LOS HUMEROS VOLCANIC CENTER, PUEBLA, MEXICO: GEOLOGY, PETROLOGY, GEOTHERMAL SYSTEM, AND GEO-ARCHAEOLOGY

A DISSERTATION

SUBMITTED TO THE DEPARTMENT OF APPLIED EARTH SCIENCES

AND THE COMMITTEE ON GRADUATE STUDIES

OF STANFORD UNIVERSITY

IN PARTIAL FULFILLMENT OF THE REQUIREMENTS

FOR THE DEGREE OF

DOCTOR OF PHILOSOPHY

By

Horacio Gerardo Ferriz-Dominguez

December 1984

I certify that I have read this thesis and that in my opinion it is fully adequate, in scope and quality, as a dissertation for the degree of Doctor of Philosophy.

Gail A. Mahood
Principal Adviser
Geology Department

I certify that I have read this thesis and that in my opinion it is fully adequate, in scope and quality, as a dissertation for the degree of Doctor of Philosophy.

Ronald J.P. Lyon

I certify that I have read this thesis and that in my opinion it is fully adequate, in scope and quality, as a dissertation for the degree of Doctor of Philosophy.

Robert G. Coleman
Geology Department

Approved for the University Committee
on Graduate Studies:

Dean of Graduate Studies & Research

LOS HUMEROS VOLCANIC CENTER, PUEBLA, MEXICO: GEOLOGY, PETROLOGY, GEOTHERMAL SYSTEM, AND GEO-ARCHAEOLOGY

Horacio Gerardo Ferriz-Dominguez
Stanford University, 1985

Los Humeros volcanic center (LHVC), located 180 km east of Mexico City, is the surface manifestation of a magma chamber zoned from rhyolitic uppermost levels to andesitic and perhaps basaltic lower levels. Three major plinian eruptions, which occurred 0.46, 0.24 and 0.1 Ma ago, represent magma volumes of 115, 10, and 12 km^3, respectively. The first resulted in emplacement of the Xăltipan Ignimbrite and collapse of the 21-by-15-km Los Humeros caldera. Collapse did not attend the second eruption, but the third led to collapse of the nested, 10-km-diameter Los Potreros caldera. Two major later episodes of lava emplacement, dated at 0.04 and 0.02 Ma, represent extrusion of 6 and 10 km^3 of magma, respectively. Large compositional and isotopical variations in all eruptive units indicate that zonation persisted throughout the lifetime of the chamber. Erupted products show an overall trend with time toward more mafic compositions, which correlates with an increase in eruptive rates from ~0.06 km^3/1000 years 0.24 Ma ago to ~0.2 km^3/1000 years in the last 0.1 Ma. Progressive disruption of the roof of the chamber by caldera-forming eruptions may have shortened the residence time of mafic and intermediate magma in the chamber, and thus the time available for regeneration of differentiated magma.

Compositional zonation of major and most trace elements seems to have been controlled largely by crystal-liquid equilibria. Partial melting of young crustal lithologies accounts best for volume relations, but must be complemented by fractional crystallization coupled with assimilation to explain compositional and isotopic variations. Systematic trends in Cr, Ni, Sr, Rb, and Ba, however, further suggest episodic magma mixing and local operation of diffusive processes.

Exploratory drilling confirms the existence of a water-dominated geothermal reservoir hosted by Plio-Pleistocene andesites. The reservoir is bounded by the ring-fracture zone of the Los Potreros caldera, and is capped by hydrothermally altered Xâltipan Ignimbrite. Faults and fractures related to intracaldera uplift provide permeability.

Inhabitants of the Caltonac archaeologic site, built on an andesite flow of LHVC, quarried obsidian from a post-Xâltipan rhyolite flow whose glassy portions are the source of the D-type obsidian found in Formative to Postclassic Mesoamerican sites.

To Fabiola

PREFACE

This dissertation consists of papers that address different aspects of the geology, petrology, geothermal potential, and geo-archaeology of the Los Humeros volcanic center, Puebla, Mexico. This large silicic volcanic center is one of five recognized to date in the Mexican Neovolcanic Belt, an east-west belt of large andesitic stratovolcanoes, silicic volcanic centers, and cinder cone fields that bisects central Mexico. Although Los Humeros is not necessarily a typical example of the silicic volcanic centers of the Neovolcanic Belt (Ferriz and Mahood, in press), because of its complex history, it does illustrate some of the problems in interpreting them, as well as some of their economically important aspects --both present and past.

The first chapter (Ferriz and Mahood, 1984) describes the evolution of the volcanic center based on field mapping and K-Ar age determinations. These data, together with a brief analysis of the ranges of composition of the products of the different eruptive units leads to the conclusions that (1) the Los Humeros magma chamber was zoned in composition from uppermost rhyolitic levels down to andesitic and perhaps even basaltic levels, (2) average eruptive rates increased with time during the 0.46 Ma lifetime of the center, and (3) the eruption rates exceeded the rates of regeneration of differentiated magma.

The second chapter is a translation of a paper in Spanish (Ferriz, in press) in which most of the mineralogical data are presented. This paper was written for didactic purposes with the Mexican geological community in mind. Thus, some basic concepts which are seldom included in a dissertation are reviewed. The analysis of the data, together with phase-equilibria considerations, leads to the conclusion that the chamber was zoned in temperature, oxygen fugacity, volatile contents, and total phenocryst contents, as well as in bulk composition.

In the third chapter (Ferriz and Mahood, in preparation) an analysis of major- and trace-element data is combined with the information presented in the previous two chapters in an attempt to discriminate among differentiation processes that could have produced the wide range of compositions erupted at Los Humeros. Partial melting of young crustal lithologies, coupled with marginal crystallization and minor assimilation, appear to have been the dominant differentiation mechanisms.

The fourth chapter is an updated analysis of the Los Humeros geothermal reservoir (Ferriz, 1982). Available geologic, geophysical, and exploratory drilling data indicate that the water-dominated reservoir is hosted by zones of secondary permeability in pre-Los Humeros andesitic and ferrobasaltic lavas, but is bounded and capped by ring-fracture zones and eruptive units linked with the evolution of the silicic volcanic center.

In the final chapter (Ferriz, in review) one of the rhyolite flows of the volcanic center is characterized as an important prehispanic source of obisidian. The results of preliminary mapping of Caltonac, a large archaeologic site located in the southwestern flank of Los Humeros, are presented as well. Caltonac seems to have developed during the Classic, probably both because of the nearby obsidian source, and because of its strategic location at the intersection of two of the natural access routes between the coastal plains and the highlands of central Mexico.

REFERENCES

Ferriz,H., 1982, Geologic and preliminary reservoir data on the Los Humeros geothermal system, Puebla, Mexico: in Proceedings Eighth Workshop Geothermal Reservoir Engineering (SGP-TR-60), p.19-24, Stanford University, Stanford, California.

Ferriz,H., in press, Zoneamiento composicional y mineralógico en los productos eruptivos del centro volcánico de Los Humeros, Puebla, Mexico: Geofísica Internacional.

Ferriz,H., in review, Caltonac, A prehispanic obsidian-mining center in Eastern Mexico? : A preliminary report: J. of Field Archaeology.

Ferriz,H., Mahood,G.A., 1984, Eruption rates and compositional trends at Los Humeros volcanic center, Puebla, Mexico: J. Geophys. Res., v.B89, p.8511-8524.

Ferriz,H., Mahood,G.A., in press, Volcanismo silícico en el Eje Neovolcanico Mexicano: International Committee for the Study of the Lithosphere, Special Issue on Mexico, Geofísica Internacional.

Ferriz,H., Mahood,G.A., in preparation, Strong compositional zonation in a silicic magmatic system of the Mexican Neovolcanic Belt: Los Humeros, Puebla: to be submitted to Contr. Mineral. Petrol.

ACKNOWLEDGEMENTS

Mi hija linda:

When many years from now you read this words you will probably wonder why it is that scientists have the tendency to dedicate incomprehensible technical books to their little daughters and, furthermore, why do they always try to explain the reasons for doing so. For a change I will not attempt to do the latter, but instead would like you to know that besides its technical content the pages of this book bear the friendship and encouragment that many people gave to me during our life at Stanford. It is so that you will remember all our wonderful friends that I write this letter.

To start chronologically, I had my first break even before we got to Stanford, when Ron Lyon decided to take the risk of accepting me as his M.Sc. student. Although he later claimed that he would never make the same mistake again Ron always rooted for me, welcomed me as a friend in his lab, and more than once got us out of financial troubles.

It was also on those early days that I found a real gold mine in the friendship of my officemates at 403. Paul Bartos, Tim Hayes, Mark Sander, Eric Seedorff, and Paul Zweng patiently put up with my ways and were always willing to help me, particularly Eric who went through an endless number of manuscripts and undertook the task of teaching me the intricacies of the English language.

A year later Gail Mahood arrived to Stanford and accepted me as her Ph.D. student. Little she knew at the time the stubborn person she was inheriting! Gail spent an incredible amount of time arguing with me in the field, listening to my half-baked ideas, and trying to make sense of what I wrote. More important, however, she never lost confidence in me and was always a caring friend.

I cannot forget our friends down in Mexico. Without the help and support of Carlos García, Gerardo López, and Camilo Yáñez I would have never been able to complete the field work at Los Humeros, and you would have never had your donkey at Perote.

Then there were the Friends of Igneous Petrology, a nickname for all of us that made talking of volcanic rocks a hobby. Long discussions with Dave Boden, Pat Dobson, Chris Fridrich, Anita Grunder, Wes Hildreth, Clark Johnson, Jenny Metz, and Steve Novak did much to clarify my ideas. They were a very exciting group to work with and I will certainly miss them. Anita in particular always managed to cheer me up when things got rough, and kindly welcomed us as part of the family in Owl Creek.

Four other friends, Pixie Couch, Yvette and Arturo Riojas, and Lori Williams took care that I would keep my sanity by not thinking geology all the time. Their friendship will always be an invaluable treasure for me.

Finally, I would like you to remember all the support that your loving grandparents, Papo y Ma, gave to us from Mexico during all these years that we had been away from home.

It is the love of these and many other friends that I have not mentioned what I dedicate to you in these pages darling. You will understand its value later, when your own time comes.

Love

Papá

TABLE OF CONTENTS

LIST OF ILLUSTRATIONS

ERUPTIVE RATES AND COMPOSITIONAL TRENDS AT LOS HUMEROS VOLCANIC CENTER, PUEBLA, MEXICO

COMPOSITIONAL AND MINERALOGICAL ZONING IN THE ERUPTIVE PRODUCTS OF THE LOS HUMEROS VOLCANIC CENTER, PUEBLA, MEXICO

STRONG COMPOSITIONAL ZONATION IN A SILICIC MAGMATIC SYSTEM OF THE MEXICAN NEOVOLCANIC BELT: LOS HUMEROS, PUEBLA

GEOLOGIC AND PRELIMINARY RESERVOIR DATA ON THE LOS HUMEROS GEOTHERMAL SYSTEM, PUEBLA, MEXICO

CALTONAC, A PREHISPANIC OBSIDIAN-MINING CENTER IN EASTERN MEXICO ? : A PRELIMINARY REPORT

LIST OF TABLES

ERUPTIVE RATES AND COMPOSITIONAL TRENDS AT LOS HUMEROS VOLCANIC CENTER, PUEBLA, MEXICO

COMPOSITIONAL AND MINERALOGICAL ZONING IN THE ERUPTIVE PRODUCTS OF THE LOS HUMEROS VOLCANIC CENTER, PUEBLA, MEXICO

STRONG COMPOSITIONAL ZONATION IN A SILICIC MAGMATIC SYSTEM OF THE MEXICAN NEOVOLCANIC BELT: LOS HUMEROS, PUEBLA

CALTONAC, A PREHISPANIC OBSIDIAN-MINING CENTER
IN EASTERN MEXICO ? : A PRELIMINARY REPORT

Ferriz,H., Mahood, G.A., 1984, Eruptive rates and compositional trends at Los Humeros volcanic center, Puebla, Mexico: J. Geophys. Res., v.B89, p.8511-8524.

CHAPTER 1

ERUPTION RATES AND COMPOSITIONAL TRENDS AT LOS HUMEROS VOLCANIC CENTER, PUEBLA, MEXICO

ABSTRACT

The Los Humeros volcanic center, located 180 km east of Mexico City, is one of several Pleistocene silicic centers in the "back-arc" portion of the Mexican Neovolcanic Belt. The eruptive history at Los Humeros suggests that average eruptive rates increased with time and exceeded rates of regeneration of differentiated magma. Silicic volcanism began ~0.47 Ma ago with extrusion of high-silica rhyolite domes. Shortly thereafter, at 0.46 Ma ago, 115 km^3 of magma zoned from high-silica rhyolite to rhyodacite were erupted, resulting in formation of the Xáltipan Ignimbrite and collapse of the 21 x 15 km Los Humeros caldera. High-silica rhyolite domes then erupted along the northwestern ring-fracture zone of the caldera. They are covered by the Faby Tuff, a dominantly rhyodacitic sequence of plinian fall deposits dated at 0.24 Ma. A second major caldera-forming event occurred ~0.1 Ma ago with the eruption of the Zaragoza Tuff, a nonwelded ignimbrite zoned from rhyodacite to andesite. Eruption of these 12 km^3 of magma led to collapse of the 10-km-diameter Los Potreros caldera, which is nested within the older Los Humeros caldera. Between 0.04 and 0.03 Ma ago, an arc of andesitic scoria cones, concentrated along the southern ring-fracture zone of the Los Humeros caldera, fed lavas that flowed southward from the volcanic center, and andesite lavas built two small shields between the eastern rims of the two calderas. Approximately 6 km^3 of andesitic magma were extruded during this stage. Activity continued up to 0.02 Ma ago with eruption of 10 km^3 of

rhyodacitic to andesitic lava flows from centers near the northern margin of the Los Potreros caldera, in the area between the eastern rims of the two calderas, and within a broad band where the southern segments of the inferred Los Humeros and Los Potreros ring-fracture zones nearly coincide. Simultaneous venting of rhyodacitic and andesitic tephra within this band led to formation of the 1.7-km-diameter El Xalapazco caldera. Minor fault-bounded uplift of the southeastern quadrant of the Los Potreros caldera followed. The latest stage of volcanic activity is represented by the eruption of ~0.25 km^3 of olivine basalt lavas along the southern ring-fracture zone of the Los Humeros caldera and on the floors of the Los Potreros and El Xalapazco calderas. Erupted magmas show an overall trend with time toward more mafic compositions. Volumetric eruptive rates increased from ~0.06 km^3 per thousand years 0.25 Ma ago to ~0.2 km^3 per thousand years in the last 0.1 Ma. The increase in eruptive rate may have been the result of a progressive decrease in the structural integrity of the roof zone of the system as successive caldera-forming eruptions reactivated old zones of weakness and created new ones. An increasingly disrupted roof allowed mafic and intermediate magmas to reach the surface relatively rapidly, decreasing their residence time in a high-level chamber and thus the time available for their differentiation.

INTRODUCTION

The purpose of this paper is to relate chemical trends in the products of the Los Humeros volcanic center to the center's physical evolution. Eruptive products of this young volcanic system span the range basalt through high-silica rhyolite, but show an overall trend with time toward increasingly mafic compositions. This pattern is most likely a product of an increasing volumetric rate of eruption that exceeded the rate of regeneration of differentiated magma. We present representative analytical and petrographic data in the context of establishing petrologic trends; a detailed account of the petrologic evolution of the Los Humeros magmatic system will appear elsewhere.

Previous geologic work at Los Humeros includes photogeologic mapping by Pêrez (1978), regional geologic mapping by YâÑez and Casique (1980), and detailed mapping by Ferriz and YâÑez (1981). Ferriz (1982) described the features of the geothermal system of Los Humeros. Reconnaissance geochemical and isotopic work has been presented by Verma and Lôpez (1983) and Verma (1983). Geophysical studies have been summarized by Alvarez (1978a) and Palacios and Garcia (1981).

GEOLOGIC SETTING

The Los Humeros volcanic center (LHVC) is located near the east end of the Late Tertiary to Quaternary Mexican Neovolcanic Belt, 55 km west-northwest of the city of

Xalapa, Veracruz. It is one of four Pleistocene silicic centers that have been identified within this belt of andesitic stratovolcanoes and cinder cones (Figure 1). All four lie near the northern boundary of the Neovolcanic Belt, well behind the front defined by active andesitic stratovolcanoes such as Volcán de Colima, Popocatépetl, and Citlaltépetl (Pico de Orizaba), each of which is situated at the end of a southward younging set of andesitic centers. A similar spatial distribution of silicic centers with respect to the andesitic stratovolcanoes is observed in the Cascade Range (e.g., Macleod and Sammel, 1982).

Paleozoic crystalline rocks, folded Mesozoic sedimentary rocks, and Tertiary intrusions and andesites crop out around the LHVC. The Teziutlán Massif (Viniegra, 1965) is a Paleozoic metamorphic and intrusive complex that crops out northeast of the volcanic center and may extend beneath it. The 3,000-m-thick Mesozoic section consists of a Triassic to Middle Jurassic clastic sequence overlain by Middle Jurassic to Upper Cretaceous calcareous rocks (Viniegra, 1965; YÁñez and Casique, 1980). Wedging of the Mesozoic section against the Teziutlán Massif (Viniegra, 1965) may reduce the thickness of the sedimentary rocks beneath the volcanic center. The Mesozoic rocks were intruded by early Tertiary syenitic and granodioritic stocks, and were later covered by Mio-Pliocene mafic volcanic rocks.

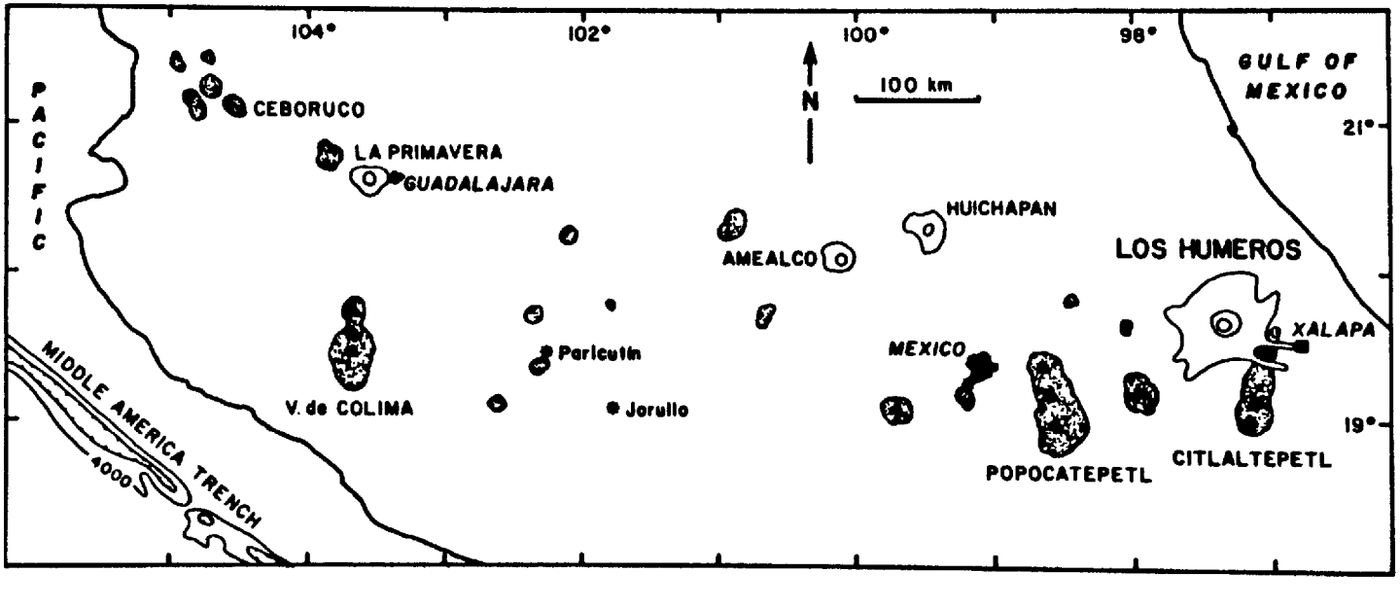

Fig. 1. Silicic and andesitic volcanic centers of the Mexican Neovolcanic Belt. Major silicic centers (calderas shown by interior lines) are unpatterned; andesitic stratovolcanoes (major vents shown with solid triangles; historically active volcanoes labeled) are shown by heavy stipple, and historically active cinder cones are shown by solid stars.

GEOLOGIC HISTORY

The following history, summarized in Table 1, is based on 1:50,000 scale field mapping (Ferriz and YÑez, 1981) and numerous K-Ar dates (Table 2). Copies of the geologic map can be obtained from the first author.

The oldest exposed volcanic rocks at LHVC are porphyritic two-pyroxene andesite lavas and breccias, and ferrobasaltic lavas of the Teziutlán Formation. K-Ar dates for two lavas from this unit are 3.5 $\pm$ 0.3 Ma (YÑez and Garcia, 1982) and 1.55 $\pm$ 0.1 Ma (Table 2). Although outcrops of the formation are limited to areas immediately north of the LHVC, this formation has been found in boreholes within the Los Humeros caldera (H1, H2, and H4 in Figure 2), where it reaches thicknesses in excess of 1000 m (Ferriz, 1982). In addition, fragments of andesite are common in all pyroclastic units of the volcanic center. Whether these lavas formed a major stratovolcano, as depicted in Figure 3a, or a group of small volcanoes cannot be determined from present exposures.

Precaldera Silicic Volcanism, Xáltipan Tuff and Los Humeros caldera.

Two crystal-poor high-silica rhyolite lavas (A and B in Figure 2) are the earliest silicic eruptive units of the LHVC. A K-Ar date of 0.47 $\pm$ 0.04 Ma for one of the lavas (Table 2) is analytically indistinguishable from that of the overlying Xáltipan Ignimbrite.

TABLE 1. Summary of the Geologic History of the Los Humeros Volcanic Center

Date, Ma	Event
>1.6	Eruption of Teziutlán lavas
0.47	Eruption of precaldera rhyolite domes
0.46	Eruption of Xáltipan Ignimbrite
	Collapse of Los Humeros caldera
0.36–0.22 (±0.02)	Eruption of postcaldera rhyolite domes
0.24 (±0.03)	Eruption of Faby Tuff
~0.10	Eruption of Zaragoza Tuff
	Collapse of Los Potreros caldera
	Gentle doming of the eastern portion of the LHVC
0.06	Eruption of Cueva Ahumada lavas
	Eruption of Xoxoctic Tuff
	Eruption of Llano Ignimbrite
0.04–0.02	Eruption of the Limón and other andesites
	Eruption of Maztaloya lavas and agglutinates
	Eruption of Cuicuiltic Tuff
	Collapse of El Xalapazco caldera
	Uplift of the SE quadrant of the Los Potreros caldera
0.03–0.02	Eruption of the San Antonio and other rhyodacites
<0.02	Eruption of olivine basalts

TABLE 2. Summary of K-Ar Dates on Eruptive Units of the Los Humeros Volcanic Center

Eruptive Unit†	Sample Coordinates	Material Dated	Sample Weight, g	K, %	$^{40}Ar^{*}$, 10^{-13} mol/g	$^{40}Ar^{atm}$, %	Calculated Age ± 1 σ‡, Ma
			Teziutlán Formation				
	19°46'49"N–97°29'41"W	whole rock	6.9253	0.618	16.6	85.5	1.55 ± 0.10
			Pre-Xáltipan Rhyolite				
B	19°35'22"N–97°23'42"W	sanidine	1.4630	4.333	35.4	69.6	0.47 ± 0.04
			Xáltipan Ignimbrite				
	19°41'36"N–97°15'15"W	biotite	1.0188	5.499§	43.5	97.4	0.46 ± 0.13
	19°41'36"N–97°15'15"W	plagioclase	8.9302	1.521	12.2	90.6	0.46 ± 0.02
			Post-Xáltipan Rhyolites				
D	19°45'47"N–97°29'28"W	sanidine	1.5005	3.022	18.7	92.4	0.36 ± 0.05
H	19°45'47"N–97°29'44"W	sanidine	1.6394	5.960	22.5	83.7	0.22 ± 0.02
			Faby Tuff				
	19°39'40"N–97°19'43"W	plagioclase	10.3559	0.696	3.3	90.0	0.27 ± 0.03
	19°39'40"N–97°19'43"W	plagioclase	6.7269	0.499	1.6	95.9	0.19 ± 0.04
			Pre-Zaragoza Rhyodacite				
L	19°39'28"N–97°24'43"W	plagioclase	8.5894	0.814	1.5	97.2	0.10 ± 0.03
			Cueva Ahumada Rhyodacite				
L	19°40'02"N–97°27'05"W	glass	2.9632	4.296	4.52	89.4	0.06 ± 0.01
			Tepeyahualco, Chiapa, and Orilla del Monte Andesites				
O	19°35'34"N–97°28'44"W	whole rock	4.2707	1.558	1.06	99.3	0.04 ± 0.03
R	19°44'57"N–97°23'09"W	whole rock	3.9366	2.149	1.28	95.2	0.03 ± 0.02
Q	19°41'28"N–97°21'08"W	whole rock	4.3924	1.540	0.49	99.7	0.02 ± 0.03
			Arenas Rhyodacite				
Y	19°38'33"N–97°28'13"W	whole rock	4.5324	3.047	1.09	94.2	0.02 ± 0.01

$\lambda_t = 0.581 \times 10^{-10}\ yr^{-1}$. $\lambda_\beta = 4.962 \times 10^{-10}\ yr^{-1}$. $^{40}K/K = 1.167 \times 10^{-4}$.
†Letters of eruptive units keyed to Figure 2.
‡Confidence interval calculated using Equation 2 of *Mahood and Drake* [1982].
§Slightly altered biotite.

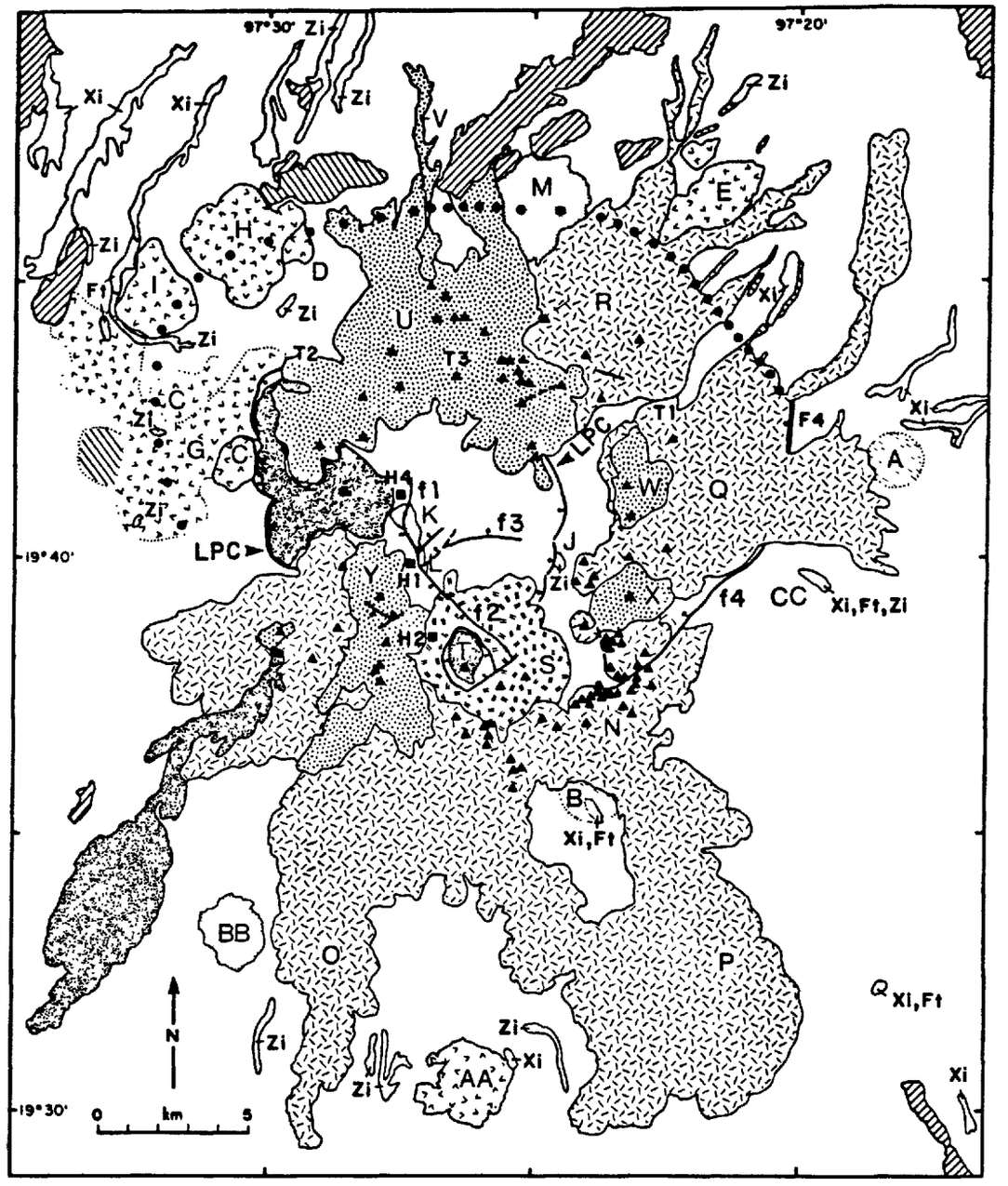

Fig. 2. Simplified geologic map of the Los Humeros volcanic center (based on *Ferriz and Yañez* [1981]). Heavy dots indicate the inferred northern topographic and structural boundary of the Los Humeros caldera. LPC indicates the eastern and western boundary faults of the Los Potreros caldera. Dotted contacts indicate largely buried units. Light stipple indicates the post-Zaragoza but pre-Xoxoctic, Las Aguilas rhyolite dome (BB) and Cueva Ahumada basaltic andesite, andesite (K), and rhyodacite lavas (L), and the Las Lineas rhyodacite dome (M). Random dashes indicate the Tepeyahualco (O), Limón (P), Orilla del Monte (Q), and Chiapa (R) andesite and basaltic andesite lavas and cinder cones. Double dashes indicate the Maztaloya (S) basaltic andesite, andesite and rhyodacite lavas and agglutinates. The heavy dot pattern indicates the San Antonio (U), Viola (W), Cuamilacas (X), and Arenas (Y) rhyodacitic lavas and tuff cones and the Papata (V) andesite flow. Unpatterned areas are outcrops of the Xáltipan Ignimbrite (Xi), Faby Tuff (Ft), and Zaragoza Ignimbrite (Zi), or alluvium and soil underlain by pyroclastic deposits of various types. Most of the area shown outside the Los Humeros caldera is underlain by the Xáltipan and Zaragoza Ignimbrites; on the east side of the map area the Faby Tuff is present as well. Within and slightly east of the Los Potreros caldera, most areas are underlain by the Xoxoctic and Cuicuiltic tuffs. T1, T2, and T3 indicate locations of telluric anomalies [*Alvarez*, 1978*b*, 1980]. Fault scarps are labeled f1 to f4. See text for other lettered units.

The Xàltipan Ignimbrite represents a minimum of 115 km^3 of magma (Table 3). The pyroclastic flows filled low areas of the rugged preexisting landscape (Figure 4a), covering ~3,500 km^2. They descended 1900 m in flowing 50 km through canyons that ran northeast to the coastal plain. To the southeast, the flows were deflected through passes on the flanks of the Cofre de Perote andesitic volcano (CP in Figure 4a), climbing as much as 600 m above the plains that surrounded LHVC to reach the area of the present-day city of Xalapa (XA in Figure 4a). South and southwest of LHVC, the pyroclastic flows covered flatter terrain, where they are now overlain by lacustrine sediments and soil. The Sierra de Tlaxco (ST in Figure 4a) was a barrier to the flows on the west, but they crossed it through passes that are now 100 m above the level of the surrounding plains. After crossing the Sierra de Tlaxco, some of the flows were deflected toward the north along the canyons of the Rio Apulco (RA) and Rio Tecuantepec (RT).

The Xàltipan Ignimbrite is mostly nonwelded; only thick accumulations in deep canyons show partial welding. Most of the pumice in the ignimbrite is aphyric high-silica rhyolite, but sparsely porphyritic biotite rhyodacite pumice is ubiquitous (Table 4). Locally, the Xàltipan Ignimbrite is covered by a co-ignimbrite ash-fall deposit that, in turn, is concordantly overlain by eight air-fall lapilli tuffs (X-3 to X-10 in Figure 5) that range in composition from rhyodacite to andesite (Table 4). These air-fall tuffs extend the compositional zonation displayed in the Xàltipan

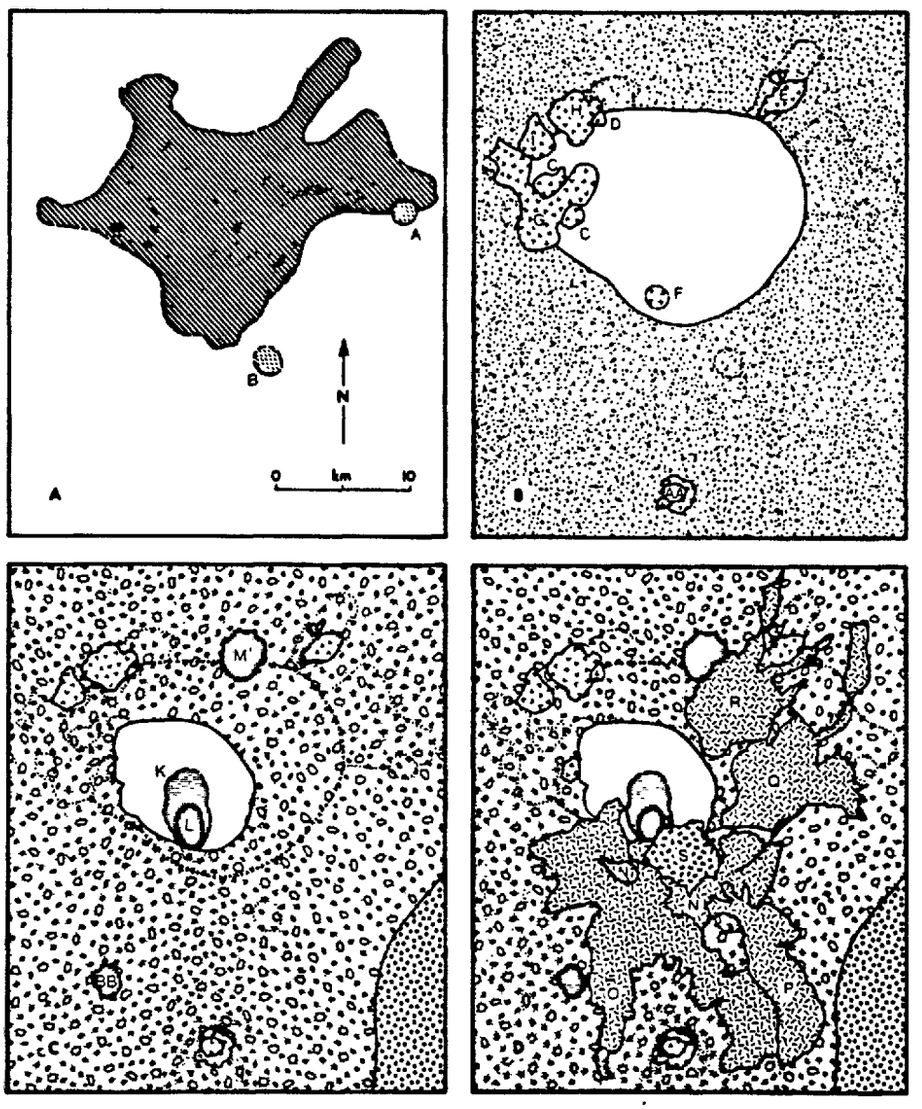

Fig. 3. Schematic geologic history of the Los Humeros volcanic center. Patterns and lettered units as in Figure 2. (*a*) Eruption of andesites and basalts of the Teziutlán Formation and later eruption of LHVC rhyolite lavas (A and B). (*b*) Eruption of the Xáltipan Ignimbrite (sandstone pattern) led to collapse of Los Humeros caldera. Intracaldera ignimbrite not shown for clarity. Collapse was followed by eruption of biotite rhyolites (C, D, E, and F), then aphyric rhyolite (G) and finally hypersthene rhyolites (H and I). (*c*) Eruption of the Faby Tuff (heavy dots). Later eruption of the Zaragoza Tuff (pebble pattern) led to collapse of Los Potreros caldera. After collapse, the Cueva Ahumada andesitic (K) and rhyodacitic (L) edifice grew within the caldera, and a rhyodacite dome (M) erupted in the north. (*d*) Formation of an arc of scoria cones (N), eruption of andesite and basaltic andesite lavas (O, P, Q, and R), and formation of the Maztaloya volcano (S). See Figure 2 for last stages of volcanic activity.

TABLE 3. Volume of the Eruptive Units of Los Humeros Volcanic Center

	Volume of Unit,* km³	Volume of Dense Rock Equivalent, km³	Maximum Thickness of Pyroclastic Units (T_{max}), m	Exponential Rate of Thickness Decay for Fall Deposits, (M)	Caldera Area, km²
Teziutlán lavas	60	60			
Pre-Xáltipan rhyolites	0.1	0.1			
Xáltipan Ignimbrite	230	115	>150		260
Post-Xáltipan rhyolites	4.7	4.7			
Faby Tuff	40	10	17.1	2.0×10^{-5}	
Zaragoza basal fall	8	2	2.5	1.6×10^{-5}	
Zaragoza Ignimbrite	20	10	>40		86
Cueva Ahumada lavas	0.1	0.1			
Xoxoctic Tuff	2.2	0.6	2.8	3.3×10^{-5}	
Llano andesitic Ignimbrite	0.2	0.1	10		
Limón and other andesites	6	6			
Cuicuiltic Tuff	0.3	0.1	5.8	14.4×10^{-5}	
San Antonio and other rhyodacites	10	10			
Olivine basalts	0.25	0.25			

*Volumes for the Teziutlán and Cueva Ahumada lavas may have considerable errors. Volume estimates for the ignimbrites do not include the unknown volume of dispersed airborne ash because of difficulties inherent in estimating this volume when the pumice in an ignimbrite is largely aphyric (Xáltipan) or has a wide range of phenocryst contents (Zaragoza) [*cf. Sparks and Walker*, 1977]. The volumes of the fall deposits were calculated by numerical integration at 0.01-m intervals, assuming elliptical isopachs. To estimate the area of the isopachs, we first calculated the exponential rate of thickness decay (M) by plotting thickness versus distance from the point of maximum thickness. Then we calculated the major axis (x) of every isopach using the equation $x = (\ln T_{max} - \ln T)/M$, where T_{max} is maximum thickness and T is thickness of interest. Third, we assumed the minor axis of the ellipse (y) to be a linear function of the major axis, $y = kx$. The value of constant k ranges from 0.9 to 0.2 for published isopach maps; an intermediate value of 0.6 is used in these calculations.

Ignimbrite; pumice in the ignimbrite ranges from 77.2 to 71.5% SiO_2 (recalculated anhydrous), whereas air-fall pumice contains 71.7 to 61.3% SiO_2. The eruption of andesitic material, although volumetrically minor, indicates that the magma chamber was strongly zoned in composition just prior to the Xáltipan eruption 0.46 Ma ago.

Eruption of the Xáltipan Ignimbrite led to collapse of the Los Humeros caldera (Figure 3b). Younger volcanic rocks obscure the caldera margin, but the original dimensions of the caldera are estimated to have been 21 x 15 km. Nowhere within the caldera is the Xáltipan Tuff exposed. Along the north half of the caldera, the structural boundary can be located either by the first appearances of the Teziutlán Formation and outflow Xáltipan Ignimbrite, or by the location of lava domes, which, based on their chemical similarity to the Xáltipan Ignimbrite, are thought to be ring-fracture rhyolites. In the northeast quadrant of the caldera, the topographic rim is well expressed in an abrupt change in the slope over which later andesites flowed. This topographic rim corresponds closely with the inferred structural margin. At locality B (Figure 2), the Xáltipan Ignimbrite is less than 5 m thick, having flowed off a preexisting high. Less than 8 km away, the ignimbrite is 250 m thick in the H2 borehole (Figures 2 and 6). The increase in thickness of the Xáltipan Ignimbrite suggests ponding within the Los Humeros caldera, and thus the boundary of the caldera must lie between localities B and H2. An arc of younger scoria cones is thought to mark the ring-fracture

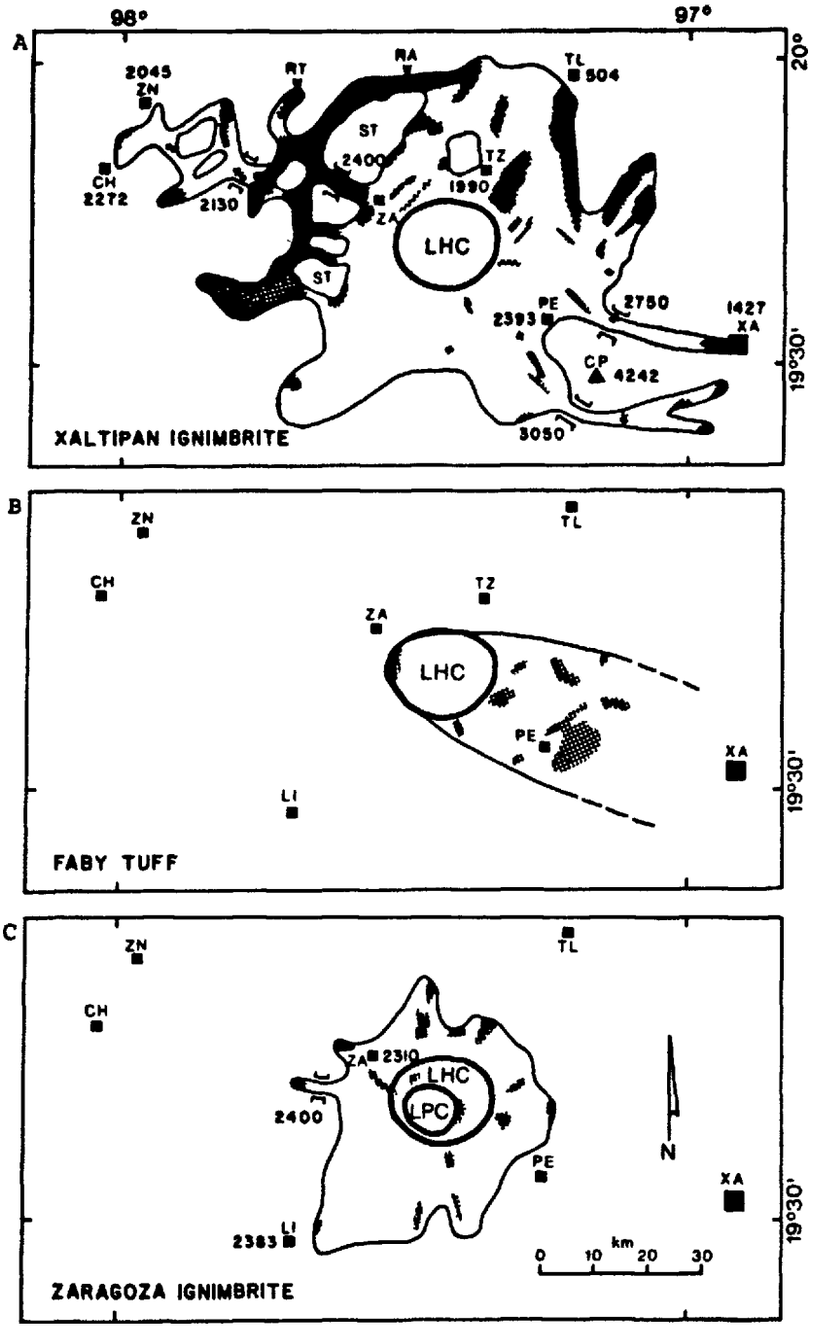

Fig. 4. Distribution of major pyroclastic units of the Los Humeros volcanic center. Present outcrops, checkered pattern; inferred extent enclosed by light solid lines. Heavy lines indicate Los Humeros (LHC) and Los Potreros (LPC) calderas. Squares indicate towns (ZN Zacatlán, CH Chignahuapan, ZA Zaragoza, TZ Teziutlán, TL Tlapacoyan, LI Libres, PE Perote, XA Xalapa); triangle, summit of the Cofre de Perote volcano (CP); ST Sierra de Tlaxco. Also shown are the canyons of the Rio Apulco (RA) and Upper Rio Tecuantepec (RT). Bridge symbols indicate passes through which the ignimbrites are inferred to have crossed mountain ranges. Numbers indicate present elevations above mean sea level in meters.

TABLE 4. Chemical Analyses of Pumice and Lavas of the Los Humeros Volcanic Center

Sample No:	LH-8	LH-11	LH-16	LH-17	LH-33	LH-41
Unit:	Xáltipan Ignimbrite Rhyolite	Xáltipan Ignimbrite Rhyodacite	Xáltipan Airfall Rhyodacite	Xáltipan Airfall Andesite	Faby Tuff	Zaragoza Basal Fall
Latitude N:	19°41'36"	19°41'36"	19°39'40"	19°39'40"	19°39'40"	19°40'01"
Longitude W:	97°15'15"	97°15'15"	97°19'43"	97°19'43"	97°19'43"	97°24'31"
T, °C:	800†	876*	870*	953†	875*	855*
$\log fO_2$:	−14.3	−12.3	−12.1	−10.3	−12.1	−13.3
SiO_2	76.6	71.5	70.6	61.3	72.2	71.1
TiO_2	0.08	0.27	0.42	0.99	0.36	0.46
Al_2O_3	12.9	16.7	14.9	16.5	14.8	14.9
Fe_2O_3	0.48	0.58	0.87	1.84	0.67	0.68
FeO	0.67	1.32	1.74	3.95	1.22	1.88
MnO	<0.02	0.04	0.04	0.10	0.04	0.04
MgO	<0.10	0.31	0.90	3.38	0.43	0.52
CaO	0.41	0.86	1.95	5.19	1.22	1.49
Na_2O	2.91	2.98	3.85	3.73	4.10	4.20
K_2O	5.80	5.35	4.58	2.83	4.88	4.66
P_2O_5	<0.05	<0.05	0.11	0.21	0.05	0.08
Rb, ppm	136	114	119	67	127	110
Sr	17	76	136	295	108	110
Ba	115	780	710	460	780	820
La	40	28	31	27	<20	32
Y	31	26	28	30	30	34
Zr	104	256	320	280	304	352

Sample No:	LH-42	LH-45	LH-53	LH-57	LH-82	LH-94
Unit:	Zaragoza Ignimbrite Rhyodacite	Zaragoza Ignimbrite Andesite	Xoxoctic Tuff	Tepeyahualco Andesite	San Antonio Rhyodacite	Humeros Olivine Basalt
Latitude N:	19°40'01"	19°31'27"	19°41'09"	19°33'56"	19°45'48"	19°37'13"
Longitude W:	97°24'31"	97°24'39"	97°24'27"	97°27'31"	97°25'44"	97°30'20"
T, °C:	879*	919*	890†	958†	907*	1067*
$\log fO_2$:	−12.6	−11.7	−11.6	−10.4	−11.7	−9.7
SiO_2	70.1	59.1	65.1	59.2	69.0	49.0
TiO_2	0.50	1.45	0.65	1.15	0.54	1.40
Al_2O_3	15.2	17.2	16.5	17.6	15.7	17.1
Fe_2O_3	0.76	1.49	1.05	1.92	0.77	1.48
FeO	2.10	5.32	3.21	4.31	2.17	8.26
MnO	0.05	0.11	0.08	0.09	0.06	0.16
MgO	0.59	2.90	1.70	2.92	0.79	8.93
CaO	1.70	6.08	3.62	6.37	1.97	10.26
Na_2O	4.38	3.93	4.45	4.06	4.72	2.90
K_2O	4.48	2.08	3.44	2.09	4.13	0.37
P_2O_5	0.11	0.39	0.17	0.28	0.14	0.19
Rb, ppm	85	57	65	52	98	5
Sr	138	427	271	458	168	357
Ba	880	560	830	570	760	78
La	34	27	33	31	35	<20
Y	30	31	33	26	28	27
Zr	326	217	400	208	343	98

Major elements determined by XRF on fused disks and Rb, Sr, and Zr on pressed pellets. Ba, La, and Y determined by emission spectrographic analysis. Analyses performed by the U.S. Geological Survey and H. Ferriz (Rb, Sr, and Zr). Analyses recalculated on anhydrous basis. Fe_2O_3* recalculated to Fe_2O_3 and FeO based on *Sack et al.* [1980] using the indicated T and fO_2.

*T and fO_2 estimated from coexisting Fe-Ti oxides [*Spencer and Lindsley*, 1981].

†T and fO_2 estimated from coexisting Fe-Ti oxides of a different sample of similar composition.

zone on the south (Figure 2). We infer that the location of a younger arc of scoria cones reflects this structural boundary (N in Figure 2). This is also the location at which the 0.05-Hz telluric response shows a large resistivity gradient (Alvarez, 1980). On the east, the caldera margin is thought to lie near fault scarp f4 (Figure 2), which as discussed below, may represent reactivation of the Los Humeros ring-fracture zone. The amount of collapse estimated by determining the offset of the lower contact of the ignimbrite is ~450 m (Figure 6), which is in excellent agreement with that estimated by relating magma volume to caldera area.

Several high-silica rhyolite domes were emplaced after collapse at or close to the inferred ring-fracture zone (Figure 3b). Sparsely porphyritic biotite rhyolites similar in composition to the Xáltipan Ignimbrite (C, D, and E in Figures 2 and 3b) were emplaced along the northern and western portions of the ring-fracture zone; an additional lava (F in Figure 3b) cut by the H2 borehole (Figure 2) may have been erupted along the southern portion of the ring-fracture zone. Probably much later, the Oyameles dome (C) was breached, and the Caltonac aphyric rhyolite flow (G) erupted through its core forming three lobes. Sparsely porphyritic hypersthene high-silica rhyolites of the Ocotepec group (H and I) later partially covered the aphyric rhyolite and one of the biotite rhyolite domes (D). Dates (Table 2) of 0.36 $\pm$ 0.05 Ma for one of the biotite rhyolite domes (D) and 0.22 $\pm$ 0.02 Ma for a hypersthene rhyolite (H)

are consistent with these field observations. Emplacement of the Pizarro high-silica rhyolite dome (AA in Figures 2 and 3b), south of the volcanic center, lifted the Xáltipan Ignimbrite locally. The younger Zaragoza Ignimbrite (discussed below) banks against this dome, which is not directly related to the Los Humeros magmatic system.

Faby Tuff

The Xáltipan Ignimbrite and the above mentioned postcaldera domes are covered discordantly by the Faby Tuff, an internally concordant sequence of one andesitic and eight rhyodacitic air-fall tuffs (F-1 to F-9 in Figure 5). The aggregate thickness of the sequence near the Los Humeros caldera rim is 16 m, with individual falls being between 1 and 3.5 m thick. At a distance of 10 km along the east-southeast oriented dispersal axis, the aggregate thickness decreases to 9 m. The internally concordant nature of the air-fall tuffs suggests that they represent a single eruptive sequence. Dates of 0.27 $\pm$ 0.03 and 0.19 $\pm$ Ma (Table 2) are irresolvable at the 95% confidence level from the 0.22 $\pm$ 0.02 Ma date on the underlying Ocotepec postcaldera dome (H in Figure 2).

The minimum area covered by the air-fall tuffs, based on present-day outcrop pattern, is ~1000 km^2 (Figure 4b). This figure greatly underestimates the original distribution, as layers F-2 and F-4 are commonly thicker than 1 m each at the boundaries of the area shown. Assuming elliptical isopachs with short-to-long-axis ratios of 0.6,

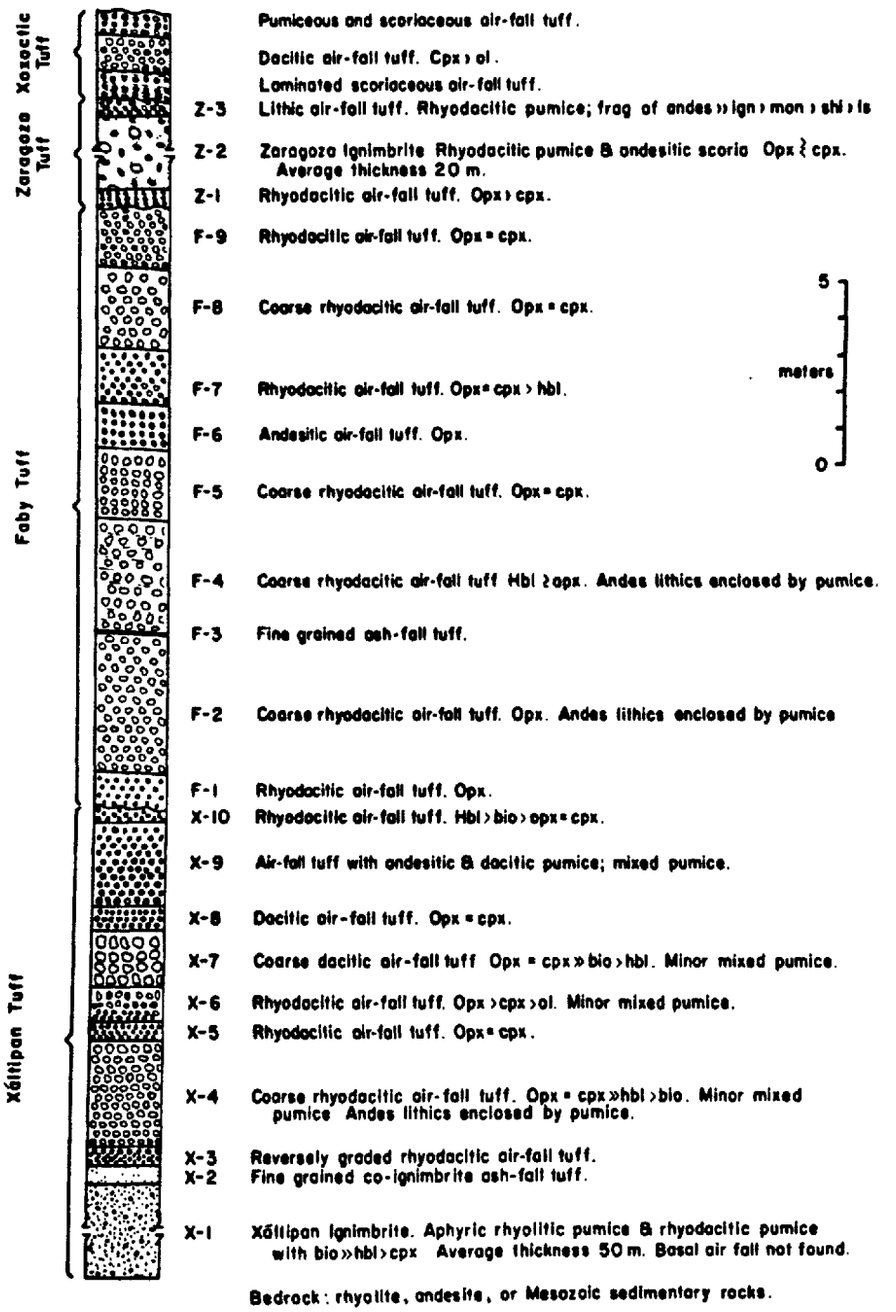

Fig. 5. Composite stratigraphic column of pyroclastic units near locality CC in Figure 2. Opx, orthopyroxene; cpx, clinopyroxene; bio, biotite; hbl, hornblende; ol, olivine; andes, andesite; ign, ignimbrite; mon, monzonite; shl, shale; ls, limestone.

the area enclosed by the 0.01 T_{max} isopach (cf. Walker, 1980) of layer F-2 would have been 25,000 km^2. The magma volume represented by the entire Faby Tuff sequence is estimated to have been ~10 km^3 (Table 3). The vent lies somewhere in the southeast quadrant of the Los Humeros caldera, as the tuff is thickest and pumice lapilli are largest near there.

The Faby Tuff is compositionally zoned. Greater than 90% by volume of the ejecta in the rhyodacitic tuffs is white ash and pumice lapilli (Table 4). The phenocryst content of pumice lapilli increases upward in the sequence from 2.5% to 15% by weight, while the silica content, recalculated anhydrous, decreases from 72.5 to 69.5%. Mixed gray and white pumice usually forms less than 5% of the ejecta, and the remaining 5% is dominated by dark green andesitic lithics. The andesitic layer F-6 consists of black ash, sparsely porphyritic scoriaceous lapilli, and 5% andesitic lithics. It appears to have erupted from the same source area as the rhyodacitic layers because their thickness variations are similar. The coeval eruption of rhyodacitic and andesitic magma may represent either (1) surging of andesite from deeper levels of a zoned chamber (cf. Hildreth, 1983), or (2) the fortuitous mixing of rhyodacite and andesite shortly before or during the eruptive event (cf. Sparks et al., 1977).

No collapse structure related to the eruption of the Faby Tuff has been recognized, despite the relatively large volume of this eruptive sequence. The lack of observed

collapse may be related to the fact that the Faby Tuff consists of nine discreet fall units, rather than a single voluminous unit; there may have been sufficient time between eruptions for replenishment of the high-level magma chamber from its root zone.

The eruption of the Faby Tuff was followed by a relatively quiescent period, during which deep gullies were cut in the Xâltipan Ignimbrite and Faby Tuff. Thin lacustrine deposits and a 0.10 ± 0.03 Ma rhyodacite flow (Locality J in Figure 2) within the Los Humeros caldera date from this period.

Zaragoza Tuff and Los Potreros Caldera

Following this period of apparent repose, a second caldera-forming eruption took place. Approximately 12 km^3 of magma erupted to form the basal plinian fall, nonwelded ignimbrite, and upper lithic-rich fall deposit of the Zaragoza Tuff (Table 3, Figure 5). This eruption led to the formation of the 10-km-diameter Los Potreros caldera (Figure 3c). We have not been succesfully date the Zaragoza Tuff, but the 0.10-Ma age of the underlying rhyodacite flow mentioned above, and the 0.06-Ma age of post-Zaragoza lavas constrain the age of the Zaragoza Tuff to ~0.1 Ma.

The dispersal axis of the basal fall deposit of the Zaragoza Tuff is poorly defined, but was probably northward. The thickness decreases from 2.5 m at the eastern rim of the Los Potreros caldera (J in Figure 2) to 2 m 15 km north of the rim. Maximum size of the pumice fragments decreases from

20 to 6 cm over this distance. Greater than 95% by volume of the air-fall tuff is formed by rhyodacitic ash and pumice lapilli (Table 4) in which phenocrysts of orthopyroxene, clinopyroxene, plagioclase, and Fe-Ti oxides form crystal clots that amount to 6.5% by weight of the pumice; andesitic scoria and lithic fragments of andesite are found in subordinate amounts. Similar crystal clots are found in the pumice of the overlying ignimbrite. This textural similarity, as well as the lack of erosional features between the air-fall tuff and the ignimbrite, suggest that the transition from fall to flow mechanism of emplacement represented a change in the physical parameters of a continuous eruptive event (cf. Sparks et al., 1973; Sparks and Wilson, 1976).

Outflow sheets of the Zaragoza Ignimbrite covered an area of ~1,300 km^2, and were generally confined to the plains that surrounded the volcanic center (Figure 4c), where it locally exceeds 20 m in thickness. On the west, the pyroclastic flows did surmount passes in the Sierra de Tlaxco, but stopped short of the Rio Apulco. Juvenile ejecta range in composition from rhyodacitic pumice to andesitic scoria (Table 4), with a minor fraction of the lapilli displaying physical mixtures of the two magmas. Chemical analyses of homogeneous lapilli lie in the ranges 71.1 to 69.9 and 59.1 to 54.4% SiO_2 (calculated anhydrous), and suggest the existence of a compositional gap within the pre-Zaragoza chamber. Clots of orthopyroxene,

clinopyroxene, plagioclase, and Fe-Ti oxides phenocrysts usually form 7.5 to 16% by weight of the rhyodacitic pumice. Phenocryst content increases to as much as 30% by weight in andesitic scoria but then decreases to as little as 4% by weight in basaltic andesite scoria. The mineralogy in the scoria is similar to that of the rhyodacitic pumice (±olivine), but the phenocrysts do not form clots.

In some exposures immediately east and west of the Los Potreros caldera rim, the lithic content of the Zaragoza Ignimbrite increases sharply from <10% by volume to ~60% within the uppermost meter. The ignimbrite is concordantly overlain by a fall deposit consisting of more than 70% by volume lithic fragments. Pumice in the lithic airfall is texturally identical to that in the ignimbrite. We interpret this high lithic concentration at the close of the eruption as signalling the onset of caldera collapse. The lithic fragments consist (in order of decreasing abundance) of aphyric and porphyritic andesite, welded ignimbrite, diorite, monzonite, shale, carbonaceous shale, slate, and limestone, and must represent lithologies overlying the magma chamber.

The eastern and western topographic walls of the Los Potreros caldera (Figure 3c) can still be recognized. The aforementioned lacustrine sediments and rhyodacite flow, covered by the Zaragoza Tuff, are exposed in the eastern wall (Locality J in Figure 2). The Oyameles biotite rhyolite dome (C in Figure 2), a rhyodacitic tephra cone, and the Caltonac aphyric rhyolite flow (G), the latter

covered by the Faby and Zaragoza Tuffs, are exposed in the western wall. Faults that form the caldera walls (LPC in Figure 2) cut the Zaragoza Tuff.

The north and south boundaries of the Los Potreros caldera are covered by younger lavas, but the forms of the west and east rims constrain rather closely where the other margins must lie (Figure 2). On the north, the ring-fracture zone is covered by the rhyodacitic to andesitic lavas of the San Antonio volcano (U in Figure 2) but is expressed in steep gradients in the telluric response (Alvarez, 1978b, 1980) at localities T2 and T3 (Figure 2). On the south, one can infer that the Los Potreros ring-fracture zone comes within 3 km of that inferred for the Los Humeros caldera. The scatter of vents between the Los Humeros ring-fracture zone and where one might reasonably draw the Los Potreros ring fracture suggests that this close approach of the two ring-fracture zones led to development of a broad intervening band of strongly faulted ground that allowed magma easy access to the surface.

The amount of collapse can be estimated from displacement of the lower contact of the Xáltipan Tuff between borehole H2, at the northern edge of the band of vents, and boreholes H1 and H4, which clearly lie within the Los Potreros caldera (Figures 2 and 6). This gives 465 and 285 m. These estimates are uncertain because some of the offset could be related to the Los Humeros caldera or to unrecognized collapse in response to eruption of the Faby

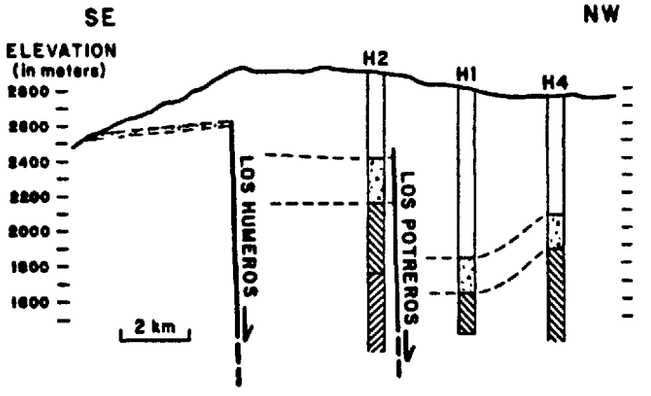

Fig. 6. Simplified cross section across the southern margin of the LHVC showing borehole constraints on the positions of the Los Humeros and Los Potreros ring-fracture zones. Xáltipan Tuff, sandstone pattern; Teziutlán Formation, right-dipping diagonal ruling; Mesozoic marls and limestones, left-dipping diagonal ruling. Descriptions of the lithologic column of each borehole are given by *Ferriz* [1982].

Tuff. On the other hand, the estimates may be too low because, as discussed below, the area near the boreholes was later uplifted and faulted. This may account for the higher elevation of the basal contact in H4 than in H1. A minimum estimate of collapse that is not subject to these uncertainties is given by the exposed height of the Oyameles dome in the western scarp of the Los Potreros caldera (C in Figure 2). This 200-m-high fault scarp exposes the dense devitrified core of the dome, the counterpart of which is not found on the down-dropped side of the fault, indicating a minimum collapse of 200 m. This amount of collapse would imply a magma volume of at least 17 km^3, taking 375 m as the average displacement of the base of the Xáltipan Tuff in the boreholes yields a collapse volume of 32 km^3. Both these estimates are greater than the 12 km^3 of magma estimated from the pyroclastic deposits themselves. This suggests that the volume of the Zaragoza Tuff has been underestimated (see footnote to Table 3) and/or that collapse was not uniform throughout the whole caldera area.

Nowhere within the Los Potreros caldera is the Zaragoza Tuff exposed, and it has not been recognized in cuttings from boreholes. This lack of significant intracaldera fill may be due to collapse occurring late in the eruptive event. Although the lower Zaragoza airfall is of normal thickness in exposures just outside the caldera, the ignimbrite is from <1 to 6 m thick, having flowed off the LHVC edifice.

The basaltic andesite and andesitic lavas of the small Cueva Ahumada volcanic edifice (K in Figures 2 and 3c),

which grew inside the Los Potreros caldera, might have been fed by magma rising through collapse-related fractures in the caldera floor. As is the case in other caldera systems (e.g. Westerveld, 1952; Christiansen and Blank, 1972; Gibson, 1974; Bailey et al., 1976; Smith, 1979; Mahood, 1980), these post-caldera lavas are more mafic than the dominant magma of the preceding Zaragoza eruption. These intermediate and mafic lavas were later intruded by a 0.06 ± 0.01 Ma biotite rhyodacite dome (L in Figures 2 and 3c). The Las Lineas orthopyroxene rhyodacite dome (M in Figures 2 and 3c), may have been intruded along the inferred northern boundary of the Los Humeros caldera at about the same time. It occupies a stratigraphic position equivalent to the Cueva Ahumada lavas; i.e., it is not covered by the Zaragoza Tuff, but is covered by the products of postcaldera andesitic volcanism.

The area east of the Los Potreros caldera was gently domed after emplacement of the Zaragoza Tuff, causing postcaldera andesites erupted east of the caldera to flow radially away from the it. It is perhaps due to doming that the Zaragoza Ignimbrite dips 12° east at locality J (Figure 2), although we cannot rule out that tilting resulted from later uplift of the southeastern quadrant of the caldera, described below. Evidence for doming west of the caldera is lacking. In contrast with resurgent calderas (Smith and Bailey, 1968), doming was not confined to the floor of the Los Potreros caldera but affected a broad region centered on

the eastern portion of the caldera (cf. Steven and Lipman, 1976; Mahood, 1980). Although several mechanisms may have contributed to postcollapse doming at Los Potreros, the continued rise of magma explains best the doming of a broad portion of the volcanic center rather than solely of the caldera floor.

Andesite and Basaltic Andesite Volcanism

Volcanic activity that followed collapse of the Los Potreros caldera and doming of a portion of the volcanic center can be divided into three stages: andesite and basaltic andesite volcanism, dominantly rhyodacitic volcanism, and basaltic volcanism. The dominant volume of each compositional type was erupted in the order listed, although there is some overlap between the first two stages.

An arc of andesite and basaltic andesite scoria cones developed along the inferred southern ring-fracture zone of the Los Humeros caldera (N in Figures 2 and 3d) after the emplacement of the Zaragoza Tuff. Approximately 50 cones can still be recognized, and a similar number lack good topographic expression, having been degraded by erosion or breached by lava flows. These cones fed ~4 km^3 of lavas that flowed south of the LHVC. One of these flows has been dated at 0.04 $\pm$ 0.03 Ma (Table 2).

Some of the southern arc lavas are compound flows consisting of several flow units (Nichols, 1936) stacked one over the other. The flow units were formed by block lava in which channelization is indicated by the presence of levees.

The average thickness of each flow unit is 10 m, and their aspect ratios (height/width between levees) range from 0.01 to 0.02. The Tepeyahualco and Limón flows (O and P, respectively, in Figures 2 and 3d) are compound flows with respective volumes of 1.25 and 0.65 km^3. They are vertically zoned in a general way in both composition and phenocryst content. Silica ranges from 56.1 to 59.5% from bottom to top in the Tepeyahualco flow, whereas in the Limón flow it ranges from 52.9 to 55.6%. Phenocryst contents increase from 2-3% by volume in the lowermost units of the Tepeyahualco flow to 15% in the uppermost units. Similarly, phenocrysts increase from 5 to 20% upward in the compound Limón flow. The least mafic portions of the Tepeyahualco compound flow resemble the andesitic portion of the Zaragoza Ignimbrite in composition and phenocryst mineralogy (plagioclase >> clinopyroxene ± orthopyroxene ± olivine).

The cause of the zoning within these compound flows has not been established. Several explanations can be proposed, but none seems entirely satisfactory. (1) Progressive fractional crystallization of basaltic magma as it rises could produce the observed zoning, but seems unlikely given the short time involved in emplacement of the compound flows. (2) A similar pattern of increasing silica content with time was observed at Paricutín and was attributed to progressive contamination of basaltic andesite magma by felsic volcanic and plutonic rocks, coupled with fractional crystallization (Wilcox, 1954). The lavas at LHVC, however, do not contain macroscopic xenoliths, and microprobe work

has shown no obvious xenocrysts. (3) Draining of the andesitic portion of the chamber from below could produce the observed zonation in a single compound flow but, given the small volumes involved, would require very strong gradients in phenocryst content and magma composition. An additional problem is that a stratified chamber would have had to contain reversals in phenocryst content, given the fact that the Limón and Tepeyahualco flows are zoned similarly with respect to phenocryst content despite silica ranges that do not overlap. (4) The position of the vents at the periphery of the LHVC allows the possibility that mafic magmas arriving from depth "knicked" the edge of the Los Humeros magma chamber and progressively mixed with andesitic magmas in the chamber as eruption proceeded.

Interbedded with the scoria of some of the older, deeply eroded cones is the Xoxoctic Tuff, a dacitic air-fall tuff (Table 4) that serves as an important marker horizon for this portion of the center's history. It is conspicuous by virtue of the light olive green color of its fresh pumice and the presence of 1-2 mm yellow-tinged euhedral olivine, which may be xenocrystic in origin. The tuff attains a maximum thickness of 2.8 m in the center of the Los Potreros caldera. It drapes the eastern and western scarps of the Los Potreros caldera and the Cueva Ahumada lavas and underlies some of the southern arc scoria cones and all the lavas they fed.

The andesitic lavas from the small Orilla del Monte and Chiapa shields, (Q and R in Figures 2 and 3d) overlie the Xoxoctic Tuff. Lavas from these shields flowed radially away from the uplifted region near the Los Potreros caldera. The total volume of magma erupted from the two volcanoes was only ~2 km^3. The ages of the Orilla del Monte and Chiapa shields are poorly constrained; single samples from each shield yielded K-Ar dates of 0.02 $\pm$ 0.03 and 0.03 $\pm$ 0.02 Ma, respectively. The phenocryst assemblage of the lavas of these shields is similar to that of the southern andesite flows. The Orilla del Monte flows contain 10-30% phenocrysts by volume, whereas the Chiapa flows contain 3-25%. Unlike the southern lavas, neither of these sequences shows a consistent trend with time in phenocryst content. Silica contents in the Chiapa shield lavas span the range 58.3-63.1%.

The nature of the structure that controlled the location of the Orilla del Monte and Chiapa shields is poorly defined. Vents are arranged in a crudely arcuate pattern that parallels the rims of the two major calderas. A structural discontinuity here is also suggested by a large gradient in the telluric response at locality T1 (Alvarez, 1978b). We do not know whether this inferred structure is related to collapse of the Los Humeros caldera, to an unrecognized collapse associated, for example, with the Faby Tuff eruption, or to the uplift that followed collapse of the Los Potreros caldera.

Fault scarp f4 (Figure 2) formed during the development of the southern arc of scoria cones. Scoria layers and the Xoxoctic Tuff are cut by the scarp, but some of the younger scoria cones cover it. Lavas from the Orilla del Monte and Chiapa shields were deflected by the scarp before finally overflowing it. The f4 scarp lies close to the inferred margin of the Los Humeros caldera and may represent reactivation of the ring-fracture zone in response to draining of magma that fed the andesite lavas.

Maztaloya Eruptive Center and El Xalapazco Caldera

The small Maztaloya eruptive center (S in Figures 2 and 3d) lies at the northern edge of the broad band of vents where the Los Humeros and Los Potreros ring fractures nearly coincide. Probably during the initial stages of this center, ~0.1 km^3 of andesitic magma was erupted as pyroclastic flows, forming the Llano Ignimbrite. One lobe of the ignimbrite flowed to the south, and is now partially covered by the Limón andesite lava flow, while two other lobes were ponded inside the Los Potreros caldera. The resulting nonwelded to partially welded ignimbrite consists of bombs, scoria blocks, lapilli, and ash, with size distribution parameters (Walker, 1971) $Md\phi$=+0.1 and σ_ϕ=2.5. Afterward, a small volcanic edifice was built by lava flows of sparsely porphyritic basaltic andesite and andesite, and by rhyodacitic agglutinates.

The Llano Ignimbrite, Maztaloya lavas, southern andesite flows, and Orilla del Monte and Chiapa shields are

all overlain by the Cuicuiltic Tuff, a visually striking sequence of interbedded rhyodacitic and andesitic air-fall lapilli tuffs that represent ~0.1 km^3 of magma. Commonly the dark-colored, scoria-dominated, andesitic layers grade vertically into light-colored, pumice-dominated, rhyodacitic layers, or vice versa. Although not abundant, mixed-magma lapilli are ubiquitous. The Cuicuiltic Tuff appears to have vented at the Maztaloya volcano, as the tuff attains a maximum thickness of 5.75 m on its slopes. Within 5 kilometers along its poorly-defined northerly dispersal axis, the sequence thins to 2.8 m. The prominent dark-colored scoria layers decrease in thickness much faster than the rhyodacitic pumice layers. The eruption of the Cuicuiltic Tuff is thought to be responsible for formation of the 1.7 km-diameter El Xalapazco caldera (T in Figure 2) on the summit of the Maztaloya volcano. The volume of the depression is ~0.2 km^3, indicating that again we may have underestimated the volume of the magma represented by the tuff (Table 3).

After eruption of the Cuicuiltic Tuff, the southeast quadrant of the Los Potreros caldera was uplifted. This roughly triangular uplift is bounded by faults f2 and f3, and a segment of f1 (Figure 2), which cut the Cuicuiltic Tuff. The fact that the faults barely propagate beyond the inferred rim of the Los Potreros caldera suggests that uplift is a consequence of magma intrusion along the Los Potreros ring-fracture zone rather than a regional tectonic event.

Dominantly Rhyodacitic Volcanism

Just prior to and following the eruption of the Cuicuiltic Tuff, rhyodacitic and minor andesitic flows erupted near the inferred northern ring-fracture of the Los Potreros caldera; the tuff covers the earliest of these flows but is overlain by most of them. These lavas form the 9 km^3 San Antonio shield volcano (U in Figure 2), which rises 450 m above the floor of the Los Potreros caldera and covers ~55 km^2. The shield is a collection of vents, each having erupted one or two flows averaging 30 m in thickness and 1.5 km in length. In general, volcanic activity began with rhyodacite lavas and concluded in the northern and eastern portions of the San Antonio volcano with eruption of andesite (e.g., V in Figure 2).

Smaller centers elsewhere in the system vented one or two stubby rhyodacite lava flows that overlie the Cuicuiltic Tuff. The small La Viola volcano (W in Figure 2) and Cuamilacas flow (X) are located in the area between the eastern rims of the two major calderas. One of the flows from the Arenas center (Y in Figure 2) in the southern band of vents is K-Ar dated at 0.02 + 0.01 Ma. Approximately 1 km^3 of magma is represented by the rhyodacite flows of centers other than the San Antonio volcano.

The lavas of the San Antonio volcano (Table 4) and the other eruptive centers that developed at this stage have sparse phenocrysts of plagioclase, orthopyroxene, and clinopyroxene in a glassy to pilotaxitic groundmass. Some contain abundant inclusions of andesite, basalt, vesicular

silicic glass, and silicified limestone, suggesting that the magmas may have interacted extensively with their wall rocks.

Basaltic volcanism

Small-volume eruptions of olivine basalt (Table 4) represent the youngest volcanic activity throughout the system. Lavas erupted on the floors of both the Los Potreros and El Xalapazco calderas, and a lava vented from the ring-fracture zone of the Los Humeros caldera spread onto the surrounding plain (Figure 2). The total volume of magma erupted at this stage was ~0.25 km^3. All three flows lack the thin veneer of pumiceous air-fall tuff that commonly covers the rhyodacitic flows of the San Antonio and Arenas volcanoes. We have not, however, successfully dated these basalts and can only state that they are younger than 0.02 Ma, the age of the youngest Arenas rhyodacite flow (Table 2). With Mg numbers of ~66 and olivine phenocrysts of Fo_{84}, these lavas represent the most primitive magmas erupted at LHVC.

DISCUSSION AND CONCLUSIONS

Silicic volcanism at the LHVC was preceeded by several million years of andesitic and basaltic volcanism. There is no evidence, however for a systematic evolution toward the high-silica rhyolite compositions that began the Los Humeros volcanic cycle ~0.47 m.y ago. These initial lavas are some of the most evolved compositions erupted at LHVC, and, since

then, there has been an overall trend toward eruption of increasingly mafic compositions (Figure 7).

Eruption of the 115 km^3 of magma represented by the Xâltipan Ignimbrite probably removed most of the rhyolitic magma (77-72% SiO_2) of the chamber, in the course of sampling down to andesitic levels (Figure 7). The post-Xâltipan, biotite-rhyolite, ring-fracture domes closely resemble in composition the first-erupted Xâltipan Ignimbrite and may represent residual rhyolitic magma from the Xâltipan event. Succeeding ring-fracture lavas are aphyric or hypersthene-bearing, slightly less silicic high-silica rhyolites. Approximately 200,000 yr later, a second major pyroclastic eruption produced the Faby Tuff, the dominant composition of which (73-69% SiO_2) overlaps part of the range of that of the Xâltipan Ignimbrite (Figure 7). After another 150,000 yr, the Zaragoza eruption tapped rhyodacitic to andesitic magma (71-54% SiO_2), which again slightly overlaps the compositional range of the preceeding eruption (Figure 7). Together, these three pyroclastic sequences represent ~85% of the volume erupted in the last 0.5 Ma.

Despite the dominance of silicic compositions in the eruptive products of the first 350,000 years of the LHVC, there is abundant evidence for subjacent more mafic magmas. All three major pyroclastic units, the Xâltipan, Faby, and Zaragoza Tuffs, contain small amounts of andesite. After Zaragoza-related collapse, small volumes of basaltic andesite and andesite erupted within the Los Potreros

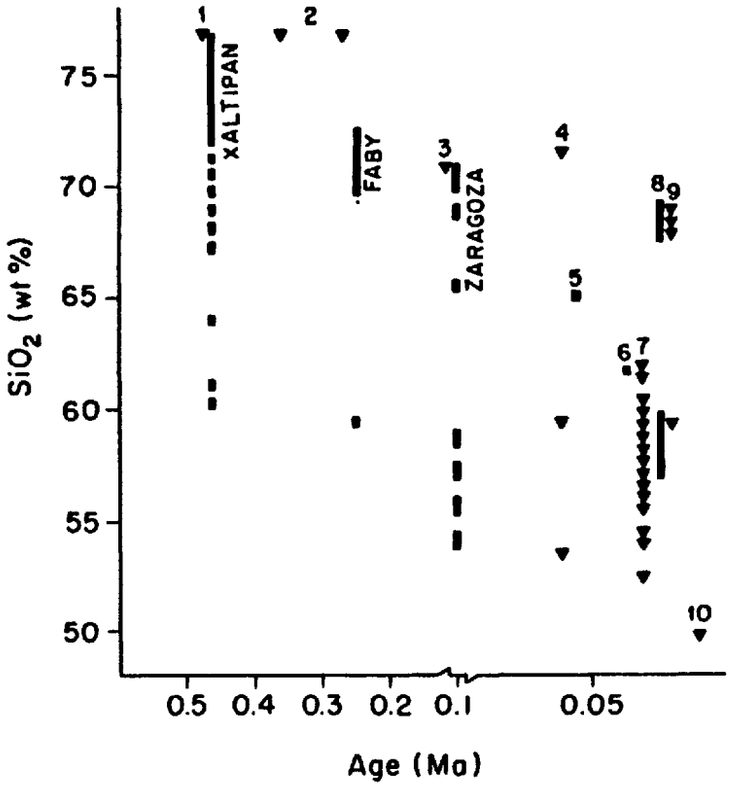

Fig. 7. SiO_2 ranges (recalculated anhydrous) versus age of major eruptive units of the LHVC. Bars indicate pyroclastic units, the continuous portion representing the predominant volume; triangles indicate lavas. 1, pre-Xáltipan rhyolites; 2, post-Xáltipan rhyolites; 3, pre-Zaragoza rhyodacite; 4, Cueva Ahumada lavas; 5, Xoxoctic Tuff; 6, Llano Ignimbrite; 7, andesites and basaltic andesites; 8, Cuicuiltic Tuff; 9, rhyodacites and minor andesites; 10, olivine basalts.

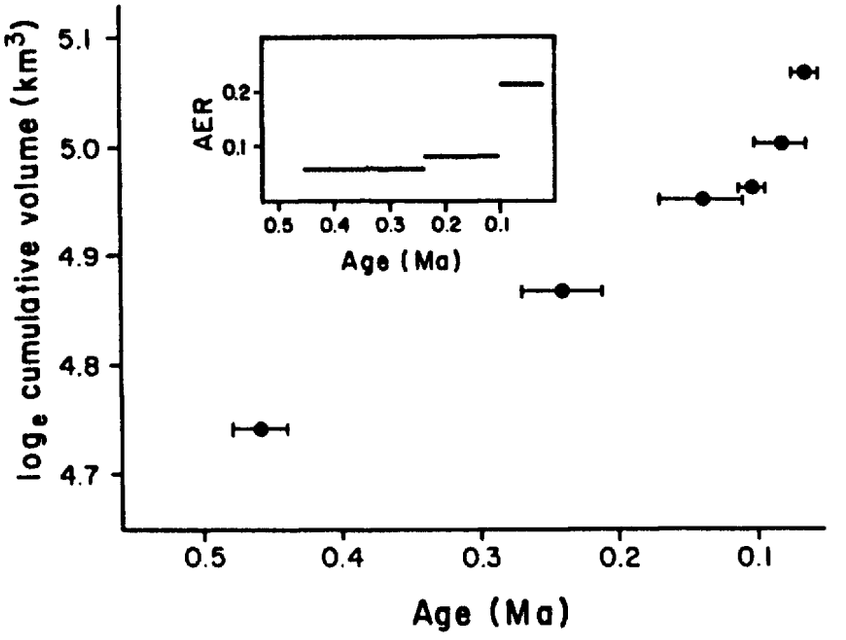

Fig. 8. Cumulative erupted magma volume versus age. Inset shows calculated average eruptive rate (AER), in cubic kilometers per thousand years, versus age. The total mass loss represented by post-Teziutlán eruptions is estimated at $\sim 3.5 \times 10^{+14}$ kg.

caldera at Cueva Ahumada. Xenocrysts of Mg-rich clinopyroxene and olivine are sparse but ubiquitous in mineral separates of rhyodacitic and dacitic lavas and pyroclastic units. These facts indicate that andesite and basalt were always present within magma reservoirs at levels only slightly deeper than those normally tapped by eruptions. "Coning" (Craft and Hawkins, 1959) of the less viscous andesitic magma toward the vent may account for the small volumes of andesite in dominantly rhyodacitic eruptions.

Just prior to eruption of the Xâltipan Tuff, high silica rhyolite magma underlay at least 260 km^2 , the area of the Los Humeros caldera. High-silica rhyolites have not erupted from this area in the last 0.25 Ma, and by ~0.03 Ma ago, the time of eruption of the Chiapa and Orilla del Monte lavas, the zone of silicic magma had contracted sufficiently to allow andesites to erupt within the Los Humeros caldera. Until the most recent activity, these mafic magmas did not erupt within a 90-km^2 area outlined crudely by the vents of the San Antonio volcano, the Orilla del Monte and Chiapa shields, and the northern margin of the band of southern vents. This area may coincide with that uplifted in post-Zaragoza, pre-Chiapa time. It does not correlate well with the positions of the ring fractures of the Los Humeros and Los Potreros calderas. For example, although some vents for the San Antonio volcano lie along the northern ring fracture of the Los Potreros caldera, others lie well away from the ring-fracture zone, both inside and outside the caldera.

These relationships may indicate that magma tapped in forming the San Antonio volcano and other centers from this period is derived from a reorganized post-Zaragoza chamber augmented by new additions of magma, whose rise may have been related to the post-Zaragoza, pre-Chiapa doming. If this magma body was zoned from rhyodacite through basaltic andesite, the composition of magma tapped by vents on the periphery of the uplifted area may have been a function of the depth at which conduits intersected the magma body and the depth at which compositional interfaces lay at the time of tapping. The latter fluctuated; removal of magma by eruptions caused compositional interfaces to move upward, whereas differentiation moved them downward.

The youngest activity in the LHVC indicates further reduction in silicic magma within a high-level reservoir. The olivine basalt lavas that erupted from the southern band of vents and within the Los Potreros and El Xalapazco calderas may represent denser, more mafic, lower portions of a zoned magma chamber that earlier had erupted andesites. Alternatively, these lavas may represent a new influx of mantle-derived mafic magma into the system. If so, their eruption implies that the magma chamber was no longer capable of acting as a density barrier (Eichelberger and Gooley, 1977; Smith, 1979). In other words, below the southern and central portions of LHVC there was no longer a considerable volume of low-density magma that would hinder the rise of dense mafic magma through it. Either low-

density magma was depleted during post-Zaragoza volcanism or it had crystallized to such a degree that it could sustain brittle fracture at the time of basaltic magma intrusion. Eruption of these relatively primitive olivine basalts indicates that the flux of mantle-derived mafic magmas through the crust continues.

We attribute the general trend toward more mafic compositions following eruption of the Xáltipan Tuff to an increasing extrusion rate that exceeded the rate of regeneration of differentiated magma (Figure 8). The rate of extrusion at LHVC increased with time, from an average of 0.06 km^3 per thousand years 0.25 Ma ago to 0.21 km^3 per thousand years during the last 0.1 Ma. We ascribe the increase in eruptive rate to a progressive decrease in the structural integrity of the roof zone of the chamber as successive caldera-forming eruptions reactivated old zones of weakness and created new ones. The lack of Quaternary faulting (Yáñez and Casique, 1980; Ferriz and Yáñez, 1981) suggests that the increased extrusion rate is not a consequence of changes in the regional strain regime of the lithosphere.

The rate of regeneration of differentiated magma is difficult to estimate, as it is a complex function of the rate of differentiation, which in turn depends on the rate of mass and energy input into the chamber and on the rate of hydrothermal convective cooling. As a minimum condition for a steady state, the rate of mass input would need to be similar to the extrusion rate. Although the rate of mass

input cannot be directly assessed, its minimum magnitude can be estimated by the rate of eruption of the late olivine basalts and of cinder cones in a nearby field. Assuming that the olivine basalts were erupted during the last 20,000 years the minimum rate of mass input can be estimated at ~0.012 km^3 per thousand years. Post-Zaragoza cinder cones surrounding the Pizarro dome (AA in Figure 2) have an average volume of 0.1 km^3 and maximum cinder cone density of 0.05 cones km^2. Given the 260-km^2 area of the Los Humeros caldera, the minimum rate of mass input estimated on this basis is 0.01 km^3 per thousand years. The same figure calculated using the data of Settle (1979) for the Paricutin field (Figure 1), yields a rate of 0.009 km^3 per thousand years. In contrast, the average eruptive rate for all magma types combined in the LHVC for the last 0.1 Ma is 0.21 km^3 per thousand years. From these figures it can be seen that unless the volume of mafic magma intruded exceeded by a factor of 20 the volume of cinder cones in the surrounding region, the magmatic system has lost mass faster than it has gained it since the eruption of the Zaragoza Tuff. Although similar calculations cannot be made for periods prior to eruption of the Zaragoza Tuff, the eruption of increasingly mafic compositions on average suggests that this condition existed for at least 0.25 Ma.

ACKNOWLEDGEMENTS

Acknowledgement is made to Mexico's Comisiòn Federal de Electricidad and Consejo Nacional de Ciencia y Tecnologìa, and to the Donors of the Petroleum Research Fund, administered by the American Chemical Society, for support of this research. We are grateful for chemical analyses provided by the Analytical Laboratories Branch of the U.S. Geological Survey. The cooperation of C. Yàñez and C. Garcìa, Comisiòn Federal de Electricidad, greatly aided the early stages of this study. Thanks are due to E. Kollman, U.S. Geological Survey Geochronological Laboratory, and J. Metz, Stanford University, for mass spectrometric measurements. D. Boden, A. Grunder, W. Hildreth, J. Luhr, and R. Wilcox provided helpful reviews of the manuscript.

REFERENCES

Alvarez,R. (Editor), 1978a, Los Humeros Caldera Special Issue: Geofis. Internacional, v.17, p.407-478.

Alvarez,R., 1978b, Telluric, self potential and surface temperature profiles on Los Humeros caldera: Geofis. Internacional, v.17, p.445-460.

Alvarez,R., 1980, Outlining tectonism and faulting with tellurics in Los Humeros-Derrumbadas geothermal area: Transactions of the Geothermal Resources Council, v.4, p.1-4.

Bailey,R.A., Dalrymple,G.B., Lanphere,M.A., 1976, Volcanism, structure, and geochronology of Long Valley caldera, Mono County, California: J. Geophys. Res., v.81, p.725-744.

Christiansen,R.L., Blank,H.R., 1972, Volcanic stratigraphy of the Quaternary rhyolite plateau in Yellowstone National Park: U.S. Geol. Surv. Prof. Pap. 729-B, 18p.

Craft,B.C., Hawkins,H.F., 1959, Applied Reservoir Engineering: Prentice-Hall, Englewood Cliffs, N.J., 437p.

Eichelberger,J.C., Gooley,R., 1977, Evolution of silicic magma chambers and their relationship to basaltic volcanism: in The Earth's Crust, Geophys. Monogr. Ser., v.20, edited by J.G. Heacock, p.57-77, AGU, Washington, D.C.

Ferriz,H., 1982, Geologic and preliminary reservoir data on the Los Humeros geothermal system, Puebla, Mexico: in Proceedings Eighth Workshop Geothermal Reservoir Engineering (SGP-TR-60), p.19-24, Stanford University, Stanford, California.

Ferriz,H., and Yáñez,C., 1981, Mapa geológico del centro volcánico de Los Humeros, estados de Puebla y Veracruz, México - Edición preliminar, (Map), Comisión Federal de Electricidad, Juan de la Barrera #37, Cd. Satelite, Edo. de Mexico, 53100, MEXICO.

Gibson,I.L., 1974, A review of the geology, petrology, and geochemistry of the volcano Fantale: Bull. Volcanol., v.38, p.791-802.

Hildreth,W., 1983, The compositionally zoned eruption of 1912 in the Valley of Ten Thousand Smokes, Katmai National Park, Alaska: J. Volcanol. Geotherm. Res., v.18, p.1-56.

Macleod,N.S., Sammel,E.A., 1982, Newberry volcano, Oregon, a Cascade Range geothermal prospect: Calif. Geol., v.35, p.235-244.

Mahood,G.A., 1980, Geological evolution of a Pleistocene rhyolitic center - Sierra La Primavera, Jalisco, Mexico: J. Volcanol. Geotherm. Res., v.8, p.199-230.

Mahood,G.A., Drake,R.A., 1982, K-Ar dating young volcanic rocks: A case study of the Sierra La Primavera, Jalisco, Mexico: Geol. Soc. Am. Bull., v.93, p.1232-1241.

Nichols,R.L., 1936, Flow units in basalts: J. Geol., v.44, p.617-630

Palacios,L.H., García,H., 1981, Informe geofísico del proyecto geotérmico Los Humeros-Derrumbadas, estados de Puebla y Veracruz: Comisión Federal de Electricidad, Mexico, 99p.

Pérez,J., 1978, Geología y petrografía de la caldera de Los Humeros: Geomimet (Mexico), v.91, p.97-106.

Sack,R.C., Carmichael,I.S.E., Rivers,M.L., Ghiorso,M.S., 1980, Ferric-ferrous equilibrium in natural silicate liquids at 1 bar: Contrib. Mineral. Petrol., v.75, p.369-376.

Settle,M., 1979, The structure and emplacement of cinder cone fields: Am. J. Sci., v.279, p.1089-1107.

Smith,R.L., 1979, Ash-flow magmatism: in Ash-flow Tuffs, edited by C.E. Chapin and W.E. Elston, Geol. Soc. Am. Spec. Pap. 180, p.5-27.

Smith,R.L., Bailey,R.A., 1968, Resurgent Cauldrons: in Studies in Volcanology: A Memoir in Honor of Howell Williams, edited by R.R. Coats, R.L. Hay, and C.A. Anderson: Geol. Soc. Am. Mem. 116, p.613-662.

Sparks,R.S.J., Walker,G.P.L., 1977, The significance of vitric-enriched air-fall ashes associated with crystal-enriched ignimbrites: J. Volcanol. Geotherm. Res., v.2, p.329-341.

Sparks,R.S.J., Wilson,L., 1976, A model for the formation of ignimbrite by gravitational column collapse: J. Geol. Soc. London, v.132, p.441-451.

Sparks,R.S.J., Self,S., Walker,G.P.L., 1973, Products of ignimbrite eruptions: Geology, v.1, v.115-118.

Sparks,R.S.J., Sigurdsson,H., Wilson,L., 1977, Magma mixing: A mechanism for triggering acid explosive eruptions: Nature, v.267, p.315-318.

Spencer,K.J., Lindsley,D.H., 1981, A solution model for coexisting iron-titanium oxides: Amer. Mineralogist, v.66, p.1189-1201.

Steven,T.A., Lipman,P.W., 1976, Calderas of the San Juan volcanic field, southwestern Colorado: U.S. Geol. Surv. Prof. Pap. 958, 35p.

Verma,S.P., 1983, Magma genesis and chamber processes at Los Humeros caldera, Mexico - Nd and Sr isotope data: Nature, v.302, p.52-55.

Verma,S.P., López,M., 1982, Geochemistry of Los Humeros caldera, Puebla, Mexico: Bull. Volcanol., v.45, p.63-79.

Viniegra,F., 1965, Geología del Macizo de Teziutlán y la Cuenca Cenozoica de Veracruz: Bol. Asoc. Mexicana Geol. Petr., v.17, p.101-163.

Walker,G.P.L., 1971, Grain size characteristics of pyroclastic deposits: J. Geol., v.79, p.696-714.

Walker,G.P.L., 1980, The Taupo pumice: product of the most powerful known (ultraplinian) eruption?: J. Volcanol. Geotherm. Res., v.8, p.69-94.

Westerveld,J., 1952, Quaternary volcanism on Sumatra: Geol. Soc. Am. Bull., v.63, p.561-594.

Wilcox,R.E., 1954, Petrology of Paricutín volcano, Mexico: U.S. Geol. Surv. Bull. 965C, p.281-349.

Yáñez,C., Casique,J., 1980, Informe geológico del proyecto geotérmico Los Humeros-Derrumbadas, estados de Puebla y Veracruz, Comisión Federal de Electricidad, Mexico, 59p.

Yáñez,C., García,S., 1982, Exploración de la región geotérmica Los Humeros-Las Derrumbadas, estados de Puebla y Veracruz: Comisión Federal de Electricidad, Mexico, Ediciones del Sector Eléctrico, 29, 98p.

Ferriz,H., in press, Zoneamiento composicional y mineralógico
en los productos eruptivos del centro volcánico de Los Humeros,
Puebla, México: Geofísica Internacional.

CHAPTER TWO

COMPOSITIONAL AND MINERALOGIC ZONING IN THE ERUPTIVE PRODUCTS OF THE LOS HUMEROS VOLCANIC CENTER, PUEBLA, MEXICO

ABSTRACT

The Los Humeros volcanic center, located 180 km east of Mexico City, is one of several silicic volcanic centers located in the "back-arc" portion of the Mexican Neovolcanic Belt. Eruptive products span the compositional range high-silica rhyolite to basalt. During the last 460,000 years, three major plinian eruptions and two major episodes of lava flow emplacement periodically "sampled" the magma chamber. The eruptive products of these events are compositionally zoned and indicate that the magma chamber was zoned from rhyolitic uppermost levels to andesitic or perhaps basaltic lower levels. Strong compositional zonation persisted throughout the lifetime of the system.

In general, the most silicic products of each plinian eruption are either aphyric or are characterized by the lowest phenocryst contents and simplest phenocryst assemblages (plagioclase, Fe-Ti oxides, and biotite or orthopyroxene). Clinopyroxene and olivine make their appearance in progressively more mafic products of each eruption. Ca/Na ratios of plagioclase and Mg/Fe ratios of the mafic phenocrysts increase as the eruptive products become more mafic. Phenocryst content increases progressively, reaches a maximum in rhyodacitic and andesitic compositions, and then decreases in basaltic andesite compositions. Changes in phenocryst assemblages and abundances are probably a consequence of superimposed gradients in composition, temperature, and volatile content in the magma chamber. Temperatures calculated from Fe-Ti-

oxide geothermometry range from 800° to 875° C for the uppermost rhyolitic levels of the chamber, 860° to 940° C for the rhyodacitic portions, and 920° to 1000° C for the andesitic portions.

INTRODUCTION

Compositional variations have been documented in individual eruptive units of several continental, island-arc, and oceanic volcanic centers (e.g., Smith, 1979, fig.10; Hildreth, 1981, fig.1), and for some centers may be the rule rather than the exception. In most cases, major-element compositional variations are accompanied by variations in trace element concentrations, phenocryst contents, modal mineralogy, mineral chemistry, and, in some instances, in isotopic ratios (Hildreth,1981). The objective of this paper is to document the variation in the chemical composition of the phenocryst minerals of the eruptive products of the Los Humeros volcanic center, Puebla, Mexico (Ferriz and Mahood, 1984), as a function of the bulk composition of the host magma. The compositions of eruptive products of this volcanic center range from high-silica rhyolite to olivine basalt. Thus, this center illustrates particularly well the ranges of composition of some of the common rock-forming minerals in a calc-alkalic suite (Figure 1).

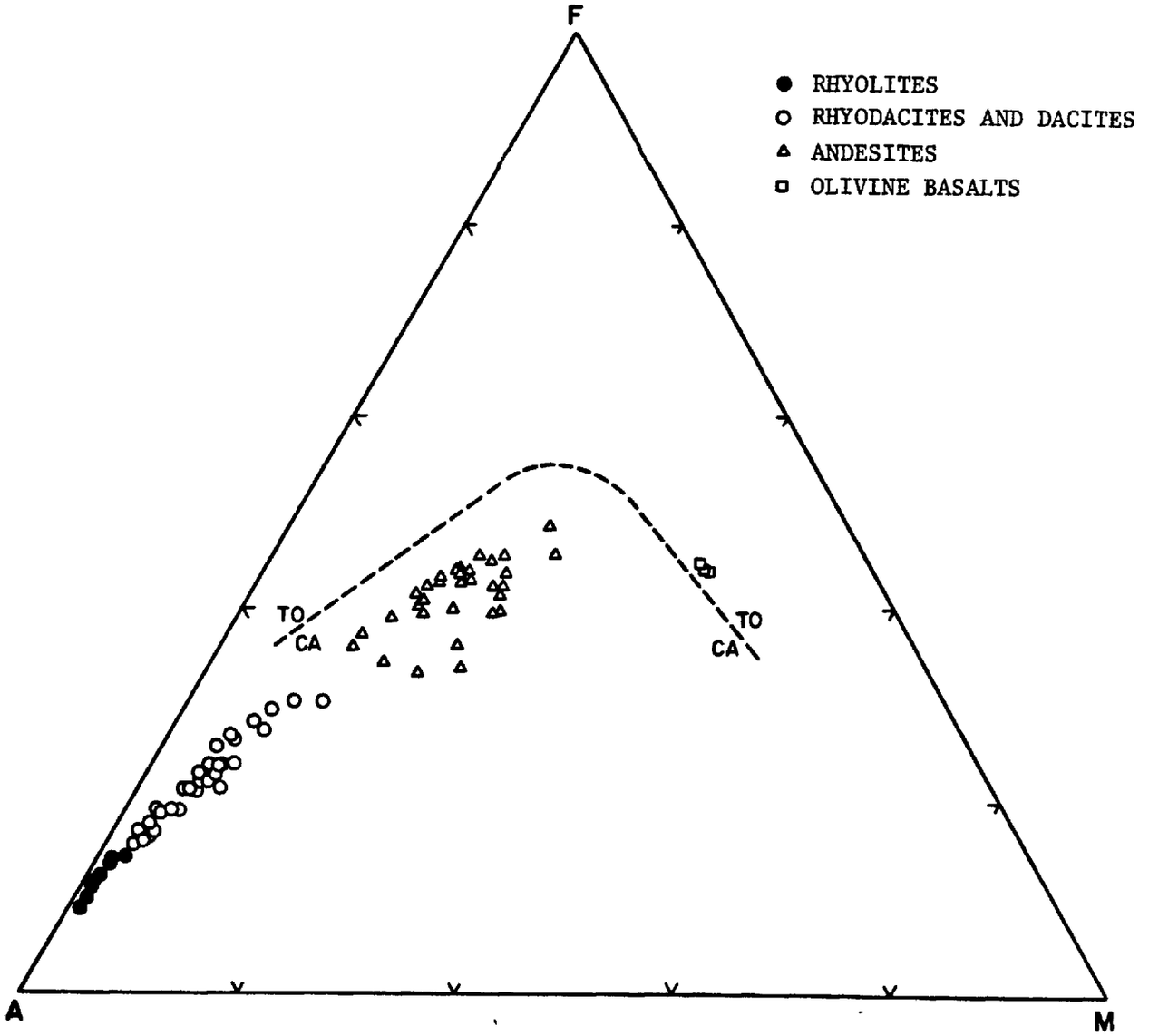

Fig. 1. AFM diagram showing data from samples of the Los Humeros volcanic center, and the boundary between calc-alkalic (CA) and tholeiitic (TO) fields based in in the criteria of Irvine and Barager (1971).

SUMMARY OF THE GEOLOGIC HISTORY

The geologic history of the Los Humeros volcanic center has been presented in Ferriz and Mahood (1984). The short summary given here provides the names of the different eruptive units, their bulk compositions, volumes, and ages. A simplified geologic map is presented in Figure 2.

The volcanic center, located 180 km east of Mexico City, is one of several Pleistocene silicic centers in the "back-arc" portion of the Mexican Neovolcanic Belt. Silicic volcanism began ~0.47 Ma ago with extrusion of high-silica rhyolite domes (A and B in Figure 2). Shortly thereafter, at 0.46 Ma ago, 115 km^3 of magma zoned from high-silica rhyolite to andesite were erupted, resulting in formation of the Xáltipan Ignimbrite and related small-volume pumice fall tuffs, and in collapse of the 21-by-15-km Los Humeros caldera. High-silica rhyolite domes then erupted, largely along the northwestern ring-fracture zone of the caldera (C, D, E, F, G, and H in Figure 2). They are covered by the 0.24- Ma Faby Tuff, a dominantly rhyodacitic sequence of plinian fall deposits that represent ~10 km^3 of magma. A second major caldera-forming event occurred ~0.1 Ma ago with eruption of the Zaragoza Tuff, a nonwelded ignimbrite zoned from rhyodacite to andesite. Eruption of these 12 km^3 of magma led to collapse of the 10-km-diameter Los Potreros caldera, which is nested within the older Los Humeros caldera. The small-volume dacitic Xoxoctic Tuff, erupted shortly thereafter, drapes the walls of the Los Poteros caldera. Between 0.08 and 0.06 Ma ago, an arc of andesitic

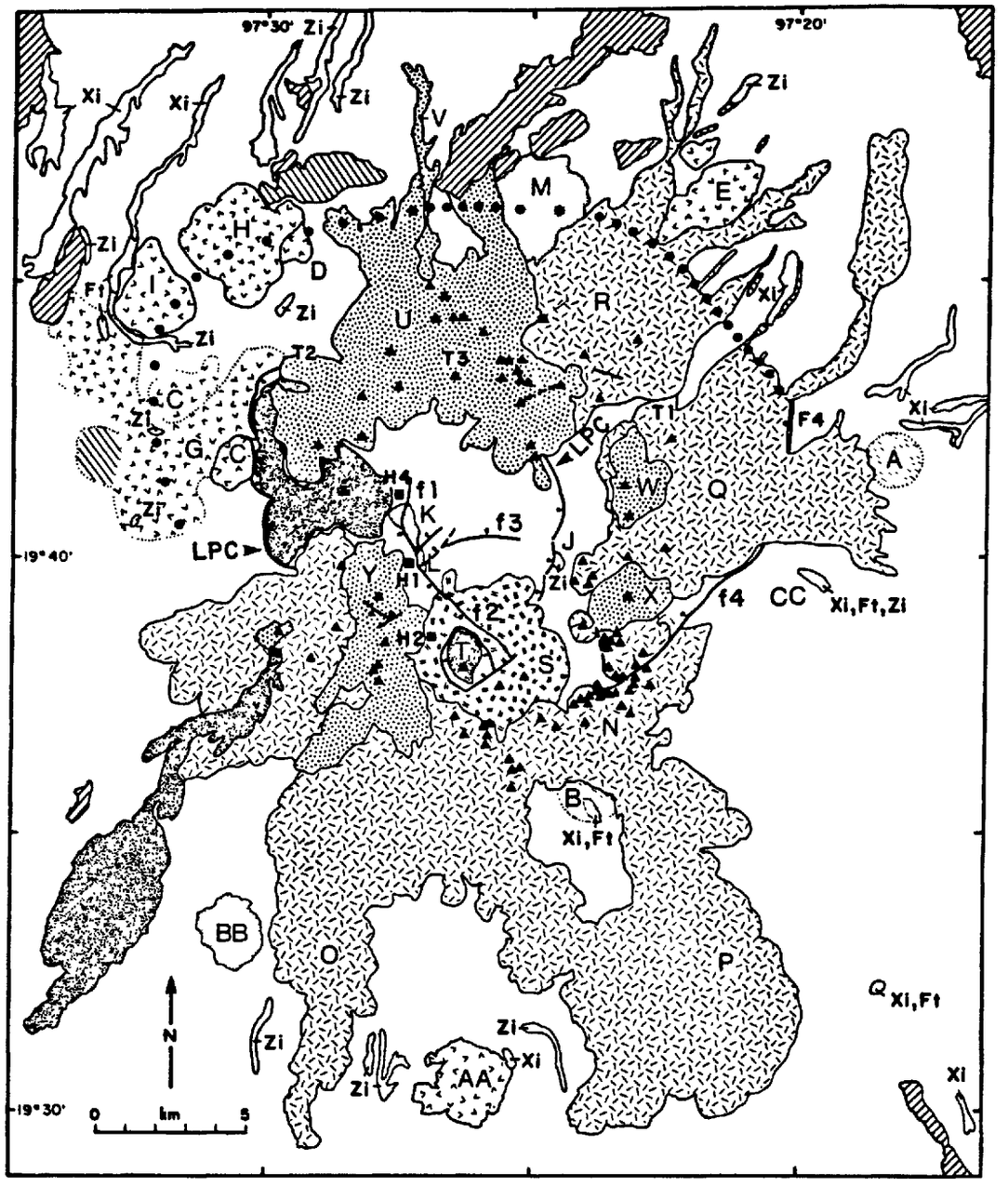

Fig. 2. Simplified geologic map of the Los Humeros volcanic center (based on *Ferriz and Yañez* [1981]). Heavy dots indicate the inferred northern topographic and structural boundary of the Los Humeros caldera. LPC indicates the eastern and western boundary faults of the Los Potreros caldera. Dotted contacts indicate largely buried units. Light stipple indicates the post-Zaragoza but pre-Xoxoctic, Las Aguilas rhyolite dome (BB) and Cueva Ahumada basaltic andesite, andesite (K), and rhyodacite lavas (L), and the Las Lineas rhyodacite dome (M). Random dashes indicate the Tepeyahualco (O), Limón (P), Orilla del Monte (Q), and Chiapa (R) andesite and basaltic andesite lavas and cinder cones. Double dashes indicate the Maztaloya (S) basaltic andesite, andesite and rhyodacite lavas and agglutinates. The heavy dot pattern indicates the San Antonio (U), Viola (W), Cuamilacas (X), and Arenas (Y) rhyodacitic lavas and tuff cones and the Papata (V) andesite flow. Unpatterned areas are outcrops of the Xáltipan Ignimbrite (Xi), Faby Tuff (Ft), and Zaragoza Ignimbrite (Zi), or alluvium and soil underlain by pyroclastic deposits of various types. Most of the area shown outside the Los Humeros caldera is underlain by the Xáltipan and Zaragoza Ignimbrites; on the east side of the map area the Faby Tuff is present as well. Within and slightly east of the Los Potreros caldera, most areas are underlain by the Xoxoctic and Cuicuiltic tuffs. T1, T2, and T3 indicate locations of telluric anomalies [*Alvarez*, 1978*b*, 1980]. Fault scarps are labeled f1 to f4. See text for other lettered units.

scoria cones, concentrated along the southern ring-fracture zone of the Los Humeros caldera, fed the Tepeyahualco (I in Figure 2), Sarabia, and Limón (J in Figure 2) compound flows that extend south of volcanic center, and andesite lavas built the small Chiapa (K in Figure 2) and Orilla del Monte (L in Figure 2) shields between the eastern rims of the two calderas. Approximately 6 km3 of andesitic magma were extruded during this stage. Simultaneous venting of the rhyodacitic and andesitic tephra of the Cuicuiltic Tuff from a small volcano in the southern ring-fracture zone of the Los Potreros caldera led to formation of the 1.7-km-diameter El Xalapazco caldera (M in Figure 2). Minor fault-bounded uplift of the southeastern quadrant of the Los Potreros caldera followed. Activity continued up to 0.04 Ma ago with eruption of 10 km3 of rhyodacitic and minor andesitic lava flows from centers near the northern margin of the Los Potreros caldera (San Antonio lavas; N in Figure 2) in the area between the eastern rims of the two calderas and within a broad band where the southern segments of the inferred Los Humeros and Los Potreros ring-fracture zones nearly coincide (Arenas lavas; O in Figure 2). The latest stage of volcanic activity is represented by the eruption of ~0.25 km^3 of olivine basalt lavas, sometime during the last 0.04 Ma, along the southern ring-fracture zone of the Los Humeros caldera and on the floors of the Los Potreros and El Xalapazco calderas. These basalts are interpreted as a new influx of mantle-derived magma into the system.

The Xáltipan, Faby, and Zaragoza Tuffs were each emplaced within periods probably ranging from hours to a few weeks, and the Tepeyahualco and Limon compound flows (Nichols,1936) were each emplaced over periods that probably ranged from weeks to months. Relative to the life span of the system these eruptions are essentially instantaneous events. Changes in chemical composition and mineralogy within each of these units are inferred to represent the compositional zonation that existed in the magma chamber just prior to their eruption. On the other hand, variations observed in lavas erupted over periods of several thousand years more likely represent variations through time of the evolving magma chamber.

COMPOSITIONAL ZONATION

A comparison of the silica contents (calculated anhydrous) of the eruptive products of each of the major eruptive units of Los Humeros (Figure 3), as well as of all the other major elements (e.g., Figure 4), indicates that the magma chamber was strongly zoned in composition throughout most of its history. Because the densities of magmas decrease as silica content increases, it is reasonable to assume that a compositionally zoned chamber would tend to be density stratified (Smith,1979), with more silicic magmas collecting in the upper portions of the chamber and more mafic, denser magmas collecting in the lower portions.

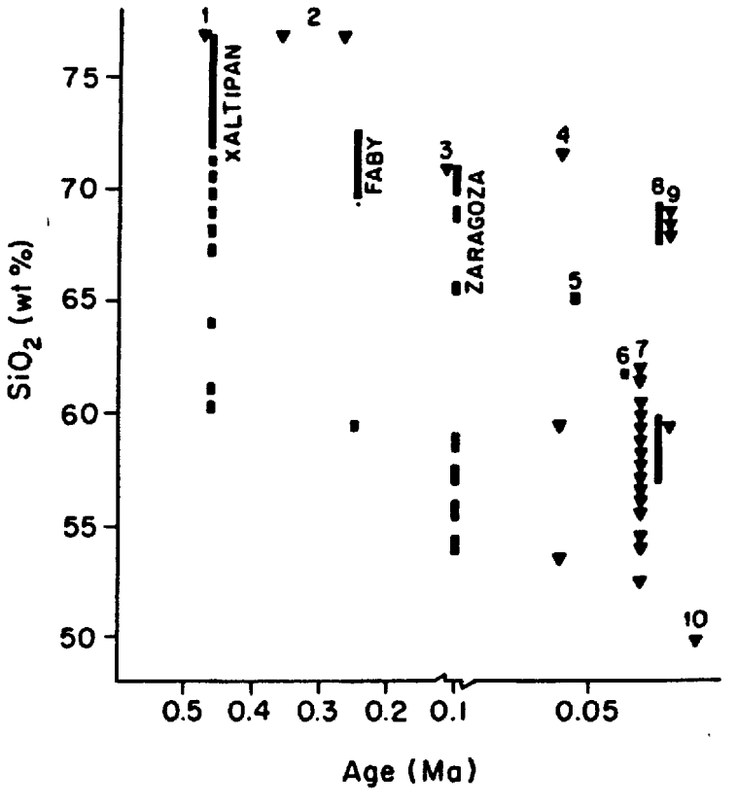

Fig. 3. SiO_2 ranges (recalculated anhydrous) versus age of major eruptive units of the LHVC. Bars indicate pyroclastic units, the continuous portion representing the predominant volume; triangles indicate lavas. 1, pre-Xáltipan rhyolites; 2, post-Xáltipan rhyolites; 3, pre-Zaragoza rhyodacite; 4, Cueva Ahumada lavas; 5, Xoxoctic Tuff; 6, Llano Ignimbrite; 7, andesites and basaltic andesites; 8, Cuicuiltic Tuff; 9, rhyodacites and minor andesites; 10, olivine basalts.

Figure 3 also illustrates a prominent compositional discontinuity between rhyodacitic and andesitic compositions, at 63 to 67 wt% SiO_2, that persisted throughout the lifetime of the system. There are a few samples whose silica content falls within this range, but, as discussed below, they represent a small volume compared to the dominant rhyolitic, rhyodacitic, and andesitic compositions, and their mineralogy suggests that these small volumes are the result of limited mixing between rhyodacitic and andesitic magma. The mechanisms that lead to development of compositional discontinuities remain uncertain, but may include processes such as (1) continuous underplating of a silicic magma chamber by mafic magmas (Eichelberger and Gooley,1977), with mixing between the two magma types being inhibited by large density and viscosity differences, (2) partial remelting of young igneous rocks in the roof of an andesitic chamber (Hildreth,1983), or (3) efficient separation of silicic magma due to marginal crystallization of an andesitic chamber and boundary-layer buoyancy (Shaw,1974; McBirney,1980).

Erupted magmas show an overall trend with time toward more mafic compositions (Figure 3), probably due to the fact that average eruptive rates increased with time and exceeded the rate of regeneration of differentiated magma. Volumetric eruptive rates increased from ~0.06 km^3 per thousand years 0.25 Ma ago to ~0.2 km^3 per thousand years in the last 0.1 Ma (Ferriz and Mahood,1984). The increase in eruptive rate was probably the result of a progressive

decrease in the structural integrity of the roof zone of the system as successive caldera-forming eruptions reactivated old zones of weakness and created new ones. An increasingly disrupted roof allowed mafic and intermediate magmas to reach the surface relatively rapidly, decreasing their residence time in a high-level chamber and thus the time available for their differentiation.

Zonation in major element composition within a magma chamber is often accompanied by large variations in trace element concentrations, as has been convincingly demonstrated by Smith and Bailey (1966), Lipman et al. (1966), Hildreth (1979, 1981), and Mahood (1981a). These variations can be graphically represented by enrichment factor diagrams (Hildreth,1979), such as those shown in Figure 4 for the Xâltipan and Zaragoza Tuffs. These diagrams represent the ratio between the concentration of a given element in the most silicic sample of an individual, compositionally zoned eruption, and its concentration in less silicic products. Assuming that the magma chamber is density stratified, this is equivalent to dividing the concentration of the element in the magma located near the top of the chamber by its concentration in magma from deeper levels tapped. The enrichment factor of elements whose concentration is highest toward the top of the magma chamber will have a value greater than one (i.e. above the base lines of Figure 4), whereas those concentrated toward the bottom will have a value less than one (i.e. below the base

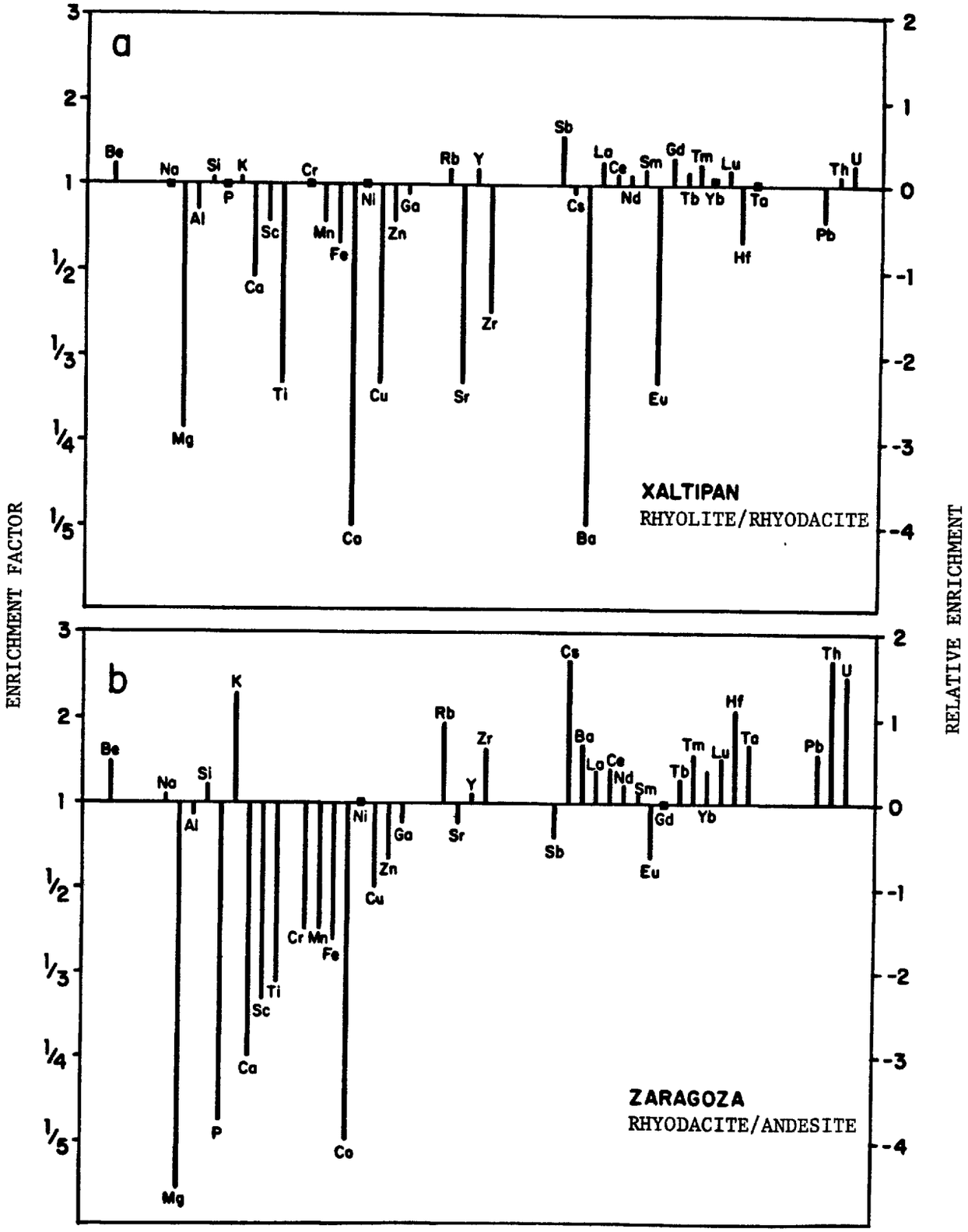

Fig. 4. Enrichment factor diagrams for the (a) Xáltipan and (b) Zaragoza Tuffs.

lines). For example, consider two samples of the same compositionally zoned eruption, one rhyolitic and one rhyodacitic; if the Rb and Sr contents of the rhyolite are 135 and 20 ppm, respectively, and those of the rhyodacite are 115 and 75 ppm, respectively, then it could be stated that Rb was enriched toward the top of the chamber by a factor of 1.17 (i.e. 135/115), whereas Sr was enriched toward the bottom, with an enrichment factor of 0.27 (i.e. 20/75).

From Figure 4a and Table 1 it can be seen that Rb, Y, La, Ce, Nd, Sm, Gd, Tb, Tm, Lu, Th, and U were concentrated toward the roof of the chamber prior to the Xâltipan eruption, whereas Mg, Al, Ca, Sc, Ti, Mn, Fe, Co, Zn, Sr, Zr, Cs, Ba, Eu, and Hf, were concentrated toward deeper levels. Enrichment factors for samples of the Zaragoza Ignimbrite show similar trends (Figure 4b, Table 1), except for Zr, Cs, Ba, Hf, and Ta which were concentrated toward the top of the chamber, and P which was concentrated toward the bottom.

A discussion on the origin of the trace element zonation in the major eruptive units of Los Humeros must be deferred until a broader petrologic discussion is presented (Ferriz and Mahood, in preparation). It is worthwhile pointing out, however, that although crystal fractionation, assimilation, and coalescence of melts derived from different partial melting events could conceptually explain such zoning patterns, the work of Shaw (1974), Hildreth (1979), Smith (1979), and Mahood (1981a) has indicated that

Table 1. Compositions of pumice and scoria of the Xaltipan and Zaragoza Tuffs.

	LH8	LH11	LH8/LH111	LH41	LH45	LH41/LH45	% σ
SiO2 (%)	76.6	71.5	1.07	71.1	59.1	1.20	
TiO2	0.08	0.27	0.30	0.46	1.42	0.32	
Al2O3	12.9	16.7	0.77	14.9	17.2	0.87	
FeO*	1.08	1.84	0.59	2.49	6.63	0.38	
MgO	<0.10	0.31	<0.32	0.52	2.84	0.18	
CaO	0.41	0.86	0.48	1.49	5.95	0.25	
Na2O	2.91	2.98	0.98	4.2	3.85	1.09	
K2O	5.8	5.35	1.08	4.66	2.04	2.28	
P2O5	<0.05	<0.05	1 ?	0.08	0.38	0.21	
Be (ppm)	5	4	1 ?	3.5	2.5	1 ?	12
Sc	2.6	3.5	0.7	5.7	17.9	0.3	5
Cr	<4	<4	1 ?	<2	5	<0.4	1
Mn	230	335	0.7	350	860	0.4	5
Co	0.3	1.5	0.2	2.5	16.3	0.2	3
Ni	3	3	1 ?	7	7	1 ?	35
Cu	1	3	1 ?	4	8	1 ?	40
Zn	26	36	0.7	49	79	0.6	4
Ga	15	16	1 ?	15	18	1 ?	13
Rb	135	110	1.2	115	60	1.9	2
Sr	30	85	0.4	120	415	0.3	3
Y	32	26	1.2	26	25	1 ?	3
Zr	125	240	0.5	310	205	1.5	3
Nb	13	15	1 ?	12	11	1 ?	9
Sb	1.1	0.7	1 ?	0.8	1.1	1 ?	9
Cs	4.3	4.8	0.9	4	1.5	2.7	3
Ba	125	720	0.2	760	460	1.7	2
La	43	34	1.3	38	28	1.4	3
Ce	73	65	1.1	68	49	1.4	5
Nd	29	26	1.1	30	25	1.2	3
Sm	5.5	4.7	1.2	5.9	5.4	1 ?	3
Eu	0.18	0.58	0.3	0.9	1.48	0.6	5
Gd	6.6	5	1.3	5.7	5.9	1 ?	3
Tb	0.83	0.73	1.1	0.86	0.68	1.3	3
Tm	0.51	0.41	1.2	0.48	0.31	1 ?	15
Yb	2.8	2.7	1 ?	2.6	1.9	1.4	5
Lu	0.51	0.44	1.2	0.48	0.32	1.5	2
Hf	4.6	7.8	0.6	8.9	4.3	2.1	3
Ta	1.9	2	1 ?	1.4	0.9	1.6	4
Pb	10	14	1 ?	17	11	1 ?	20
Th	21.6	20	1.1	15.4	5.8	2.7	3
U	5.4	4.4	1.2	3.7	1.5	2.5	2

Major elements, Rb, Sr, Y, Zr and Nb determined by X-ray Fluorescence. Ba, Co, Cr, Cs, Hf, Sb, Ta, Th, U, Zn, Sc, La, Ce, Nd, Sm, Eu, Gd, Tb, Tm, Yb, and Lu determined by Instrumental Neutron Activation Analysis. Be, Mn, Ni, Cu, Ga, and Pb determined by Emission Spectroscopy. Analyses performed by the U.S. Geological Survey except for Rb, Sr, Y, Zr, and Nb (*H. Ferriz*).

% σ is an estimate of the reproducibility based in duplicate analyses. Queries indicate elements for which the validity of enrichment factors is uncertain due to the fact that both values are indistinguishable at the 95% confidence level.

liquid-state differentiation processes such as thermogravitational diffusion, volatile transfer, or gradients in melt structure may, in some cases, be the main mechanisms by which strong trace element zonation develops.

MINERAL ASSEMBLAGES

Nomenclature

Most of the rock-forming minerals can be envisaged as solid solutions of end members that have relatively simple compositions. Giving the molecular proportion of each end member is a convenient and condensed way of expressing the chemical composition of a mineral species. For example, the composition of a plagioclase can be expressed as $Ab_{43}An_{55}Or_2$ indicating that this particular plagioclase can be described as the result of mixing 43 mol% albite, 55 mol% anorthite and 2 mol% orthoclase. This notation can be further simplified to $Ab_{43}An_{55}$, which would imply that the solid solution is formed by 43 mol% albite and 55 mol% anorthite, with the remainder being formed by orthoclase. These conventions will be used throughout this paper. The end members used, and their abbreviations, have been compiled in Table 2 for reference.

The magma types erupted at Los Humeros can be loosely divided into five groups: rhyolites (>72% SiO_2, recalculated anhydrous), rhyodacites (72 to 67% SiO_2), dacites (63 to 67% SiO_2), andesites (63 to 52% SiO_2), and basalts (<52% SiO_2). This division, while convenient for the purposes of discussion, is completely arbitrary. As

Table 2. Nomenclature

			COMPONENTS		
	plagioclase	pl	An	anorthite	$CaAl_2Si_2O_8$
	sanidine	san	Ab	albite	$NaAlSi_3O_8$
			Or	orthoclase	$KAlSi_3O_8$
	quartz	qz			
	clinopyroxene	cpx	Wo	wollastonite	$CaSiO_3$
	orthopyroxene	opx	En	enstatite	$MgSiO_3$
			Fs	ferrosilite	$FeSiO_3$
	olivine	ol	Fo	forsterite	Mg_2SiO_4
			Fa	fayalite	Fe_2SiO_4
	biotite	bio			
	hornblende	hbl			
Fe-Ti oxides (ox)	titanomagnetite	tmt	mt	magnetite	Fe_3O_4
			usp	ulvospinel	Fe_2TiO_4
	ilmenite	ilm	ilm	ilmenite	$FeTiO_3$
			hem	hematite	Fe_2O_3

X^{opx}_{FeSiO3} = molecular proportion of the $FeSiO_3$ component in orthopyroxene.

a^{bio}_{annite} = activity of the annite ($KFe_3AlSi_3O_{10}(OH_2)$) component in biotite.

X^{M1}_{Fe2+} = molecular proportion of Fe 2+ in the M1 octahedral site of orthopyroxene.

X^{y}_{Fe2+} = molecular proportion of Fe 2+ in the y octahedral site of biotite.

$X_{Fe2+,S2+}$ = molar fraction of Fe 2+ with respect to the total number of 2+ cations in titanomagnetite.

$n_{Fe3+,F}$ = total number of Fe 3+ per formula unit in tmt.

shown in Figure 5 rhyolitic, rhyodacitic, and andesitic compositions constitute the bulk of the volume of magma erupted at Los Humeros.

Variations in mineral assemblages

The mineral assemblages of the products of a compositionally zoned eruption show major changes, as shown in Table 3 (see also Hildreth,1981, table 2). These changes include variations in the total phenocryst content (discussed in a later section), variations in the relative proportions of the different phenocryst phases, and appearance or disappearance of some mineral phases as progressively more mafic (and presumably deeper) levels of the chamber were tapped. The following paragraphs summarize the variations in mineral assemblages observed in the major eruptive units of Los Humeros.

The Xâltipan Ignimbrite and related air-fall tuffs represent, as stated before, a single eruptive event which tapped magmas of rhyolitic to andesitic composition. The bulk of the pumice in the Xâltipan Ignimbrite is high-silica rhyolite in composition and crystal free, but, as illustrated by samples 1 through 8 in Table 3, the ejecta become porphyritic as their silica content decreases. The mineral assemblage of the porphyritic rhyolitic pumice changes, again as a function of decreasing SiO_2 or increasing MgO, from (pl-bio-ox-cpx) to (pl-bio-ox-cpx$\pm$san). As rhyodacitic compositions are reached, the mineral assemblage becomes (pl-bio-san-ox-cpx$\pm$opx) and progressively

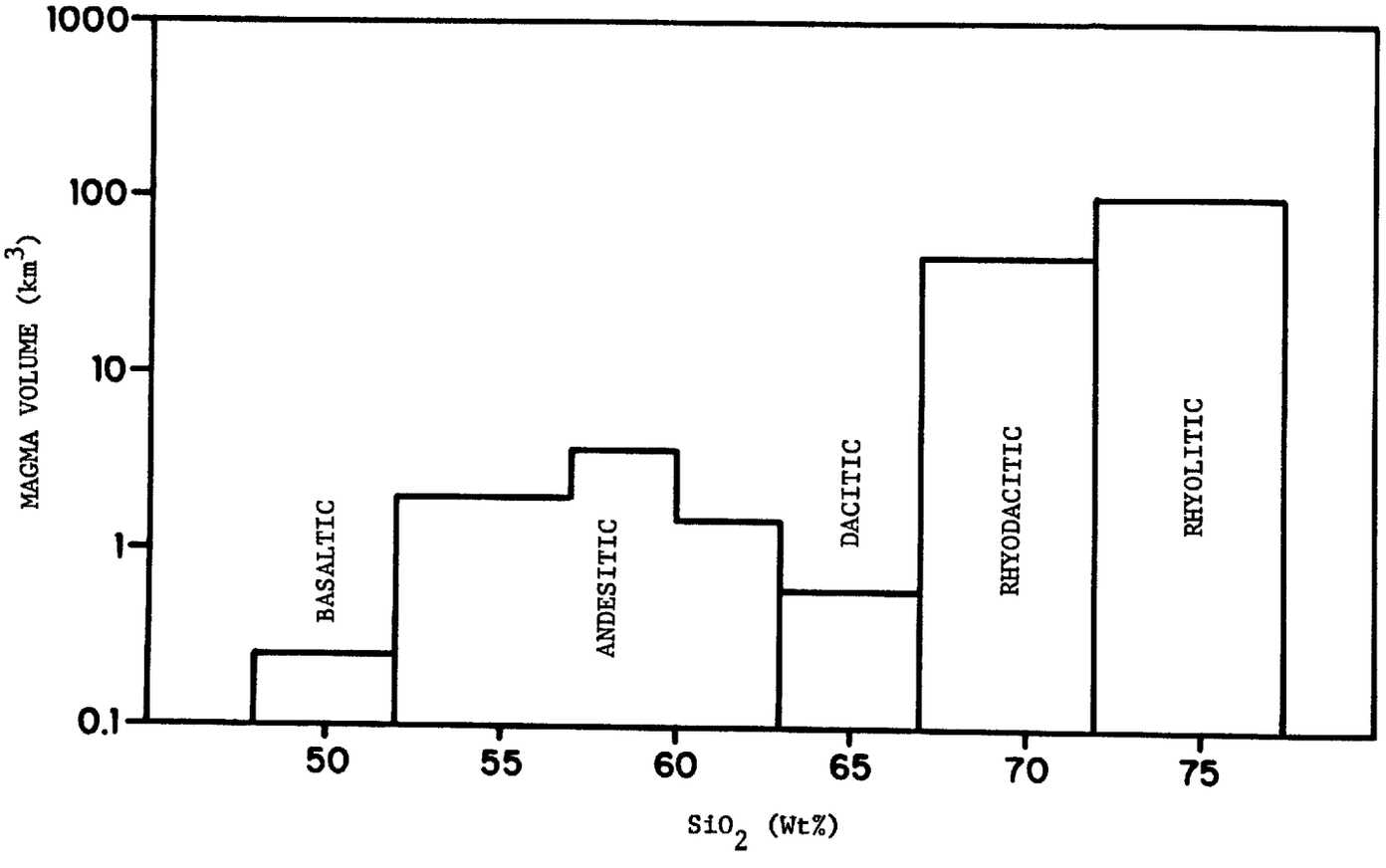

Fig. 5. Volumes of different magma types erupted at Los Humeros during the last 0.46 Ma (based on Ferriz and Mahood, 1984, table 3).

changes to (pl-opx-cpx-ox±bio) and then to (pl-opx-cpx-ox±bio±hbl). Finally, andesitic scoria typically exhibit the assemblage (pl-cpx-ol±ox). The relatively sparse pumice of dacitic composition contains (pl-opx-cpx-ox±bio±hbl±ol); the presence of forsteritic olivine (7 in Table 8) suggests that the small volume of dacitic magma was formed by limited mixing between the dominant silicic and mafic magmas.

The post-Xâltipan rhyolites can be divided into three types in terms of both age and mineralogy. The first type (sample 9 in Table 3; C, D, and E in Figure 2) is formed by rhyolite domes that were emplaced shortly after collapse of the Los Humeros caldera. They are inferred to represent rhyolitic magma remaining in the chamber after the Xâltipan eruption (Ferriz and Mahood,1984). Their phenocryst content ranges from 5 to 10 wt%, and they are characterized by the presence of (san-pl-bio-ox±opx±qz). The second type (sample 10; F in Figure 2) is the aphyric rhyolite of the Caltonac flow, which erupted through the core of one of the biotite rhyolites and is cut in turn by one of the rhyolite domes of the third type (Ferriz and Mahood,1984). This last type (sample 11; G and H in Figure 2) comprises two rhyolite domes that were emplaced probably only shortly before the Faby Tuff eruption. They contain only 3-4 wt% phenocrysts of (pl-opx-ox-san).

The bulk of the volume of the Faby Tuff is formed by pumice that spans a small silica range (72.5-69.4 wt% SiO_2; samples 12, 13, and 14 in Table 3). In spite of this restricted compositional range the Faby Tuff shows major

Table 3. Modal mineralogy (in weight %) of selected samples.

	SAMPLE (a)	CRYSTALS IN WT% (b)	(c)	SiO2 (%)	MgO (%)	san	pl	bio	hbl	opx	cpx	ol	tmt	ilm
	1 LH7	0		77.2	<0.10									
	2 LH15		5.3	76.2	0.12		0.6	2.5			0.6			1.6
	3 LH13		7.7	73.1	0.28	tr	1	4			0.7			2
XALTIPAN	4 LH11	9	7.8	71.5	0.31	0.5	1	4		tr	0.7			1.6
TUFF	5 LH16	6	6.4	70.6	0.90		2	tr		1.5	0.7	tr		1.6
	6 LH19	7	9.2	69.8	0.91		3	tr	tr	3	1	tr		1.6
	7 LH20	4	7.7	66.8	1.07		3	0.5	tr	1.5	1	tr		1.6
	8 LH17		6.8	61.3	3.38		2				2.5	1.5	0.8	
	9 LH25		5.1	76.6	0.14	2	1	1		0.3				0.8
POST-XALTIPAN RHYOLITE DOMES AND FLOWS	10 LH27	0		76.1	0.13									
	11 LH30		3.9	76.1	0.13	0.5	2			0.7	tr			0.8
	12 LH31	2.5	4.3	72.5	0.37		2			1.5				0.8
FABY	13 LH33	4.5	5.5	72.2	0.43		2	tr	1	1.5		tr		0.8
TUFF	14 LH34	15	18	69.4	0.75		8			4	4			2
	15 LH35	1		59.1	3.55		tr			tr	tr	tr	tr	
	16 LH41	6.5	9	71.1	0.52		3			3	1			2
	17 LH48	12	14.2	70.4	0.57		9			3	0.6			1.6
ZARAGOZA	18 LH44	16	18.7	69.9	0.63		11			4	0.7			2
TUFF	19 LH46	40	43	65.4	1.28		33			7				3
	20 LH45	29	32	59.1	2.90		22			1.5	6.5			2
	21 LH47	3.5	4.8	54.4	4.08		1			1	0.5	0.3		2
XOXOCTIC TUFF	22 LH53	2	2.5	65.1	1.70		0.5				1	0.6	0.4	
	23 LH60		3.1	59.5	2.65		2				0.7		0.4	
TEPEYAHUALCO	24 LH61		17.9	59.2	2.92		11			1.5	4	0.6		0.8
FLOW	25 LH55		3	57.8	3.14		2				0.7	0.3		
	26 LH57		3.8	56.1	3.78		2				0.7	0.7	0.4	
LIMON	27 LH65		22.5	56.5	3.23		16				5	1.5		
FLOW	28 LH62		5.7	53.6	4.64		3					2.7		
CHIAPA	29 LH72		4.4	63.1	1.81		2			0.6	1			0.8
FLOWS	30 LH70		9.1	58.3	2.81		7.5				1	0.6		
	31 LHB2		14	69.0	0.79		8			1.5	2.5			2
	32 LHB1		7.4	68.7	0.80		3		0.3	1.5	0.7	tr		1.6
SAN ANTONIO	33 LHB3		18.5	69.2	0.77		11			1.5	4			2
FLOWS	34 LHB4		4.7	60.8	2.35		2			0.6	0.7	0.6		0.8
	35 LHB5		3.7	60.5	2.46		1			0.6	0.7	0.6		0.8
	36 LHB9		4.7	59.6	2.61		3				1	0.7		
OLIVINE BASALT	37 LH94		6.6	49.0	8.93		1					5		0.6

(a) Sample identification number.
(b) Measured by weighting crystal and glass concentrates separately.
(c) Estimated from point-counting modal analysis.

changes in mineral assemblages and total phenocryst contents. The (pl-opx-ox) assemblage of the most silicic pumice is replaced by (pl-opx-ox-hbl) and (pl-opx-cpx-ox) in progressively less silicic rhyodacitic pumice. In the andesitic scoria (sample 15) the assemblage becomes (pl-cpx-ol-opx-tmt).

The variation in the rhyodacitic pumice of the Zaragoza Tuff (samples 16, 17 and 18 in Table 3) is restricted to changes in the total phenocryst contents (discussed in a later section). Its (pl-opx-cpx-ox) assemblage is replaced, however, by (pl-cpx-opx-ox) and (pl-cpx-opx-ol-ox) in progressively more mafic andesitic scoria (samples 19 and 20). Pumice of dacitic composition is notoriously sparse, and is characterized by very high total phenocryst contents (sample 18). The fact that this pumice yields Fe-Ti-oxide temperatures significantly lower than those of rhyodacitic pumice or andesitic scoria (Table 11) suggests that they might represent fragments torn from the partially crystallized margins of the chamber, rather than part of the main compositionally zoned magma body.

No major variations have been observed in the (pl-cpx-ol-mt) assemblage of the dacitic pumice of the Xoxoctic Tuff (sample 22 in Table 3), which represents ~0.6 km3 of magma. As in the case for the Xàltipan dacitic pumice, the presence of highly magnesian clinopyroxene and olivine (Tables 6 and 8) in pumice with a bulk silica content of 65 wt% suggests that this small volume of dacitic magma was formed by mixing between felsic and mafic magmas.

The andesitic Tepeyahualco (samples 23 to 26 in Table 3) and Limón (samples 27 and 28) compound flows, which respectively span the ranges 59.5-56.1 and 56.5-53.6 wt% SiO2, also show changes in mineralogy. In the former, the phenocryst assemblage changes with decreasing silica content from (pl-cpx-opx±ox) to (pl-cpx-ol±ox), whereas in the latter it changes from (pl-cpx-ol) to (pl-ol). Variation in the andesitic lavas of the Chiapa (samples 29 and 30) and Orilla del Monte shields is similar to that of the Tepeyahualco flow.

The San Antonio rhyodacitic lavas (samples 31 to 33 in Table 3) are characterized by an assemblage of (pl-opx-cpx-ox), joined in some flows by rare hornblende. Mafic inclusions containing (pl-ol-cpx-ox) are ubiquitous; as discussed later they are interpreted as quenched inclusions of andesitic magma. The mineral assemblage of the San Antonio andesitic lavas (samples 34 to 36) changes from (pl-cpx-opx-ol-ox) to (pl-cpx-ol±ox) with decreasing silica content.

Olivine basalt flows (sample 37 in Table 3), which erupted during the latest stage of volcanic activity at Los Humeros, are characterized by a simple mineralogy: Ol-pl±ox phenocrysts are set in an intersertal or ophitic groundmass. In the former glass clouded with oxide granules occupies the interstices between subhedral plagioclase laths of the groundmass. In the latter the groundmass plagioclase laths are enclosed within anhedral crystals of titanaugite.

MINERALOGY

Analytical procedure

Microprobe analyses of feldspars and mafic minerals were obtained with Stanford University's JEOL Superprobe (TM), at an accelerating voltage of 15 kv, a sample current of 15 nA, a beam diameter of 10 μm, and a counting time of 20 s. Fe-Ti oxide analyses were obtained with University of California at Berkeley's ARL microprobe, at an accelerating voltage of 15 kv, a sample current of 30 nA, a beam diameter of 2 μm, and a counting time of 10 s. Analyses shown in Tables 4 to 11 are averages of 10 to 50 point analyses.

Plagioclase

Plagioclase is present in all the phyric eruptive products, and in most cases represents the most abundant phenocryst phase. It is also a prominent groundmass phase in andesitic lavas. As shown in Figure 6 and Table 4, average compositions of plagioclase phenocrysts change as a function of the bulk composition of the host rock, being more Ab-rich in rhyolitic ejecta and lavas and more An-rich in progressively more mafic material. Plagioclase has a restricted range of average compositions in rhyolitic and rhyodacitic products, commonly being oligoclase in the former and andesine in the latter. In andesitic compositions the range is much wider, comprising both bytownite and labradorite.

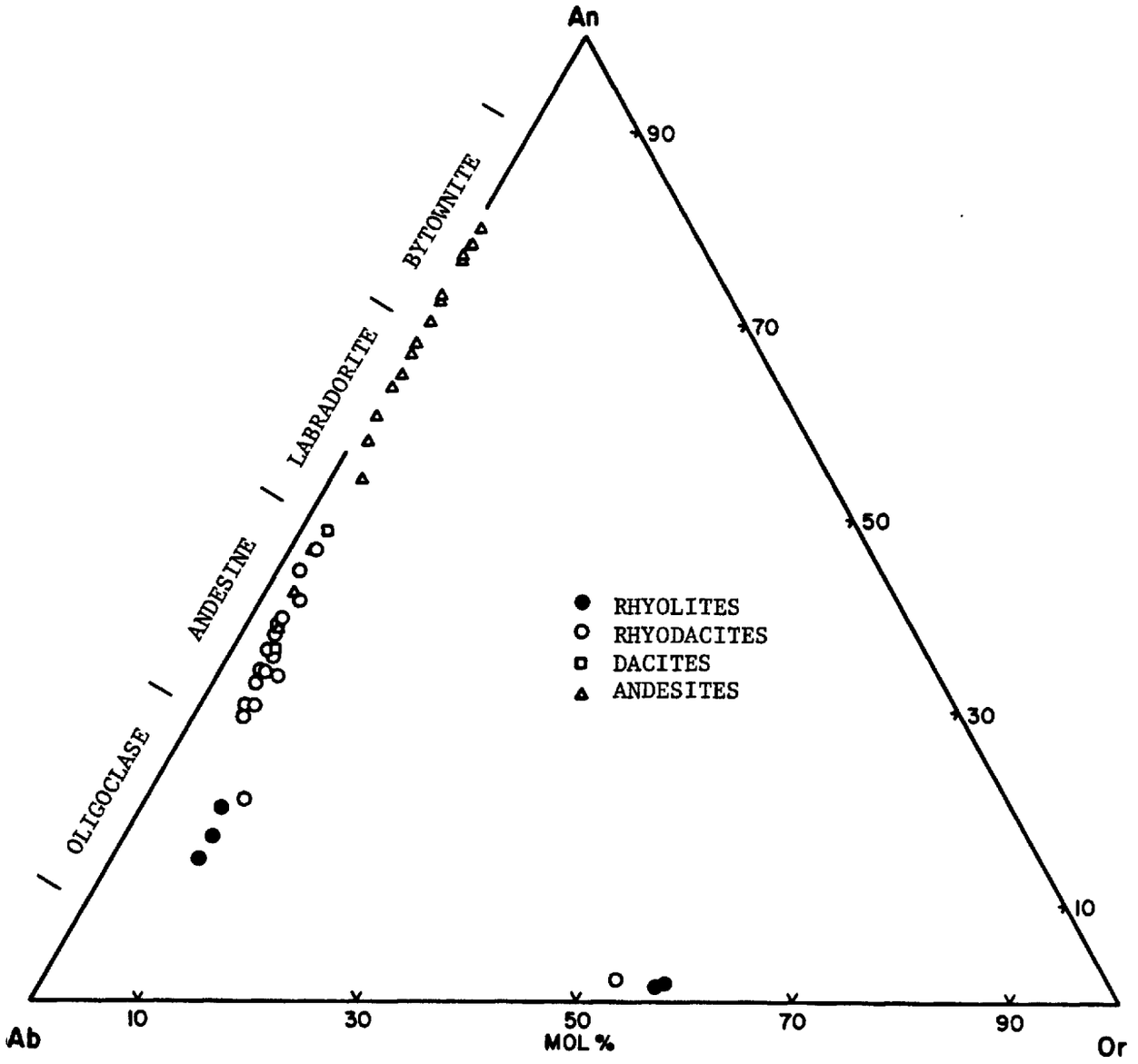

Fig. 6. Molar plagioclase and sanidine compositions of selected samples from Los Humeros volcanic center.

Crystals within individual rhyolitic samples rarely vary by more than 3 mol% An. They are characteristically unresorbed, faintly zoned, and lack prominent glass or mineral inclusions. Normal zoning toward more sodic and potassic rims is much more common than reverse zoning.

Variations in average composition within individual rhyodacitic eruptive sequences, such as the Faby or Zaragoza Tuffs, are usually smaller than 6 mol% An, but within a single sample or a single crystal may exceed 15 mol% An. Zoning and resorption are common features, the latter being more widely developed in lavas than in pyroclastic products. Zoning can be normal, reverse, or oscillatory, but is generally gradual. Abrupt compositional discontinuities are sparse; where present they are commonly restricted to a thin outermost rim. Abrupt changes from a homogeneous core to a zoned mantle are observed in some instances.

Compositions within individual andesitic samples are highly variable, covering a range from 5 to 25 mol% An. The average An content of small phenocrysts and groundmass plagioclase is generally less than that of the larger phenocrysts, ocassionally by as much as 20 mol% An, perhaps due to crystallization of the former at lower water pressures (Mathez, 1973; Gill, 1981, fig.6.1). Inclusions of glass or its devitrification products are common and impart a sieve-like texture to some of the phenocrysts. In any given sample, however, both inclusion-bearing and inclusion-free phenocrysts can be found. Zoning can be normal, reverse, or oscillatory, the first being the most

Table 4. Average composition of plagioclase in selected samples.

	XALTIPAN TUFF						POST-XALTIPAN RHYOLITES		FABY TUFF				ZARAGOZA TUFF				
	3	4	5	6	7	8	9	11	12	13	14	15	16	17	18	20	21
	LH13	LH11	LH16	LH19	LH20	LH17	LH25	LH30	LH31	LH33	LH34	LH35	LH41	LH48	LH44	LH45	LH47
SiO2	62.8	63.6	59.9	57.7	58.9	51.3	65.4	65.4	59.1	60.2	58.4	54.7	60.4	59.9	59.3	52.4	52.2
Al2O3	22.5	23.6	24.2	25.9	25.3	30.2	21.9	22.3	24.7	24.2	25.8	29.0	24.2	24.8	25.6	29.7	29.7
FeO		0.23	0.42	0.45					0.30	0.33	0.33	0.49	0.35		0.35	0.48	
CaO	4.12	4.55	6.85	8.60	7.46	13.36	3.13	3.59	6.97	6.32	7.81	11.25	5.99	6.73	7.50	12.19	12.69
Na2O	8.28	8.45	6.86	6.32	6.77	3.56	9.05	8.74	7.02	7.46	6.76	4.97	7.46	7.13	6.94	4.30	3.96
K2O	1.28	1.65	0.95	0.62	0.66	0.16	1.42	1.43	0.62	0.71	0.54	0.51	0.79	0.67	0.58	0.16	0.14
	98.98	102.0	99.18	99.59	99.09	98.58	100.9	101.4	98.71	99.22	99.64	100.9	99.19	99.23	100.2	99.23	98.69
An	20	21	34	41	36	67	15	17	34	31	38	54	29	33	36	60	63
Ab	73	70	61	55	60	32	77	75	62	65	59	43	66	63	61	39	36
Or	7	9	5	4	4	1	8	8	4	4	3	3	5	4	3	1	1

	XOXOCTIC TUFF	TEPEYAHUALCO FLOW			LIMON FLOW		CHIAPA FLOWS		SAN ANTONIO FLOWS						OLIVINE BASALT
	22	24	25	26	27	28	29	30	31	32	33	34	35	36	37
	LH53	LH61	LH55	LH57	LH65	LH62	LH72	LH70	LH82	LH81	LH83	LH84	LH85	LH89	LH94
SiO2	55.7	48.3	51.3	48.8	48.2	48.4	57.0	49.2	60.0	59.0	59.1	55.6	59.1	53.3	51.9
Al2O3	27.4	32.8	30.4	32.9	32.1	32.6	26.4	30.7	25.4	26.1	25.9	26.7	26.0	28.8	29.8
FeO							0.37	0.57							
CaO	9.85	16.08	12.93	15.35	15.16	15.45	8.58	14.73	7.04	7.87	7.50	9.41	7.93	11.71	12.35
Na2O	5.47	2.16	3.77	2.48	2.49	2.34	6.18	3.02	7.08	6.69	6.91	5.73	6.65	4.55	4.07
K2O	0.39	0.10	0.18	0.06	0.10	0.08	0.45	0.13	0.74	0.57	0.65	0.34	0.54	0.25	0.20
	98.81	99.44	98.58	99.59	98.05	98.87	98.98	98.35	100.3	100.2	100.0	97.78	100.2	98.61	98.32
An	49	80	65	77	77	78	42	72	34	38	36	47	39	58	62
Ab	49	19	34	23	23	22	55	27	62	59	60	51	58	41	37
Or	2	1	1				3	1	4	3	4	2	3	1	1

common. As in the case of rhyodacitic compositions, gradual transitions are much more abundant than abrupt ones.

The striking zoning patterns of plagioclase have been the object of several studies, recently summarized by Gill (1981, p.171-172). Normal zoning is probably due to incomplete equilibration between crystals and melt during isobaric cooling or isothermal ascent of hydrous magma. Reverse zoning could result from isothermal ascent of anhydrous magma, inward growth of originally skeletal crystals during isobaric crystallization, local rise in temperature, magma mixing, or settling of plagioclase crystals into more mafic portions of a chamber. Finally, oscillatory zoning could be related to rhythmic changes in intrinsic parameters such as pressure or water fugacity, or be the result of diffusion rate-controlled compositional gradients at crystal-liquid interfaces. As stated by Gill (1981), the zoning, inclusions, and resorptions of plagioclase phenocrysts may provide a good record of magma history, but their complexity makes interpretation difficult.

K_2O and FeO are minor but important components of plagioclase. K_2O or molar orthoclase contents increase with increasing Ab content, from 0.3 mol% Or in An_{80} plagioclase to about 8 mol% Or in An_{20} plagioclase. FeO content ranges from 0.2 to 0.6 wt%, generally increasing with increasing An content.

Quartz and Sanidine

Despite the fact that the bulk of the magma erupted at Los Humeros had silica contents in excess of 75 wt%, and that K_2O contents were relatively high, quartz and sanidine are rarely observed. They occur in trace amounts in the crystal concentrates of a few rhyolitic pumice fragments of the Xàltipan Ignimbrite and in some of the post-Xàltipan rhyolites.

Sanidine compositions (Table 5, Figure 6) vary from Or57Ab41An2 to Or51Ab47An2, the rims of individual crystals being slightly more sodic than the cores. This zoning is probably due to incomplete equilibration of the feldspar during cooling of the melt.

Although the absence of quartz and sanidine from the bulk of the rhyolitic and rhyodacitic eruptive products would seem anomalous at first sight, Carmichael et al. (1974, p.228-236) have shown that during crystallization of rhyolitic magma that contains even small amounts of CaO, the first phase to crystallize would be plagioclase, which may or may not be joined later by sanidine. Quartz would coprecipitate with plagioclase $\pm$ sanidine only at a later stage in the crystallization sequence. The scarcity of quartz and sanidine is thus probably due both to the small degree of crystallization suggested by the low phenocryst contents of the Los Humeros rhyolites, and to the presence of small but significant quantities of CaO in the liquid.

Table 5. Average composition of sanidine.

	XALTIPAN TUFF		POST-XALTIPAN RHYOLITE
	3	4	9
	LH13	LH11	LH25
SiO2	66.8	65.2	65.9
Al2O3	19.4	18.8	19.2
CaO	0.45	0.36	0.30
Na2O	4.79	4.56	4.68
K2O	8.47	9.71	9.59
	99.91	98.63	99.67
Or	53	57	57
Ab	45	41	42
An	2	2	1

Pyroxenes

Augite (clinopyroxene) and orthopyroxene are the most abundant mafic phenocrysts in the rhyodacitic to andesitic products of Los Humeros, being subordinate in abundance only to plagioclase in most samples. Other pyroxenes such as pigeonite and subcalcic augite are only very rarely found as groundmass phases in some andesite flows. Augite is a common groundmass mineral in andesites, and in some of the late olivine basalts occurs as anhedral masses poikilitically enclosing plagioclase. Variations in the average compositions of augite are small (Table 6, Figure 7). They lie between Wo_{41-40} En_{35-31} Fs_{24-30} in rhyolitic samples, between Wo_{42-41} En_{45-35} Fs_{14-23} in most rhyodacitic ones, and between Wo_{40} En_{50-42} Fs_{11-18} in andesitic products. Variations within individual samples or crystals rarely exceed 4 mol% of the En and Fs components and 1 mol% of the Wo component, regardless of composition. Molar proportions of Fs within augites show a weak positive correlation with the FeO*/MgO ratios of the whole rock.

Orthopyroxene is commonly the dominant pyroxene in rhyolitic and rhyodacitic samples, but is only found in small amounts or not at all in andesitic ones. It is also a rare groundmass phase in andesites at Los Humeros. Orthopyroxene phenocrysts have more variable average compositions, ranging between Wo_{3} En_{39-62} Fs_{58-35} in rhyolitic compositions, Wo_{2-3} En_{56-65} Fs_{41-33} in rhyodacitic ones, and Wo_{3} En_{60-79} Fs_{37-18} in andesitic scoria and lavas. Variations within individual samples or crystals rarely

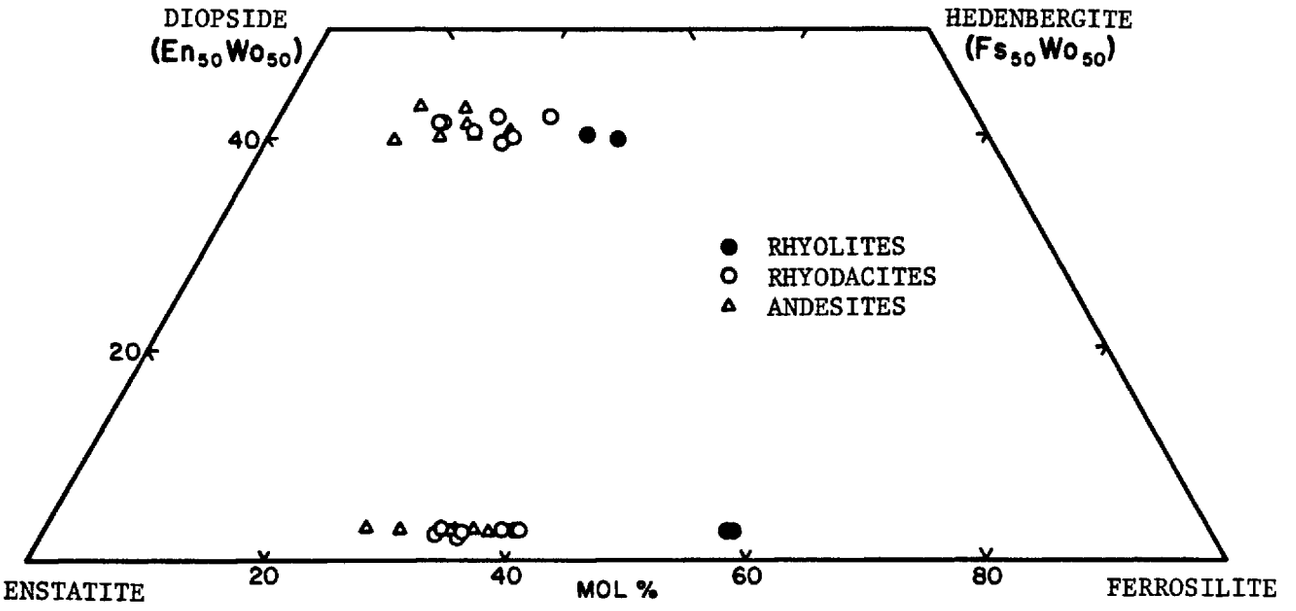

Fig. 7. Molar pyroxene compositions of selected samples from Los Humeros volcanic center.

Table 6. Average composition of clinopyroxene and orthopyroxene in selected samples.

	XALTIPAN TUFF						POST-XALTIPAN RHYOLITES		FABY TUFF				ZARAGOZA TUFF				
	3	4	5	6	7	8	9	11	12	13	14	15	16	17	18	20	21
	LH13	LH11	LH16	LH19	LH20	LH17	LH25	LH30	LH31	LH33	LH34	LH35	LH41	LH48	LH44	LH45	LH47
SiO2	51.7	50.4	51.3	50.2	51.5	50.6					51.8	51.5	51.0	51.9	51.6	51.0	51.7
TiO2	0.17	0.19	0.59	0.98	0.41	1.06					0.35	0.70	0.42	0.33	0.32	0.64	0.64
Al2O3	0.71	0.53	1.84	3.19	1.48	3.33					1.27	2.42	1.25	1.01	0.97	2.07	1.90
FeO	13.9	17.6	10.2	8.2	12.2	7.8					10.1	7.6	13.1	11.9	13.1	9.9	8.8
MgO	11.4	8.8	15.0	15.6	13.1	14.5					14.4	16.9	13.2	13.0	13.4	15.0	15.0
CaO	19.7	18.9	19.6	21.7	19.2	20.4					20.7	20.5	19.4	19.5	19.7	20.2	20.0
Na2O	0.39	0.38	0.36	0.37	0.36	0.39					0.40	0.27	0.36	0.37	0.34	0.32	0.30
MnO	0.83		0.36		0.57	0.20					0.45		0.45	0.49	0.46	0.26	0.26
Cr2O3	0.01		0.06		0.00	0.09					0.00		0.00	0.02	0.00	0.01	
	98.81	96.8	99.31	100.2	98.82	98.37					99.47	99.89	99.18	98.52	99.89	99.4	98.6
Wo	43	42	40	43	41	44					43	42	41	42	41	41	42
En	34	27	43	44	39	43					41	46	38	38	38	43	44
Fs	23	31	17	13	20	13					16	42	21	20	21	16	14
SiO2			51.6	52.5	51.6		51.6	51.2	52.8	52.7	51.9	52.8	51.3	52.3	51.7	52.6	53.2
TiO2			0.11	0.21	0.24		0.11	0.09	0.18	0.18	0.17	0.24	0.19	0.23	0.18	0.33	0.31
Al2O3			0.44	0.72	0.59		0.23	0.19	0.35	0.50	0.52	0.70	0.45	0.53	0.39	1.14	0.93
FeO			27.1	24.1	25.6		31.3	34.3	24.3	22.4	22.6	22.0	25.2	23.9	24.3	17.9	18.7
MgO			19.8	21.8	18.5		15.3	13.1	19.7	21.6	22.7	22.4	20.4	19.7	20.4	24.8	23.8
CaO			1.15	1.30	1.37		1.00	1.10	1.24	1.16	1.15	1.36	1.46	1.38	1.33	1.53	1.45
Na2O			0.03	0.02					0.02	0.02	0.01	0.00					
MnO			0.90		1.04		2.02	1.53			0.95		0.86	0.86	0.89	0.47	0.50
Cr2O3			0.01		0.02		0.01	0.01			0.02		0.01	0.02	0.01	0.00	0.02
			101.1	100.6	98.96		101.57	101.6	98.59	98.58	100.0	99.5	99.87	98.92	99.2	98.77	98.91
Wo			2	3	3		2	3	3	2	2	3	3	3	3	3	3
En			55	60	55		46	39	57	62	63	63	57	58	58	69	67
Fs			43	37	42		52	58	40	36	35	34	40	39	39	28	30

	XOXOCTIC TUFF	TEPEYAHUALCO FLOW			LIMON FLOW	CHIAPA FLOWS		SAN ANTONIO FLOWS						OLIVINE BASALT
	22	24	25	26	27	29	30	31	32	33	34	35	36	37
	LH53	LH61	LH55	LH57	LH65	LH72	LH70	LH82	LH81	LH83	LH84	LH85	LH89	LH94
SiO2	52.1	52.3	50.6	50.1	51.0	52.2	51.1	52.5	52.8	52.4	51.3	51.7	50.8	48.3
TiO2	0.43	0.62	0.92	1.25	0.68	0.43	0.85	0.37	0.34	0.33	0.55	0.78	0.75	2.09
Al2O3	2.37	2.33	3.20	3.73	2.49	1.23	2.86	1.07	1.01	1.02	1.79	2.32	2.26	4.11
FeO	4.9	7.1	8.1	9.1	7.4	12.5	9.3	11.2	10.7	11.1	10.5	9.4	8.5	9.7
MgO	16.3	16.1	15.2	15.0	15.6	13.9	15.3	13.8	14.4	13.7	14.8	14.7	14.9	12.7
CaO	21.4	20.9	20.3	19.5	20.2	19.7	19.7	20.0	20.0	20.6	19.2	20.5	20.2	20.0
Na2O	0.25	0.28	0.34	0.33	0.31	0.36	0.38	0.40	0.34	0.36	0.36	0.34	0.33	0.50
MnO	0.13	0.16	0.19	0.22	0.16	0.49	0.17	0.45	0.48	0.43	0.35	0.28	0.23	0.18
Cr2O3			0.09			0.00	0.07			0.00	0.02			0.22
	97.88	99.79	98.94	99.23	97.84	100.8	99.73	99.79	100.0	99.94	98.87	100.0	97.97	97.8
Wo	45	43	43	41	42	40	41	42	42	43	40	43	42	44
En	47	46	44	44	46	40	44	40	41	39	43	42	44	40
Fs	8	11	13	15	12	20	15	18	17	18	17	15	14	17
SiO2		53.5				53.3		53.0	53.8	52.8	52.0	53.1		
TiO2		0.24				0.24		0.21	0.21	0.17	0.21	0.24		
Al2O3		0.49				0.57		0.54	0.57	0.42	0.54	0.53		
FeO		21.9				22.6		23.5	20.9	23.5	22.2	23.0		
MgO		22.4				21.7		20.9	22.7	20.7	21.4	21.0		
CaO		1.49				1.49		1.37	1.51	1.41	1.44	1.36		
Na2O														
MnO		0.81				0.84		0.88	0.66	0.86	0.79	0.84		
Cr2O3		0.00				0.02		0.02	0.15	0.03	0.02	0.00		
		100.8				100.8		100.4	100.5	99.89	98.6	100.0		
Wo		3				3		3	3	3	3	3		
En		63				61		60	64	59	61	60		
Fs		34				36		37	33	38	36	37		

exceed 5 mol% of the En and Fs components. As for augites, Fs molar proportions in orthopyroxene show a weak but positive correlation with whole rock FeO*/MgO ratios. Fe/Mg ratios are always higher in orthopyroxene than in coexisting augite.

Pyroxenes contain significant amounts of cations such as Al, Na, Ti, and Mn. For crystal-chemical reasons (Huebner, 1980), the first three elements are enriched in clinopyroxene with respect to orthopyroxene, whereas the reverse is true for Mn. The ranges in minor-element concentrations in the different magma types erupted at Los Humeros are shown in Table 7. Interpretation of these differences is uncertain, however, as it has been demonstrated experimentally that they might reflect different conditions of temperature, pressure, bulk composition, a_{SiO_2}, f_{O_2}, coexisting mineral assemblages, and cooling rates (Huebner, 1980).

Olivine

Olivine is the dominant phenocryst in olivine basalts, and a sparse but ubiquitous phase in andesitic products (Table 8). Olivine xenocrysts are found in some dacitic, rhyodacitic, and rhyolitic samples.

Some olivine phenocrysts in basalts are zoned from cores of composition Fo_{84} to rims of Fo_{75}. This latter value is similar to that of groundmass olivine (Fo_{74}), which suggest that the rims are a product of late stage crystallization, probably during eruption. Average olivine

Table 7. Concentrations of minor oxides in pyroxenes.

	Clinopyroxene	Orthopyroxene
TiO2		
Rhyolites	0.16-0.17	0.09-0.13
Rhyodacites	0.19-0.98	0.11-0.33
Andesites	0.55-1.19	0.20-0.33
Ol- basalt	2.09	
Al2O3		
Rhyolites	0.56-0.75	0.15-0.66
Rhyodacites	0.53-1.83	0.35-0.73
Andesites	1.23-4.21	0.49-1.14
Ol- basalt	4.11	
Na2O		
Rhyolites	0.32-0.39	0.01
Rhyodacites	0.31-0.83	0.01-0.06
Andesites	0.27-0.41	
Ol- basalt	0.50	
MnO		
Rhyolites	0.71-0.75	1.49-2.02
Rhyodacites	0.31-0.83	0.66-0.95
Andesites	0.15-0.49	0.24-0.96
Ol- basalt	0.18	

Table 8. Average compositions of olivine in selected samples.

	7	8	15	21	22	24	26	27	28	34	36	37
	LH20	LH17	LH35	LH47	LH53	LH61	LH57	LH65	LH62	LH84	LH89	LH94
SiO2	38.1	39.2	39.1	40.0	39.3	39.5	39.1	38.6	38.4	37.4	37.4	39.6
FeO	24.2	20.2	19.0	16.6	16.0	19.4	22.3	20.7	21.6	25.3	25.3	14.8
MgO	36.2	40.1	41.7	42.7	43.2	41.3	40.3	40.1	39.2	36.0	35.0	44.5
MnO	0.34	0.27		0.21	0.23	0.27	0.32	0.26	0.29	0.36	0.34	0.20
CaO			0.14		0.15							
	98.84	99.77	99.94	99.51	98.88	100.4	102.0	99.66	99.49	99.06	98.04	99.10
Fo	73	78	80	82	83	79	76	78	76	72	71	84
Fa	27	22	20	18	17	21	24	22	24	28	29	16

phenocryst compositions in andesites range from Fo_{80} to Fo_{71}. Compositions within individual samples are often as variable. Chromian spinel granules and glass inclusions, some bearing a gas bubble, are found in some phenocrysts. As in the case of the basaltic lavas, groundmass olivine in andesites is normally less magnesian than phenocrystic olivine, typically ranging between Fo_{65} and Fo_{60}. Phenocrystic and groundmass olivines are characteristically unrimmed and unresorbed.

FeO/MgO ratios in olivine are always lower than those of the whole rock and, where present, of coexisting orthopyroxene. They can be both smaller or larger than the ratios in coexisting clinopyroxene. MnO contents of olivine range from 0.20 to 0.36 wt% and have a weak positive correlation with their FeO*/MgO ratio. CaO contents were not systematically measured, but in the few andesitic samples analyzed were found to range between 0.14 and 0.20 wt%. These CaO contents are high enough to suggest crystallization at pressures lower than 10 kb (Finnerty and Boyd, 1978).

Biotite

Biotite is the predominant ferromagnesian mineral in the porphyritic rhyolitic and rhyodacitic pumice of the Xáltipan Ignimbrite and in the early post-Xáltipan high-silica rhyolite domes. Biotite plates are characteristically euhedral and unresorbed, their largest dimensions varying between 0.5 and 2 mm. The larger crystals ocassionally

Table 9. Selected biotite analyses.

	3	4	7	9
	LH13	LH11	LH20	LH25
SiO2	36.3	35.6	36.1	37.4
TiO2	5.0	4.9	5.3	4.9
Al2O3	13.2	13.3	13.1	12.9
FeO	19.9	21.3	19.7	21.6
MgO	10.2	9.7	10.3	10.5
CaO	0.03	0.02	0.00	0.00
Na2O	0.73	0.73	0.69	0.54
K2O	8.36	8.41	8.49	8.74
MnO	0.25	0.23	0.18	0.21
Cl		0.08		
F		0.35		
	93.97	94.62	93.86	96.79

enclose submillimetric inclusions of apatite and zircon. Unfortunately, most of the biotite microprobe analyses show large potassium deficiencies, suggesting posteruptive exchange with meteoric water. No correlation that might suggest syneruptive alteration has been found between degree of biotite alteration and phenocryst content or stratigraphic position (e.g., Hildreth,1979). The analyses with the smaller deficiencies are shown in Table 9.

Amphibole

Amphibole is a scarce phase occuring in small amounts in dacitic pumice of the Xâltipan air-fall tuffs, in some of the rhyodacitic layers of the Faby and Cuicuiltic Tuffs, and in a few of the San Antonio rhyodacitic lavas.

All amphiboles (Table 10) are calcic (Ca>1.34 per 23 oxygens) and are largely magnesian hastingsitic hornblendes or magnesian hastingsites, following the nomenclature of Leake (1968). In general, the crystals are slightly zoned, with the Fe/Mg ratio increasing toward the rim. FeO*/MgO ratios lie between 0.83 and 1.46, and are always smaller than the ratio of the rock, although correlation between the two ratios is erratic. Hornblende FeO*/MgO ratios are always larger than those of coexisting clinopyroxene, but may be larger or smaller than those of coexisting orthopyroxene. K/Na ratios of the whole rock are characteristically two to three times larger than those of the amphiboles.

Table 10. Average compositions of amphiboles.

	7	13	32
	LH20	LH33	LH81
SiO2	42.1	42.5	42.4
TiO2	3.6	3.7	3.8
Al2O3	11.0	11.0	11.2
FeO	16.1	12.4	13.8
MgO	11.0	13.2	12.7
CaO	10.60	11.20	10.90
Na2O	2.49	2.67	2.70
K2O	0.73	0.65	0.61
MnO	0.33	0.24	0.27
	97.95	97.56	98.38

Oxides

Three oxides occur as primary minerals in the eruptive products of Los Humeros: an Fe-Ti spinel phase (hereafter called titanomagnetite), an Fe-Ti rhombohedral phase (hereafter called ilmenite), and a chromian spinel phase. Fe-Ti oxides are the only phases that have FeO*/MgO ratios much larger than that of the host rock, and thus their potential fractionation may become the dominant mechanism for limiting magmatic iron enrichment.

Titanomagnetite and ilmenite are probably among the first crystallized phases in rhyolitic and rhyodacitic samples, where they are commonly present as inclusions in mafic phases. In andesites and basalts, titanomagnetite is a scarce but ubiquitous phase; ilmenite is even more sparse or is entirely absent. Chromian spinel occurs only as inclusions in olivine phenocrysts of andesites and basalts.

Calculated following the method of Carmichael (1967), ulvospinel contents in titanomagnetite phenocrysts usually vary between 30 and 45 mol% (Table 11), and R_2O_3 (Fe_2O_3 + Al_2O_3 + Cr_2O_3) contents of ilmenite phenocrysts range from 8 to 17 mol%. Titanomagnetite is enriched in Al_2O_3, Cr_2O_3, and SiO_2 with respect to coexisting ilmenite, which in turn is enriched in MgO and MnO. Although not measured in this study, the work of Carmichael (1967) has shown that Fe-Ti oxides can have as much as 1.5 wt% V_2O_3 and 0.3 wt% ZnO.

Table 11. Average composition of titanomagnetite and ilmenite in selected samples.

	XALTIPAN TUFF					POST-XALTIPAN RHYOLITE	FABY TUFF				ZARAGOZA TUFF				
	3	4	5	6	7	11	12	13	14	15	16	18	19	20	21
	LH13	LH11	LH16	LH19	LH20	LH25	LH31	LH33	LH34	LH35	LH41	LH44	LH46	LH45	LH47
SiO2	0.09	0.08	0.07	0.10	0.08	0.15	0.06	0.07	0.07	0.08	0.08	0.08	0.09	0.08	0.14
TiO2	14.6	13.9	12.3	13.6	16.7	14.5	12.6	12.7	12.2	14.7	16.8	16.2	16.5	15.9	15.0
Al2O3	1.39	1.30	1.72	1.75	2.46	1.08	1.68	1.67	1.81	2.13	1.56	1.66	1.65	2.86	3.21
Cr2O3	0.02	0.03	0.08	0.01	0.00	0.04	0.01	0.02	0.02	0.02	0.01	0.02	0.03	0.03	0.06
FeO	77.0	78.2	77.9	76.1	73.3	78.2	77.9	78.0	77.9	74.1	75.7	75.0	74.0	72.1	71.0
MnO	0.80	0.80	0.51	0.58	0.60	0.57	0.68	0.67	0.53	0.51	0.55	0.54	0.56	0.43	0.33
MgO	0.78	0.79	1.73	1.94	2.54	0.56	1.63	1.63	1.86	2.74	1.38	1.48	1.58	2.76	3.09
CaO	0.00	0.01	0.03	0.01	0.00	0.01	0.05	0.00	0.01	0.03	0.02	0.02	0.02	0.01	0.01
	94.68	95.11	94.34	94.09	95.68	95.11	94.61	94.76	94.4	94.31	96.1	95	94.43	94.17	92.84
mol% usp	42.0	39.9	35.1	38.6	46.7	42.0	35.9	36.2	34.7	41.7	47.4	46.2	47.4	45.0	43.1
SiO2	0.00	0.02	0.03	0.04	0.00	0.07	0.05	0.02	0.02		0.04	0.02	0.06	0.03	0.06
TiO2	48.7	48.1	46.6	44.3	48.1	46.1	46.0	45.7	45.6		48.5	47.8	48.7	47.2	45.4
Al2O3	0.06	0.05	0.16	0.31	0.22	0.06	0.13	0.14	0.15		0.13	0.13	0.12	0.24	0.34
Cr2O3	0.01	0.02	0.00	0.03	0.03	0.00	0.00	0.02	0.00		0.00	0.00	0.00	0.00	0.01
FeO	47.0	47.1	46.0	45.2	46.0	48.1	47.2	48.3	48.1		46.7	46.8	45.4	45.3	44.5
MnO	1.15	1.27	0.62	0.49	0.73	0.98	0.90	0.87	0.70		0.69	0.71	0.67	0.51	0.41
MgO	1.62	1.29	4.10	3.99	3.08	1.20	2.84	2.00	3.03		2.36	2.48	2.59	4.28	4.46
CaO	0.02	0.04	0.05	0.03	0.04	0.02	0.04	0.05	0.05		0.02	0.04	0.02	0.02	0.01
	98.56	97.89	97.56	94.39	98.2	96.53	97.16	97.1	97.65		98.44	97.98	97.56	97.58	95.19
mol% R2O3	7.9	8.0	12.8	14.4	9.8	10.6	12.8	12.6	14.2		8.6	9.7	7.5	11.8	13.2
T (°C)	802	793	870	*	884	874	876	875	890		855	879	821	919	934
-log fO2	14.3	14.4	12.1		12.5	12.5	12.0	12.1	11.6		13.3	12.6	14.2	11.7	11.2

	XOXOCTIC TUFF	TEPEYAHUALCO FLOW		SAN ANTONIO FLOWS					OLIVINE BASALT
	22	24	26	31	32	33	34	35	37
	LH53	LH61	LH57	LH82	LH81	LH83	LH84	LH85	LH94
SiO2	0.14	0.26	0.37	0.11	0.11	0.11	0.17	0.16	0.12
TiO2	16.8	16.0	19.3	14.3	15.1	14.8	16.0	15.5	21.2
Al2O3	2.29	2.05	1.77	2.04	2.11	2.20	2.30	2.62	0.50
Cr2O3	0.05	0.02		0.11	0.05	0.08	0.03	0.05	0.21
FeO	71.4	73.2	71.3	74.2	75.1	74.6	73.9	74.5	70.4
MnO	0.56	0.35	0.42	0.46	0.55	0.52	0.41	0.24	0.45
MgO	2.32	2.53	2.10	1.97	1.75	2.00	2.30	2.02	1.88
CaO	0.04	0.03	0.26	0.03	0.10	0.02	0.03	0.02	0.09
	93.6	94.44	95.52	93.22	94.87	94.33	95.14	95.11	94.85
mol% usp	48.5	46.0	55.6	41.3	43.0	42.3	45.4	44.0	61.1
SiO2		0.06		0.04	0.08	0.08	0.13	0.52	0.10
TiO2		44.5		46.0	45.5	45.5	45.8	46.7	47.4
Al2O3		0.18		0.20	0.19	0.18	0.25	0.32	4.11
Cr2O3		0.04		0.02	0.03	0.03	0.01	0.02	0.04
FeO		48.4		46.6	47.3	47.3	46.0	46.0	43.3
MnO		0.38		0.63	0.74	0.63	0.56	0.39	0.63
MgO		3.45		3.07	2.95	3.07	3.87	3.28	2.89
CaO		0.05		0.05	0.01	0.05	0.06	0.06	0.19
		97.06		96.61	96.8	96.84	96.68	97.29	98.66
mol% R2O3		16.0		12.4	13.4	13.5	13.2	10.8	12.7
T (°C)		1005		907	936	934	951	891	1067
-log fO2		10.0		11.7	11.2	11.2	11.0	12.2	9.7

* Tmt-ilm pair in apparent desequilibrium according to C. Bacon's criterion (see caption of Figure 8).

Xenocrysts and inclusions

Xenocrysts of calcic plagioclase, magnesian olivine and orthopyroxene, and perhaps Fe-Ti oxides, are present in some crystal concentrates from rhyolitic and rhyodacitic products. In most cases xenocrysts can be recognized as such by petrographic criteria or by extreme differences between their composition and that of the dominant phenocrysts. However, with some minerals, such as Fe-Ti oxides, neither criteria is robust enough to make an unequivocal identification of xenocrysts. In these cases, we can do little more than suspect their presence when microprobe analyses indicate the existence of two different generations of the same mineral phase.

Two types of inclusions are observed at Los Humeros, particularly in the post-Zaragoza rhyodacitic lavas: mafic porphyritic clots and accidental inclusions of pre-Xáltipan lavas and silicified limestone. The mafic porphyritic clots have quench textures, and phenocrysts of plagioclase, olivine, clinopyroxene, and titanomagnetite in a glassy to hyalopilitic groundmass. They are interpreted as andesitic magma that was quenched when mixed with rhyodacitic magma.

The ubiquitous presence of mafic xenocrysts and quenched inclusions in the silicic magmas of Los Humeros implies that the two types of magmas were in continuous, albeit limited, interaction within the chamber. This observation supports the conclusion reached above that the magma chamber was strongly zoned in composition throughout the lifetime of the system. Unfortunately, it also makes the

interpretation of trends based on the composition of mineral phases present in trace amounts more difficult.

INTENSIVE PARAMETERS

Temperature and oxygen fugacity

The experimental work of Buddington and Lindsley (1964) demonstrated that the extent of magnetite-ulvospinel and ilmenite-hematite solid solution is strongly dependent on temperature and oxygen fugacity. Thus, the composition of coexisting Fe-Ti oxide phases can be used as a geothermometer and as a geobarometer of oxygen fugacity (Spencer and Lindsley, 1981). In order to apply this geothermometer, it is first necessary to assess whether the two coexisting Fe-Ti phases are in equilibrium. Bacon (written comm.,1980) has shown empirically that the logarithms of (Mg/Mn) ratios in titanomagnetite-ilmenite pairs in apparent equilibrium are related to each other by a simple linear relationship over rather wide ranges of T, P, and f_{O_2}. The data from Los Humeros are compared with the equilibrium field proposed by Bacon in Figure 8. Out of the 45 data points plotted, seven fall clearly outside this field, and are rejected from the data base.

The results of applying the Fe-Ti oxide geothermometer to the Los Humeros data are shown in Figure 9. Given the precision of microprobe data, the uncertainty of the calculated temperatures is probably $\pm 30^{o}$ C (Spencer and Lindsley,1981), so without further work the fine-scale thermal structure of the magma chamber cannot be resolved.

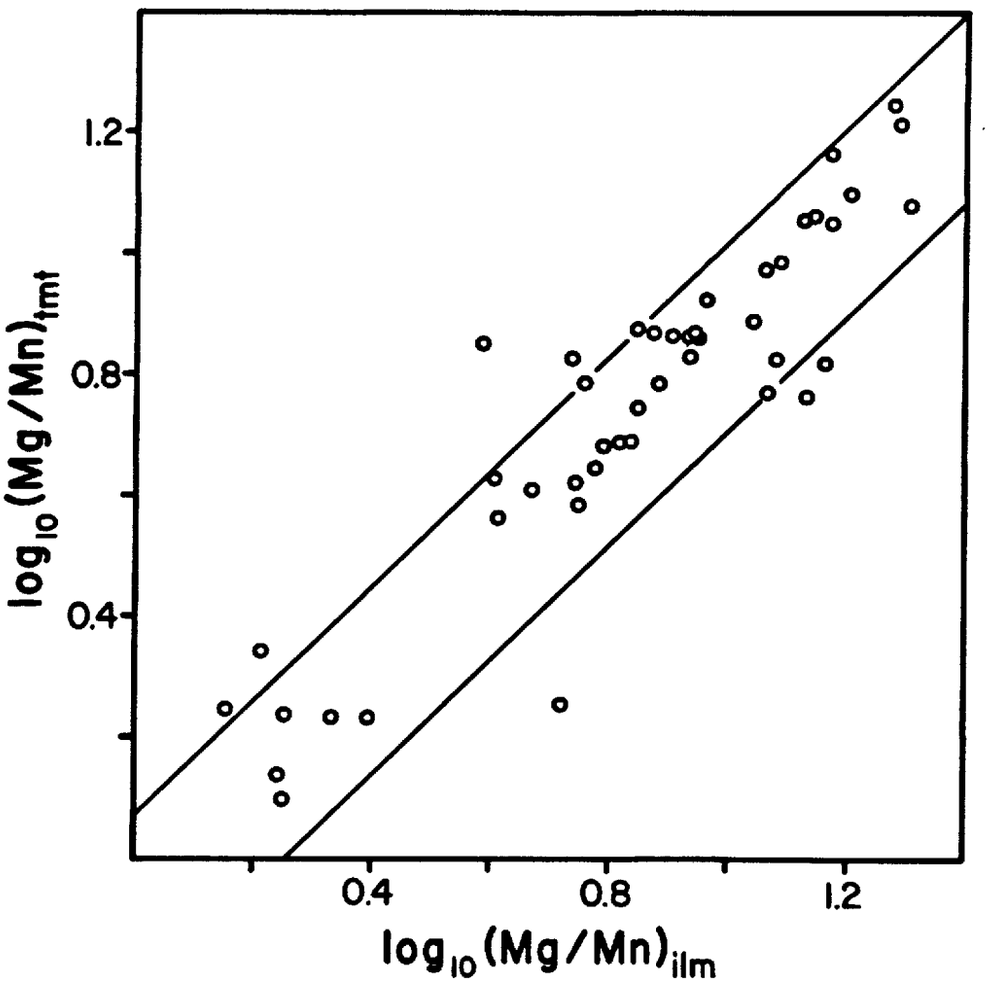

Fig. 8. Mg/Mn ratios of coexisting titanomagnetite-ilmenite pairs. The two lines bound the empirical equilibrium field defined by the equation proposed by Bacon (written comm.,1980):

$$\log(Mg/Mn)_{il} = 1.0462 \log(Mg/Mn)_{mt} + 0.07961 \pm 0.1$$

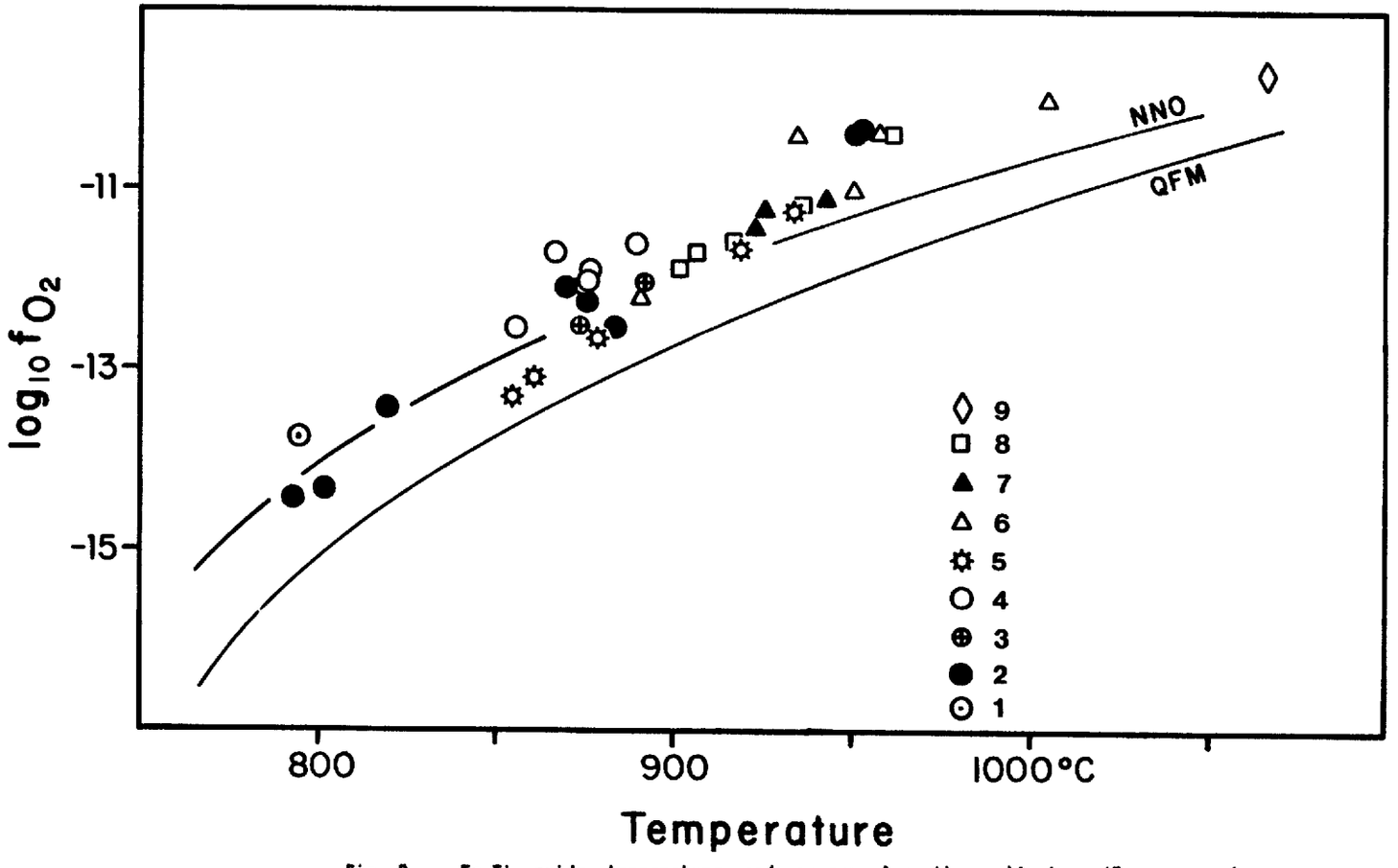

Fig. 9. Fe-Ti oxide temperature and oxygen fugacity estimates (Spencer and Lindsley,1981) for samples of Los Humeros volcanic center. 1 pre-Xăltipan rhyolite, 2 Xăltipan Tuff, 3 post-Xăltipan biotite-rhyolite and pre-Faby opx-rhyolite, 4 Faby Tuff, 5 Zaragoza Tuff, 6 Tepeyahualco, Chiapa, and San Antonio andesites, 7 Cuicuiltic Tuff, 8 San Antonio and Arenas rhyodacites, 9 olivine basalt.

Pre-eruptive temperatures of rhyolitic magma were probably in the range 800° - 875° C, 860° - 940° C for rhyodacitic magma, 920° - 1000° C for andesitic magma, and greater than 1100° C for the late-erupted olivine basalts.

An independent assesement of the validity of the calculated temperatures can be obtained by comparing the results obtained from two different geothermometers. Such a comparison is done in Figure 10, where Fe-Ti oxide temperatures are plotted against temperatures obtained through the pyroxene geothermometer of Lindsley (1973), for samples in which the coexisting pyroxenes contain less than 10 mol% of non-quadrilateral components. Of the 16 points plotted, 12 fall within the $\pm$50° C uncertainty of the pyroxene geothermometer. Although based on a small data base, this comparison should again be a reminder of the rather large errors that could be associated with estimated temperatures due to disequilibrium, analytical errors, and uncertainities in the formulation of the geothermometers.

Total pressure

The presence of collapse structures at Los Humeros is the strongest indication that the magma chamber was emplaced at a shallow level in the crust. In contrast, stress relaxation linked to voluminous magma withdrawal from a deep-seated chamber would be expected to be distributed throughout the crust, and not to be reflected at the surface in a significant way. For example, Swanson et al. (1975) demonstrated that eruption of the voluminous (>1500 km^3),

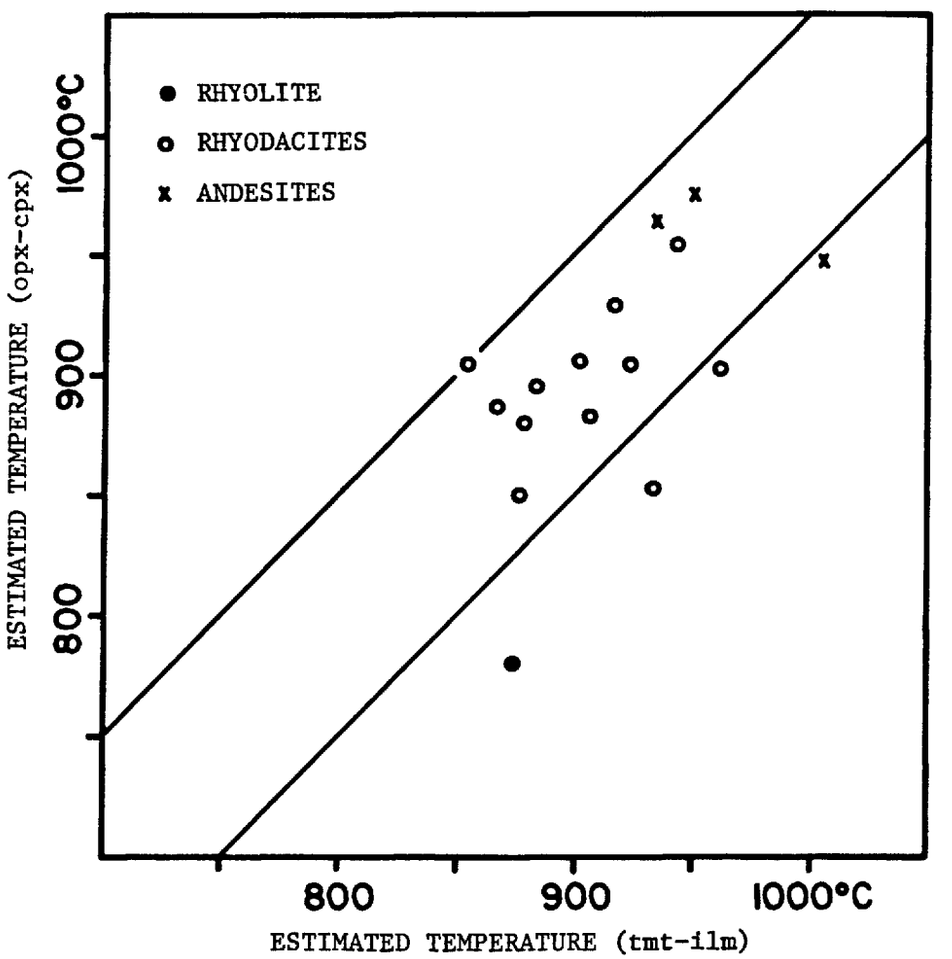

Fig. 10. Comparison between Fe-Ti oxide and cpx-opx temperature estimates (Spencer and Lindsley,1981; Lindsley,1983) for selected samples of Los Humeros volcanic center. The two lines delimit the ± 50° C uncertainty field of the pyroxene geothermometer.

mantle-derived, Roza Basalt Flow of the Columbia River Plateau, USA, which was probably emplaced within a period of a few weeks, was at most accompanied by gentle regional subsidence. Major collapse structures have not been documented. On the other hand, in cases like the Yellowstone volcanic center, USA, where the depth to the top of the magma chamber has been determined by geophysical methods to be ~5 km (Eaton et al.,1975), major eruptions produced well-defined collapse structures (Christiansen and Blank,1972; Christiansen,1979).

Ideally, total pressure could be calculated with mineral geobarometers. In reality, the utility of geobarometry is limited by the number of mineral assemblages for which thermodynamic properties are known, the imprecision of the thermodynamic data, limited understanding of mineral solution models, analytical errors, and the potential for non-equilibrium conditions among coexisting mineral phases. The results obtained through geobarometry should thus be interpreted with caution. Table 12 shows total pressures calculated using the titanomagnetite-quartz-orthopyroxene geobarometer, using the formulation of Hildreth (1977) and mineral data from the rhyolitic portion of the Xàltipan Ignimbrite and one of the post-Xàltipan biotite rhyolites. The calculated total pressures range from 1.1 to 2.4 kbars, which would correspond to depths between 4 and 9 km. Although these figures are reasonable in the light of the geologic evidence, the reader must be

Table 12. Estimates of total pressure.

a^{opx}_{FeSiO3}	a^{tmt}_{Fe3O4}	a^{quartz}_{SiO2}	T °C	$-\log f_{O2}$	Pressure (kb)
0.504	0.5159	1	793	14.42	2.4
0.504	0.4935	1	802	14.32	2.1
0.504	0.5877	1	802	14.32	1.1

Pressure was calculated using the expression:

$$P = \frac{12399 - T\,(\log K + 3.621)}{0.0859} + 1 \qquad \text{(Hildreth, 1977)}$$

where P is pressure in bars, T is temperature in degrees Kelvin, and:

$$K = \frac{a^{tmt}_{Fe3O4}\,(a^{quartz}_{SiO2})^3}{a^{opx}_{FeSiO4}\,(f_{O2})^{\frac{1}{2}}}$$

$$a^{tmt}_{Fe3O4} = 0.5\; n_{Fe3+,F}\; (X_{Fe2+,S2+})\; (X_{Fe3+,S3+}) \qquad \text{(Stormer, 1983)}$$

$$a^{opx}_{FeSiO3} = (X^{M1}_{Fe} \cdot X^{M2}_{Fe})^{\frac{1}{2}} \qquad \text{(Ewart et al., 1975)}$$

$$a^{quartz}_{SiO2} = X^{quartz}_{SiO2}$$

A BASIC program that performs these calculations can be requested from the author.

aware that the calculated values are extremely sensitive to small variations in the chosen parameters, particularly T and f_{O_2}.

Water contents

Water contents of dense rhyolitic and rhyodacitic vitrophyres are summarized in Table 13, but they are unlikely to represent magmatic values, due to potential degassing during magma ascent and the common phenomenon of post-emplacement hydration (e.g., Taylor, 1968).

Magmatic water contents can be estimated, in principle, from phase-equilibria considerations when a hydrous mineral is present. For example, within a magma where biotite, titanomagnetite, and sanidine are in equilibrium, water fugacity can be estimated by the method originally proposed by Wones and Eugster (1965), and later revised by Wones (1972) and Hildreth (1977). The later revisions were based on the original experimental data, but incorporated refinements in the thermodynamic properties of the control buffers of Wones and Eugster (1965). Unfortunately, the corrections are neither trivial nor without qualifications, the main uncertainty being introduced by the present lack of understanding of biotite solution models (Bohlen et al., 1980). Water fugacities calculated assuming a total pressure of 2 kb, and using Hildreth's (1977) formulation and mineral data from two biotite-bearing rhyolitic samples of the Xâltipan Ignimbrite and one of the post-Xâltipan biotite rhyolites range between 0.4 and 1 kb, depending on

Table 13. Weight percent H2O contents in vitrophyres, pumice and scoria.

Rhyolitic vitrophyres	1.1	1.1	1.0 (LH27)	0.78 (LH30)
Rhyodacitic vitrophyres	0.79	0.73 (LH82)	0.84	0.88
Andesitic lavas	0.45 (LH72)	0.45	0.90 (LH70)	0.98
Rhyolitic and rhyodacitic pumice	2.5 (LH7)	3.1 (LH11)	2.9 (LH32)	3.7 (LH41)
Andesitic scoria	2.0 (LH45)	0.40 (LH35)	0.77	

Analyses performed by the U.S. Geological Survey by the Penfield method.

the way in which the activity of annite in biotite is calculated (Table 14). These values would be equivalent to a P_{H_2O} between 0.44 and 1.2 kb (Burnham et al.,1969). Since the water pressures are smaller than the assumed total pressure of 2 kb, the magma presumably was not saturated with water. Assuming a mean value of 65.8 for the gram formula mass of the melt and a total pressure of 2 kb, water fugacities can be converted to weight percent water contents using the method of Carmichael et al. (1977). Water fugacities between 0.40 and 1 kb would be equivalent to water contents between 3.3 and 5.5 wt%.

The virtual absence of hydrous phases in the major post-Xàltipan eruptive units does not necessarily imply that the magma itself was anhydrous. More mafic compositions and higher average temperatures could have inhibited the crystallization of minerals such as biotite and hornblende. For example, Naney (1983) found that in a synthetic rhyodacitic melt at 2 kbars the assemblage opx-pl is stable only at water contents between 2 and 3 wt% for temperatures similar to those of the Faby and Zaragoza Tuffs. At lower water contents cpx becomes stable, whereas at higher water contents plagioclase becomes unstable. The transition from opx-pl to opx-cpx-pl dominated assemblages observed in the Faby Tuff could be a natural example of a gradient in water content in an anhydrous mineral assemblage. Comparisons with experimentally determined water content values should be undertaken with care, however, as small changes in major element melt compositions may lead to major changes in

Table 14. Estimates of H2O content (wt%) in rhyolitic magma.

a^{bio}_{annite}		a^{tmt}_{Fe304}	$a^{san}_{KAlSi308}$	T °C	-log f_{O2}	f_{H2O} (bars)	Wt% H2O
0.1190	(1)	0.5159	0.5567	793	14.42	1027	5.4
0.0672	(2)	0.5159	0.5567	793	14.42	580	3.9
0.0655	(3)	0.5159	0.5567	793	14.42	565	3.9
0.0972	(1)	0.4935	0.6075	802	14.32	770	4.5
0.0548	(2)	0.4935	0.6075	802	14.32	434	3.3
0.0539	(3)	0.4935	0.6075	802	14.32	427	3.3
0.1121	(1)	0.5877	0.5995	802	14.32	756	4.5
0.0656	(2)	0.5877	0.5995	802	14.32	442	3.3
0.0643	(3)	0.5877	0.5995	802	14.32	433	3.3

(1) $a^{bio}_{annite} = (X^{y}_{Fe2+})^3$ (Wones, 1972)

(2) $a^{bio}_{annite} = X^{x}_{K} (X^{y}_{Fe2+})^3 (X^{hyd}_{OH})^2$ (Hildreth, 1977)

(3) $a^{bio}_{annite} = (X^{x}_{K} (X^{y}_{Fe2+})^3 X^{z}_{Al} (X^{z}_{Si})^3 (X^{hyd}_{OH})^2)/0.105$ (Bohlen et al., 1980)

Total pressure is inferred to be 2 kb, and the average molar mass of the magma is calculated as 65.8. The fugacity of H2O is calculated using the expression:

$$\log f_{H2O} = \frac{G^o}{2.303RT} + \log a^{bio}_{annite} + \tfrac{1}{2} \log f_{O2} - \log a^{tmt}_{Fe304} - \log a^{san}_{KAlSi308}$$

a^{tmt}_{Fe304} is calculated as in Table 12, and the $a^{san}_{KAlSi308}$ is taken to be equal to $X^{san}_{KAlSi308}$. Hildreth (1977) has expressed the first term of the equation as:

$$\frac{G^o}{2.303RT} = \frac{8674}{T} + 2.461 + \frac{3.92 \times 10^{-3}}{T} (P-1)$$

where P is the pressure in bars and T is the temperature in degrees Kelvin.

The weight% H2O in the magma has been calculated from f_{H2O} values using the formulation of Carmichael et al. (1977). A BASIC program that performs these calculations can be requested from the author.

mineral stabilities (for example, compare Naney,1983 with Maaloe and Wyllie,1975).

The data available for the eruptive units of Los Humeros are too scant to address the question of whether a volatile gradient was superimposed on the compositional and thermal zonation of the magma chamber. However, Hildreth (1977,1981) has convincingly argued that a roofward enrichment of volatiles might be a characteristic trait of silicic magma chambers based on: (1) the increase in phenocryst content in progressively more mafic products of major compositionally zoned eruptions (see next section), (2) the enrichment of F and Cl in the most silicic ejecta of some eruptions, (3) water fugacity estimates in a large number of samples of the Bishop Tuff, USA, (4) the restriction of hydrous silicates to the more silicic products of some eruptive units, and (5) the progressive evolution from plinian-fall to pyroclastic flow emplacement mechanisms documented in several voluminous eruptions (e.g. the Zaragoza Tuff; Ferriz and Mahood,1984).

PHENOCRYST CONTENT

Perhaps one of the most striking features of the data presented in Table 3 is the large variations in phenocryst content that occur within each of the major eruptive units of Los Humeros. These variations are summarized in Figure 11, in which the phenocryst content, in weight percent, has been plotted against the bulk MgO content of each sample. MgO has been selected because it is a good indicator of the mafic character of a given sample.

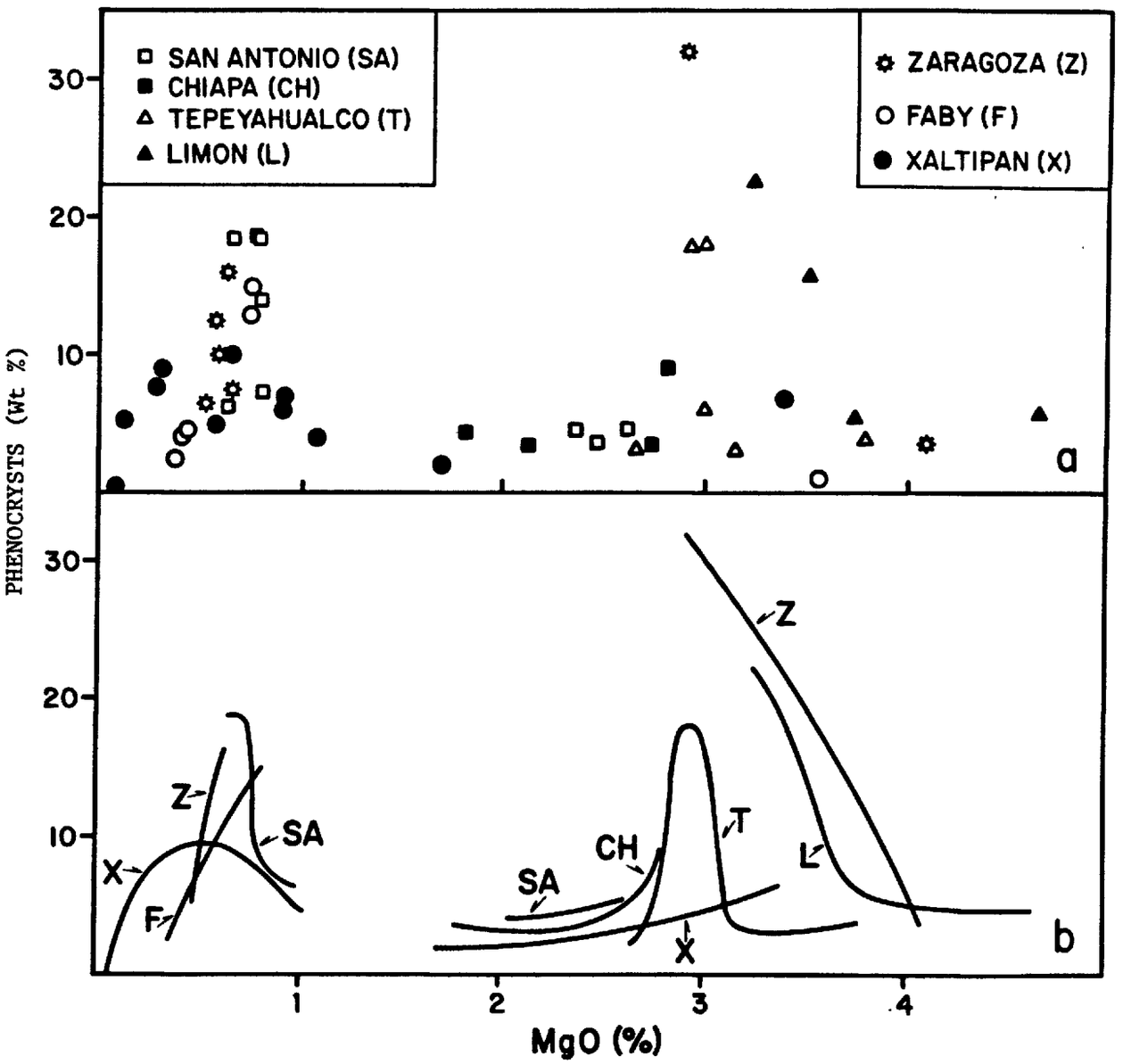

Fig. 11. Variations in phenocryst content for the major eruptive units of Los Humeros volcanic center. (a) Data points. (b) Smoothed trends.

The silicic portions of the three major eruptive units (Xaltipan, Faby, and Zaragoza Tuffs) show similar trends of increasing crystal content as the mafic character of the pumice increases. These trends are not, however, the extension of each other; for example, the most crystal-poor pumice of the Faby Tuff has the same MgO content as some of the most crystal-rich pumice of the Xaltipan Ignimbrite. This indicates that during the 220,000 and 140,000 years of repose between these eruptions a crystal-poor silicic melt was regenerated in the uppermost portions of the magma chamber.

Being adjacent to the main cooling surface, the uppermost portions of the magma chamber would be expected to have the lowest temperature. At first glance, there seems to be a contradiction with the fact that they are characterized by the lower phenocryst contents. The solution to this apparent contradiction lies in the decrease in the liquidus temperature of a magma as its mafic character decreases and as its volatile content increases.

The liquidus temperature is defined as that temperature at which crystals first form in a cooling magma. Excluding nucleation problems, the phenocryst content of a melt will increase as the difference between its actual temperature and the liquidus temperature increases. Experimental work has demonstrated that as the mafic character of a melt decreases, so does the liquidus temperature (Figure 12). Thus, in a magma chamber zoned from more silicic compositions near the top to more mafic compositions toward

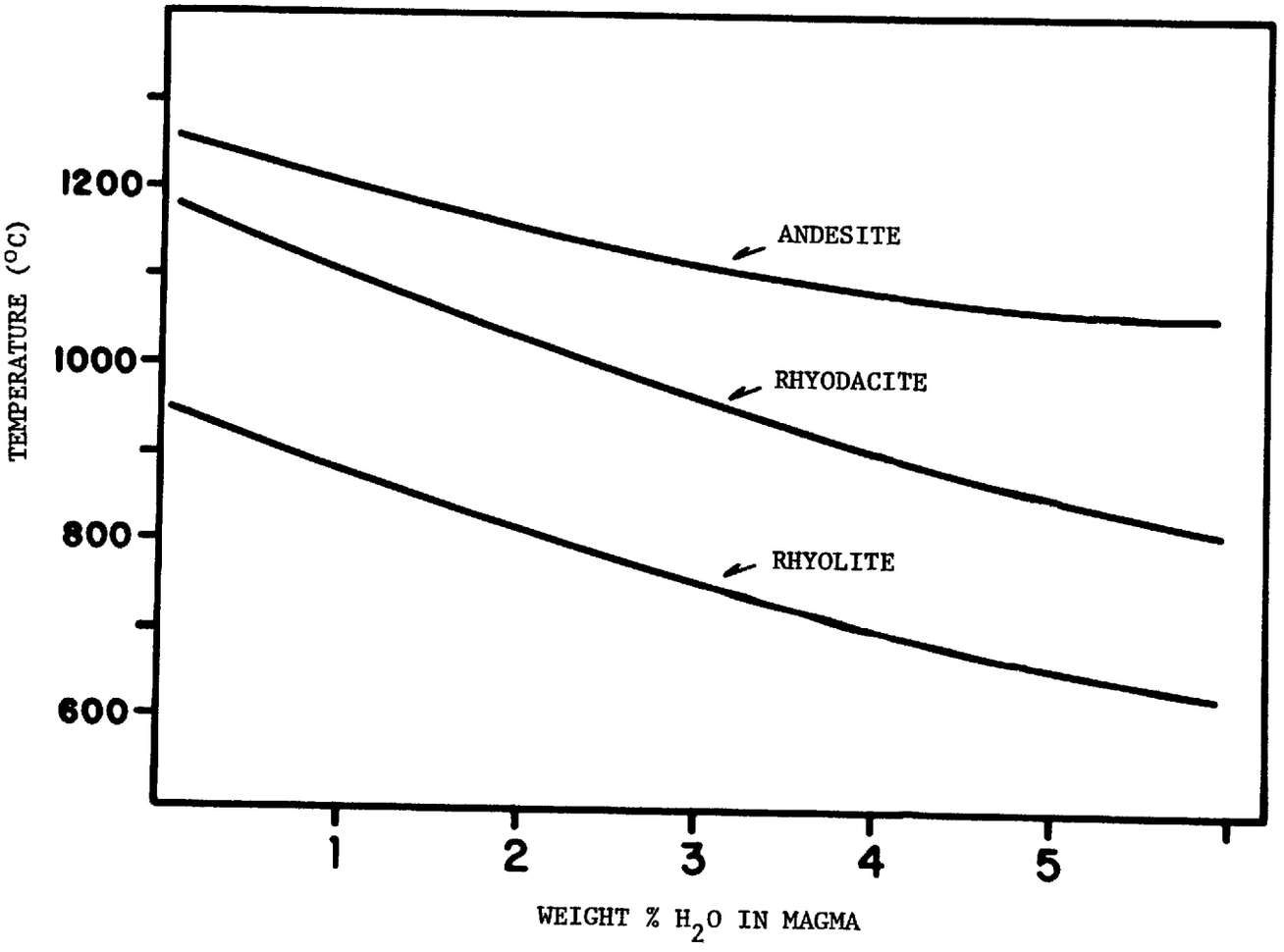

Fig. 12. Effect of bulk composition and water content on the liquidus temperature of a melt from experimental data by Burnham and Jahns (1962), Eggler (1972), and Maaloe and Wyllie (1975).

the bottom, there would be a corresponding increase in the liquidus temperature from top to bottom (Figure 13). An additional decrease in the liquidus temperature is induced by increases in the volatile content of the melt (Figure 12). Therefore, if in addition to the compositional zonation there is roofward enrichment of volatiles (Shaw,1974; Smith,1979; Hildreth,1981), the liquidus temperature will be depressed even farther, and the gradient in liquidus temperature would be particularly large in the uppermost portion of the chamber.

Changes in phenocryst content within the products of a zoned eruption can be explained by the difference between the liquidus temperature gradient and the actual temperature gradient in the magma chamber, as exemplified in Figure 13a. Figure 13a can be considered an idealized snapshot of the conditions prevailing in the magma chamber just prior to the Xâltipan eruption, and it illustrates three points: (1) A temperature gradient existed within the chamber, the least mafic portions being at a lower temperature than the most mafic portions. (2) Although the temperature is lowest in the most silicic part of the chamber, in the presence of roofward enrichment of volatiles the magma might lie above or just slightly below the strongly depressed liquidus temperature. Thus, the magma would be crystal-free or would have a low phenocryst content. This prediction is in agreement with the crystal-free (Xâltipan) or crystal-poor (Faby and Zaragoza) nature of the most silicic pumice of the three major eruptions. (3) As the melt becomes more mafic

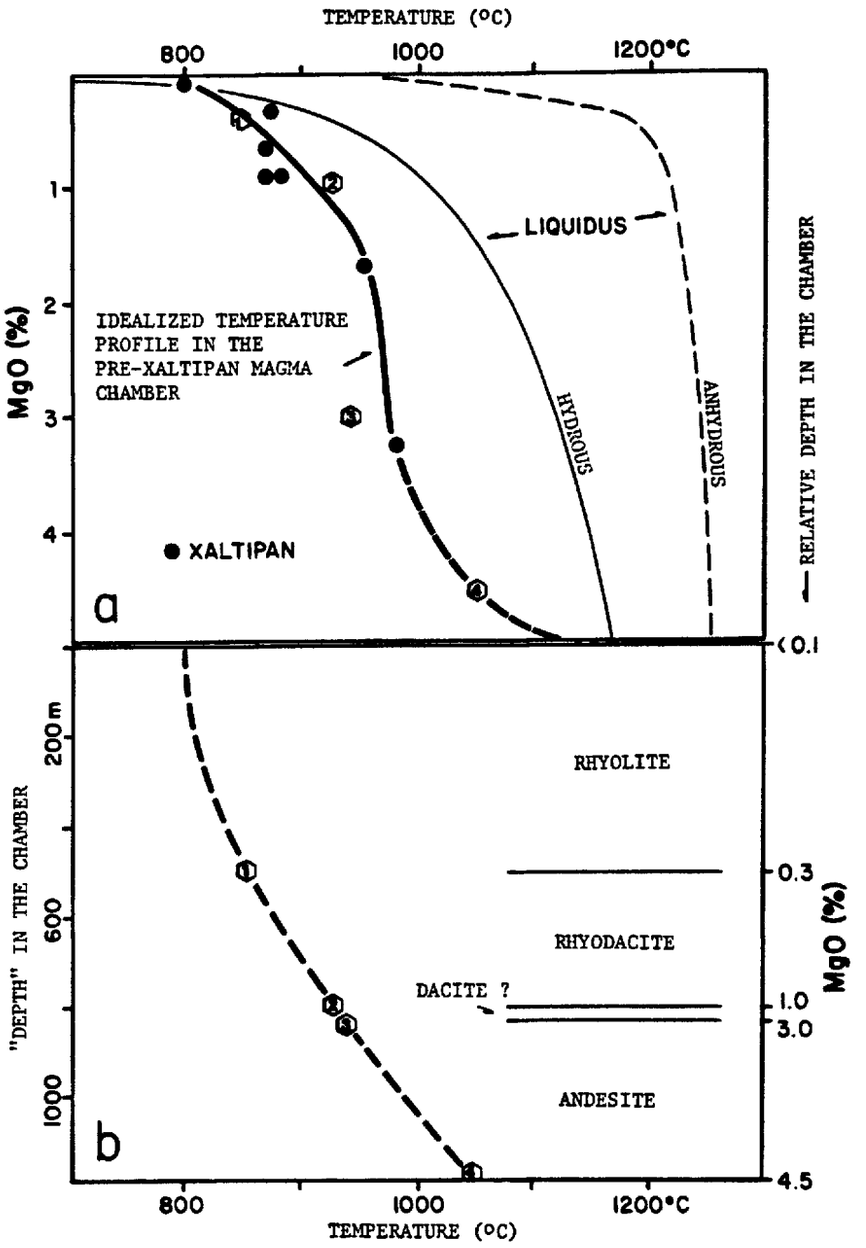

Fig. 13. (a) Comparison of hypothetical magma temperature versus liquidus temperature profiles. The magma temperature profile is loosely constrained by Fe-Ti oxide temperature estimates of Xáltipan Tuff samples; the dashed extension is hypothetic. Liquidus temperature profiles are based on Burnham and Jahns (1962), Maaloe and Wyllie (1975), and Eggler (1972). The curve labeled "hydrous" assumes a smooth water content gradient between 5 wt% a the top of the chamber to 2 wt% in the lower portions. (b) Hypothetical magma temperature gradient as a function of "depth" in the magma chamber. The "depth" has been estimated from the erupted magma volumes, and by idealizing the chamber as a cilinder 16 km in diameter (the average diameter of the Los Humeros caldera). The numbered hexagons represent arbitrary but equivalent points in (a) and (b).

the difference between the magma temperature and the liquidus temperature initially increases, so the phenocryst content would be expected to increase. Again this is confirmed by the general increase in phenocryst content observed in the silicic portion of the three major eruptions.

After the initial increase the phenocryst content of some units tends to diminish. For example, in Figure 11 it can be seen that the phenocryst content of the Xăltipan ejecta eventually reaches a maximum, diminishes as more MgO-rich compositions are reached, and finally seems to increase again in the most mafic ejecta. The andesitic portion of the Zaragoza Tuff shows a very strong reversal in phenocryst content (Figure 11), but it is uncertain whether the silicic and andesitic trends join through a maximum, or represent two different maxima with an intervening phenocryst-poor interval. The post-Zaragoza Tepeyahualco and Limón compound flows, which were emplaced within a few thousand years of each other, also show strong variations in their phenocryst contents (Figure 11). In the former, a pronounced maximum is developed, whereas in the latter the phenocryst content decreases abruptly with increasing MgO content. The patterns of the more mafic portion of the Zaragoza Tuff and those of the Tepeyahualco and Limón flows are similar, but it again must be stressed that they are not the extension of each other, and, in fact, they do not overlap. For example, the most phenocryst-rich flow unit of the Limón flow has the

same MgO content as the most crystal-poor flow unit of the Tepeyahualco flow.

The link between the trends observed in the more silicic compositions is, as stated above for the Zaragoza Tuff, uncertain. The trend observed in the Xâltipan ejecta suggests the existence of a minimum at intermediate compositions. A minimum at intermediate compositions is also suggested when the trends of the Chiapa and San Antonio lavas are considered together (Figure 11). The San Antonio lavas show a decreasing phenocryst content with increasing MgO content. The trend of the Chiapa andesites partially overlaps that of the San Antonio lavas, but at its most mafic composition the phenocryst content increases again. However, the validity of this combined trend is uncertain because, although closely related in time and space, neither the eruption of the San Antonio or Chiapa lavas can be considered an instantaneous event. The apparent trends between them could therefore be fortuitous.

The reversals in phenocryst content, or the bimodal distribution of phenocrysts within a compositionally zoned magma chamber can be explained with reference to Figure 13a, where the magma temperature gradient for the Xaltipan event has been hypothetically extended. The slope of this gradient does not decrease monotonically, since the temperature of the magma is not dependant on its MgO content but on the volume or "thickness" of the different compositional levels. It is because of this that although it would be expected for the magma temperature gradient to

be monotonic in a graph of temperature vs. "depth" in the chamber (e.g., Figure 13b), this same gradient adopts a sigmoidal shape in the T-MgO graph (Figure 13a). In contrast, the liquidus gradient depends only in the composition of the magma and is thus monotonic in the T-MgO graph. The fact that each gradient is controlled by a different parameter makes them have opposite overall curvatures (Figure 13a), so that although the difference between the two gradients initially increases, it could in principle reach a maximum and then decrease, which will result in an inversion in the total phenocryst content.

CONCLUSIONS

During the last 460,000 years, several major eruptive events periodically tapped the magma chamber of the Los Humeros volcanic center. All of these major eruptions are zoned with respect to major- and trace-element concentrations, total phenocrysts contents, and modal mineralogy. Estimation of intrinsic parameters indicates that the chamber was also zoned in temperature, oxygen fugacity, and most probably volatile content, with uppermost volatile-rich rhyolitic and rhyodacitic levels being at a lower temperature than the deeper, less volatile-rich andesitic and perhaps even basaltic levels. Similarities in the range of compositions present in each of the main eruptive units, and thermal continuity among the different compositions, indicate that the coexistence of silicic and andesitic magmas within the same chamber was a stable

process, and not the result of the fortuitous injection of andesitic magma in a silicic chamber.

Petrogenetic interpretation of the Los Humeros magmatic system must incorporate a larger data base than that presented here, namely with regard to rock chemistry (Ferriz and Mahood, in preparation). The mineralogic study, however, imposes some restrictions that must be incorporated in any petrologic model: (1) Since each major eruption sampled a wide range of compositional levels within the magma chamber, crystal fractionation models are constrained by the mineralogy and relative modal proportions of phenocrysts observed in the products of each eruption, as well as by the relative volumes of the different magma types. (2) The existence of mineral phase boundaries within the magma chamber prior to each major eruption indicates that either magma extraction mechanisms were abnormally efficient, or that some, if not all, of the minerals present in each assemblage formed after the compositional zonation of the chamber had developed. (3) The process of magma mixing is widely documented by the ubiquitous occurrence of xenocrysts and quenched mafic magma inclusions in felsic eruptive products. However, its relative petrogenetic importance remains to be assessed. The small erupted volumes of dacitic magma suggest that magma mixing was limited, but even minor mixing may have strong effects in petrogenetic indicators such as isotopic ratios and trace-element concentrations. (4) There is no indication that the

temperature of the different magma types changed much during the last 460,000 years. Simple conductive cooling models (e.g., Smith and Shaw, 1978, fig.3) suggest that this condition could not have persisted for such a large time span unless the system received additional and sustained energy input, for example in the form of hot basaltic magma injections. Petrogenetic theories should thus address the potential open-system nature of the magma chamber.

ACKNOWLEDGEMENTS

Acknowledgement is made to Mexico's Comisiòn Federal de Electricidad and Consejo Nacional de Ciencia y Tecnologia, to the Donors of the Petroleum Research Fund, administered by the American Chemical Society, and to the U.S. National Science Foundation (Grant EAR-8121380 to G.Mahood) for support of this research. Mayor element analyses provided by the Anaytical Laboratories Branch of the U.S. Geological Survey, and trace element analyses provided by courtesy of R.L.Smith (U.S. Geological Survey) are grately appreciated. Thanks are due to M.Rivers and C.Ueng for assistance in operating the microprobes, and to D.Boden, G.Mahood, D.Pohl, and C.E.Seedorff for providing helpful reviews of the manuscript.

REFERENCES

Bohlen,S.R., Peacor,D.R., Essene,E.J., 1980, Crystal chemistry of a metamorphic biotite and its significance in water barometry: Am. Mineral., v.68, p.477-493.

Buddington,A.F., Lindsley,D.H., 1964, Iron-titanium oxide minerals and synthetic equivalents: J. Petrology, v.5, p.310-357.

Burnham,C.W., Jahns,R.H., 1962, A method for determining the solubility of water in silicate melts: Am. J. Science, v.260, p.721-745.

Burnham,C.W., Holloway,J.R., Davis,N.F., 1969, Thermodynamic properties of water to 1000° C and 10,000 bars: Geol.Soc.Amer. Spec. Paper 132, 96p.

Carmichael,I.S.E., 1967, The iron-titanium oxides of salic volcanic rocks and their associated ferromagnesian silicates: Contrib. Mineral. Petrol., v.14, p.36-64.

Carmichael,I.S.E., Nicholls,J., Spera,F.J., Wood,B.J., Nelson,S.A., 1977, High-temperature properties of silicate liquids: Applications to the equilibration and ascent of basic magma: Philos. Trans. R. Soc. Lond., Ser.A, v.286, p.373-431.

Carmichael,I.S.E., Turner,F.J., Verhoogen,J., 1974, Igneous Petrology: McGraw-Hill Book Co., New York, 739p.

Christiansen,R.L., 1979, Cooling units and composite sheets in relation to caldera structure: in Chapin,C.E., and Elston,W.E., eds., Ash-flow Tuffs: Geol. Soc. Am. Spec. Paper 180, p.29-42.

Christiansen,R.L., Blank,H.R., 1972, Volcanic stratigraphy of the Quaternary rhyolite plateau in Yellowstone National Park: U.S. Geol. Surv. Prof. Pap. 82, 246p.

Eaton,G.P., Christiansen,R.L., Iyer,H.M., Pitt,A.M., Mabey,D.R., Bank,H.R., Zietz,I., Gettings,M.E., 1975, Magma beneath Yellowstone National Park: Science, v.188, p.787-796.

Eggler,D.H., 1972, Water-saturated and undersaturated melting relations in a Paricutin andesite and an estimate of water content in the natural magma: Contrib. Mineral. Petrol., v.34, p.261-271.

Eichelberger,J.C.; Gooley,R., 1977, Evolution of silicic magma chambers and their relationships to basaltic volcanism: in The Earth's Crust, Geophys. Monograph 20, Amer. Geophys. Union, p.57-77.

Ewart,A., Hildreth,W., Carmichael,I.S.E., 1975, Quaternary acid magma in New Zealand: Contr. Mineral. Petrol., v.51, p.1-27.

Ferriz,H., Mahood,G.A., 1984, Eruption rates and compositional trends at Los Humeros volcanic center, Puebla, Mexico: J. Geophys. Res., v.B89, p.8511-8524.

Ferriz,H., Mahood,G.A., in preparation, Petrology of the Los Humeros volcanic center, Puebla, Mexico: to be submitted to Contr. Mineral. Petrol.

Ferriz,H. and Yàñez,C., 1981, Mapa geolôgico del centro volcânico de Los Humeros, estados de Puebla y Veracruz, Mèxico -Edición preliminar, (Map): Comisión Federal de Electricidad, Juan de la Barrera #37, Cd. Satelite, Edo. de Mèxico, 53100, MEXICO.

Finnerty,A.A., Boyd,F.R., 1978, Pressure-dependent solubility of calcium in forsterite coexisting with diopside and enstatite: Carnegie Inst. Wash. Year Book, v.77, p.713-717.

Gill,J.B., 1981, Orogenic Andesites and Plate Tectonics: Springer-Verlag, New York, 390p.

Hildreth,E.W., 1977, The magma chamber of the Bishop Tuff: Gradients in temperature, pressure, and composition [Ph.D. thesis]: Berkeley, University of California, 328p.

Hildreth,E.W., 1979, The Bishop Tuff: Evidence for the origin of compositional zonation in silicic magma chambers, in Chapin,C.E., and Elston,W.E., eds., Ash-flow Tuffs: Geol. Soc. Am. Spec. Paper 180, p.43-75.

Hildreth,E.W., 1981, Gradients in silicic magma chambers: Implications for lithospheric magmatism: J. Geophys. Res., v.B86, p.10153-10192.

Hildreth,E.W., 1983, The compositionally zoned eruption of 1912 in the Valley of Ten Thousand Smokes, Katmai National Park, Alaska: J. Volcanol. Geotherm. Res., v.18, p.1-56.

Huebner,J.S., 1980, Pyroxene phase equilibria at low pressure, in Prewitt,C.T., ed., Pyroxenes: Mineral. Soc. Am. Reviews in Mineralogy, v.7, p.213-288.

Irvine,T.N., Baragar,W.R., 1971, A guide to the chemical classification of the common igneous rocks: Can.J. Earth Sci., v.8, p.523-548.

Leake,B.E., 1978, Nomenclature of amphiboles, Am. Mineral., v.63, p.1023-1052.

Lindsley,D.H., 1983, Pyroxene thermometry: Am. Mineral., v.68, p.477-493.

Lipman, P.W., Christiansen,R.L., O'Connor,J.T., 1966, A compositionally zoned ash-flow sheet in Southern Nevada: U.S. Geol. Surv. Prof. Pap. 524-F, 47p.

Maaloe,S., Wyllie,P.J., 1975, Water content of a granite magma deduced from the sequence of crystallization determined experimentally with water-undersaturated conditions, Contrib. Mineral. Petrol., v.52, p.175-191.

Mahood,G.A., 1981a, Chemical evolution of a Pleistocene rhyolitic center: Sierra La Primavera, Jalisco, Mexico: Contrib. Mineral. Petrol., v.77, p.129-149.

McBirney,A.R., 1980, Mixing and unmixing of magmas: J. Volcanol. Geotherm. Res., v.7, p.357-371.

Mathez,E.A., 1973, Refinement of the Kudo-Weill plagioclase thermometer and its application to basaltic rocks: Contrib. Mineral. Petrol., v.41, p.61-72.

Naney,M.T., 1983, Phase equilibria of rock-forming ferromagnesian silicates in granitic systems: Am.J.Science, v.283, p.993-1033.

Nichols,R.L., Flow units in basalts, J. Geol., 44, 617-630, 1936.

Shaw,H.R., 1974, Diffusion of H_2O in granitic liquids: Part I. Experimental data; Part II. Mass transfer in magma chambers: in Geochemical Transport and Kinetics, edited by A.W.Hofmann, B.J.Giletti, H.S.Yoder, R.A.Yund, Carnegie Inst. Wash. Publ. 634, p.139-170.

Smith,R.L., 1979, Ash-flow magmatism: in Chapin,C.E., and Elston,W.E., eds., Ash-flow Tuffs: Geol. Soc. Am. Spec. Paper 180, p.5-27.

Smith,R.L., and Bailey,R.A., 1966, The Bandelier Tuff: A study of ash-flow eruption cycles from zoned magma chambers: Bull. Volcanol., v.29, p.83-104.

Smith,R.L., and Shaw,H.R., 1978, Igneous-related geothermal systems: U.S. Geol. Surv. Circular 790, p.12-17.

Spencer,K.J., and Lindsley,D.H., 1981, A solution model for coexisting iron-titanium oxides: Am. Mineral., v.66, p.1189-1201.

Stormer,J.C., 1983, The effects of recalculation on estimates of temperature and oxygen fugacity from analyses of multicomponent iron-titanium oxides: Am. Mineral., v.68, p.586-594.

Swanson,D.A., Wright,T.L., and Helz,R.T., 1975, Linear vent systems and estimated rates of magma production and eruption for the Yakima basalt on the Columbia Plateau: Am. J. Science, v.275, p.877-905.

Taylor,H.P., 1968, The oxygen isotope geochemistry of igneous rocks: Contrib. Mineral. Petrol., v.19, p.1-71.

Wones,D.R., 1972, Stability of biotite - a reply: Am. Mineral., v.57, p.316-317.

Wones,D.R., and Eugster,H.P., 1965, Stability of biotite: experiment, theory and application: Am. Mineral., v.62, p.687-691.

Ferriz,H., Mahood,G.A., in preparation, Strong compositional zonation in a silicic magmatic system of the Mexican Neovolcanic Belt: Los Humeros, Puebla: To be submitted to Contrib. Mineral. Petrol.

CHAPTER 3

STRONG COMPOSITIONAL ZONATION IN A SILICIC MAGMATIC SYSTEM OF THE MEXICAN NEOVOLCANIC BELT: LOS HUMEROS, PUEBLA

ABSTRACT

The Los Humeros volcanic center, located 180 km east of Mexico City, is one of several silicic volcanic centers located in the "back-arc" portion of the Mexican Neovolcanic Belt. Eruptive products span the compositional range high-silica rhyolite to basalt. During the last 460,000 years, three major plinian eruptions and an extended period of lava flow emplacement periodically "sampled" the magma chamber. The eruptive products of these events are compositionally zoned and indicate that the magma chamber was zoned from rhyolitic uppermost levels to andesitic and perhaps basaltic lower levels.

Major-element variations seem to have been controlled, to a large extent, by crystal-liquid equilibria. Partial melting of young crustal lithologies accounts best for volume relations, but must be complemented by fractional crystallization coupled with assimilation to explain compositional and isotopic variations. The distribution patterns of elements such as Ni, Cr, Sr, and Rb, further suggest episodic events of magma mixing.

Strong compositional zonation persisted throughout the lifetime of the system, although erupted magmas show an overall trend with time toward more mafic compositions because eruptive rates seem to have exceeded the rate of regeneration of differentiated magma. During the last 0.5 Ma the thermal input was apparently small enough to inhibit generation of differentiated magma by partial melting of the

wall rocks, but large enough to offset conductive or hydrothermal cooling that would promote crystallization.

INTRODUCTION

Voluminous eruptions represent instantaneous samples of a magma reservoir, and hence contain information about magma compositions, phenocryst assemblages, pressure, temperatures, and volatile fugacities prevailing in the chamber just before the eruption. Furthermore, a sequence of voluminous eruptions provides a record of the chemical and physical evolution of the magma reservoir. The objectives of this paper are (1) to document the compositional variations of the eruptive units of Los Humeros volcanic center, which represents the surface expression of a magma chamber where strong compositional zonation persisted for at least 0.46 Ma, (2) to evaluate the roles of different mechanisms that may have led to development of this zonation, and (3) to speculate about the physical parameters that controlled an overall trend with time toward eruption of more mafic compositions.

Previous geologic work at Los Humeros includes photogeologic mapping by Pêrez (1978), regional geologic mapping by Yâñez and Casique (1980), and detailed mapping by Ferriz and Yâñez (1981). Ferriz and Mahood (1984) describe the physical evolution of the center. Reconnaissance geochemical and isotopic data are presented by Verma and Lôpez (1983) and Verma (1983, 1984).

For the purpose of discussion, we have arbitrarily divided the magma types erupted at Los Humeros into five groups based on their silica content, recalculated on an anhydrous basis: rhyolites (>72% SiO_2), rhyodacites (72 to 67% SiO_2), dacites (67 to 63% SiO_2), andesites (63 to 53% SiO_2), and basalts (<53% SiO_2).

SUMMARY OF THE GEOLOGIC HISTORY

The following summary, based on Ferriz and Mahood (1984), provides the names of the different eruptive units and their bulk compositions, volumes, and K-Ar ages. A simplified geologic map is presented in Figure 1, and a summary of the geologic history is presented in Table 1.

The Los Humeros volcanic center, located 180 km east of Mexico City, is one of several Pleistocene silicic centers in the "back-arc" portion of the Mexican Neovolcanic Belt (Ferriz and Mahood, in press). The oldest exposed volcanic rocks at Los Humeros are Pliocene tholeiitic andesites and ferrobasalts of the Teziutlán Formation. Silicic volcanism began ~0.47 Ma ago with extrusion of high-silica rhyolite domes (A and B in Figure 1). Shortly thereafter, at 0.46 Ma ago, 115 km^3 of magma zoned from high-silica rhyolite to andesite were erupted as the Xáltipan Ignimbrite and related small-volume air-fall tuffs. Resultant collapse formed the 21-by-15-km Los Humeros caldera. High-silica biotite rhyolite domes, erupted shortly thereafter along the ring-fracture zone (C, D, and E in Figure 1), are interpreted as residual rhyolitic magma from the Xáltipan event. Later

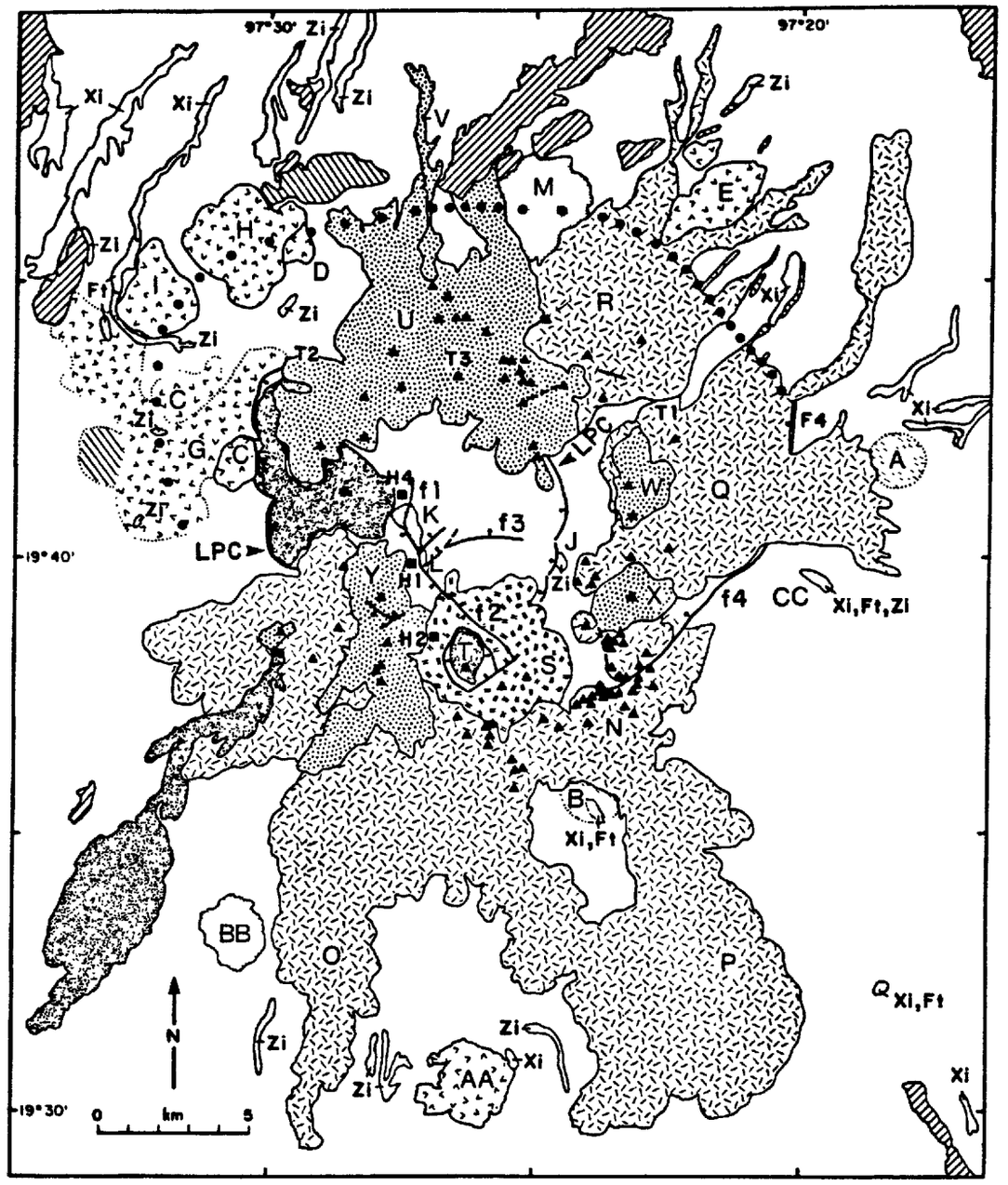

Fig. 1. Simplified geologic map of the Los Humeros volcanic center (based on *Ferriz and Yañez* [1981]). Heavy dots indicate the inferred northern topographic and structural boundary of the Los Humeros caldera. LPC indicates the eastern and western boundary faults of the Los Potreros caldera. Dotted contacts indicate largely buried units. Light stipple indicates the post-Zaragoza but pre-Xoxoctic, Las Aguilas rhyolite dome (BB) and Cueva Ahumada basaltic andesite, andesite (K), and rhyodacite lavas (L), and the Las Lineas rhyodacite dome (M). Random dashes indicate the Tepeyahualco (O), Limón (P), Orilla del Monte (Q), and Chiapa (R) andesite and basaltic andesite lavas and cinder cones. Double dashes indicate the Maztaloya (S) basaltic andesite, andesite and rhyodacite lavas and agglutinates. The heavy dot pattern indicates the San Antonio (U), Viola (W), Cuamilacas (X), and Arenas (Y) rhyodacitic lavas and tuff cones and the Papata (V) andesite flow. Unpatterned areas are outcrops of the Xáltipan Ignimbrite (Xi), Faby Tuff (Ft), and Zaragoza Ignimbrite (Zi), or alluvium and soil underlain by pyroclastic deposits of various types. Most of the area shown outside the Los Humeros caldera is underlain by the Xáltipan and Zaragoza Ignimbrites; on the east side of the map area the Faby Tuff is present as well. Within and slightly east of the Los Potreros caldera, most areas are underlain by the Xoxoctic and Cuicuiltic tuffs. T1, T2, and T3 indicate locations of telluric anomalies [*Alvarez*, 1978*b*, 1980]. Fault scarps are labeled f1 to f4. See text for other lettered units.

ring-fracture high-silica rhyolite lavas are aphyric (Caltonac flow; G) or hypersthene-bearing (Ocotepec rhyolites; H and I), and are interpreted as the early manifestations of the second major eruptive cycle. This second cycle culminated in eruption of the 0.24-Ma Faby Tuff, a dominantly rhyodacitic sequence of plinian fall deposits that represents ~10 km^3 of magma. A third major event occurred ~0.1 Ma ago with eruption of the Zaragoza Tuff, a nonwelded ignimbrite zoned from rhyodacite to andesite. Eruption of the 12 km^3 of magma represented by this tuff led to collapse of the 10-km-diameter Los Potreros caldera, which is nested within the older Los Humeros caldera. The 0.6-km^3 dacitic Xoxoctic Tuff, erupted ~0.05 Ma ago, drapes the walls of the Los Potreros caldera. Between 0.04 and 0.03 Ma ago, an arc of andesitic scoria cones, concentrated along the southern ring-fracture zone of the Los Humeros caldera, fed the Tepeyahualco (O), Sarabia, and Limón (P) compound flows that extend south of volcanic center, and andesite lavas built the small Orilla del Monte (Q) and Chiapa (R) shields between the eastern rims of the two calderas. Approximately 6 km^3 of andesitic magma were extruded during this stage. Simultaneous venting of the rhyodacitic and andesitic tephra of the 0.1-km^3 Cuicuiltic Tuff from a small volcano in the southern ring-fracture zone of the Los Potreros caldera led to formation of the 1.7-km-diameter El Xalapazco caldera (T). Minor fault-bounded uplift of the southeastern quadrant of the Los Potreros caldera followed. Activity continued up to 0.02 Ma ago with

Table 1. Summary of the geologic history of the Los Humeros volcanic center.

Date, Ma	Event	Estimated magma volume (km3)
>1.6	Eruption of Teziutlan lavas	60
0.47	Eruption of precaldera rhyolite domes	0.1
0.46	Eruption of Xaltipan Ignimbrite	115
	Collapse of Los Humeros caldera	
0.36	Eruption of post-Xaltipan biotite rhyolites	3
0.22 (±0.02)	Eruption of pre-Faby orthopyroxene rhyolites	2
0.24 (±0.03)	Eruption of Faby Tuff	10
~0.10	Eruption of Zaragoza Tuff	12
	Collapse of Los Potreros caldera	
	Gentle doming of eastern portion of the LHVC	
0.06	Eruption of Cueva Ahumada lavas	0.1
	Eruption of Xoxoctic Tuff	0.6
	Eruption of Llano Ignimbrite	0.1
0.04-0.02	Eruption of the Limon and other andesites	6
	Eruption of Maztaloya lavas and agglutinates	1
	Eruption of Cuicuiltic Tuff	0.1
	Collapse of El Xalapazco caldera	
	Uplift of the SE quadrant of Los Potreros caldera	
0.03-0.02	Eruption of the San Antonio and other rhyodacites	10
<0.02	Eruption of olivine basalts	0.25

From Ferriz and Mahood (1984, tables 1 and 3).

eruption of 10 km^3 of rhyodacitic and minor andesitic lava flows from centers near the northern margin of the Los Potreros caldera (San Antonio lavas; U), in the area between the eastern rims of the two calderas (W and X), and within a broad band where the southern segments of the inferred Los Humeros and Los Potreros ring-fracture zones nearly coincide (Arenas lavas; Y). The latest stage of volcanic activity is represented by ~0.25 km^3 of olivine basalts erupted during the last 0.02 Ma along the southern ring-fracture zone of the Los Humeros caldera and on the floors of the Los Potreros and El Xalapazco calderas (Figure 1).

Large systematic variations in major-element contents of the products of the main eruptive events at Los Humeros, as illustrated for SiO_2 in Figure 2, indicate that the magma chamber was strongly zoned in composition throughout most of its history. Because the densities of metaluminous magmas decrease as they become more silicic, a compositionally zoned chamber would tend to be density stratified (Smith,1979), with more silicic magmas collecting in the upper portions of the chamber. Figure 2 also illustrates the conspicuous dearth of material in the range 63 to 67 wt% SiO_2 throughout the lifetime of the system. There are a few dacitic samples whose silica content falls within this gap, but the presence of strongly magnesian olivine and clinopyroxene (Ferriz, in press) suggests that these small volumes of dacite are the result of limited mixing between rhyodacitic and andesitic magma.

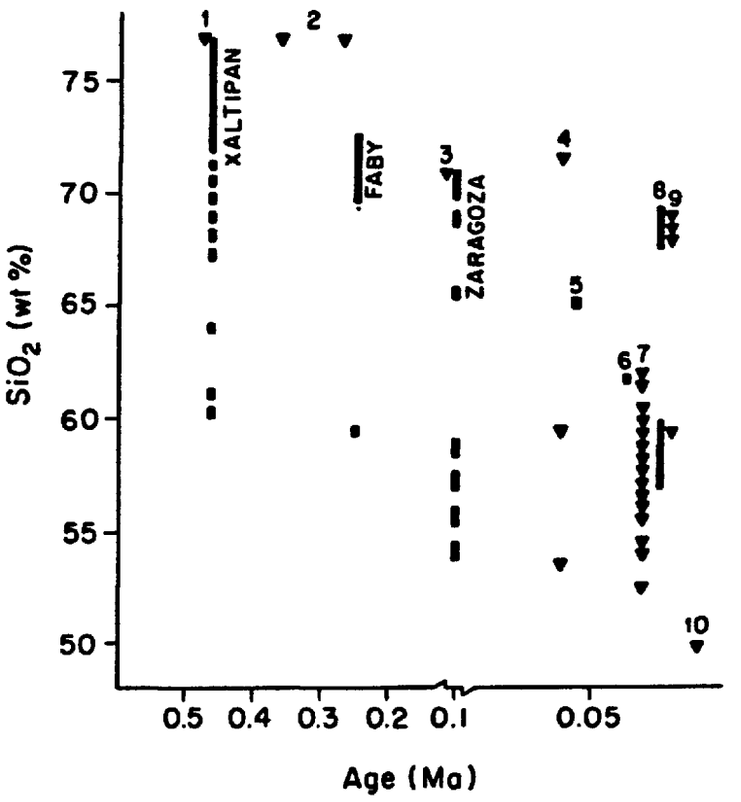

Fig. 2. SiO_2 ranges (recalculated anhydrous) versus age of major eruptive units of the LHVC. Bars indicate pyroclastic units, the continuous portion representing the predominant volume; triangles indicate lavas. 1, pre-Xáltipan rhyolites; 2, post-Xáltipan rhyolites; 3, pre-Zaragoza rhyodacite; 4, Cueva Ahumada lavas; 5, Xoxoctic Tuff; 6, Llano Ignimbrite; 7, andesites and basaltic andesites; 8, Cuicuiltic Tuff; 9, rhyodacites and minor andesites; 10, olivine basalts.

Erupted magmas show an overall trend with time toward more mafic compositions (Figure 2), perhaps because average eruptive rates increased with time and eventually exceeded the rate of regeneration of differentiated magma. Volumetric eruptive rates increased from ~0.06 km^3 per thousand years 0.24 Ma ago to ~0.2 km^3 per thousand years in the last 0.1 Ma (Ferriz and Mahood, 1984). The increase in eruptive rate was probably the result of a progressive decrease in the structural integrity of the roof zone of the system as successive caldera-forming eruptions reactivated old zones of weakness and created new ones. An increasingly disrupted roof may have allowed mafic and intermediate magmas to reach the surface relatively rapidly, decreasing their residence time in a high-level chamber and thus the time available for their differentiation.

MINERALOGY

All the major eruptive units of Los Humeros show both changes in mineral assemblages and large ranges in total phenocryst content (Table 2). A detailed description of these variations, together with representative microprobe analyses of the principal phenocrystic phases, is presented in Ferriz (in press; Chapter 2 of this thesis).

Plagioclase phenocrysts are present in all porphyritic products. Biotite, in some cases containing inclusions of apatite and zircon, is present only in the rhyodacitic portions of the Xáltipan Tuff and the early post-Xáltipan rhyolite domes. Hornblende is rare; in the Faby and

Table 2. Modal mineralogy (in weight %) of selected samples. *

	SAMPLE	SiO2 (%)	MgO (%)	CRYSTALS IN WT%	san	pl	bio	hbl	opx	cpx	ol	tot-ile
	LH7	77.2	<0.10	0								
	LH13	73.1	0.28	8	tr	1	4			0.5		2
XALTIPAN	LH11	71.5	0.31	8	0.5	1	4		tr	0.5		1.5
TUFF	LH19	69.8	0.91	9		3	tr	tr	3	1	tr	1.5
	LH20	66.8	1.07	8		3	0.5	tr	1.5	1	tr	1.5
	LH17	61.3	3.38	7		2				2.5	1.5	1
POST-XALTIPAN RHYOLITE	LH25	76.6	0.14	6	2	1	1		0.5			1
PRE-FABY	LH27	76.1	0.13	0								
RHYOLITES	LH30	76.1	0.13	5	0.5	2			1	tr		1
	LH31	72.5	0.37	3		1.5			1			0.5
FABY	LH33	72.2	0.43	6		2	tr	1	1.5		tr	1
TUFF	LH34	69.4	0.75	18		8			4	4		2
	LH35	59.1	3.55	1		tr			tr	tr	tr	tr
	LH41	71.1	0.52	7		3			2	1		1
	LH48	70.4	0.57	14		9			3	0.5		1.5
ZARAGOZA	LH44	69.9	0.63	18		11			4	1		2
TUFF	LH45	59.1	2.90	33		22			2	7		2
	LH47	54.4	4.08	5		1			1	0.5	0.5	2
XOXOCTIC TUFF	LH53	65.1	1.70	2		0.5				1	0.5	0.5
	LH60	59.5	2.65	3		2				1		0.5
TEPEYAHUALCO	LH61	59.2	2.92	18		11			1.5	4	0.5	1
FLOW	LH55	57.8	3.14	3		2				1	0.5	
	LH57	56.1	3.78	4		2				1	1	0.5
LIMON	LH65	56.5	3.23	22		16				5	1.5	
FLOW	LH62	53.6	4.64	6		3					3	
CHIAPA	LH72	63.1	1.81	4		2			0.5	1		1
FLOWS	LH70	58.3	2.81	9		8				1	0.5	
	LH82	69.0	0.79	15		8			1.5	3		2
SAN ANTONIO	LH81	68.7	0.80	9		3		0.5	1.5	1	tr	1.5
FLOWS	LH84	60.8	2.35	5		2			0.5	1	0.5	1
	LH89	59.6	2.61	5		3				1	1	
OLIVINE BASALT	LH94	49.0	8.93	7		1					5	0.5

* Simplified from Ferriz (in press, table 3).

Table 3. Average compositions of the predominant mineral phases. *

	Magma composition		
	Rhyolitic	Rhyodacitic	Andesitic
Plagioclase			
Xáltipan	An(15-20)Ab(77-73)Or(8-7)	An(21-41)Ab(70-55)Or(9-4)	An(67)Ab(32)Or(1)
Faby		An(31-38)Ab(65-59)Or(3-4)	An(57)Ab(43)Or(3)
Zaragoza		An(29-36)Ab(66-61)Or(5-3)	An(60-63)Ab(39-36)Or(1)
Post-Zaragoza lavas		An(34-38)Ab(62-59)Or(4-3)	An(39-80)Ab(58-19)Or(0-3)
Orthopyroxene			
Xáltipan	En(46)Fs(52)Wo(2)	En(55-60)Fs(37-42)Wo(2-3)	
Faby		En(57-63)Fs(40-35)Wo(3-2)	En(63)Fs(35)Wo(2)
Zaragoza		En(57-58)Fs(40-39)Wo(3)	En(67-69)Fs(30-28)Wo(3)
Post-Zaragoza lavas		En(59-64)Fs(38-33)Wo(3)	En(60-63)Fs(37-34)Wo(3)
Clinopyroxene			
Xáltipan	En(27-34)Fs(31-23)Wo(42-43)	En(43-44)Fs(37-42)Wo(40-43)	En(43)Fs(13)Wo(44)
Faby		En(41)Fs(16)Wo(43)	En(46)Fs(12)Wo(42)
Zaragoza		En(38)Fs(21-20)Wo(42-41)	En(43-44)Fs(16-14)Wo(41-42)
Post-Zaragoza lavas		En(39-41)Fs(18-17)Wo(43-42)	En(40-46)Fs(20-11)Wo(40-43)

* From Ferriz (in press, tables 4 and 6).

Cuicuiltic Tuffs it is present in the moderately silicic pumice but absent in the most and least silicic ones. Augite and orthopyroxene are the most abundant mafic phases in most post-Xâltipan eruptive units, although orthopyroxene is in some cases absent in the more mafic products of each unit, in which olivine is commonly present. Titanomagnetite and ilmenite are among the first-crystallized phases in rhyolitic and rhyodacitic products, but the latter is scarce or completely absent in andesitic ones. Very small amounts of quartz and sanidine have been observed only in a few rhyodacitic pumice fragments of the Xâltipan Ignimbrite and in the post-Xâltipan and pre-Faby rhyolites. As shown in Table 3, the compositions of the dominant phases change with the bulk composition of the host (and presumably with depth, temperature, and volatile content within the zoned magma chamber).

Ferriz (in press) suggested that, in general, the large changes in the phenocryst content of each eruptive unit, some of which show reversals in phenocryst content (Table 2), reflect the relative difference between the magma temperature gradient within the chamber and the composition-dependent liquidus gradient (Figure 3). The depression of the liquidus due to changes in composition alone seems insufficient, however, to explain abrupt transitions like the one observed in the Faby Tuff, in which the phenocryst content increases abruptly from 3 to 15 wt% as the silica content of the host changes from 72.5 to 69.4 wt%. Such an abrupt roofward decrease in crystal content accompanying

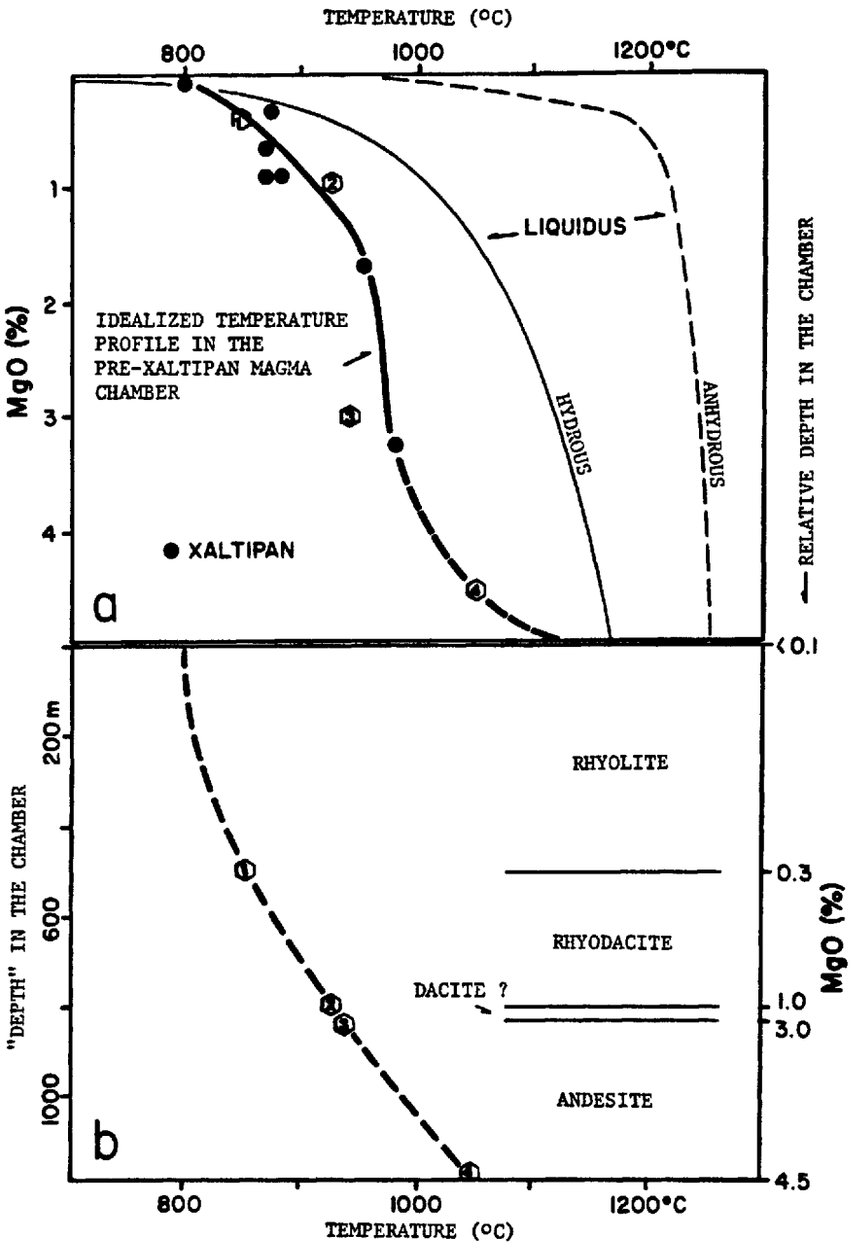

Fig. 3. (a) Comparison of hypothetical magma temperature versus liquidus temperature profiles. The magma temperature profile is loosely constrained by Fe-Ti oxide temperature estimates of Xaltipan Tuff samples; the dashed extension is hypothetic. Liquidus temperature profiles are based on Burnham and Jahns (1962), Maaloe and Wyllie (1975), and Eggler (1972). The curve labeled "hydrous" assumes a smooth water content gradient between 5 wt% a the top of the chamber to 2 wt% in the lower portions. The sigmoidal shape of the magma temperature gradient is due to the fact that the temperature of the magma is not dependant on its MgO content but on the volume or "thickness" of the different compositional levels. (b) Hypothetical magma temperature gradient as a function of "depth" in the magma chamber. The "depth" has been estimated from the erupted magma volumes, and by idealizing the chamber as a cilinder 16 km in diameter (the average diameter of the Los Humeros caldera). The numbered hexagons represent arbitrary but equivalent points in (a) and (b).

only minor changes in bulk composition seems to point to a strong depression of the liquidus by concentration of volatiles in the upper portion of the magma chamber (Mahood, 1981b). The similar patterns of increasing phenocryst content in progressively less silicic pumice observed in the silicic portions of the three major pyroclastic eruptions (XÃltipan, Faby, and Zaragoza) indicates that the 220,000 and 140,000 years of repose between them provided ample time for regeneration of crystal-poor (and probably volatile-rich) upper levels within the chamber. The strong reversals in the phenocryst content of the major eruptive units (Table 2), the correlation between mineral and whole-rock chemistry, and the progressive changes in phenocryst assemblages within each compositionally zoned unit argue against crystal settling as an explanation for the large changes in total phenocryst contents.

INTENSIVE PARAMETERS

Temperature and oxygen fugacity

Temperatures and oxygen fugacities estimated from coexisting Fe-Ti oxides (Spencer and Lindsley, 1981) are shown in Figure 4. Pre-eruptive temperatures of rhyolitic magmas were probably in the range 800° - 875° C, 860° - 940° C for rhyodacitic magmas, 920° - 1000° C for andesitic magmas, and greater than 1100° C for the late-erupted olivine basalts. Temperatures of magmas of similar composition did not change significantly during the last 0.46 Ma, which suggests that the magma chamber received

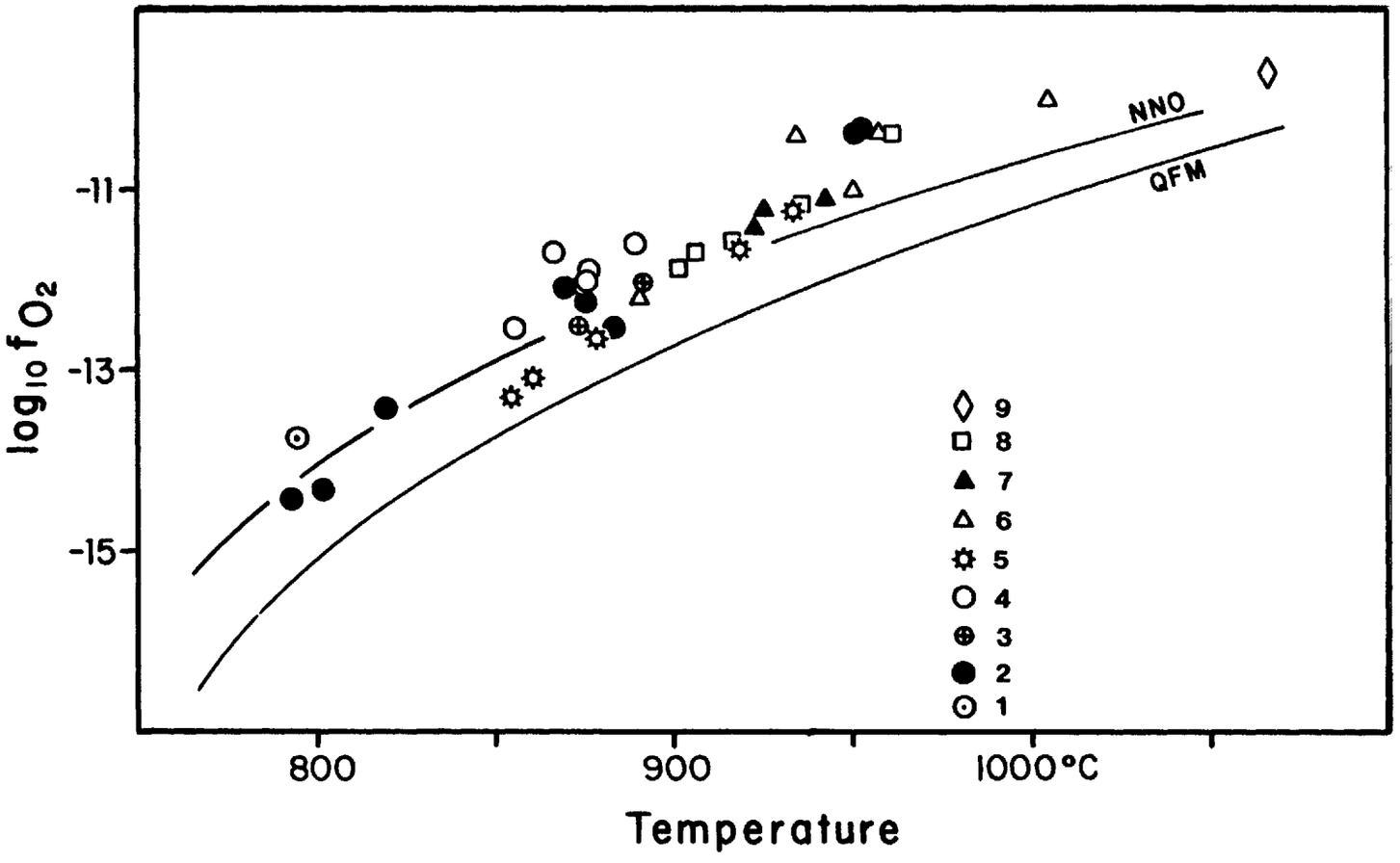

Fig. 4. Fe-Ti oxide temperature and oxygen fugacity estimates (Spencer and Lindsley,1981) for samples from the Los Humeros volcanic center. 1 pre-Xàltipan rhyolite, 2 Xàltipan Tuff, 3 post-Xàltipan biotite rhyolite and pre-Faby opx rhyolite, 4 Faby Tuff, 5 Zaragoza Tuff, 6 Tepeyahualco, Chiapa, and San Antonio andesites, 7 Cuicuiltic Tuff, 8 San Antonio and Arenas rhyodacites, 9 olivine basalt.

continuous although perhaps episodic thermal energy input during its lifetime, probably through underplating of basaltic magma (e.g, Lachenbruch et al., 1976; Smith and Shaw,1978). Addmitedly, in a chamber without sustained thermal input the heat loss to the wall rocks could be balanced by the latent heat of crystallization, but then one would expect to see a progressive increase with time of the phenocryst content of equivalent magma types or a significant degree of regeneration of differentiated magma (cf. Thorarinsson, 1967). Neither of these features is evident at Los Humeros.

Total pressure

The presence of collapse structures at Los Humeros is the strongest evidence that the magma chamber was emplaced at a shallow level in the crust, as stress relaxation linked to voluminous magma withdrawal from a deep-seated chamber would be expected to be distributed throughout the crust. Total pressures calculated with the titanomagnetite-quartz-orthopyroxene geobarometer, using the formulation of Hildreth (1977) and mineral data from the rhyolitic portion of the Xâltipan Ignimbrite and one of the post-Xâltipan biotite rhyolites range from 1.1 to 2.4 kb (Table 4). These pressures correspond to depths between 4 and 9 km.

Water fugacity

Water fugacities are estimated from the biotite-titanomagnetite-sanidine geobarometer (Wones and Eugster,1965), using Hildreth's (1977) formulation. Assuming

Table 4. Estimates of total pressure.

a^{opx}_{FeSiO3}	a^{tmt}_{Fe3O4}	a^{quartz}_{SiO2}	T °C	$-\log f_{O2}$	Pressure (kb)
0.504	0.5159	1	793	14.42	2.4
0.504	0.4935	1	802	14.32	2.1
0.504	0.5877	1	802	14.32	1.1

Pressure was calculated using the expression:

$$P = \frac{12399 - T\ (\log K + 3.621)}{0.0859} + 1 \qquad \text{(Hildreth, 1977)}$$

where P is pressure in bars, T is temperature in degrees Kelvin, and:

$$K = \frac{a^{tmt}_{Fe3O4}\ (a^{quartz}_{SiO2})^3}{a^{opx}_{FeSiO4}\ (f_{O2})^{\frac{1}{2}}}$$

$$a^{tmt}_{Fe3O4} = 0.5\ n_{Fe3+,F}\ (X_{Fe2+,S2+})\ (X_{Fe3+,S3+}) \qquad \text{(Stormer, 1983)}$$

$$a^{opx}_{FeSiO3} = (X^{M1}_{Fe} \cdot X^{M2}_{Fe})^{\frac{1}{2}} \qquad \text{(Ewart et al., 1975)}$$

$$a^{quartz}_{SiO2} = X^{quartz}_{SiO2}$$

a total pressure of 2 kb, data from two biotite-bearing rhyolitic samples of the Xâltipan Ignimbrite and from a sample of one of the post-Xâltipan rhyolites indicate water fugacities between 0.4 and 1 kb, depending on the way in which the activity of annite in biotite is calculated (Table 5). These values would be equivalent to a P_{H2O} of 0.44 and 1.2 kb (Burnham et al., 1969). Because the calculated water pressures are smaller than the assumed total pressure of 2 kb, the magma presumably was not water-saturated. Assuming a mean value of 65.8 for the gram formula mass of the melt and a total pressure of 2 kb, water fugacities can be converted to weight percent water contents using the method of Carmichael et al. (1977). Water fugacities between 0.4 and 1 kb are equivalent to water contents between 3.3 and 5.5 wt%.

The virtual absence of hydrous phases in the major post-Xâltipan eruptive units does not necessarily imply that the magma itself was relatively dry. More mafic compositions and higher average temperatures could have inhibited crystallization of biotite and hornblende. For example, Naney (1983) found that in a synthetic rhyodacitic melt at 2 kb the assemblage opx-plag is stable at water contents between 2 and 3 wt% for temperatures similar to those of the Faby and Zaragoza Tuffs. At lower water contents clinopyroxene joins the assemblage, whereas at higher water contents plagioclase becomes unstable. The transition from opx-pl-tmt-ilm to opx-cpx-pl-tmt-ilm$\pm$hbl assemblages observed in the Faby Tuff could be a natural

Table 5. Estimates of H2O content (wt%) in rhyolitic magma.

a^{bio}_{annite}		a^{tmt}_{Fe3O4}	$a^{san}_{KAlSi3O8}$	T °C	-log f_{O2}	f_{H2O} (bars)	Wt% H2O
0.1190	(1)	0.5159	0.5567	793	14.42	1027	5.4
0.0672	(2)	0.5159	0.5567	793	14.42	580	3.9
0.0655	(3)	0.5159	0.5567	793	14.42	565	3.9
0.0972	(1)	0.4935	0.6075	802	14.32	770	4.5
0.0548	(2)	0.4935	0.6075	802	14.32	434	3.3
0.0539	(3)	0.4935	0.6075	802	14.32	427	3.3
0.1121	(1)	0.5877	0.5995	802	14.32	756	4.5
0.0656	(2)	0.5877	0.5995	802	14.32	442	3.3
0.0643	(3)	0.5877	0.5995	802	14.32	433	3.3

(1) $a^{bio}_{annite} = (X^{y}_{Fe2+})^3$ (Wones, 1972)

(2) $a^{bio}_{annite} = X^{x}_{K} (X^{y}_{Fe2+})^3 (X^{hyd}_{OH})^2$ (Hildreth, 1977)

(3) $a^{bio}_{annite} = (X^{x}_{K} (X^{y}_{Fe2+})^3 X^{z}_{Al} (X^{z}_{Si})^3 (X^{hyd}_{OH})^2)/0.105$ (Bohlen et al., 1980)

Total pressure is inferred to be 2 kb, and the average molar mass of the magma is calculated as 65.8. The fugacity of H2O is calculated using the expression:

$$\log f_{H2O} = \frac{G^o}{2.303RT} + \log a^{bio}_{annite} + \tfrac{1}{3} \log f_{O2} - \log a^{tmt}_{Fe3O4} - \log a^{san}_{KAlSi3O8}$$

a^{tmt}_{Fe3O4} is calculated as in Table 4, and the $a^{san}_{KAlSi3O8}$ is taken to be equal to $X^{san}_{KAlSi3O8}$. Hildreth (1977) has expressed the first term of the equation as:

$$\frac{G^o}{2.303RT} = \frac{8674}{T} + 2.461 + \frac{3.92 \times 10^{-3}}{T} (P-1)$$

where P is the pressure in bars and T is the temperature in degrees Kelvin.

The weight% H2O in the magma has been calculated from f_{H2O} values using the formulation of Carmichael et al. (1977).

example of anhydrous mineral assemblages that indicate a gradient in water content in a magma chamber.

WHOLE-ROCK CHEMISTRY

Major- and trace-element X-ray fluorescence analyses of 99 samples of homogeneous pumice, scoria, and lavas constitute our major data base. This is augmented by INAA, emission spectroscopy, and oxygen isotopic analyses for selected samples, which along with the Sr and Nd isotopic data of Verma (1983) are the basis for the following discussion.

We believe that all the units erupted at Los Humeros in the last 0.46 Ma were derived from a single unified but strongly compositionally zoned magma chamber, perhaps with the exception of the olivine basalts. Evidence for this include: (1) the nested character of the two major collapse structures, (2) the similarities in the major- and trace-element trends for all eruptive units (e.g. Figure 5), (3) the near-identity of REE patterns in rhyolitic and rhyodacitic material regardless of eruptive unit (Figure 8e), (4) similar ranges of phenocryst composition and abundance in the different units (Tables 2 and 3; Ferriz, in press), and (5) restricted temperature ranges of compositionally similar magma types.

The series as a whole is strictly calc-alkalic in the sense defined by Peacock (1931; Peacock Index = 59; Figure 5a), and fulfills all the calc-alkalic criteria of Irvine and Baragar (1971). In a K_2O vs. SiO_2 diagram (Figure 5b)

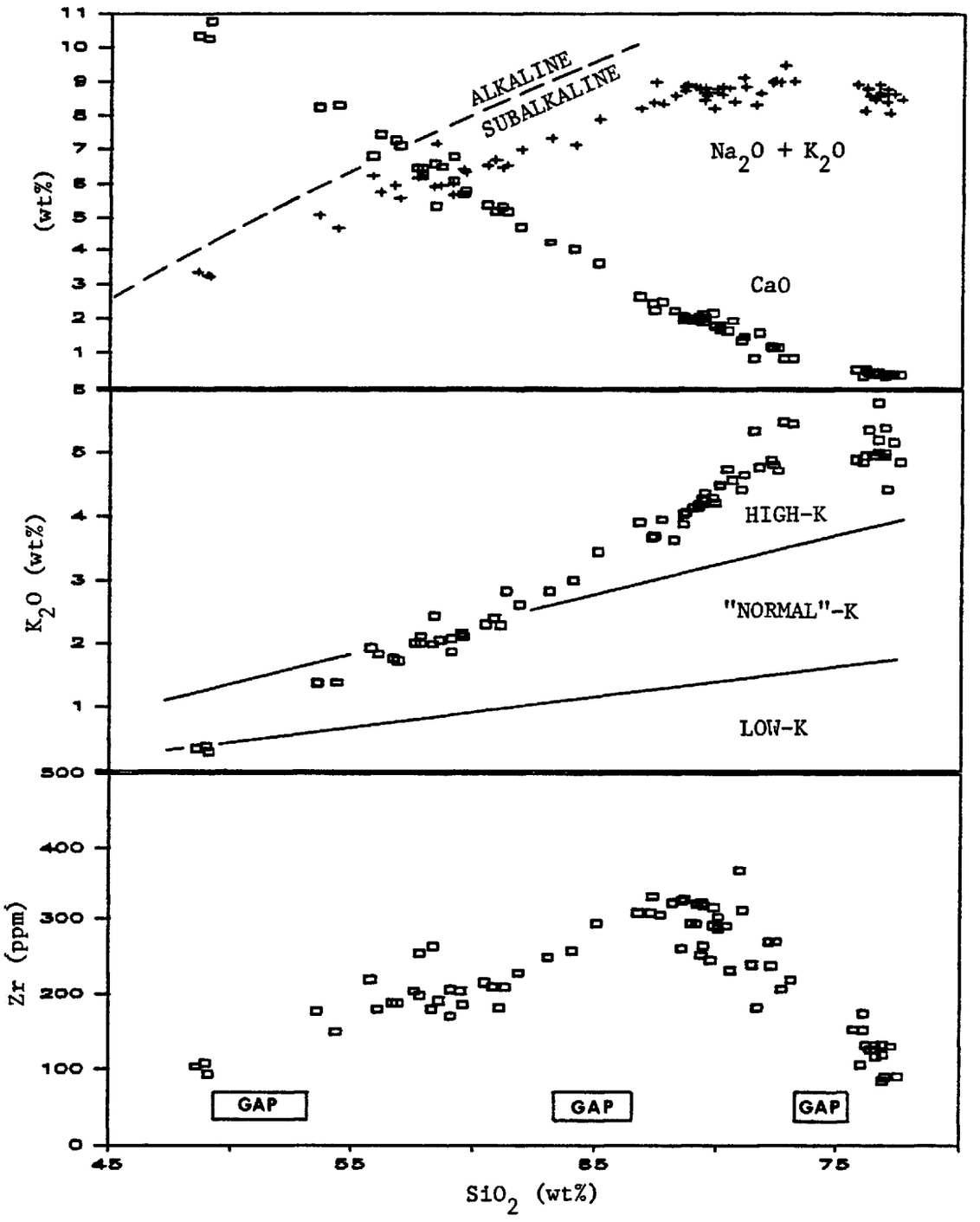

Fig. 5. (a) Alkali-lime diagram for all units erupted during the last 0.46 Ma at Los Humeros. The dashed line indicates the alkaline-subalkaline boundary of Irvine and Baragar (1971). (b) K_2O vs. SiO_2 variation diagram. The solid line indicates the classification boundaries of Peccerrillo and Taylor (1976). (c) Zr vs. SiO_2 variation diagram. The bottom bars indicate SiO_2 ranges for which there is a paucity of products at Los Humeros.

the data extend from the "normal"-K to the high-K fields of Peccerrillo and Taylor (1976) or Gill (1981). Based on a different data set, Verma and López (1983) took the crossover from "normal"-K to high-K fields as evidence that two different magma series were represented at Los Humeros. We attach little petrogenetic significance to this crossover given that chemical classifications are by nature arbitrary.

Pre-Xáltipan lavas

The relation between the tholeiitic Teziutlán lavas (Table 6), which preceded eruption of the Xáltipan Ignimbrite by at least 1 Ma, and the calc-alkalic volcanism of the last 0.46 Ma is uncertain. Their presence indicates, however, that the area had been a focus of magmatism for an extended period of time, and their supporting intrusions may locally form a significant component of the crust. The lavas erupted only shortly before the Xáltipan Tuff are already highly evolved high-silica rhyolites (Table 6), but exposure is insufficient to establish whether the onset of silicic volcanism followed a period of volcanic quiescence or whether there was a gradual transition between mafic Teziutlán volcanism and silicic volcanism.

Xáltipan Tuff and post-Xáltipan biotite rhyolites

The bulk of the pumice of the Xáltipan Tuff is aphyric and high-silica rhyolite in composition. Lapilli of porphyritic rhyolitic and rhyodacitic pumice are common, however, and andesitic scoria is found in small amounts. Dacitic pumice (LH20 in Table 7) is notably sparse, and the

Table 6. Analyses (recalculated volatile-free) of pre-Xáltipan lavas.

		TEZIUTLAN LAVAS				PRE-XALTIPAN RHYOLITES	
		LH2	LH4	LH1	LH3	LH5	LH6
SiO2	(wt%)	61.3	48.4	48.1	47.6	76.9	76.0
TiO2	"	1.04	2.52	2.19	2.84	0.09	0.09
Al2O3	"	16.9	17.4	17.5	16.7	12.7	14.2
Fe2O3	"	1.37	1.97	1.86	2.19	0.35	0.34
FeO	"	4.64	9.59	9.82	10.46	0.56	0.60
MnO	"	0.11	0.18	0.18	0.20	0.02	0.04
MgO	"	2.01	6.01	6.81	5.93	0.14	0.11
CaO	"	4.35	8.98	9.31	9.01	0.43	0.36
Na2O	"	4.98	3.59	3.13	3.59	3.38	3.31
K2O	"	3.00	0.88	0.72	0.95	5.40	4.86
P2O5	"	0.27	0.52	0.37	0.53	<0.05	<0.05
LOI	(900°C)	0.79	1.49	0.75	0.69	3.59	4.75
Rb	ppm	73	9	7	11	114	119
Sr	"	354	486	531	474	30	23
Y	"	50	30	31	34	26	31
Zr	"	394	186	176	210	119	106
Nb	"	24	13	15	13	11	15
Ni	"	8	23	51	25	0	0
Cr	"	17	49	94	49	0	1

Major element values reported in Tables 6, 7, 9, 10, and 11 were determined by XRF on fused disks. Rb, Sr, Y, Zr, Nb, Ni, and Cr were determined by XRF on pressed pellets. Ba and V were determined by emission spectrographic analysis. F and Cl determined by specific ion electrode techniques. Analyses performed by the U.S. Geological Survey and H. Ferriz (Rb, Sr, Y, Zr, Nb, Ni, and Cr). Fe2O3* recalculated to Fe2O3 and FeO based on Sack et al. (1980).
Loss on ignition (LOI) is included as an indicator of the degree of hydration of the different samples.

Table 7. Analyses (recalculated volatile-free) of homogeneous pumice and scoria from the Xaltipan Tuff, and of the post-Xaltipan biotite-rhyolites.

		XALTIPAN TUFF															POST-XALTIPAN BIO-RHYOLITES			
		LH7	LH10	LH8	LH9	LH15	LH13	LH14	LH18	LH11	LH16	LH22	LH19	LH20	LH21	LH17	LH23	LH26	LH24	LH25
SiO2	(wt%)	77.2	76.6	76.6	76.4	76.2	73.1	72.7	71.7	71.5	70.6	70.1	69.8	66.8	64.1	61.3	77.5	77.0	76.9	76.6
TiO2	"	0.05	0.10	0.08	0.11	0.07	0.22	0.26	0.38	0.27	0.42	0.47	0.52	0.76	1.13	0.99	0.08	0.07	0.06	0.10
Al2O3	"	12.5	12.7	12.9	13.2	13.3	14.7	14.7	14.7	16.7	14.9	15.6	15.3	16.2	16.2	16.5	12.5	13.4	13.1	13.1
Fe2O3	"	0.33	0.33	0.33	0.38	0.35	0.64	0.48	0.75	0.58	0.93	0.90	0.96	1.05	1.81	1.89	0.31	0.33	0.32	0.35
FeO	"	0.76	0.76	0.79	0.77	0.85	1.11	1.17	1.47	1.32	1.68	1.64	1.98	2.93	3.33	3.91	0.54	0.60	0.58	0.62
MnO	"	0.02	0.02	<0.02	0.02	0.03	0.03	0.03	0.04	0.04	0.04	0.06	0.06	0.08	0.09	0.10	0.02	0.04	0.05	0.02
MgO	"	<0.10	<0.10	<0.10	<0.10	0.12	0.28	0.29	0.57	0.31	0.90	0.65	0.91	1.07	1.69	3.38	0.11	0.10	0.11	0.14
CaO	"	0.40	0.40	0.41	0.42	0.44	0.87	0.86	1.60	0.86	1.95	1.81	2.16	2.66	4.05	5.19	0.39	0.39	0.35	0.47
Na2O	"	3.48	3.90	2.91	3.52	3.21	3.55	3.98	3.89	2.98	3.85	4.12	3.95	4.31	4.15	3.73	3.64	3.67	3.48	3.38
K2O	"	5.17	5.02	5.80	4.97	5.37	5.47	5.50	4.78	5.35	4.58	4.50	4.29	3.91	3.00	2.83	4.87	4.43	4.95	5.21
P2O5	"	<0.05	<0.05	<0.05	<0.05	<0.05	<0.05	0.06	0.08	<0.05	0.11	0.12	0.13	0.21	0.36	0.21	0.05	0.05	0.05	0.05
LOI (900°C)		3.39	2.91	3.34	3.57	4.32	3.70	3.01	4.15	5.24	4.47	3.60	4.41	3.99	1.97	1.77	0.30	1.30	2.71	3.32
F	ppm			400						600							400			
Cl	"			1000						<500							700			
Rb	ppm	139	140	133	133	127	127	124	101	112	115	124	115	93	74	68	126	116	106	112
Sr	"	25	15	28	28	37	64	58	91	86	134	167	147	217	312	281	23	15	22	28
Y	"	32	30	32	31	30	24	24	22	26	25	30	27	29	29	25	24	27	25	23
Zr	"	131	132	126	126	132	219	207	182	239	232	287	245	308	257	209	91	90	85	116
Nb	"	14	16	13	14	13	16	13	10	15	12	12	14	14	11	13	12	15	15	12
Ni	"	0	0	0	0	1	0	0	0	0	1	0	2	0	1	19	0	0	0	0
Cr	"	0	2	3	0	1	3	2	4	0	6	0	5	4	2	20	6	1	5	1
Ba	ppm			115					720	780	710	870	700	820	660	460	190	66	45	620
V	"			<10					<10	<10	29	<10	36	34	70	120	<10	<10	<10	<10

presence of Fo_{72} olivine within it suggests that it formed by limited mixing between silicic and andesitic magma. Compositions of homogeneous pumice of the Xáltipan Tuff indicate the existence of a compositional gap between 73 and 76 wt% SiO_2 (Figure 6).

Compositional trends of the units erupted at Los Humeros during the last 0.46 Ma are remarkably consistent, although, because of the general trend with time toward eruption of more mafic compositions, their ranges of overlap are restricted (cf. Figures 6, 9, 10, and 11). For the Xáltipan Tuff, Al_2O_3, FeO*, MnO, MgO, and CaO decrease monotonically as the SiO_2 content increases (Figure 6). The concentrations of TiO_2 and P_2O_5 initially increase with increasing silica content, reach a maximum at 64 wt% SiO_2, and then decrease; significantly, ilmenite and apatite are notably scarce in andesitic products. Na_2O also seems to reach a maximum at ~68 wt% SiO_2, although its pattern is somewhat scattered. K_2O is the only major component that increases monotonically with increasing SiO_2 contents.

An enrichment factor diagram (Hildreth, 1979) depicting the ratio of elemental concentrations (Tables 7 and 8) in a rhyolitic sample (LH8) over those in a rhyodacitic one (LH11) --which would presumably be equivalent to the ratio of concentrations in the roofward portion of the chamber over the abundances in a deeper level-- is presented in Figure 7a. This diagram shows modest roofward enrichment of Rb, Y, REE (except for Eu), Th, and U, and roofward depletion of Sc, Co, Zn, Sr, Zr, Ba, Eu, and Hf.

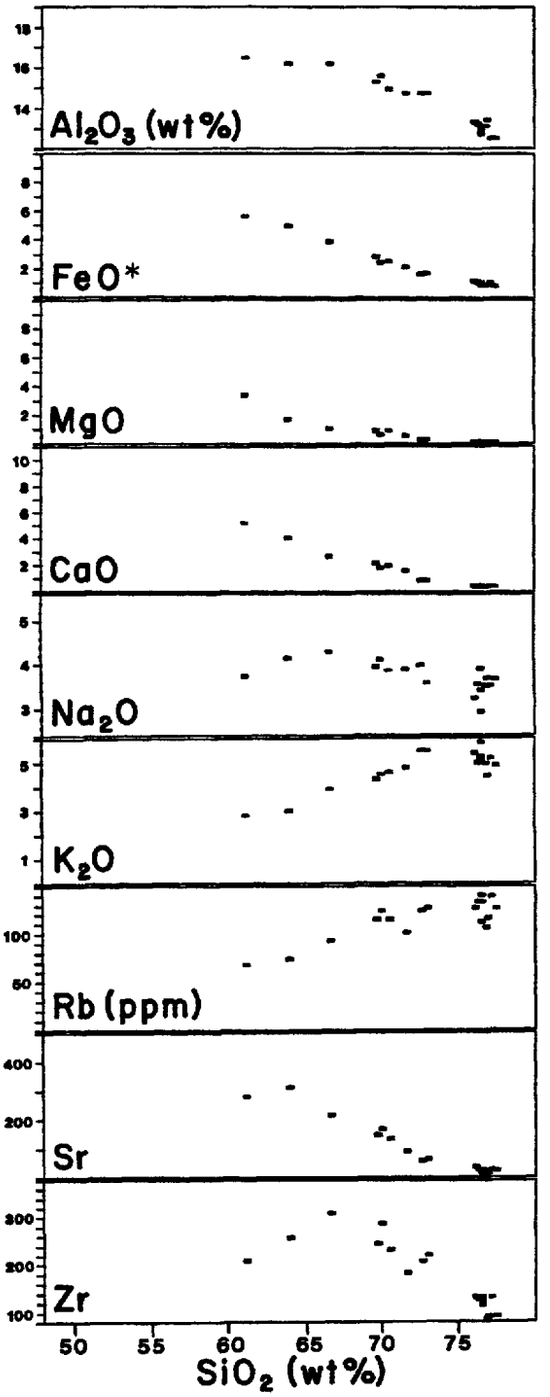

Fig. 6. Variation diagrams for samples of Xáltipan Tuff and post-Xáltipan biotite rhyolites (analyses recalculated volatile-free).

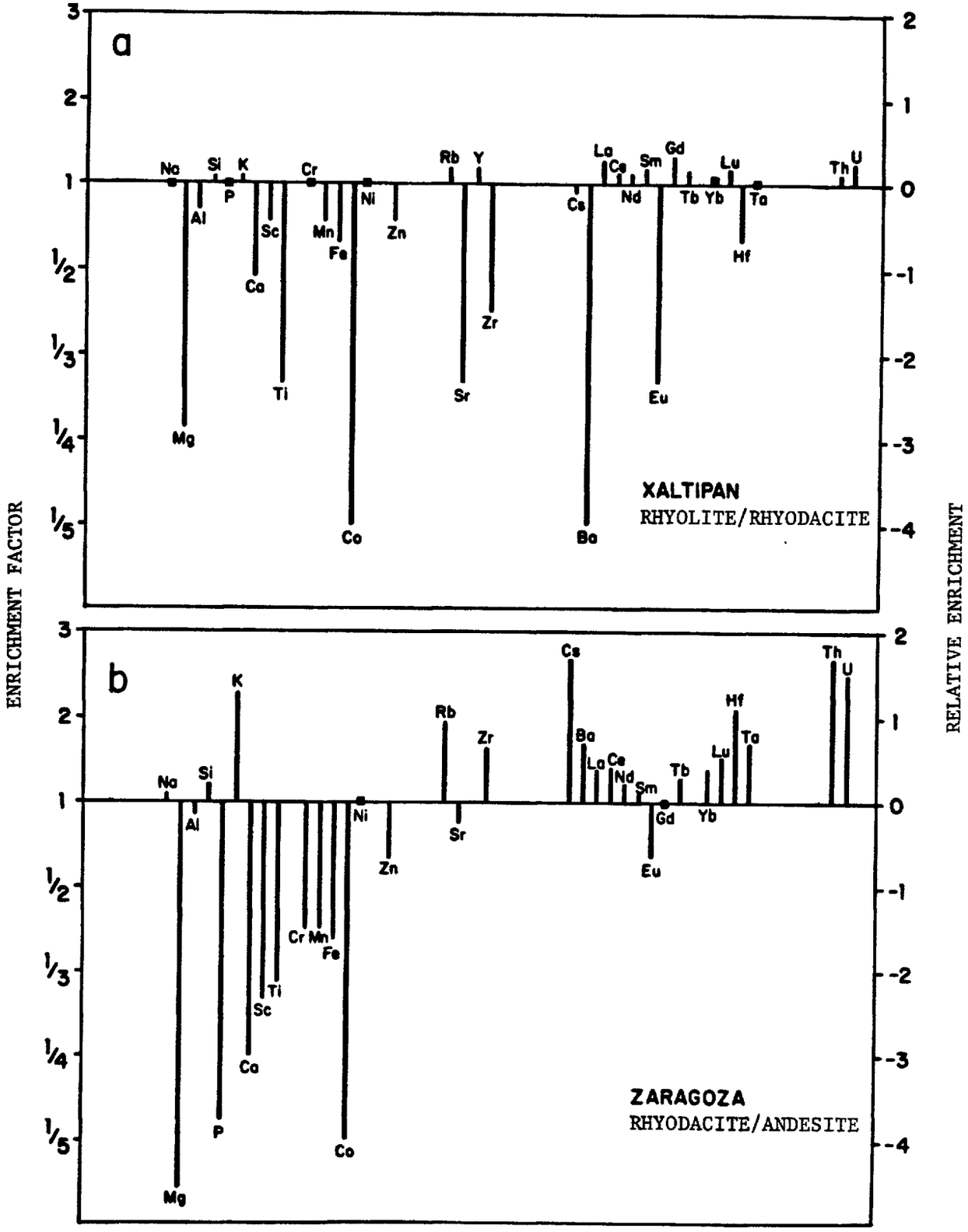

Fig. 7. Enrichment factor diagrams for the (a) Xáltipan and (b) Zaragoza Tuffs.

Table 8. Instrumental neutron activation analyses of selected samples.

	LH6	LH8	LH11	LH23	LH30	LH41	LH44	LH45	LH86	LH90	σ (%)
Sc	2.77	2.64	3.47	2.54	2.94	5.74	5.80	17.90	5.04	5.31	5
Co	0.3	0.3	1.5	0.2	0.6	2.5	2.9	16.3	4.4	3.9	3
Zn	31	26	36	31	36	49	47	79	49	52	4
Sb	1.0	1.1	0.7	0.9	0.9	0.8	1.2	1.1	1.2	0.8	9
Cs	3.9	4.3	4.8	4.0	4.1	4.0	3.9	1.5	4.3	3.7	3
La	43	43	34	43	43	38	40	28	38	39	3
Ce	81	73	65	70	73	68	68	49	67	68	5
Nd	30	29	26	29	29	30	27	25	30	32	3
Sm	5.8	5.5	4.7	4.9	5.3	5.9	5.6	5.4	5.5	5.9	3
Eu	0.19	0.18	0.58	0.17	0.41	0.90	1.03	1.48	1.06	1.10	5
Gd	5.3	6.6	5.0	4.8	5.2	5.7	5.9	5.9	5.6	5.1	3
Tb	0.91	0.83	0.73	0.68	0.83	0.86	0.85	0.68	0.81	0.81	3
Yb	3.3	2.8	2.7	2.5	2.9	2.6	2.6	1.9	2.6	2.7	5
Lu	0.55	0.51	0.44	0.47	0.53	0.48	0.45	0.32	0.48	0.49	2
Hf	4.6	4.6	7.8	3.9	5.6	8.9	8.6	4.3	8.9	8.9	3
Ta	2.55	1.89	2.03	1.92	1.79	1.44	1.41	0.86	1.66	1.56	4
Th	26.8	21.6	20.0	22.3	20.7	15.4	14.6	5.8	16.8	15.5	3
U	5.7	5.4	4.4	5.4	5.0	3.7	3.8	1.5	4.6	4.3	2

Analyst: G. A. Wandless (U.S. Geological Survey). σ (%) is an estimate of the reproducibility based in two replicate analyses.

Chondrite-normalized REE patterns of rhyolitic and rhyodacitic pumice samples of the Xâltipan Tuff are shown in Figure 8a, together with that of a single post-Xâltipan biotite rhyolite sample. The patterns of the two rhyolitic samples are similar, although not identical. The post-Xâltipan lava has slightly smaller HREE contents than the Xâltipan rhyolitic pumice. In addition, these lavas have slightly higher MgO and P_2O_5 contents, and slightly lower FeO*, Rb, and Zr contents (Table 7). Except for Zr these differences are small, however, and could have resulted from minor fractionation of biotite (with zircon inclusions).

Caltonac and Ocotepec rhyolites, and Faby Tuff

The relationship between the Caltonac and Ocotepec rhyolites and the overlying Faby Tuff is uncertain. We regard them as essentially contemporaneous samples of the magma chamber on account of: (1) Similarity in compositions of the Caltonac and Ocotepec rhyolites; (2) irresolvable K-Ar dates of one of the Ocotepec rhyolite domes (0.22±0.02 Ma) and the Faby Tuff (0.24±0.03 Ma); (3) similar phenocryst assemblages of the Ocotepec rhyolites and the most silicic pumice of the Faby Tuff (Table 9); and (4) identical Fe-Ti oxide temperatures of 875° for the Ocotepec rhyolites and the most silicic pumice of the Faby Tuff (Ferriz, in press, table 11). As a working hypothesis, we will thus consider the pre-Faby rhyolites as end-members of the compositional zonation in the magma chamber just prior to eruption of the Faby Tuff.

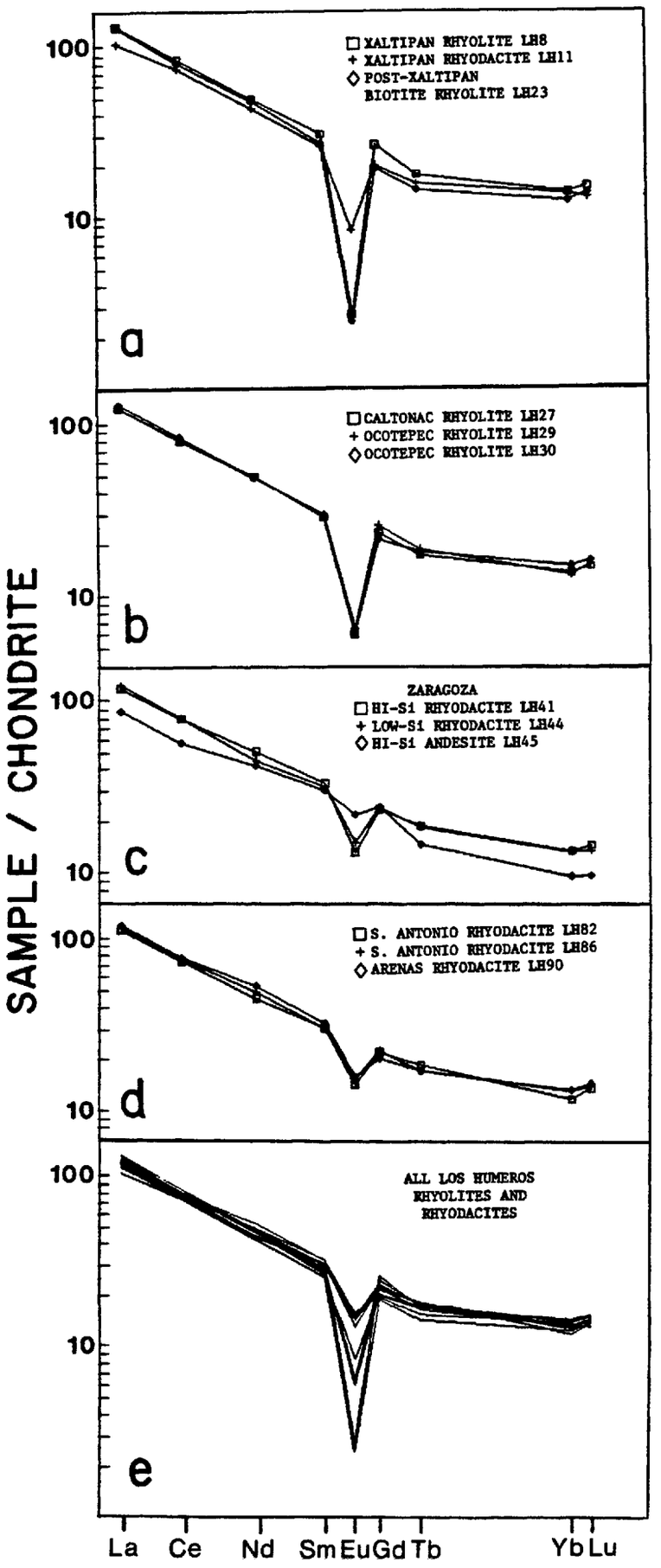

Fig. 8. Plot of chondrite-normalized (Haskin et al., 1968) rare earth element abundances for selected samples from Los Humeros volcanic center. Analyses performed by the U.S. Geological Survey.

Table 9. Analyses (recalculated volatile-free) of the pre-Faby Caltonac and opx-rhyolites, and of pumice and scoria from the Faby Tuff.

		CALTONAC RHYOLITE	OPX-RHYOLITES			FABY TUFF					
		LH27	LH28	LH29	LH30	LH31	LH32	LH33	LH34	LH36	LH35
SiO2	(wt%)	76.1	76.9	75.7	76.1	72.5	72.3	72.2	69.4	69.5	59.1
TiO2	"	0.13	0.10	0.14	0.12	0.33	0.34	0.36	0.56	0.56	1.15
Al2O3	"	13.0	12.6	13.1	12.9	14.7	14.8	14.8	15.6	15.5	17.1
Fe2O3	"	0.48	0.42	0.49	0.49	0.66	0.68	0.71	1.05	1.13	1.61
FeO	"	0.80	0.70	0.81	0.81	1.15	1.20	1.26	1.87	1.62	4.59
MnO	"	0.02	0.02	0.02	0.02	0.04	0.04	0.04	0.05	0.05	0.10
MgO	"	0.13	0.10	0.13	0.13	0.37	0.40	0.43	0.75	0.74	3.55
CaO	"	0.51	0.42	0.53	0.50	1.17	1.16	1.22	2.15	2.02	6.79
Na2O	"	3.84	3.66	4.03	3.87	4.25	4.21	4.10	4.18	4.32	3.82
K2O	"	4.96	4.99	4.90	4.96	4.73	4.82	4.88	4.27	4.37	1.87
P2O5	"	0.05	0.05	0.05	0.05	0.06	0.05	0.05	0.14	0.14	0.31
LOI	(900°C)	0.62		0.40	0.32	4.40	4.47	4.49	3.71	3.86	0.29
F	ppm	500		500	600		500	500		200	
Cl	"	700		700	800		1000	1000		1100	
Rb	ppm	117	132	114	137	121	109	119	98	96	39
Sr	"	39	18	34	37	93	94	107	161	171	380
Y	"	26	29	24	31	25	22	26	23	24	18
Zr	"	152	133	153	175	270	238	269	252	265	171
Nb	"	10	12	11	12	13	12	10	10	9	10
Ni	"	0	0	0	0	0	0	0	0	0	8
Cr	"	1	0	5	3	1	2	3	2	3	9
Ba	ppm	540	330	550	570	910	750	780	900	840	580
V	"	<10	<10	<10	<10	<10	<10	<10	36	<10	140

As shown in Figure 9, the data for the pre-Faby and Faby samples once again suggest the existence of a compositional gap between 73 and 75 wt% SiO_2. Dacitic compositions also are conspicuously absent, but as for the Xàltipan Tuff the data base is far too limited to ascertain the existence of a discontinuity between rhyodacitic and andesitic compositions. Major-element trends are like those described for the Xàltipan Tuff, except that Na_2O contents go through a maximum between 69 and 72 wt% SiO_2. On the average, the pre-Faby rhyolites are also slightly more mafic than the Xàltipan rhyolitic pumice and the post-Xàltipan biotite rhyolites, being enriched in MgO, CaO, TiO_2, and FeO*.

Rb contents increase monotonically with increasing SiO_2, Sr contents decrease monotonically, and Zr contents go through a maximum between 69 and 72 wt% SiO_2 (Figure 9) although all samples contain zircon. Chondrite-normalized REE patterns of the Caltonac and Ocotepec rhyolites are essentially identical, and parallel those of the rhyolitic pumice of the Xàltipan Tuff (Figures 8b and 8e), but they show a less pronounced Eu anomaly.

Zaragoza Tuff

Approximately 80% of the juvenile ejecta of the Zaragoza Tuff is rhyodacitic pumice which, in spite of wide variations in color and phenocryst content, spans a very limited compositional range (e.g., 71.1 to 69.9 wt% SiO_2; Figure 10, Table 10). The rest of the ejecta is formed by

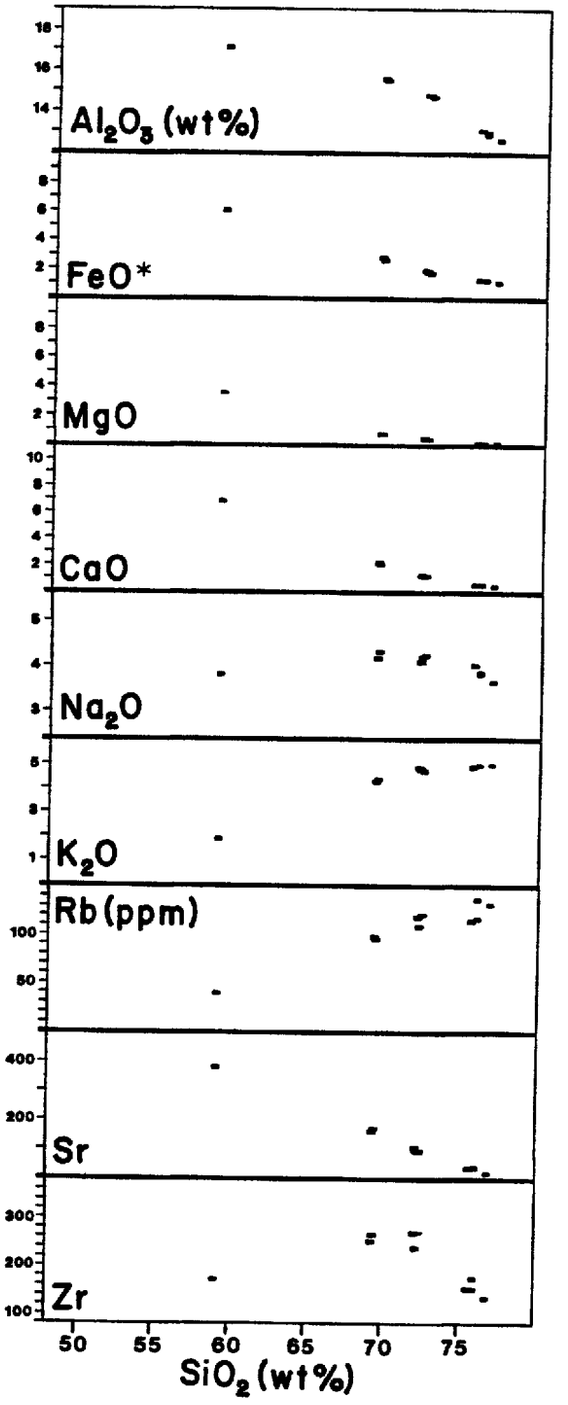

Fig. 9. Variation diagrams for samples of pre-Faby rhyolites and Faby Tuff (analyses recalculated volatile-free).

Table 10. Analyses (recalculated volatile-free) of homogeneous pumice and scoria from the Zaragoza Tuff.

		ZARAGOZA TUFF						
		LH41	LH48	LH42	LH43	LH44	LH45	LH47
SiO2	(wt%)	71.1	70.4	70.1	69.9	69.9	59.1	54.4
TiO2	"	0.46	0.48	0.50	0.51	0.51	1.45	2.01
Al2O3	"	14.9	15.3	15.2	15.3	15.4	17.2	17.5
Fe2O3	"	0.69	0.71	0.79	0.81	0.78	1.69	2.06
FeO	"	1.88	1.87	2.07	2.17	1.99	5.13	6.42
MnO	"	0.04	0.05	0.05	0.05	0.05	0.11	0.12
MgO	"	0.52	0.57	0.59	0.65	0.63	2.90	4.08
CaO	"	1.49	1.67	1.70	1.79	1.82	6.08	8.31
Na2O	"	4.20	4.06	4.38	4.49	4.56	3.93	3.30
K2O	"	4.66	4.75	4.48	4.22	4.23	2.08	1.39
P2O5	"	0.08	0.10	0.11	0.11	0.10	0.39	0.41
LOI (900°C)		3.91	3.12	2.53	2.60	2.45	1.36	0.61
Rb	ppm	113	101	108	110	102	58	34
Sr	"	121	121	126	140	139	415	404
Y	"	26	24	23	25	25	25	18
Zr	"	312	291	303	316	292	206	150
Nb	"	12	10	11	12	12	11	10
Ni	"	0	0	0	0	0	0	1
Cr	"	3	6	3	5	2	15	5
Ba	ppm	820	880	880	870	860	560	
V	"	<10	<10	<10	<10	18	160	

andesitic scoria that ranges from 59.1 to 54.4 wt% SiO_2 as a minimum. Na_2O and K_2O increase monotonically with increasing SiO_2 content, and all other oxides major and minor oxides decrease monotonically. Even though some of the samples have phenocryst contents as high as 30% there is no evidence in the Harker diagrams of Figure 10 for any of these samples being cumulative.

Differences in the concentrations of trace elements in the most and least silicic rhyodacitic samples are irresolvable at the 95% confidence level (Tables 8 and 10), in spite of the fact that their phenocryst content varies by at least 10 wt%. Between the most silicic rhyodacitic and andesitic samples, however, there are pronounced differences (Figure 7b). Rb, Zr, Cs, Ba, LREE, HREE, Hf, Ta, Th, and U were enriched in the rhyodacitic magma, whereas Sc, Cr, Co, Zn, Sr, and Eu were enriched in the andesitic one. The most silicic andesitic sample is relatively depleted in the lightest and heaviest REE with respect to the rhyodacitic samples, which, as shown by Model 9 in Tables 13 and 14, is consistent with the fractionation of clinopyroxene. Although it contains over 20 wt% plagioclase phenocrysts, the andesitic scoria still displays a slight negative Eu anomaly (Figure 8c).

Post-Zaragoza units

We attribute the volcanism of the last 0.06 Ma to tapping of a reorganized post-Zaragoza chamber which was zoned from rhyodacite through basaltic andesite and

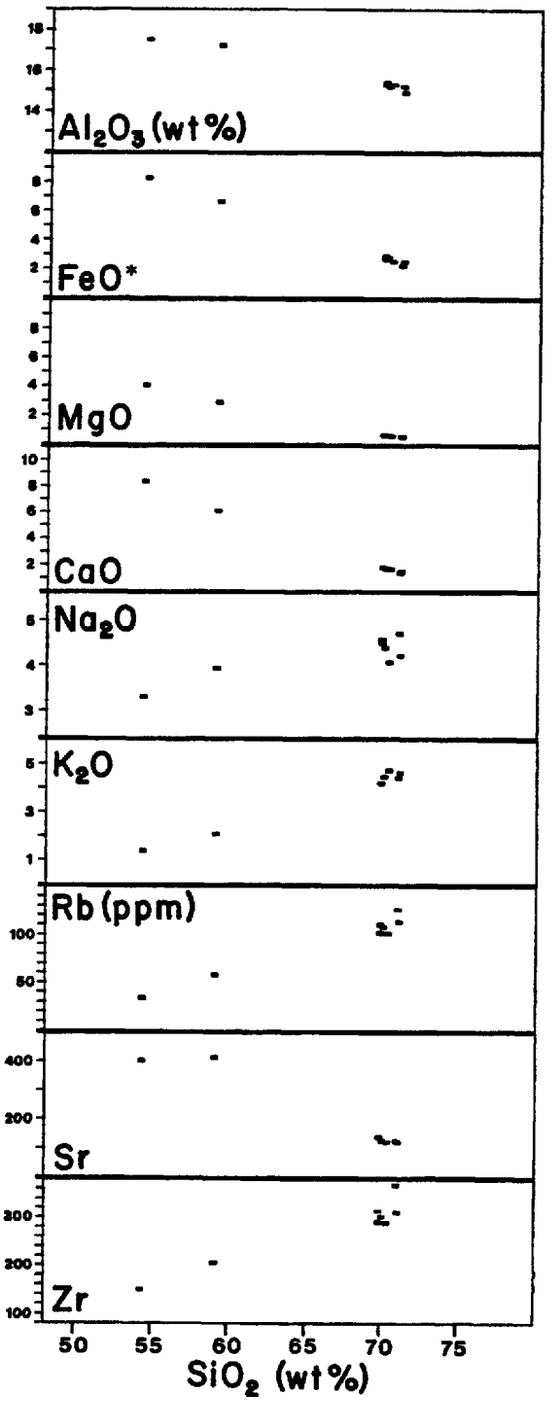

Fig. 10. Variation diagrams for samples of Zaragoza Tuff (analyses recalculated volatile-free).

probably received mass and thermal input through the injection of mantle-derived basaltic magma in its root zone (Ferriz and Mahood, 1984).

Although the compositions of the eruptive products of the last 0.06 Ma span a very wide range, rhyodacite (69 to 67 wt% SiO_2) and andesite (63 to 53 wt% SiO_2) predominate volumetrically. Of the ~17 km^3 of magma erupted during this interval only the silica content of the pumice of the 0.6-km^3 Xoxoctic Tuff falls in the range 63 to 67 wt%. A fourth magma type is represented by the 0.25 km^3 of olivine basalts erupted during the last 0.02 Ma. With Mg numbers of ~66 and olivine phenocrysts of Fo_{84}, these lavas represent the most primitive magmas erupted at Los Humeros.

X-ray fluorescence analyses of selected post-Zaragoza units are shown in Table 11. Samples LH59, LH68, LH65, and LH64 have over 20 wt% phenocrysts and are shown by a different symbol in the variation diagrams of Figure 11. The last three have abnormally high Al_2O_3 and CaO contents and abnormally low FeO* contents, and mass balance calculations suggest that over half of their plagioclase phenocrysts could be cumulative. The fact that chemical evidence for crystal accumulation is restricted to lavas and not observed in pyroclastic products (cf. LH45 in Tables 2 and 10) leads us to believe that crystal concentration in these samples could be related to flow emplacement.

For the group as a whole, Na_2O and K_2O contents increase with increasing SiO_2 but the former shows considerable scatter. Al_2O_3 decreases slightly with

Table 11. Analyses (recalculated volatile-free) of pumice, scoria and lavas from selected post-Zaragoza eruptive units.

		XOXOCTIC TUFF	TEPEYAHUALCO FLOW							SARABIA FLOW			LIMON FLOW				CHIAPA FLOWS			
		LH53	LH60	LH61	LH58	LH55	LH56	LH59	LH57	LH67	LH68	LH66	LH63	LH65	LH64	LH62	LH72	LH71	LH69	LH70
SiO2	(wt%)	65.1	59.5	59.2	57.8	57.8	57.6	57.5	56.1	58.4	56.3	55.8	56.7	56.5	56.1	53.6	63.1	61.9	58.6	58.3
TiO2	"	0.65	1.43	1.15	1.53	1.50	1.49	1.28	1.42	1.53	1.02	1.65	1.37	1.06	1.31	1.54	1.13	1.21	1.51	1.50
Al2O3	"	16.5	16.8	17.6	16.9	16.7	17.1	18.1	17.5	16.7	19.4	17.0	17.4	19.3	18.4	18.0	16.4	16.6	17.3	17.4
Fe2O3	"	1.47	2.21	1.92	2.04	2.02	1.99	2.05	1.93	2.41	1.91	2.17	2.19	1.99	1.99	2.00	1.65	1.73	1.71	1.69
FeO	"	2.83	4.79	4.31	5.57	5.55	5.52	4.76	5.64	5.09	3.85	6.15	5.04	4.02	4.78	6.38	3.96	4.30	5.26	5.25
MnO	"	0.08	0.10	0.09	0.12	0.12	0.12	0.10	0.12	0.14	0.08	0.13	0.11	0.09	0.10	0.13	0.09	0.09	0.10	0.10
MgO	"	1.70	2.65	2.92	2.99	3.14	3.14	2.99	3.78	2.71	3.36	3.65	3.62	3.23	3.53	4.64	1.81	2.12	2.73	2.81
CaO	"	3.61	5.71	6.37	6.25	6.45	6.47	7.08	7.44	5.36	8.70	6.82	7.27	8.54	8.01	8.26	4.26	4.74	6.50	6.59
Na2O	"	4.45	4.25	4.06	4.36	4.12	4.18	3.88	3.92	4.75	3.56	4.31	4.18	3.42	3.73	3.72	4.52	4.39	3.90	3.93
K2O	"	3.44	2.17	2.09	2.03	2.12	2.02	1.90	1.84	2.44	1.57	1.93	1.78	1.60	1.70	1.38	2.83	2.62	2.06	2.00
P2O5	"	0.17	0.36	0.28	0.38	0.38	0.37	0.34	0.34	0.43	0.25	0.38	0.35	0.26	0.32	0.35	0.29	0.30	0.39	0.38
LOI (900°C)		2.67	0.01	0.38	0.01	0.44	0.44	0.50	0.32	0.37	0.36	0.14	0.56	0.79	0.52	0.70	0.15	0.14	0.85	0.94
Rb	ppm	81	48	46	40	49	41	36	31	47	31	39	35	31	33	26	63	56	41	40
Sr	"	233	405	421	350	464	375	404	389	317	463	358	411	472	403	442	307	330	412	403
Y	"	24	23	21	26	29	24	17	22	32	13	28	24	18	18	24	21	19	20	21
Zr	"	295	205	190	199	254	204	157	180	263	129	220	188	138	140	178	249	228	191	181
Nb	"	12	13	11	11	14	11	11	11	13	11	11	11	10	10	10	11	11	10	10
Ni	"	7	5	9	2	4	5	4	13	4	11	6	13	12	12	23	1	3	5	5
Cr	"	8	3	21	15	26	19	14	45	10	22	24	39	22	35	39	8	5	13	14
Ba	ppm	830	580	570	610	580	540	590	480								750	710	610	590
V	"	52	190	170	210	160	180	180	200								120	130	160	180

continues . . .

Table 11. (continued)

		CUICUILTIC TUFF					SAN ANTONIO FLOWS									ARENAS FLOWS			OLIVINE BASALTS		
		LH76	LH77	LH79	LH80	LH78	LH87	LH83	LH86	LH82	LH81	LH88	LH84	LH85	LH89	LH90	LH91	LH92	LH96	LH94	LH95
SiO2	(wt%)	69.5	67.7	67.3	61.1	56.9	69.4	69.2	69.2	69.0	68.7	68.6	60.8	60.5	59.6	68.6	68.2	67.4	49.1	49.0	48.6
TiO2	"	0.51	0.67	0.70	1.30	1.51	0.54	0.54	0.51	0.54	0.60	0.57	1.36	1.41	1.37	0.55	0.63	0.68	1.39	1.40	1.49
Al2O3	"	15.5	15.7	16.2	16.7	17.1	15.4	15.4	15.6	15.7	15.7	15.9	16.5	16.5	16.9	15.9	15.9	16.0	17.4	17.1	17.1
Fe2O3	"	0.96	1.13	1.14	1.60	1.84	1.08	0.99	1.04	0.95	1.00	1.19	1.78	1.81	1.90	0.96	1.09	1.14	1.49	1.48	1.52
FeO	"	1.95	2.53	2.63	4.71	5.96	1.91	2.05	1.87	2.00	2.10	2.15	4.84	4.99	5.11	2.13	2.42	2.49	8.06	8.26	8.39
MnO	"	0.05	0.07	0.07	0.09	0.12	0.06	0.05	0.05	0.06	0.06	0.07	0.10	0.10	0.10	0.06	0.07	0.07	0.16	0.16	0.16
MgO	"	0.78	1.11	0.92	2.44	3.55	0.66	0.77	0.79	0.79	0.80	0.63	2.35	2.46	2.61	0.81	0.73	0.83	8.29	8.93	8.90
CaO	"	2.04	2.50	2.46	5.33	7.10	1.92	2.03	2.00	1.97	2.02	2.00	5.21	5.39	5.80	2.08	2.25	2.26	10.76	10.26	10.34
Na2O	"	4.33	4.41	4.72	4.17	3.84	4.65	4.66	4.65	4.72	4.84	4.85	4.32	4.24	4.22	4.83	4.95	5.30	2.95	2.90	3.03
K2O	"	4.26	3.96	3.68	2.30	1.74	4.19	4.18	4.15	4.13	4.07	3.89	2.40	2.31	2.12	4.04	3.64	3.70	0.28	0.37	0.34
P2O5	"	0.14	0.17	0.18	0.31	0.35	0.14	0.14	0.13	0.14	0.15	0.14	0.35	0.36	0.34	0.14	0.15	0.19	0.16	0.19	0.20
LOI	(900°C)	3.54	3.44	3.59	1.05	0.61	0.39	0.37	0.44	0.55	0.76	0.27	0.06	0.17	0.01	0.21	0.59	0.37	0.01	0.01	0.01
Rb	ppm	108	92	81	52	36	97	95	111	97	100	87	52	55	43	82	84	86	0	3	0
Sr	"	175	181	202	399	369	142	156	167	161	169	168	352	391	388	136	223	212	308	324	308
Y	"	23	24	23	20	23	24	24	25	23	25	26	21	22	22	22	28	27	20	20	20
Zr	"	319	306	308	182	188	322	294	320	295	326	325	210	215	187	261	322	330	94	107	104
Nb	"	12	12	14	12	13	14	13	14	14	16	12	12	12	11	10	12	14	10	10	10
Ni	"	2	0	1	3	10	0	0	0	1	0	0	2	0	0	0	0	0	92	111	104
Cr	"	5	2	6	9	41	0	0	8	3	2	0	6	12	9	4	3	5	195	268	268
Ba	ppm	780	760	880	660	520	870	850	780	760	780	940	710	690	650	810	890		69	78	87
V	"	23	44	24	150	170	27	31	27	29	25	19	150	170	190	19	20		180	160	190

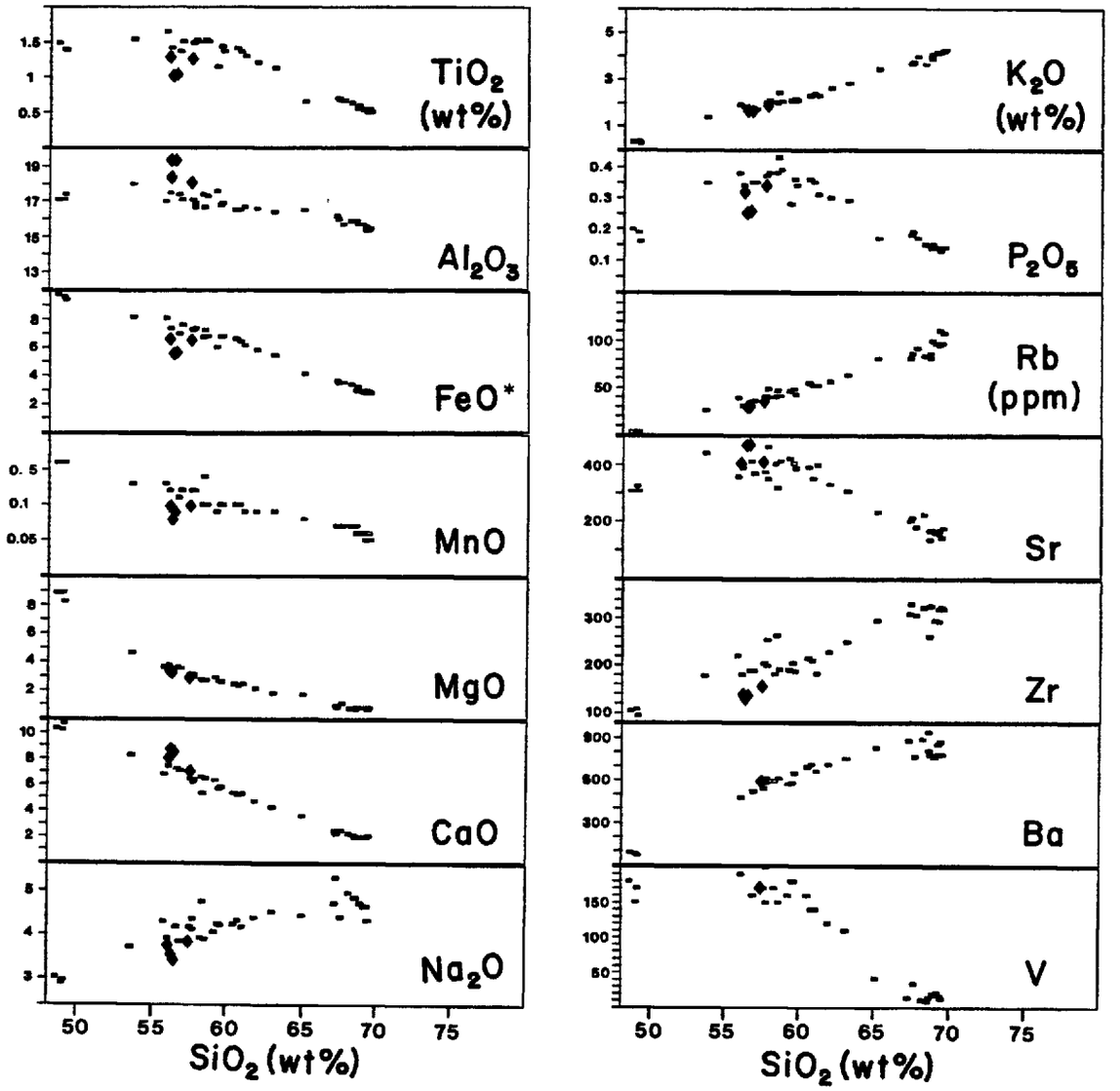

Fig. 11. Variation diagrams for samples of selected post-Zaragoza eruptive units (analyses recalculated volatile-free). The black rhombs indicate samples with over 20 wt% phenocrysts.

increasing SiO_2 content; data for andesites show considerable scatter despite the fact that the majority of the samples have phenocryst contents below 5 wt%. FeO*, MnO, MgO, and CaO contents show pronounced monotonic decreases with increasing SiO_2. TiO_2 remains relatively constant, though scattered, in samples with SiO_2 contents smaller than 59 wt%, but decreases sharply in samples with higher silica content. Finally, P_2O_5 contents go through a maximum at 59 wt% SiO_2; the maximum coincides roughly with the minimum silica content of products that contain apatite (~61 wt%).

Rb, Zr, and Ba increase monotonically with increasing SiO_2 content. Sr and V remain relatively constant up to 60 wt% SiO_2 and decrease rapidly at higher silica contents. Chondrite-normalized REE patterns of three San Antonio and Arenas rhyodacitic lavas (Figure 8d) are essentially identical to those of the Zaragoza rhyodacitic pumice.

ISOTOPIC DATA

Isotopic values of $E_{Sr}=-3.5\pm1.1$ and $E_{Nd}=+1.4\pm0.6$ (Table 12; LH8 in Figure 12) measured in one of our samples of Xâltipan high-silica rhyolite pumice (recalculated from Verma, 1983) are remarkably "primitive" for such a highly evolved major-element composition, and rule out the involvement of lower continental crust or old upper continental crust in the generation of this magma (cf. Figure 16). The $d^{18}O$ values of the high-silica rhyolite portion of the Xâltipan Tuff are unknown on account of its aphyric nature, but sanidine (Ab_{40}) of immediately pre- and post-Xâltipan high-silica rhyolite lavas have values of +6.9

Table 12. Summary of isotopic data.

Sample *	SiO2 "	ESr #	ENd ^	dO18 ~
		PRE-XALTIPAN RHYOLITE		
LH5	76.9			6.9
		XALTIPAN TUFF		
LH8 (HF15)	76.6	-3.5 ± 1.1	1.4 ± 0.6	
LH14	72.7			6.4
LH11	71.5			6.5
		POST-XALTIPAN RHYOLITE		
LH25	76.6			7.3
		PRE-FABY RHYOLITES		
LH27 (HF239)	76.1	-2.8 ± 0.9		
LH28	76.9			6.7
LH29 (HF238)	75.7	-5.1 ± 1.3		7.2
		FABY TUFF		
LH33 (HF76)	72.2	-0.9 ± 0.6		6.8
		ZARAGOZA TUFF		
LH44 (HF2)	69.9	2.1 ± 0.6		7.1
		LIMON FLOW		
LH62 (CH33)	53.6	-7.7 ± 0.7	2.5 ± 0.4	6.3
LH64 (CH31)	56.1	-4.5 ± 0.7		
LH65 (CH28)	56.5	-1.4 ± 1.0	0.4 ± 0.6	6.7
		TEPEYAHUALCO FLOW		
LH57 (CH47)	56.1	-7.5 ± 0.9		
LH56 (CH46)	57.6	-4.3 ± 1.1		
		SARABIA FLOW		
LH66 (CH40)	55.8	-6.7 ± 0.9		
		SAN ANTONIO RHYODACITE		
LH87	69.4			6.6
		SAN ANTONIO ANDESITE		
LH85 (CH4)	60.5	-5.1 ± 0.8	1.2 ± 0.8	
		OLIVINE BASALT		
LH94 (HF117)	49	-9.1 ± 2.6	4.1 ± 0.6	5.8
		PIZARRO RHYOLITE		
LH99 (CH42)	76.5	4.4 ± 0.6	-1.4 ± 0.4	8.4

* Labels in brackets are those used by Verma (1983). HF samples are splits from LH samples collected by H. Ferriz; CH samples, collected by S.P. Verma, are from the same outcrop as equivalent LH samples.

" Reported SiO2 contents are those of LH samples (analyses recalculated volatile-free).

Recalculated according to DePaolo and Wasserburg (1976) from whole-rock 87Sr/86Sr values reported by Verma (1983). ESr = 0 is equivalent to 87Sr/86Sr = 0.7045. Discrepancies between the values on this table and those of Verma (1983) are due to age correction based on the K-Ar dates of Ferriz and Mahood (1984).

^ Recalculated according to DePaolo and Wasserburg (1976) from whole-rock 143Nd/144Nd values reported by Verma (1983). ENd = 0 is equivalent to 143Nd/144Nd = 0.51265.

~ dO18 analyses by C. Johnson (U.S. Geological Survey) on plagioclase concentrates of LH samples. Estimated 1σ = 0.1.

and +7.3, respectively. They contrast with values of +6.5 and +6.4 obtained on plagioclase (An_{20}) concentrates of two Xâltipan rhyodacitic samples.

E_{Sr} values of the Caltonac and Ocotepec rhyolites are -2.8 ± 0.9 and -5.1 ± 1.3, respectively (recalculated from Verma, 1983; LH27 and LH29 in Figure 12). They are comparable with the -3.5 ± 1.1 value of the rhyolitic Xâltipan pumice at the 95% confidence level but contrast with the $E_{Sr}= -0.9\pm0.6$ value of one of our Faby pumice samples (recalculated from Verma, 1983; LH33 in Figure 12). $d^{18}O$ measurements on sanidine concentrates of two of the Ocotepec rhyolite domes yielded values of +7.2 and +6.7. The former compares well with the +7.3 value of one of the post-Xâltipan biotite rhyolites, whereas the latter compares with the +6.8 value of a plagioclase (An_{30}) concentrate of a Faby pumice sample. It is uncertain whether this difference in values is significant.

Verma (1983) reported a value of $E_{Sr}= +2.1\pm0.6$ for our least silicic Zaragoza rhyodacitic sample (LH44 in Figure 12). This is the highest value that has so far been measured in any of the units directly related to the volcanic center and sharply contrasts with the negative values of the high-silica rhyolites and the post-Zaragoza andesites. A plagioclase (An_{35}) concentrate from this same sample yielded a $d^{18}O$ value of +7.1. No isotopic data are available for samples from the andesitic portion of this unit.

Isotopic data for some post-Zaragoza units are shown in Figure 12. Of particular interest are the trends defined by

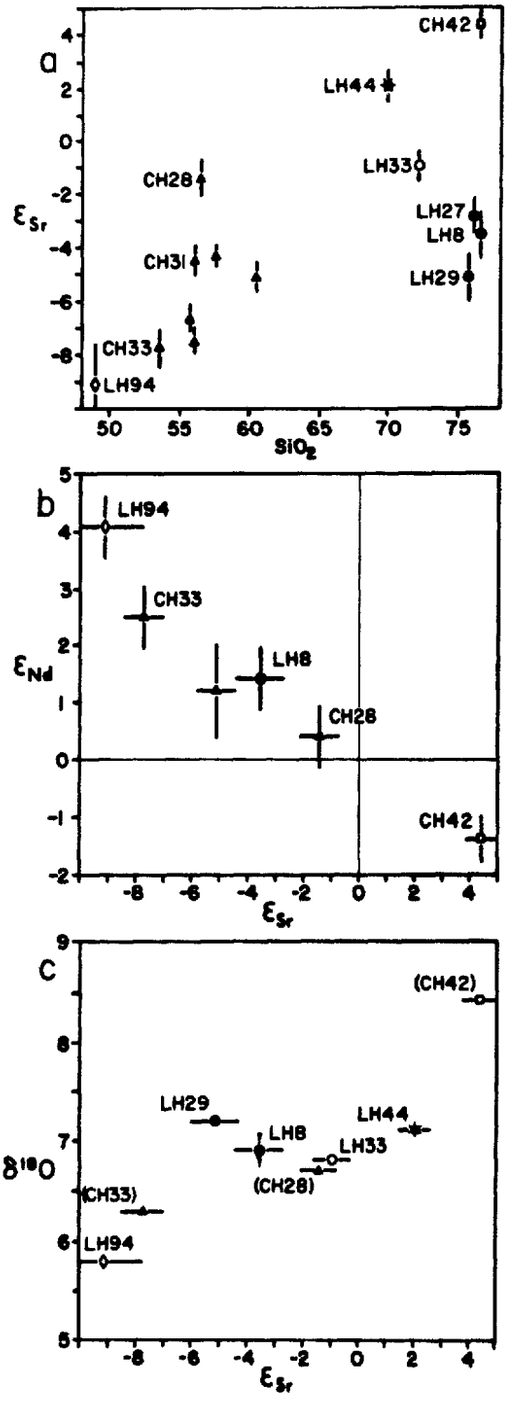

Fig. 12. Graphical summary of isotopic data (Table 12) for selected samples of Los Humeros volcanic center. ● represents rhyolitic pumice from the Xàltipan Tuff and pre-Faby rhyolites. ○ represents rhyodacitic pumice from the Faby Tuff. * represents rhyodacitic pumice from the Zaragoza Tuff. △ represents post-Zaragoza andesites. ◇ represents a sample from one of the late-erupted olivine basalts. Shown for comparison purposes is a sample from the unrelated Pizarro dome (□; AA in Figure 1).

samples CH33, CH31, and CH28 of Verma (1983), which correspond to our samples LH62, LH64, and LH65, and respectively represent the bottom, middle, and upper flow units of the Limón compound flow (P in Figure 1). The samples from this compositionally zoned flow indicate that the andesitic portion of the magma chamber was zoned both in composition and isotopic ratios. In the SiO_2 vs. E_{Sr} diagram the data from these samples bridge the gap between the high E_{Sr} of the rhyodacitic portion of the Zaragoza Tuff and the low E_{Sr} of the late-erupted olivine basalts.

Figure 12 also shows the isotopic values of a sample from the Pizarro rhyolite dome, which is located south of the volcanic center (AA in Figure 1). Despite its close spatial relation this dome is not related to the magmatic system of Los Humeros, as suggested by its isotopic values, its mineralogy, and its REE pattern (Ferriz and Mahood, in press). In the next section we will use the isotopic values of this dome as those of one potential crustal contaminant for modeling purposes.

Five major hypotheses, which we will discuss in the next section, are advanced as possible explanations of the primitive isotopic values of the rhyolitic portion of the chamber: (1) partial fusion of young andesitic and ferrobasaltic intrusions, (2) crystal fractionation of mantle-derived magmas, (3) coupled assimilation-fractional crystallization of basaltic or andesitic magma, (4) assimilation of young mafic roof rocks by crustal-derived

rhyolitic magmas, and (5) mixing of basaltic and crustal-derived rhyolitic magmas.

The trend observed between the E_{Sr} data for the rhyolitic pumice of the Xáltipan Tuff, the pre-Faby rhyolites, and the rhyodacitic pumice of the Faby and Zaragoza Tuffs could in principle be explained in two ways: (1) collapse-related contamination of the residual magma after each major eruption, and (2) limited mixing between low E_{Sr} rhyolitic magma and high E_{Sr} low-Si rhyodacitic magma. Finally, the Zaragoza-andesite-basalt trend can in principle be explained by (1) coalescence of mafic magmas derived from partial melting of an heterogeneous source, (2) coupled assimilation-fractional crystallization of mafic magma, or (3) mixing between rhyodacitic and basaltic magma.

ORIGIN OF THE COMPOSITIONAL ZONATION

Several simple differentiation mechanisms can explain the development of the strong compositional zonation of the Los Humeros magma chamber. Besides explaining the elemental trends, however, differentiation models must ideally also explain: (1) the volumetrical predominance of high-silica rhyolitic magma over all other magma types, (2) the persistence of the compositional zonation for over 400,000 years; (3) the development of the compositional gaps between 75 and 73 wt%, and between 67 and 63 wt%; (4) the isotopic variations; (5) the existence of mineralogic zonation within the chamber; (6) the remarkable similarity in the REE

patterns of the rhyolitic and rhyodacitic products for the last 400,000 years; and (7) the decrease in the maximum SiO_2 content of successive eruptive units. Since most likely several process operated simultaneously or sequentially during the growth and active life of the chamber, it is not surprising that no single-stage process is capable of explaining all of the aforementioned traits. Our objective in this section is thus to evaluate the degree to which different differentiation mechanisms may have operated in the magmatic system, rather than to select the "best" process.

As we discuss in the next pages, major-element variations seem to have been controlled, to a large extent, by crystal-liquid equilibria. Partial melting of young crustal lithologies is best suited to explain volume relations, but needs to be complemented by fractional crystallization coupled with assimilation to explain compositional and isotopic variations. The distribution patterns of some elements (e.g., Ni, Cr, Sr, and Rb), however, seem to record episodic periods of magma mixing.

Partial Melting

Partial melting provides the simplest solution to the problem of generating the very large volumes of silicic magma at Los Humeros. For example, the experimental results of Busch et al. (1974), Helz (1976), Dixon and Rutherford (1983), coupled with the analysis of Marsh (1984), suggest that the 100 km^3 of Xâltipan rhyolitic magma could be

reasonably generated from partial melting of less than 1000 km^3 of rock.

The relatively primitive isotopic ratios of most Los Humeros magmas seem to rule out the possibility that they could be primary melts derived from partial melting of old upper continental crust, and the positive E_{Nd} values rule out lower crustal rocks. Furthermore, the necessity for any melt extracted from a peridotitic source to be in equilibrium with residual forsteritic olivine precludes the derivation of the rhyolitic and rhyodacitic portions of the chamber, and for that matter of the Los Humeros andesites (cf. Gill, 1981, pp.251-256), as primary partial melts of the mantle. These arguments limit the potential sources to young continental crust, such as the early Tertiary plutons that crop out around Los Humeros (YÁÑez and Casique, 1980) or the inferred supporting intrusives of the late Tertiary andesitic and ferrobasaltic lavas. Melting of the volcanic pile itself is rejected on the basis of the small thickness (~1,000 m) established by drilling (Ferriz, 1982).

The low Al_2O_3 and CaO contents of the Los Humeros rhyolites, as well as the high K_2O contents, contrast markedly with those derived experimentally from mafic and intermediate rocks (Busch, 1974; Helz,1976; Dixon and Rutherford, 1983). The composition of the experimental products reflects the early melting of plagioclase, which will probably make Sr and Eu contents to be much higher than the ones observed in for example the XÁltipan pumice (e.g. Figure 13c). The generation of the Los Humeros rhyolitic

magma from a silicic primary melt would thus seem to require a significant amount of plagioclase fractionation at higher levels in the crust.

Admitting as a temporary hypothesis that silicic primary melts could have been formed by partial melting of young mafic continental crust, it could be argued that the generation of more mafic melts could result from larger degrees of partial melting. Features like the compositional gaps could then be explained by accretion of magmas generated by consecutive episodes of batch melting. The volumetric predominance of rhyolitic magma over all other types, however, imposes a severe constraint in a model based in an increasing degree of partial melting, and for that matter in all simple differentiation mechanisms that imply a common origin for all the different magma types erupted at Los Humeros. That these magma types coexisted in the same chamber during the last 0.46 Ma is demonstrated by the similar compositional ranges of the major eruptive units, but the integration of the chamber may have involved the generation of a large volume of silicic magma through partial melting, later coalescence of more mafic melts derived from different sources, and final modification of original compositional traits by high-level differentiation mechanisms.

Crystal Fractionation

Conceptually, the different compositions observed within any single eruptive unit could be the result of crystal

fractionation process such as crystal settling or marginal crystallization with ascent of a buoyant boundary layer. Table 13 shows the results of modeling the diverse major-element compositions as the result of simple crystal fractionation through a least-squares approximation (Bryan et al., 1968). The phenocryst compositions used in modeling are those of the presumed parent (indicated by an asterisk for any given model) and are reported by Ferriz (in press). For the sake of simplicity we have assigned equal weights to all the major and minor oxides, as weighted models improved the sum of the squares of the residuals but barely affected the proportions of the fractionated phases. We consider the residuals of all models as acceptable, so at least from the mathematical point of view the crystal fractionation hypothesis provides a suitable explanation for the major-element variations.

Enrichment trends defined by the data available on the Xâltipan and Zaragoza Tuffs (Figure 7) are also qualitatively consistent with a crystal fractionation mechanism. Fractionation of plagioclase ($\pm$ sanidine) and biotite (presumably with zircon inclusions) from Xâltipan rhyodacitic magma to generate Xâltipan high-silica rhyolite magma (models 1 and 1b) is congruent with the relative depletion of the latter in Al, Ca, Na, Sr, Eu, Ba, Sc, Ti, Mn, Fe, Co, Zn, Zr, and Hf and with its relative enrichment in K, Rb, Y, REE (except Eu), Th, and U. Fractionation of plagioclase, clinopyroxene, orthopyroxene, magnetite, and

Table 13. Least-squares approximations of crystal fractionation models

	Sample	1	1b	2	3	4	5	6	7	8	9	10	11	12	13	14	15	16	17	18	19
Xaltipan rhyolite	LH7	75	70																		
Xaltipan rhyodacite	LH14	*	*	58																	
Xaltipan andesite	LH17			*	18																
Ocotepec rhyolite	LH29					86															
Faby hi-Si rhyodacite	LH31					*	85														
Faby low-Si rhyodacite	LH34						*	48													
Faby andesite	LH35							*	22												
Zaragoza hi-Si rhyodacite	LH41									92											
Zaragoza low-Si rhyodacite	LH44									*	53										
Zaragoza hi-Si andesite	LH45										*	65									
Zaragoza low-Si andesite	LH47											*	32								
Tepeyahualco hi-Si andesite	LH61													84							
Tepeyahualco low-Si andesite	LH57													*	27						
Limon hi-Si andesite	LH65															91					
Limon low-Si andesite	LH62															*	35				
Chiapa hi-Si andesite	LH72																	71			
Chiapa low-Si andesite	LH70																	*	22		
San Antonio rhyodacite	LH83																			57	
San Antonio andesite	LH84																			*	18
Olivine basalt	LH94				*				*				*		*		*		*		*
Plagioclase		17	9	25	44	13	12	32	42	7	29	20	36	8	39	2	34	18	42	27	44
Sanidine			19																		
Clinopyroxene				7	16		1	10	16		7	9	13	4	15		14	6	16	7	16
Orthopyroxene							1	5		1	5									4	
Olivine				5	12			1	12			2	12	2	12	4	11	2	12		13
Biotite		8	2																		
Magnetite				4	10	1	1	3	9		4	3	8	2	8	3	7	2	9	4	9
Ilmenite				1							1	1						1		1	
Sum r2		0.9	0.02	0.4	0.2	0.4	0.1	0.3	0.08	0.07	0.1	0.01	0.1	0.1	0.08	0.4	0.06	0.01	0.08	0.01	0.07

The * indicates the presumed parent in each model. The diagonal numbers opposite to the presumed daughter indicate the % residual melt it represents. The lower columns indicate the weight percent of the modeled fractionated phases. The large residuals of models 1 and 2 are largely due to poor fits for the alkalies (perhaps due to remobilization of the alkalies during hydration of the pumice). The least-square approximations were calculated using the formulation of Bryan et al. (1968). A program in BASIC that performs these calculations can be requested to the first author.

ilmenite from Zaragoza andesitic magma to generate Zaragoza rhyodacitic magma (model 9) is also consistent with the relative depletion of the latter in Mg, Al, Ca, Sc, Ti, Cr, Zn, Sr, and Eu, and with its relative enrichment in Na, K, Rb, Zr, Cs, Ba, REE (except Eu), Th, and U. The opposite directions of enrichment for Zr, Hf, Pb, and Ba between the Xáltipan and Zaragoza Tuffs seem to reflect the presence of biotite, zircon, and perhaps sanidine, in the fractionating assemblage of the former.

Most of the models, however, are only moderately successful in reproducing the absolute concentrations of some selected trace elements (Table 14). Relatively poor fits are particularly noticeable for Cr and Rb, which are underestimated in intermediate and mafic compositions, and for Ba, which is overestimated in silicic compositions but underestimated in intermediate ones. O'Hara (1977) has argued that relative enrichment in highly compatible elements like Cr, and in the large-ion lithophile elements, could result from fractionation in a chamber that is periodically replenished by less differentiated magma; this process needs not to be constrained to the more mafic portions of the chamber, and could conceptually take place at the scale of individual compositional levels (cf. Christiansen, 1984). Replenishment will have little effect in the major-element composition of derivative magmas, but in diagrams like those shown in Figure 13 it will shift the trend of the differentiates toward the upper right corner, hindering a straightforward correlation with the

Table 14. Estimates of elemental concentrations in residual magma.

	Model	1	1b	2	3	4	5	6	7	8	9
V	Estimated			70 ± 65	135 ± 135		15 ± 5	110 ± 100	135 ± 135	20 ± 2	90 ± 85
	Observed			<10	120		<10	36	140	<10 *	18
Cr	Estimated			2 ± 2	8 ± 8			1 ± 1	15 ± 15		1 ± 1
	Observed			<1	20 *			2	9		2
Rb	Estimated	130 ± 10	138 ± 19	112 ± 3	15 ± 2	140 ± 3	115 ± 3	75 ± 5	10 ± 3	110 ± 1	105 ± 5
	Observed	139	139	124 *	68 *	114 *	121 *	98 *	49 *	113	102
Sr	Estimated	35 ± 25	25 ± 15	230 ± 85	300 ± 235	55 ± 30	100 ± 55	290 ± 140	290 ± 215	105 ± 35	315 ± 135
	Observed	25	25	58 *	281	37	93	161	380	121	139 *
Ba	Estimated	450 ± 300	400 ± 390	690 ± 90	305 ± 100	955 ± 60	960 ± 60	980 ± 190	235 ± 95	885 ± 30	885 ± 105
	Observed	115 *	115	780	460 *	550 *	910	900	580 *	820 *	860
La	Estimated	25 ± 15	38 ± 7							38 ± 1	45 ± 5
	Observed	43	43							38	40
Eu	Estimated	0.5 ± 0.1	0.3 ± 0.3							0.9 ± 0.1	2.1 ± 0.4
	Observed	0.2 *	0.2							0.9	1.0 *
Yb	Estimated	3 ± 0.3	3.5 ± 0.4							2.8 ± 0.1	3 ± 0.3
	Observed	2.8	2.8 *							2.6	2.6

	Model	10	11	12	13	14	15	16	17	18	19
V	Estimated			135 ± 75	130 ± 130			115 ± 75	135 ± 135	75 ± 70	150 ± 150
	Observed			170	200			120	180	31	150
Cr	Estimated			5 ± 5	10 ± 10	5 ± 5	10 ± 10	1 ± 1	10 ± 10	1 ± 1	10 ± 10
	Observed			21 *	45 *	22 *	39 *	8 *	14	<1	6
Rb	Estimated	50 ± 2	10 ± 2	35 ± 1	10 ± 1	30 ± 2	10 ± 3	55 ± 1	10 ± 3	85 ± 5	15 ± 3
	Observed	58 *	34 *	46 *	31 *	31	26 *	63 *	40 *	95 *	52 *
Sr	Estimated	350 ± 95	285 ± 175	375 ± 40	290 ± 190	460 ± 10	290 ± 160	345 ± 85	290 ± 215	280 ± 110	295 ± 235
	Observed	415	404	421 *	389	472	442	307	403	156 *	352
Ba	Estimated			550 ± 20	205 ± 70			760 ± 60	235 ± 95	995 ± 85	275 ± 130
	Observed			570	480 *			750	590 *	850 *	710 *

Elemental concentrations calculated using equations (8) and (11) of Arth (1976). The +/- values encompass the solutions obtained assuming either surface equilibrium or total equilibrium between crystals and melt, as well as spread in partition coefficients. Maximum and minimum partition coefficients were compiled from Arth (1976), Hanson (1978), Irving (1978), Luhr and Carmichael (1980), Crecraft et al. (1981), Gill (1981), and Mahood and Hildreth (1983). The * indicates a poor fit.

replenishing magma. The low Ba contents in silicic products could be a consequence of sanidine fractionation (model 1b). We have excluded sanidine in most fractionation models because it is absent as a phenocryst in the presumed parent magmas, but are aware that it may had been a significant component of the phenocryst assemblage at larger degrees of crystallization.

Volume relations remain a major problem with any simple crystal-fractionation hypothesis. For example, from the models of Table 13 it can be concluded that to obtain the ~100 km^3 of rhyolitic magma erupted during the Xâltipan event through crystal fractionation of basalt, the original volume of the parental magma would need to have been of ~1200 km^3. There is no eruptive center in the Mexican Neovolcanic Belt that could serve as an analog to support the vigorous intrusion of mafic magma implied by this large volume.

Crystal settling is unlikely to have been a major fractionation mechanism because: (1) The aphyric nature of the voluminous high-silica rhyolite portion of the Xâltipan Tuff would imply abnormally efficient settling of phenocrysts of very different specific gravities in a magma of high viscosity. Superheating of the magma prior to eruption, or a drastic increase in the volatile content of the melt could conceivably lead to resorption of phenocrysts, but again resorption would have had to be abnormally efficient for all traces of even refractory minerals such as iron-titanium oxides and zircon to

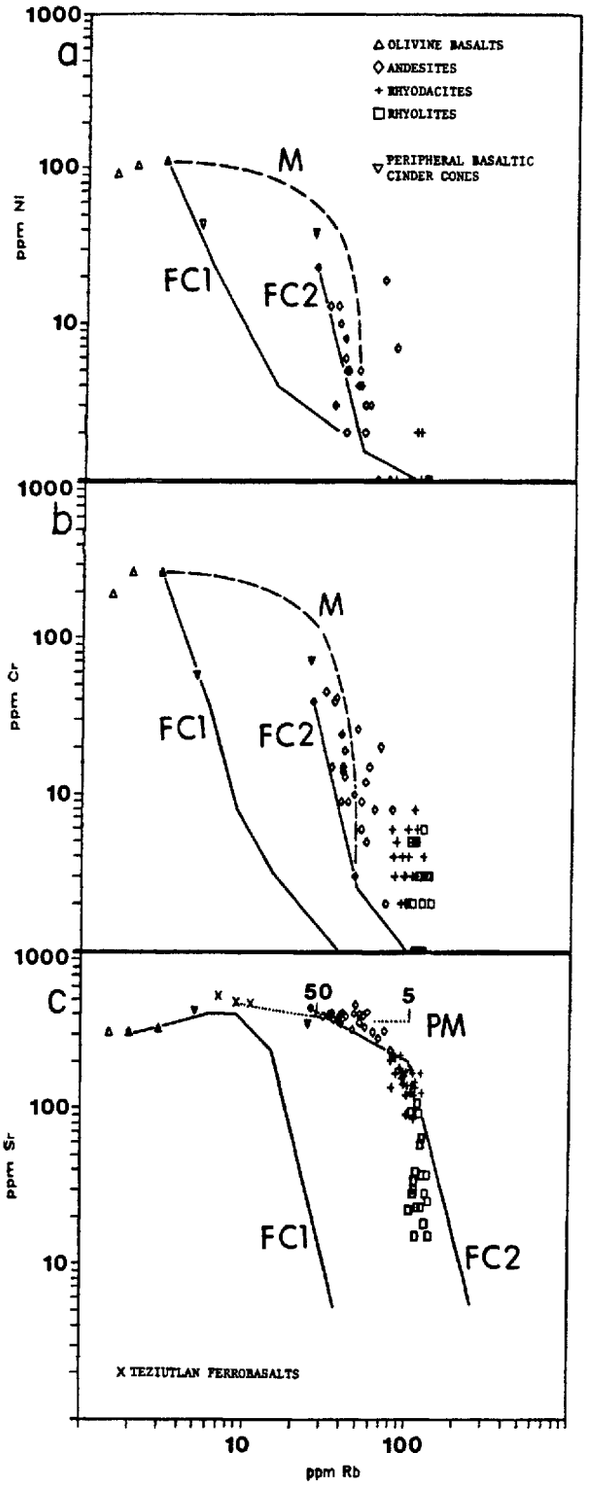

Fig. 13. Ni, Cr, and Sr contents plotted against Rb contents for samples from Los Humeros volcanic center and for two samples of basaltic cinder cones erupted at its periphery. Line FC1 is the trend that would result from fractional crystallization of the late-erupted olivine basalts, and line FC2 is the trend that would result from fractional crystallization of the most mafic flow unit of the Limón compound flow (LH62 in Table 11). Bulk partition coefficients were calculated using the mineral proportions of Table 13. Line M in (a) and (b) represents mixing between olivine basalt and the least mafic flow unit of the Tepeyahualco compound flow (LH60 in Table 11). Numbered tick marks on line PM in (c) indicate percent fusion at P_{H2O} = 5 kb of an amphibolite with major element composition similar to that of the Teziutlán ferrobasalts. Bulk partition coefficients were calculated using mineral proportions from the experimental results of Helz (1976).

completely disappear. (2) Crystal settling would not lead to the development of the compositional gaps observed in all major units. (3) Proportions of modeled fractionated phases are in most cases different from the observed proportions of phenocrysts (Table 15). (4) Crystal settling would not lead to the development of the apparent isotopic zonation of the chamber.

A better alternative for a fractionation mechanism is crystallization along the margins of the magma chamber. As pointed out by the experimental work of Shaw (1974), McBirney (1980), Turner and Gustafson (1981), and Huppert et al. (1984), the heat loss along the cooling surfaces represented by the margins of the chamber would lead to the development of a crystallization interface or boundary layer. Since the magma at this crystallization interface would be more differentiated and thus less dense than the magma farther from the boundary layer, the former may migrate to higher levels in the chamber (but see Spera et al., 1984). This type of crystal fractionation mechanism could explain the development of one or more compositional gaps; ascent of a differentiated boundary layer might not be a continuous process but occur only after crystallization has advanced to such a degree that the density of the layer is low enough to generate buoyant forces that exceed the yield strength. Marginal crystallization may also explain the difference between modeled proportions of fractionated phases and the observed modal mineralogy, as parameters that control the crystallizing assemblage (e.g., temperature,

Table 15. Comparison of relative proportions of modeled fractionating phases (Table 12) and relative weight proportions of the modal mineralogy of the presumed parent (Ferriz, in press, table 3).

Model	1	2	3	4	5	6	7	8	9	10	11	12	13	14	15	16	17	18	19
Modeled																			
Plagioclase	0.7	0.6	0.5	0.9	0.8	0.6	0.5	0.9	0.6	0.6	0.5	0.5	0.5	0.2	0.5	0.6	0.5	0.6	0.5
Clinopyroxene		0.2	0.2		0.1	0.2	0.2		0.2	0.3	0.2	0.3	0.2		0.2	0.2	0.2	0.2	0.2
Orthopyroxene					0.1	0.1		0.1	0.1									0.1	
Olivine		0.1	0.2				0.2			0.1	0.2	0.1	0.2	0.5	0.2	0.1	0.2		0.2
Biotite	0.3																		
Magnetite		0.1	0.1	0.1	0.1	0.1	0.1		0.1	0.1	0.1	0.1	0.1	0.3	0.1	0.1	0.1	0.1	0.1
Ilmenite																			
Observed																			
Plagioclase	0.1	0.3	0.2	0.5	0.4	0.3	0.2	0.6	0.7	0.2	0.2	0.5	0.2	0.5	0.2	0.8	0.2	0.4	0.2
Clinopyroxene	0.1	0.4	0.1		0.2	0.3	0.1		0.2	0.1	0.1	0.2	0.1		0.1	0.1	0.1	0.2	0.1
Orthopyroxene				0.4	0.2	0.1		0.2	0.1	0.2								0.1	
Olivine		0.2	0.7			0.3	0.7			0.1	0.7	0.2	0.7	0.5	0.7	0.1	0.7	0.1	0.7
Biotite	0.5																		
Magnetite	0.1	0.1	0.1	0.1	0.1	0.1	0.1	0.1		0.2	0.1	0.1	0.1	0.1	0.1		0.1	0.1	0.1
Ilmenite	0.1		0.1	0.1	0.1		0.1	0.1		0.2	0.1		0.1		0.1		0.1		0.1

Note: Proportions may not add to 1.0 because of rounding.

volatile fugacity) could be significantly different between the boundary layer and the predominant volume of the chamber. Simple marginal crystallization does not explain, however, the apparent zonation of heavy isotopes in the chamber, although Shaw (1974) has argued that, given enough contrast between the chemical potential of two components across the crystallization interface, diffusional exchange with the wall rocks of the chamber may significantly affect the isotopic ratios of the boundary layer.

Assimilation

Assimilation, most probably coupled with crystallization (Taylor, 1980; DePaolo, 1981), is perhaps the simplest way to explain the apparent isotopic variations and zonation of the Los Humeros magmas, particularly since our limited knowledge of the nature of the crust under eastern Mexico allows unlimited choices of hypothetical contaminants! In this section we will thus limit ourselves to inquire upon some scenarios that might explain (1) the relatively "primitive" isotopic ratios of the high-silica rhyolite portion of the chamber, (2) the apparent trend observed between the Xáltipan, Faby, and Zaragoza Tuffs in the E_{Sr} vs. SiO_2 diagram (Figure 12a), and (3) the E_{Sr} trend observed between the basaltic, andesitic, and Zaragoza magmas.

For modeling purposes we have initially taken the isotopic values of the Pizarro dome (AA in Figure 1) as an end-member representing a potential crustal contaminant,

akin perhaps to the Tertiary intrusions that crop out around the volcanic center, and the values of the olivine basalt as an end-member representing a relatively primitive, mantle-derived magma. For lack of data, the other lithologies from the local "basement" are treated in a qualitative way.

A simplified assimilation-fractional crystallization (AFC) model for Xâltipan rhyolitic magma is represented by line A-B in Figure 14. Under the conditions of the model (Table 16), rhyolitic magma with the isotopic signatures of the Xâltipan pumice could be obtained after 80% crystallization of a mixture of 80% by weight basaltic magma and 20% contaminant. These figures suggest that the 100 km^3 of the silicic portion of the tuff could have formed by AFC of an integrated volume of ~400 km^3 of basaltic magma. This volume is not unreasonable since the edifices of the andesitic stratovolcanoes of eastern Mexico have volumes approaching 200 km^3. Similar models with other hypothetical contaminants such as lower crust granulites, Paleozoic schists, Triassic sandstones, and Jurassic and Cretacic limestones, imply either a minimum amount of contamination, and thus a very large volume of basaltic magma, or E_{Sr} and E_{Nd} values significantly different from those of the Xâltipan rhyolitic pumice (Figure 16).

The low E_{Sr} values of the rhyolitic portion of the chamber can also be explained through assimilation by originally radiogenic magma of young, isotopically primitive, Sr-rich roof rocks. Given the very low Sr contents of the Xâltipan rhyolitic melt, small amounts of

Table 16. Conditions for the models for the isotope systematics.

Model	Initial magma						Contaminant						Model conditions		
	ESr	ENd	d018	Sr	Nd	SiO2	ESr	ENd	d018	Sr	Nd	SiO2	r	DSr	DNd
A	-9.1	4.1	5.8	370	15	49	4.4	-1.4	8.4	75	35	70	0.2	2.0	0.6
B	-7.1	2.0	6.5	70	33	67	4.4	-1.4	8.4	75	35	70	0.2	5.0	0.6
C	4.4	1.4	6.9	10	25	77	-9.1	4.1	5.8	360	15	49	1.0	2.0	0.6
D	2.1		7.1	160		70	-3.5		6.9	10		77			
E	2.1		7.1	160		70	-3.5		6.9	10		77	0.99	0.15	
F	-9.1	4.1	5.8	370	10	49	4.4	-1.4	8.4	400	40	65	0.4	0.2	0.6
G	-7.7	2.5	6.0	470	15	52	4.4	-1.4	8.4	400	40	65	0.4	0.77	0.6
H	-4.5	1.0	6.5	540	30	55	4.4	-1.4	8.4	400	40	65	0.4	0.89	0.6
I	-1.4	0.4	6.7	540	35	56	4.4	-1.4	8.4	400	40	65	0.4	2.0	0.6
J	-9.1	4.1	5.8	367	10	49	-1.4	0.4	6.7	540	20	56	0.9	0.65	0.6
L	-9.1	4.1	5.8	370	10	49	75	-6		500	5	10	0.2	2.5	0.6
M	-9.1	4.1	5.8	370	10	49	110	-22		150	30	70	0.2	2.5	0.6
N	-9.1	4.1	5.8	370	10	49	110	-7		200	15	60	0.2	2.5	0.6
O	-9.1	4.1	5.8	370	10	49	0	-15		250	20	70	0.2	2.5	0.6

Models have been calculated using equations (3), (6), (13), (15), (19), and (20) of DePaolo (1981); r is the ratio of the rate of assimilation to the rate of crystallization. All models are consistent with observed variations in silica content. The bulk partition coefficient for 18O has been assumed to be zero in all models.

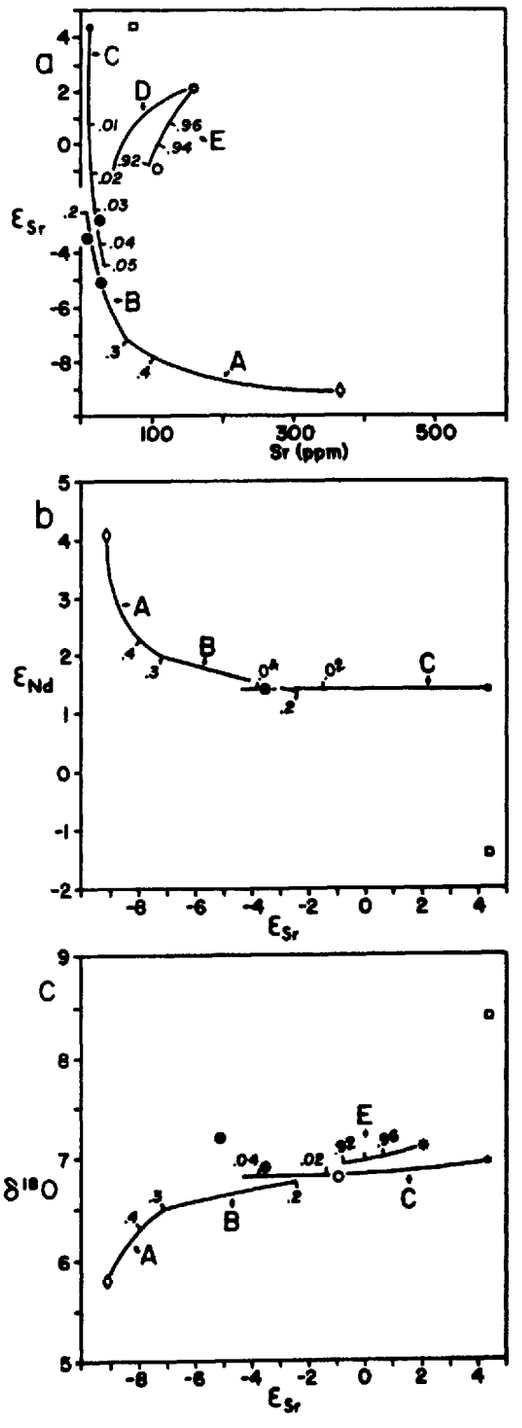

Fig. 14. Assimilation-fractional crystallization and mixing models (Table 16) for the silicic portion of the chamber. Symbols as in Figure 12. The tick marks in curves A, B, and E are labeled with fraction of melt remaining. The tick marks in curve C are labeled with weight percent of mixed basaltic magma.

assimilation of material similar in composition to, for example, the Teziutlán lavas would result in a large shift in the E_{Sr} of the magma (cf. with discussion of Curve C in the next section). Addmitedly, the temperature of the rhyolitic magma may be insufficient to completely melt a rock of ferrobasaltic composition. However, the early melting of plagioclase, where a significant amount of the Sr of the rock would be expected to reside, could produce the shift toward lower E_{Sr} at even incipient degrees of melting of the contaminant. Note that the $d^{18}O$ values of the pre- and post-Xáltipan rhyolites preclude assimilation of hydrothermally altered rock.

The trend defined by the data of the Xáltipan, Faby, and Zaragoza Tuffs could have been a consequence of the eruptive and collapse processes themselves. The disequilibrium induced in the magma chamber and its host rocks by major magma withdrawal and caldera collapse might have favoured entrainment and later assimilation of host-rock fragments. In fact, fragments of andesite are occasionally found within pumice of the Faby Tuff. They have not been found, however, within pumice fragments of the Zaragoza Tuff. Furthermore, the isotopic values of the pre-Faby rhyolites indicate that the rhyolitic portion of the chamber retained its low E_{Sr} values for nearly 0.2 Ma after the Xáltipan eruption, thereby suggesting that this mechanism is not responsible for the higher E_{Sr} of the Faby Tuff. As we point out below, limited mixing within the

silicic portion of the chamber provides a better explanation.

The main constraint in modeling the Zaragoza-andesite-basalt trend as a simple AFC process is the fact that the Sr contents of the magmas involved do not increase monotonically (Taylor, 1980), but attain a maximum value in the more silicic andesitic compositions. This may be due to the fact that the bulk partition coefficient of Sr would increase as the degree of differentiation increases. The result of such an increase is depicted by the composite curve F-G-H-I in Figure 15a. Under the conditions assumed this model provides a poor fit to the E_{Sr}-$d^{18}O$ and E_{Sr}-E_{Nd} systematics, although its general shape is consistent with the data.

Magma Mixing

Perhaps the most compelling evidence that magma mixing took place at Los Humeros is the presence of euhedral xenocrysts of strongly magnesian clinopyroxene ($En_{47}Fs_{8}Wo_{45}$) and olivine (Fo_{85}) in the dacitic Xoxoctic Tuff (Ferriz, in press), which erupted sometime between 0.06 and 0.04 Ma ago. At Los Humeros, the only other magma type with such strongly magnesian mineralogy are the late-erupted olivine basalts, so the euhedral Xoxoctic xenocrysts are indicative of at least one period of injection of basaltic magma in the Los Humeros chamber at ~0.05 Ma ago. Very sparse, strongly magnesian olivine xenocrysts also have been found in some crystal concentrates of Xáltipan dacitic and rhyodacitic

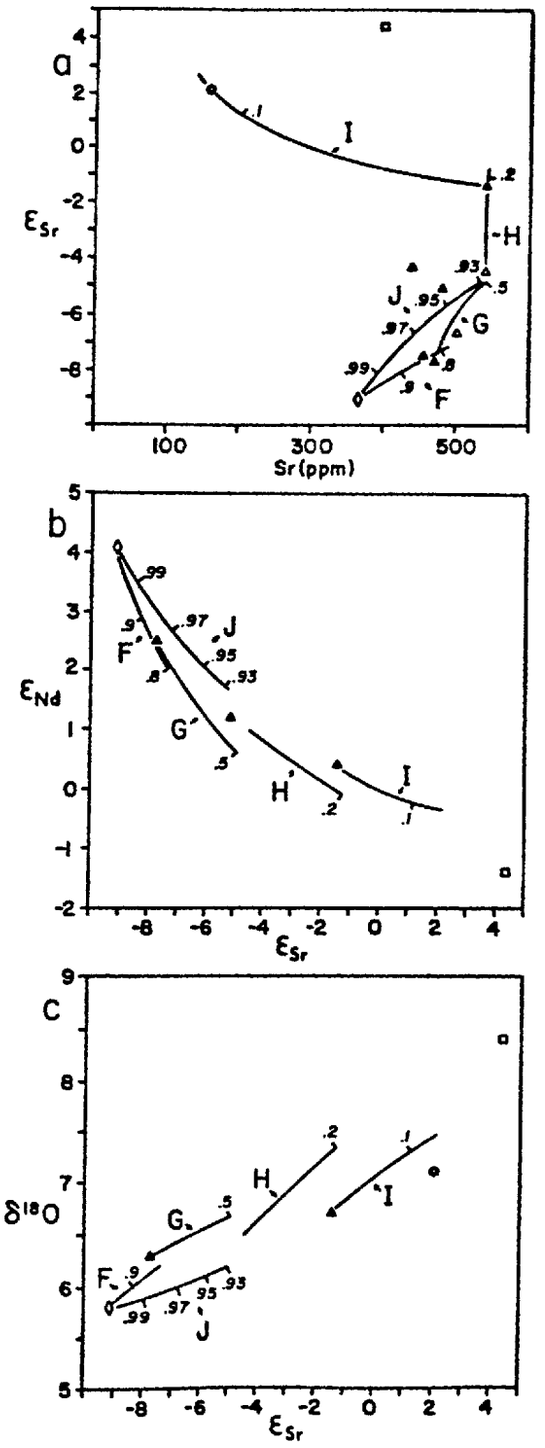

Fig. 15. Assimilation-fractional crystallization and mixing models (Table 16) for the andesitic portion of the chamber. Symbols as in Figure 12. Tick marks are labeled with fraction of melt remaining.

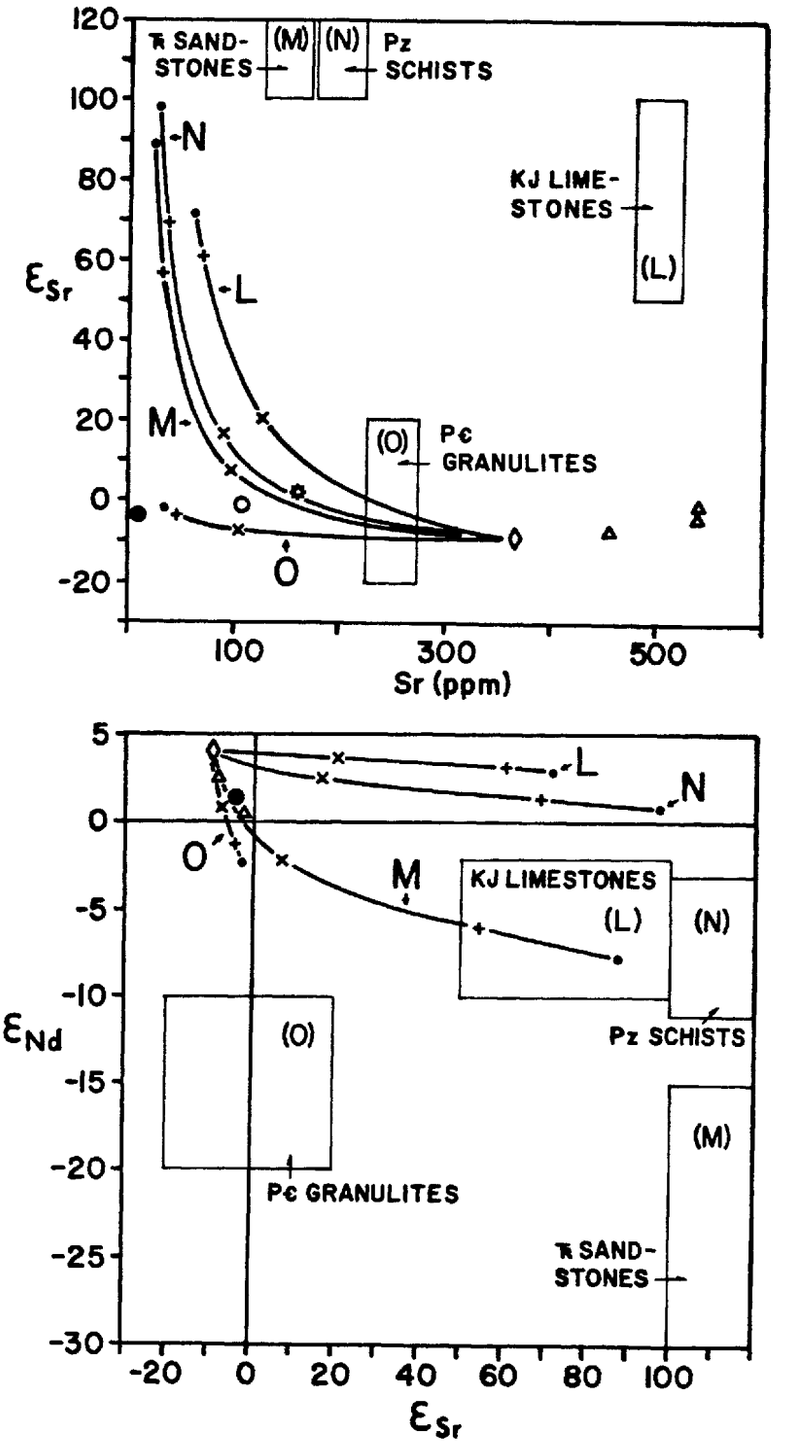

Fig. 16. Assimilation-fractional crystallization models between olivine basalt and lithologies of the local "basement" (Table 16). The assumed contaminant is identified by the same label as the AFC model. The isotopic values of the assumed contaminants are hypothetical, although we consider them reasonable. The x, +, and • along each curve represent andesitic, rhyodacitic, and rhyolitic compositions, respectively. Symbols for Los Humeros samples as in Figure 12.

pumice and of Zaragoza rhyodacitic pumice, which suggests that the injection of basalt has occurred several times (perhaps continuously) at Los Humeros.

Although there is mineralogic evidence of magma mixing throughout the active lifetime of Los Humeros, its role as a major mechanism in the development of the major-element compositional zonation is uncertain. The small volume of erupted dacitic magma, and the persistence of compositional gaps for nearly 0.5 Ma, are difficult to reconcile with large scale mixing. On the other hand, isotopic and some of the trace-element trends discussed in a previous section could in principle be the result of combined fractionation and small amounts of mixing.

Curve C in Figure 14 is an example of the effect that small amounts of mixing can have in isotopic ratios. As shown by this model, the low E_{Sr} of the Xáltipan ignimbrite could have resulted from contamination of a formerly high E_{Sr} rhyolitic magma with low E_{Sr} basaltic magma. Given the very low Sr contents of the Xáltipan rhyolitic magma, as little as 4% by weight contamination with basaltic magma would be enough to decrease the E_{Sr} value from +4.4 to -3.5. This scenario, however, will force us to explain the low E_{Sr} of the pre-Faby rhyolites through a practically identical repetition of the contamination process shortly before their emplacement. We consider this alternative unlikely, although possible. As mentioned before, however, the same shift could be produced by assimilation of isotopically primitive roof

rocks, which would be better suited to explain the persistence of low E_{Sr} in the upper levels of the chamber.

The Xàltipan-Faby-Zaragoza E_{Sr} trend could also be interpreted as the result of limited mixing between low E_{Sr} high silica rhyolite Xàltipan magma and high E_{Sr} Zaragoza rhyodacitic magma. Curves D and E in Figure 14a represent simple binary mixing and mixing coupled with fractional crystallization, respectively, between Xàltipan and Zaragoza magmas. The simple mixing hyperbola would imply very low Sr contents or very high E_{Sr} values for the products of mixing, which contrasts with the intermediate values of the Faby Tuff. Curve E was calculated assuming that the mixing of lower temperature rhyolitic magma with higher temperature rhyodacitic magma would induce some crystallization of the latter (Table 16). Under these conditions the mixing of 5% by weight of Xàltipan rhyolitic magma with Zaragoza magma would be enough for the latter to attain the isotopic signatures of the Faby magma. It must be pointed out that explaining the Xàltipan-Faby-Zaragoza E_{Sr} trend through a magma mixing-fractional crystallization process implies that the Zaragoza magma acquired its isotopic signature before coalescing with the rhyolitic chamber and that mixing was limited, perhaps due to density stabilization.

Finally, to explain the basalt-andesite E_{Sr} trend a scenario could be envisaged in which a magma chamber having a silicic upper portion and a Sr-rich andesitic lower portion is repeatedly underplated with basalt, which would then partially mix with the andesitic portion of the

chamber. Independently of whether the silicic and andesitic portions of the chamber did or did not have the same isotopic ratios, the final ratios in the andesitic portion would be a function of the degree of mixing between the original andesitic magma and the basaltic magma. This model is exemplified by Curve J in Figure 15, which was again calculated under the assumption that mixing with lower temperature magma would induce a small amount of crystallization in the higher temperature magma (Table 16). The fit of Curve J could be improved if magma mixing is envisaged as a multistage rather than a single-stage process but the small data base does not warrant such a refinement.

The trends observed in compatible-incompatible trace-element diagrams is consistent with small amounts of mixing between basaltic magma and high-silica andesite (Curve M in Figure 13). Addmitedly, the trends themselves could result from simple crystal fractionation of basaltic andesite magma like that of the lowermost flow unit of the Limón compound flow (Curve FC2 in Figure 13). At least for the andesitic portion of the chamber, however, the consistent displacement of the data toward values higher than those predicted by model FC2 can be explained as well by mixing between the olivine basalts and high-silica andesitic magma (Model J in Figure 15).

Liquid State Processes

The work of Kennedy (1955), Shaw (1974), Shaw et al. (1976), Hildreth (1979, 1981), McBirney and Noyes (1979),

and Mahood (1981a,b) has pointed out the potential importance of liquid state processes, such as diffusion under thermal and gravitational gradients, volatile transfer, and gradients in melt structure, in differentiation. Unfortunately, the "fingerprints" of these processes remain as yet poorly characterized.

Hildreth (1979, 1981) has suggested that in magma chambers that have differentiated enough to develop a high-silica rhyolite portion, liquid state processes could (as opposed to more "classic" differentiation mechanisms) lead to: (1) decreases in progressively less silicic products of the same eruption in the Na/K ratio and Mn contents, (2) strong depletion (<100 ppm) in the most silicic pumice of Sr, Ba, P, and Mg, (3) antithetic directions of enrichment of some of the elements in the first transition series (Sc to Zn), and (4) relative LREE depletion and HREE enrichment in the most silicic products. Except for the strong depletion of Sr, Ba, P and Mg, which might be applicable to the most silicic portion of the Xáltipan Tuff, the Los Humeros data seem largely inconsistent with the previous observations. The data for single eruptive units at Los Humeros can at best be considered scanty, however, and minor contributions to differentiation through liquid state processes might be beyond our resolution.

CONCLUSION

The previous analysis of differentiation mechanisms shows that no simple single-stage process is capable of

explaining the chemical, isotopic, and mineralogic traits of the Los Humeros volcanic products. Quantification of the role of some mechanisms is severely limited by our scanty knowledge of the nature of the crust in eastern Mexico and by our poor understanding of the physical aspects of magma generation, ascent, and coalescence in shallow chambers. Despite the oversimplifications that we have been forced to make, however, we believe that the inadequacy of our models indicates that magma generation and differentiation at Los Humeros was complex, and that several processes operated simultaneously or sequentially during the growth and active life of the chamber.

The multi-stage differentiation history of the Los Humeros system seems to record the initial stages of the growth of a large silicic system. Further evolution was inhibited, however, because the rate of differentiation processes which regenerate silicic magma were unable to compensate for the rate at which mass was lost during several major eruptions. The regeneration of crystal-poor, and presumably volatile-rich, uppermost levels during the 220,000 and 140,000 years of repose between the Xáltipan, Faby, and Zaragoza eruptions and the evidence for episodic injection of basaltic magma demonstrate that the chamber did not remain static between the various eruptions. As we have argued elsewhere (Ferriz and Mahood, 1984), the increasing rate of eruption may have reduced the residence time of intermediate magma in the system, thus decreasing

the time available for its differentiation, and for at least the last 100,000 years the eruption rate seems to have exceeded the rate of basaltic magma input.

Although in terms of mass balance the output rate seems to have exceeded the input rate, this may have not been the case with the thermal balance, which seems to have stayed constant during the lifetime of the system. Assuming cooling by conduction alone and a simplified formulation akin to that of Huppert and Sparks (1980), we estimate that for the thermal gradient to have remained relatively constant the chamber must have received mafic magma input at a minimum rate of 0.1 km^3 per thousand years; under hydrothermal cooling conditions the rate of mafic magma input may need to be as high as 10 km^3 per thousand years. The minimum estimated rate is an order of magnitude larger than the rate of extrusion of mafic magma, as estimated from the volumes and ages of the late-erupted olivine basalts and from a cinder cone field nearby (Ferriz and Mahood, 1984). This rate of injection of mafic magma can still be considered modest, however, when compared with the rates of 0.5 to 5 km^3 per thousand years estimated for Japanese and Central American volcanoes (Nakamura, 1974; Wood, 1978), 10 to 100 km^3 per thousand years for oceanic islands such as Hawaii and Iceland (Swanson, 1972; Schilling et al., 1978), and 50 km^3 per thousand years for silicic centers like Yellowstone and those of the Taupo volcanic zone (Wilson et al., 1984).

The rate of injection of mafic magma may have been much larger during the period of eruption of the Teziutlán lavas and the initial stages of integration of the chamber. During the last 0.5 Ma, however, the input of mafic magma seems to have been small enough that no significant volumes of differentiated magma were generated by partial melting of the wall rocks, but large enough to offset conductive or hydrothermal cooling that could lead to fractional crystallization.

ACKNOWLEDGEMENTS

Acknowledgement is made to Mexico's Comisión Federal de Electricidad and Consejo Nacional de Ciencia y Tecnología, to the Donors of the Petroleum Research Fund, administered by the American Chemical Society, and to the U.S. National Science Foundation (Grant EAR-8121380 to Mahood) for support of this research. Major-element XRF analyses provided by the Anaytical Laboratories Branch of the U.S. Geological Survey, and $d^{18}O$ analyses provided by courtesy of C.M.Johnson (U.S. Geological Survey) are greatly appreciated. We also owe thanks to M.Hochella for guidance in operating the XRF equipment, to R.L.Smith for providing INA analyses, and to A.Grunder and C.E.Seedorff for helpful reviews of the manuscript.

REFERENCES

Alvarez,R., 1978, Telluric, self-potential and surface temperature profiles on Los Humeros caldera: Geofisica Internacional, v.17, p.445-460.

Alvarez,R., 1980, Outlining tectonism and faulting with tellurics in Los Humeros-Derrumbadas geothermal area: Trans. Geotherm. Resour. Counc., v.4, p.1-4.

Arth,J.G., 1976, Behavior of trace elements during magmatic processes - A summary of theoretical models and their applications: Jour. Research U.S. Geol. Surv., v.4, p.41-47.

Bohlen,S.R., Peacor,D.R., Essene,E.J., 1980, Crystal chemistry of a metamorphic biotite and its significance in water barometry: Am. Mineral., v.68, p.477-493.

Bryan,W.B., Finger,L.W., Chayes,F., 1969, Estimating proportions in petrographic mixing equations by least-squares approximation: Science, v.163, p.926-927.

Burnham,C.W., Jahns,R.H., 1962, A method for determining the solubility of water in silicate melts: Am. J. Science, v.260, p.721-745.

Burnham,C.W., Holloway,J.R., Davis,N.F., 1969, Thermodynamic properties of water to 1000° C and 10,000 bars: Geol.Soc.Amer. Spec. Paper 132, 96p.

Busch,W, Schneider,G., Mehnert,K.R., 1974, Initial melting at grain boundaries, Part II: Melting in rocks of granodioritic, quartzdioritic, and tonalitic composition: N.Jb. Miner. Mh., v.8, p.345-370.

Carmichael,I.S.E., Nicholls,J., Spera,F.J., Wood,B.J., Nelson,S.A., 1977, High-temperature properties of silicate liquids: Applications to the equilibration and ascent of basic magma: Philos. Trans. R. Soc. Lond., Ser.A, v.286, p.373-431.

Carmichael,I.S.E., Turner,F.J., Verhoogen,J., 1974, Igneous Petrology: McGraw-Hill Book Co., New York, 739p.

Christiansen,E.H., 1984, Geochemical evolution of a magmatic system open to self-contamination --An examination of fractionation in a double-diffusive magma system: in M.A. Dungan, T.L. Grove, and W. Hildreth (eds.), Proceedings of the Conference on Open Magmatic Systems: Inst. Study Earth Man, S. Method. Univ., Dallas, Texas, August 21-28, p.26-28.

Crecraft,H.R., Nash,W.P., Evans,S.H., 1981, Late Cenozoic volcanism at Twin Peaks, Utah. Part I: Geology and petrology: J. Geophys. Res., v.B86,p.10303-10320.

DePaolo,D.J., 1981, Trace element and isotopic effects of combined wallrock assimilation and fractional crystallization: Earth Planet. Sci. Lett., v.53, p.189-202.

DePaolo,D.J., Wasserburg,G.J., 1976, Nd isotopic variations and petrogenetic models: Geophys. Res. Lett., v.3, p.249-252.

Eggler,D.H., 1972, Water-saturated and undersaturated melting relations in a Paricutin andesite and an estimate of water content in the natural magma: Contrib. Mineral. Petrol., v.34, p.261-271.

Ewart,A., Hildreth,W., Carmichael,I.S.E., 1975, Quaternary acid magma in New Zealand: Contr. Mineral. Petrol., v.51, p.1-27.

Ferriz,H., 1982, Geologic and preliminary reservoir data on the Los Humeros geothermal system, Puebla, Mexico: in Proceedings Eighth Workshop Geothermal Reservoir Engineering (SGP-TR-60), p.19-24, Stanford University, Stanford, California.

Ferriz,H., in press, Zoneamiento composicional y mineralógico en los productos eruptivos del centro volcánico de Los Humeros, Puebla, Mexico: Geofísica Internacional.

Ferriz,H., Mahood,G.A., 1984, Eruption rates and compositional trends at Los Humeros volcanic center, Puebla, Mexico: J. Geophys. Res., v.B89, p.8511-8524.

Ferriz,H., Mahood,G.A., in press, Volcanismo riolítico en el Eje Neovolcánico Mexicano: International Committee for Study of the Lithosphere, Special Issue on Mexico, Geofísica Internacional.

Ferriz,H., Yáñez,C., 1981, Mapa geológico del centro volcánico de Los Humeros, estados de Puebla y Veracruz, México - Edición preliminar, (Map), Comisión Federal de Electricidad, Juan de la Barrera #37, Cd. Satelite, Edo. de Mexico, 53100, MEXICO.

Gill,J.B., 1981, Orogenic Andesites and Plate Tectonics: Springer-Verlag, New York, 390p.

Hanson,G.N., 1978, The application of trace elements to the petrogenesis of igneous rocks of granitic composition: Earth Planet. Sc. Let., v.38, p.26-43.

Haskin,L.A., Haskin,M.A., Frey,F.A., Wildeman,T.R., 1968, Relative and absolute terrestrial abundances of the rare earths: in L.H. Ahrens (ed.), Origin and Distribution of the Elements, Int. Ser. Mon. Earth Sci., v.30, p.45-54.

Heltz,R.T., 1976, Phase relations of basalts in their melting ranges at P_{H2O} = 5 kb., Part II, Melt compositions: J. Petrol., v.17, p.139-193.

Hildreth,E.W., 1977, The magma chamber of the Bishop Tuff: Gradients in temperature, pressure, and composition [Ph.D. thesis]: Berkeley, University of California, 328p.

Hildreth,E.W., 1979, The Bishop Tuff: Evidence for the origin of compositional zonation in silicic magma chambers, in Chapin,C.E., and Elston,W.E., eds., Ash-flow Tuffs: Geol. Soc. Am. Spec. Paper 180, p.43-75.

Hildreth,E.W., 1981, Gradients in silicic magma chambers: Implications for lithospheric magmatism: J. Geophys. Res., v.B86, p.10153-10192.

Huppert,H.E., Sparks,R.S.J., 1980, The fluid dynamics of a basaltic magma chamber replenished by influx of hot dense ultrabasic magma: Contrib. Mineral. Petrol., v.75, p.279-289.

Huppert,H.E., Sparks,R.S.J., Turner,J.S., 1984, Some effects of viscosity on the dynamics of replenished magma chambers: J. Geophys. Res., v.B89, p.6857-6877.

Irvine,T.N., Baragar,W.R., 1971, A guide to the chemical classification of the common igneous rocks: Can.J. Earth Sci., v.8, p.523-548.

Irving,A.J., 1978, A review of experimental studies of crystal/liquid trace element partitioning: Geochem. Cosmochem. Acta, v.42, p.743-770.

Kennedy,G.C., 1955, Some aspects of the role of water in rock melts: Geol. Soc. Am. Spec. Pap. 62, p.489-504.

Lachenbruch,A.H., Sass,J.H., Munroe,R.J., Moses Jr.,T.H., 1976, Geothermal setting and simple heat conduction models for the Long Valley caldera, J. Geophys. Res., v.B81, p.769-784.

Luhr,J.F., Carmichael,I.S.E., 1980, The Colima volcanic complex. Part I. Post-caldera andesites from Volcán Colima: Contrib. Mineral. Petrol., v.71, p.343-372.

Maaloe,S., Wyllie,P.J., 1975, Water content of a granite magma deduced from the sequence of crystallization determined experimentally with water-undersaturated conditions: Contrib. Mineral. Petrol., v.52, p.175-191.

Mahood,G.A., 1981a, Chemical evolution of a Pleistocene rhyolitic center: Sierra La Primavera, Jalisco, Mexico: Contrib. Mineral. Petrol., v.77, p.129-149.

Mahood,G.A., 1981b, A summary of the geology and petrology of the Sierra La Primavera, Jalisco, Mexico: J. Geophys. Res., v.B86, p.10137-10152.

Mahood,G.A., Hildreth,W., 1983, Large partition coefficients for trace elements in high-silica rhyolites: Geochem. Cosmochem. Acta, v.47, p.11-30.

Marsh,B.D., 1984, Mechanisms and energetics of magma formation and ascension: in Explosive Volcanism: Inception, Evolution, and Hazards, National Academy Press (Studies in Geophysiscs), Washington, D.C., p.67-83.

McBirney,A.R., 1980, Mixing and unmixing of magmas, J. Volcanol. Geotherm. Res., v.7, p.357-371.

McBirney,A.R., Noyes,R.M., 1979, Crystallization and layering of the Skaergaard intrusion: J. Petrol., v.20, p.487-554.

Nakamura,K., 1974, Preliminary estimate of global volcanic production rate: in Utilization of Volcanic Energy, edited by J.L. Golp and A.S. Furumoto: Sandia Laboratories, Albuquerque, New Mexico, p.273-285.

Naney,M.T., 1983, Phase equilibria of rock-forming ferromagnesian silicates in granitic systems: Am.J.Science, v.283, p.993-1033.

O'Hara,M.J., 1977, Geochemical evolution during fractional crystallization of a periodically refilled magma chamber: Nature, v.266, p.503-507.

Peacock,M.A., 1931, Classification of igneous rock series: J. Geol., v.39, p.54-67.

Peccerrillo,A., Taylor,S.R., 1976, Geochemistry of Eocene calc-alkaline volcanic rocks from the Kastamonu area, northern Turkey: Contrib. Mineral. Petrol., v.58, p.63-81.

Pèrez,J., 1978, Geologia y petrografia de la caldera de Los Humeros: Geomimet (Mexico), v.91, p.97-106.

Sack,R.C., Carmichael,I.S.E., Rivers,M.L., Ghiorso,M.S., 1980, Ferric-ferrous equilibrium in natural silicate liquids at 1 bar: Contrib. Mineral. Petrol., v.75, p.369-376.

Schilling, J-G., Unni,C.K., Bender,M.L., 1978, Origin of chlorine and bromine in the oceans: Nature, v.273, p.631-636.

Shaw,H.R., 1974, Diffusion of H_2O in granitic liquids: Part I. Experimental data; Part II. Mass transfer in magma chambers: in Geochemical Transport and Kinetics, edited by A.W.Hofmann, B.J.Giletti, H.S.Yoder, R.A.Yund, Carnegie Inst. Wash. Publ. 634, p.139-170.

Shaw,H.R., Smith,R.L., Hildreth,W., 1976, Thermo-gravitational mechanisms for chemical variations in zoned magma chambers: Geol. Soc. Am. Abstr. Prog., v.8, p.1102.

Smith,R.L., and Shaw,H.R., 1978, Igneous-related geothermal systems: U.S. Geol. Surv. Circular 790, p.12-17.

Spencer,K.J., Lindsley,D.H., 1981, A solution model for coexisting iron-titanium oxides: Amer. Mineralogist, v.66, p.1189-1201.

Spera,F.J., Yuen,D.A., Kemp,D.V., 1984, Mass transfer rates along vertical walls in magma chambers and marginal upwelling: Nature, v.310, p.764-767.

Stormer,J.C., 1983, The effects of recalculation on estimates of temperature and oxygen fugacity from analyses of multicomponent iron-titanium oxides: Am. Mineral., v.68, p.586-594.

Swanson,D.A., 1972, Magma supply rate at Kilauea volcano, 1952-1971: Science, v.175, p.169-170.

Taylor,H.P., 1980, The effects of assimilation of country rocks by magmas on $^{18}O/^{16}O$ and $^{87}Sr/^{86}Sr$ systematics in igneous rocks: Earth Planet. Sci. Lett., v.47, p.243-254.

Thorarinsson,S., 1967, The eruptions of Hekla in historical times: A tephrachronological study: in Einarsson, T. et al., eds., The Eruption of Hekla, 1947-1948, Reykjavik, Societas Scientiarum Islandica, 183p.

Turner,J.S., Gustafson,L.B., 1981, Fluid motions and compositional gradients produced by crystallization or melting at vertical boundaries: J. Volcanol. Geotherm. Res., v.11, p.93-125.

Verma,S.P., 1983, Magma genesis and chamber processes at Los Humeros caldera, Mexico - Nd and Sr isotope data: Nature, v.302, p.52-55.

Verma,S.P., 1984, Alkali and alkaline earth element geochemistry of Los Humeros caldera, Puebla, Mexico: J. Volcanol. Geotherm. Res., v.20, p.21-40.

Verma,S.P., López,M., 1983, Geochemistry of Los Humeros caldera, Puebla, Mexico: Bull. Volcanol., v.45, p.63-79.

Wilson,C.J.N., Rogan,A.M., Smith,I.E.M., Northey,D.J., Nairn,I.A., Houghton,B.F., 1984, Caldera volcanoes of the Taupo volcanic zone, New Zealand: J. Geophys. Res., v.B89, p.8463-8484.

Wones,D.R., and Eugster,H.P., 1965, Stability of biotite: experiment, theory and application: Am. Mineral., v.62, p.687-691.

Wones,D.R., 1972, Stability of biotite - a reply: Am. Mineral., v.57, p.316-317.

Wood,C.A., 1978, Morphometric evolution of composite volcanoes: Geophys. Res. Lett., v.5, p.437-439.

Yáñez,C., Casique,J., 1980, Informe geológico del proyecto geotérmico Los Humeros-Derrumbadas, estados de Puebla y Veracruz, Comisión Federal de Electricidad, Mexico, 59p.

Ferriz,H., 1982, Geologic and Preliminary Reservoir Data on the Los Humeros Geothermal System, Puebla, Mexico: Proceedings Eight Workshop Geothermal Reservoir Engineering (SGP-TR-60), Stanford University, Stanford, California, December 1982, p.19-24.

CHAPTER 4

GEOLOGIC AND PRELIMINARY RESERVOIR DATA ON THE LOS HUMEROS GEOTHERMAL SYSTEM, PUEBLA, MEXICO

ABSTRACT

Exploratory drilling has confirmed the existence of a geothermal system in the Los Humeros volcanic center, located 180 km east of Mexico City. Volcanic activity in the area began with the eruption of andesites and ferrobasalts, followed by two major caldera-forming pyroclastic eruptions. The younger Los Potreros caldera is nested inside the older Los Humeros caldera. At later stages, andesitic, rhyodacitic, and olivine basalt lavas erupted along the ring-fracture zones of both calderas.

Geologic interpretation of structural, geophysical, and drilling data suggests that: (1) The water-dominated geothermal reservoir is hosted by the early andesitic and ferrobasaltic volcanic pile, is bounded by the ring-fracture zone of the Los Potreros caldera, and is capped by the products of the oldest caldera-forming eruption. (2) Permeability within the andesitic pile is provided by faults and fractures related to intracaldera uplift. (3) The geothermal system has potential for a large influx of meteoric water through portions of the ring-fracture zones of both calderas. (4) Volcanic centers with similar magmatic and structural conditions can be found in the eastern Cascades, U.S.A.

INTRODUCTION

The Los Humeros volcanic center (LHVC) is located in the eastern end of the Mexican Neovolcanic Belt, 20 km northwest of Perote, Veracruz. Mild fumarolic activity

sparked interest in the geothermal potential of the area in the mid-1960's. Preliminary geological and geophysical reconnaissance surveys (Mooser, 1964; Pèrez, 1978; Alvarez, 1978) led Mexico's Comisiòn Federal de Electricidad to undertake an extensive exploration program that included regional geologic mapping (Yàñez and Casique, 1980), detailed geologic mapping of the volcanic center (Ferriz and Yàñez, 1981), resistivity, self-potential, and aeromagnetic surveys (Palacios and Garcìa, 1981), geochemical surveys (Molina, 1979), and exploration drilling (Rivera, 1982; Lòpez, 1982a; Gutièrrez, 1982). This paper integrates some of the information collected during the exploration program, under the framework of detailed geologic mapping, to provide preliminary data on the characteristics of the geothermal reservoir.

REGIONAL GEOLOGY AND LOCAL "BASEMENT"

The Quaternary Mexican Neovolcanic Belt is an irregular belt of large andesitic stratovolcanoes, cinder-cone fields, and a few silicic centers, which bisects central Mexico in an east-west direction. Molnar and Sykes (1969) suggested that magmatism along this belt is related to the subduction of the Cocos Plate below Mexico along the Middle America Trench. LHVC is one of several silicic centers located in the "back-arc" portion of the belt. Two other of these silicic centers, Los Azufres and La Primavera (Mahood, 1980), also host significant geothermal systems.

The local basement of LHVC is formed by a Mesozoic sedimentary sequence and Tertiary intrusions and andesites. The Mesozoic rocks (Viniegra, 1965; YÁÑez and Casique, 1980) can be divided in a Triassic to Middle Jurassic clastic sequence, and a Middle Jurassic to Upper Cretaceous sequence of marls and limestones of inferred low permeabilities.

GEOLOGIC HISTORY

The oldest exposed rocks at Los Humeros are dense porphyritic to sparsely porphyritic andesitic and ferrobasaltic flows of the Teziutlán Formation. K-Ar age determinations on these flows range from 3.5 $\pm$ 0.3 to 1.6 $\pm$ 0.1 Ma. These flows crop out in the northern portion of LHVC, but similar rock types have been found during drilling in its central and southern portions. Similar rock fragments are common in all the younger pyroclastic units. Thus, these andesite and basalts seem to have covered most of the area now occupied by LHVC. Mapping of flow directions, breccia pipes, and fossil hydrothermal alteration zones indicates that the vents for these flows were located in the area now occupied by LHVC. This inference is reinforced by an increase in the thickness of the Teziutlán Formation from 60 m in the northern outcrops to more than 1000 m in a borehole drilled in the central portion of LHVC (H-4 in Figure 1). It is in these dense and brittle rocks that fluid production has been found during exploration drilling.

Fig. 1. Simplified geologic map of the Los Humeros volcanic center. LHC, Los Humeros caldera rim; LPC, Los Potreros caldera rim; caldera rims discontinuous where inferred, dotted where buried. Heavy lines, faults. Triangles, boreholes. Sandstone pattern, Xáltipan Ignimbrite; boulder pattern, Zaragoza Ignimbrite; dashes and "v" patterns, rhyolitic and rhyodacitic domes; breccia pattern, scoria cones; dash-arrow and cross patterns, andesites; dash-dot pattern, rhyodacites; arrow pattern, olivine basalts; blank, tuffs younger than the Zaragoza Ignimbrite.

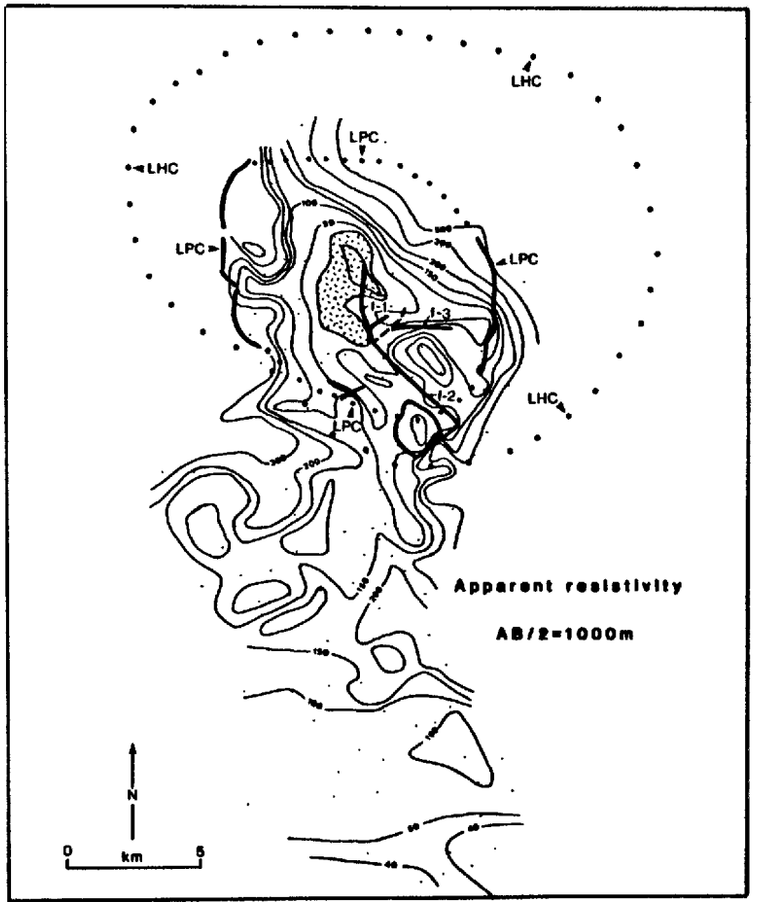

Fig. 2. Apparent resistivity isopleth map for AB/2 = 1 km. Resistivities in ohm-m. LHC, Los Humeros caldera; LPC, Los Potreros caldera. Heavy lines, faults. Dash pattern, area enclosed by the 20 ohm-m apparent resistivity contour. Light dots, center of sounding. Modified from Palacios and García, 1981.

The onset of silicic volcanism is marked by the intrusion of two high-silica rhyolite domes, one of which has been K-Ar dated at 0.47 ± 0.04 Ma. Later eruption of the 230 km^3 rhyolitic (77% SiO_2) to rhyodacitic (71% SiO_2) Xâltipan Ignimbrite led to the collapse of the Los Humeros caldera (LHC in Figure 1). The rim of this 21 by 15 km caldera is covered by younger volcanic rocks, so its configuration has been determined by the location of ring-fracture volcanism, as well as by topographic expression. Given the volume of magma equivalent to the Xâltipan Ignimbrite (~115 km^3) and the area of the caldera, one can estimate the average amount of collapse as 450 m. Nowhere is the Xâltipan Ignimbrite exposed inside the Los Humeros caldera, but a 200 m-thick moderately welded ignimbrite found at 965 m depth in the H-1 borehole is its intracaldera equivalent.

After collapse, several high-silica rhyolite domes were emplaced along the northwestern, northern, and southern (?) portions of the inferred ring-fracture zone. Their emplacement was followed by the eruption of ~40 km^3 of Faby rhyodacitic (72-69% SiO_2) air-fall tuffs.

The eruption of the 28 km^3 rhyodacitic (71% SiO_2) to andesitic (54% SiO_2) Zaragoza Ignimbrite resulted in the formation of the 10-km-diameter Los Potreros caldera (LPC in Figure 1), nested within the older Los Humeros caldera. Its eastern and western topographic walls can still be recognized in the field, but the northern and southern portions of the caldera rim have been obliterated by younger

ring-fracture volcanism. A minimum of 200 m of collapse has been estimated from reconstruction of precaldera topography. Outflow sheets of the Zaragoza Ignimbrite tilted up to 12°, and postcaldera lavas that flowed radially away from the Los Potreros caldera, indicate doming of the caldera and its surroundings shortly after collapse. Contemporaneously, a small andesitic volcanic edifice occupied the central portion of the caldera. This edifice was later intruded by a biotite rhyodacite dome.

After the emplacement of the Zaragoza Ignimbrite an arc of andesitic scoria cones developed along the southern ring-fracture zone of the Los Humeros caldera (Figure 1). The cinder cones fed approximately 4 km^3 of andesitic (53-59% SiO_2) lava that flowed south of LHVC. Similar lavas erupted from two small shield volcanoes located between the eastern and northeastern rims of the two nested calderas. The lavas from these volcanoes, which flowed radially away from the Los Potreros caldera, have a total volume of ~2 km^3.

Activity continued with the eruption of 10 km^3 of rhyodacitic (68-69% SiO_2) flows from centers located between the northern, eastern, and southern portions ring-fracture zones of the calderas. The simultaneous venting of rhyodacitic and andesitic tephra, approximately coeval with the eruption of the earliest rhyodacite flows, led to the collapse of the 1.7-km-diameter El Xalapazco caldera along the south-southeastern ring-fracture zone of the Los Potreros caldera. This eruption was followed by minor

fault-bounded uplift of the southeastern quadrant of the Los Potreros caldera, perhaps due to upward movement of magma.

The final stage of volcanic activity at LHVC is represented by the eruption of olivine basalts (49% SiO_2) on the floor of the Los Potreros and El Xalapazco calderas, and along the southwestern ring-fracture zone of the Los Humeros caldera. The total volume represented by these basalts is ~0.25 km^3.

The apparently erratic composition of the products of LHVC appears to represent tapping of different levels of a magma chamber that was zoned from rhyolite to basaltic andesite in composition, and probably underplated by olivine basalts. This tapping of different levels would be possible only because of the existence of two nested collapse structures of significantly different size, the ring-fracture zone of the larger structure tapping deeper levels of the magma chamber than that of the smaller structure. Perhaps more relevant for the development of the geothermal system is that: (1) the mere existence of the collapse structures suggests that the magma chamber was lodged at a shallow depth, (2) the volume of the eruptive products indicates that the magma chamber was a voluminous one, (3) the long magmatic history implies a prolonged period of heating of the rocks that hosted the magma chamber, (4) the ring-fracture zones of both calderas have persisted as zones of structural weakness or discontinuity for an extended period of time, thus providing favorable structural conditions for the development of a hydrothermal system.

GEOPHYSICAL DATA

Aeromagnetic surveys of the area (Flores et al., 1978; J. Ruiz in Palacios and García, 1981) show a change in polarity along the southern ring-fracture zone of the Los Humeros caldera, and a major bipolar anomaly on the northeastern quadrant of the Los Potreros caldera. The center of this bipolar anomaly corresponds with a small gravity high (Mena and González, 1978) and, from what is known about the geology of LHVC, could correspond to a swarm of basaltic dikes, to the thick central portion of the eruptive center(s) that fed the Teziutlán andesites, or to an intracaldera intrusion.

The LHVC corresponds with a broad negative low in the residual anomaly gravity map of Mena and González (1978), which they modeled as a $\leq$ 1-km-thick accumulation of material with an average density of 2.35 g/cm^3 and a density contrast of 0.32 g/cm^3 with respect to the surrounding rocks. An average thickness of 1 km for low-density intracaldera deposits is not unreasonable in the light of the results of boreholes H-1 and H-4 (Figure 1), in which the dense Teziutlán andesites were cut at depths of 1155 and 874 m respectively. I attribute other negative anomalies around LHVC to thick accumulations of the outflow sheets of the Xaltipan Ignimbrite.

Palacios and García (1981) reported the results of 184 Schlumberger vertical electric soundings with maximum electrode spacings (AB/2) of 2 km, and 32 soundings with maximum spacings of 4 km. Their results have been used to

construct the simplified isopleth map of apparent resistivities, for an AB/2 spacing of 1 km, shown in Figure 2; the major structural features defined by geologic mapping are also shown as heavy lines and dots. A zone of low resistivity, delineated by the 20 ohm-m contour, occupies the central portion of the Los Potreros caldera; the general shape of the low seems to be controlled by fault f-1 and by the northwestward projection of fault f-2. Fault control in the central portion of the Los Potreros caldera seems to be better expressed by the 50 ohm-m contour, spurs of which are aligned along faults f-2 and f-3; however, the major southern spur of this contour does not correspond to any mappable fault or fracture zone. Apparent resistivities increase abruptly toward the rim of the Los Potreros caldera, except at the southern caldera rim and along a narrow "channel" through the northwestern rim. Thus, the Los Potreros ring-fracture zone seems to constitute an impermeable barrier that partially bounds the geothermal system, except for the southward and northwestern "openings", which, as discussed below, may represent zones of meteoric water influx into the system. Structural control by intracaldera faults can still be recognized in apparent resistivity maps with AB/2 of 1.5 and 2 km (Palacios and García,1981) but, in addition, the southern ring-fracture zone of the Los Potreros caldera seems to become a major controlling structure.

BOREHOLE DATA

Up to 1982 three boreholes had been completed in the area (Figure 1). The data obtained during drilling have been reported by Gutiérrez (1982), López (1982a,1982b), and Rivera (1982a).

The first exploratory borehole, H-1 in Figure 1, was sited near the intersection of faults f-1 and f-2. In its 1458 m it cut 700 m of intracaldera lavas and tuffs, 265 m of lithic tuff that may correlate with the Upper Zaragoza Tuff, 190 m of Xáltipan Ignimbrite, and 303 m of Teziutlán lavas. Two permeable zones, found at 1250 m and 1400 m depth, probably represent the down-hole intersections of faults f-1 and f-2. Maximum temperatures of 270° to 276° C were measured at the depth of the lower permeable zone during initial production tests in September, 1981 (López,1982a).

As of December, 1982 the H-1 well was producing a 200 tonne/hr steam-water mixture at a wellhead pressure of 14 kg/cm^2 and with an enthalpy of 300 kcal/kg. One analysis of brine collected at atmospheric pressure (López, 1982a) showed, in ppm, Na^+=265, K^+=31, Li^+=5, Ca^{++}=1.9, Mg^{++}=0.2, B=195, NH_4=7, F^-=0.4, Cl^-=100, HCO_3^-=270, $CO_3^=$=120, $SO_4^=$=115, SiO_2=480, and pH=8.5. Incondensable gases collected at the wellhead formed 0.5% by volume of the steam phase; their analysis (López, 1982a) showed, in mole %, CO_2=87.1, H_2S=0.03, H_2=0.03, and CH_4=0.4.

Borehole H-2 is located near, but on the outside, of the inferred rim of the Los Potreros caldera. According to

Gutièrrez (1982), in its 2301 m it cut 495 m of postcaldera lavas and tuffs, 245 m of ignimbrite, 400 m of Teziutlàn lavas, and 1161 m of Mesozoic marls. Although bottom temperatures as high as 280° C were recorded no permeable zones were found in this borehole.

Borehole H-4 is located near the northern end of fault f-1, on the down-thrown side of the fault. According to Rivera (1982b), in its 1880 m the borehole cut 108 m of postcaldera tuffs, 766 m of ignimbrite (which may represent the aggregate thickness of the Xàltipan and Upper Zaragoza Tuff), and 1006 m of Teziutlàn lavas. Because several intervals of circulation loss were found at depths greater than 1000 m, production casing was installed between 1100 and 1880 m depth. A bottom temperature of 299° C was recorded prior to the start of production tests. The well began producing dry steam at a pressure of 116 kg/cm^2 by September,1982; pressure soon stabilized at 17 kg/cm^2 and the dry steam flow rate stabilized at 160 tonne/hr. After a short period, however, pressure and flow rate began declining again and, by mid-November,1982, had values of 4.6 kg/cm^2 and 47 tonne/hr respectively (Lòpez, 1982b). The field operators have attributed this decline to plugging of the well during production tests, although decreased permeability due to flashing of the fluid within the formation cannot be ruled out with the available data.

Incondensable gases, analyzed during the stage of stable pressure, formed 2.9% by volume of the steam. Their

analysis (López, 1982b) showed, in mole %, CO_2=78.5, H_2S=9.4, H_2=11.9, CH_4=0.04, and N_2=0.15.

DISCUSSION

The preliminary geophysical and drilling data can be interpreted in light of the detailed geologic study (Ferriz and Mahood, *1984*) to estimate some of the parameters needed in reservoir engineering, namely the boundaries of the system; the location, nature, and extent of the major permeability controls; and the potential water influx into the system. These parameters will support and complement those obtained through transient pressure analyses once more boreholes are drilled. In the meantime they may prove useful in siting exploration boreholes.

It has already been suggested that the system is bounded laterally by the ring-fracture zone of the Los Potreros caldera. Of the major units found inside the caldera only the Xáltipan and Zaragoza ignimbrites could be expected to have significant primary permeabilities. However, production zones in wells H-1 and H-4 are within the very dense Teziutlán lavas, suggesting that the hot-water aquifer is confined to steeply dipping zones of secondary permeability such as fault f-1. Although mapped faults cut both lavas and ignimbrites, open fractures would be more likely to persist in the brittle ferrobasalts and andesites than in the moderately consolidated overlying ignimbrites. In addition, hydrothermal alteration will tend to reduce the primary permeability of the ignimbrites, which

would then operate as a semi-impermeable cap for the reservoir. The restriction of mild fumarolic activity to the trace of fault f-1 implies the existence of such a cap. In summary, the geothermal system seems to be hosted by the essentially homogeneous Teziutlán lavas, and capped by impermeable intracaldera ignimbrite, within the Los Potreros caldera.

The resistivity surveys (Figure 2), and the results obtained from wells H-1 and H-4, suggest that permeable zones are controlled by the faults that bound the uplifted southeastern quadrant of the Los Potreros caldera (faults f-1, f-2, and f-3). If this uplift is indeed the result of magma intrusion, its boundary faults would not be expected to propagate beyond the inferred rim of the Los Potreros caldera, as has been confirmed by geologic mapping. The location of at least a group of permeable zones seems thus to be well constrained. However, spurs in the contours of the apparent resistivity maps (Figure 2 and Palacios and García, 1981) suggest fracture control in areas within the Los Potreros caldera in which no evidence of such fracture zones can be found in the surface. To confirm the existence of such zones, and to characterize them, is one of the tasks faced by the field operator. These inferred fractures are perhaps related to the regional doming experienced by the Los Potreros caldera shortly after its collapse, and thus would have been formed much earlier than the faults associated with the uplift of the southeastern quadrant of the caldera. Tensional faulting and fracturing related to

somewhat similar doming has been documented in other caldera systems (Smith and Bailey,1968); the faults thus formed are commonly parallel and do not extend beyond the boundaries of the caldera.

The apparent resistivity isopleths of Figure 2 suggest that there could be flow of fluid into or outwards from the geothermal system through the northwestern rim of the Los Potreros caldera; the idea that flow is into the system is favored due to the lack of thermal indicators in the northern portion of LHVC. Peculiar regional topographic conditions cause precipitation in the northern portion of LHVC to be more intense than in the southern portion; an average of 1200 and 600 mm/yr respectively (Reyes, 1979). Precipitation infiltrates quickly through the permeable unconsolidated and unaltered pyroclastic deposits, but not so through the unfractured domes and lava flows. Taking into account the distribution of impermeable lavas shown in Figure 1, and the difference in precipitation intensity, a larger infiltration rate would be expected in the northwestern portion of LHVC. Assuming 50% evapotranspiration a potential water influx of 10^7 m^3/yr might be expected from the area enclosed by the northwest ring-fracture zones of both calderas into the Los Potreros caldera.

Another potential source of water influx is groundwater from the closed basin that extends south of LHVC, which forms its northern boundary. The basin has an area of

approximately 5250 km^2, and an average annual precipitation of 620 mm; 40% of the precipitation infiltrates to later move outwards from the basin to the north (Reyes,1979), where the groundwaters could be intercepted by the plumbing system of the volcanic center. Water influx would explain the "opening" in the resistivity contours south of the Los Potreros caldera (Figure 2). Alternatively, such "opening" could indicate migration of fluids from the geothermal system into the hydrologic system of the closed basin.

CONCLUSIONS

I currently see the geothermal reservoir as a water-dominated system bound by the Los Potreros caldera, hosted by the Teziutlán lavas, and sealed by the Xáltipan Ignimbrite and younger volcanic units. Permeable zones are controlled by the fault zones that bound an intracaldera uplift. Additional permeable zones are perhaps provided by fractures related to post-collapse doming of the caldera area; these fractures are not expected to propagate beyond the rim of the Los Potreros caldera. The heat that is now being tapped by the geothermal fluid was probably derived from a compositionally zoned magma chamber that developed in a shallow level of the crust within the last 0.5 Ma. A potentially large influx of water into the system may be structurally controlled by portions of the ring-fracture zones of the Los Humeros and Los Potreros calderas.

The conclusions obtained through geologic, geophysic, and hydrologic studies of this center, coupled with the

development of the reservoir, shall be of interest for the exploration and development of reservoirs hosted by volcanic centers in the Eastern Cascades. Centers such as the Newberry and Medicine Lake volcanoes have many similarities with Los Humeros, such as similar tectonic environment, complex magmatic histories, the potential for nested collapse structures and post-collapse doming and fracturing, and potentially high influx of cold water into the systems.

ACKNOWLEDGMENTS

I want to thank the technical personnel of Mexico's Comisiôn Federal de Electricidad for their continuing support and access to unpublished data, in particular to C. Garcia, C. YáÑez, C. Fernàndez, J.M. Lôpez, L.C.A. Gutièrrez, and O. Rivera. G. Mahood, J. Gudmundsson, P.J. Bartos, and J. Ortiz reviewed the manuscript and made useful suggestions. Acknowledgment is made to Mexico's Comisiôn Federal de Electricidad, and Consejo Nacional de Ciencia y Tecnologia, and to the Donors of the Petroleum Research Fund, administered by the American Chemical Society, for the support of this research.

REFERENCES

Alvarez,R. (ed.), 1978, Los Humeros caldera special issue: Geof. Internacional, v.17, p.407-478.

Ferriz,H., Mahood,G.A., 1984, Eruption rates and compositional trends at Los Humeros volcanic center, Puebla, Mexico: J. Geophys. Res., v.B89, p.8511-8524.

Ferriz,H., Yáñez,C., 1981, Mapa geológico del centro volcánico de Los Humeros, Edición preliminar: Comisión Federal de Electricidad, México, Juán de la Barrera#37, Cd. Satélite, Edo. de Mexico, 53100, MEXICO.

Flores,C., Alvarez,R., Singh,S.K., Urrutia,J., 1978, Aeromagnetic survey of Los Humeros caldera, Mexico: Geof. Internacional, v.17, p.415-428.

Gutiérrez,L.C.A., 1982, Litología y zoneamiento hidrotermal en los pozos H-1 y H-2 del campo geotérmico de Los Humeros,Puebla: Comisión Federal de Electricidad, México, 45p.

López,J.M., 1982a, Geoquímica del agua y gases separados del Pozo Humeros-1, campo geotérmico de Los Humeros, Puebla, México: Comisión Federal de Electricidad, México, 15p.

López,J.M., 1982b, Geoquímica de gases separados del Pozo Humeros-4, campo geotérmico de Los Humeros, Puebla, México: Comisión Federal de Electricidad, México.

Mahood,G.A., 1980, Geological evolution of a Pleistocene rhyolitic center - Sierra La Primavera, Jalisco, Mexico: J. Volcanol. Geotherm. Res., v.8, p.199-230.

Mena,M., González,T., 1978, Regional gravity of Los Humeros volcanic area: Geof. Internacional, v.17, p.429-444.

Molina,R., 1979, Geoquímica de los gases de la región geotérmica Los Humeros - Las Derrumbadas, Puebla: Comisión Federal de Electricidad, México, 33p.

Molnar,P., Sykes,L.R., 1969, Tectonics of the Caribbean and Middle America regions from focal mechanisms and seismicity: Geol. Soc. Am. Bull., v.80, p.1639-1684.

Mooser,F., 1964, Geología de la Cuenca de Oriental (map): Comisión Hidrológica Cuenca Valle de México, México.

Palacios,L.H., García,H., 1981, Informe geofísico del proyecto geotérmico Los Humeros - Derrumbadas, estados de Puebla y Veracruz: Comisión Federal de Electricidad, México, 99p.

Pèrez,J., 1978, Geologìa y petrografìa de la caldera de Los Humeros: Geomimet, No.91, p.97-106.

Reyes,M., 1979, Geologìa de la Cuenca de Oriental, estados de Puebla, Veracruz, y Tlaxcala: Colecciòn Cientìfica INAH, Mèxico, v.71, 62p.

Rivera,O., 1982a, Reporte geològico del Pozo Humeros-1, campo geotèrmico de Los Humeros, Puebla, Mèxico: Comisiòn Federal de Electricidad, Mèxico.

Rivera,O., 1982b, Personal communication.

Smith,R.L., Bailey,R.A., 1968, Resurgent cauldrons: Geol. Soc. Am. Mem. 116, p.613-662.

Viniegra,F., 1965, Geologìa del Macizo de Teziutlàn y la Cuenca Cenozoica de Veracruz: Bol. Asoc. Mexicana Geol. Petr., v.17, p.101-163.

Yàñez,C., Casique,J., 1980, Informe geològico del proyecto geotèrmico Los Humeros - Derrumbadas, estados de Puebla y Veracruz: Comisiòn Federal de Electricidad, Mèxico, 59p.

Ferriz,H., in review, Caltonac, A prehispanic obsidian-mining center in eastern Mexico? : A preliminary report: J. Field Archaeology.

CHAPTER 5

CALTONAC, A PREHISPANIC OBSIDIAN-MINING CENTER IN EASTERN MEXICO?: A PRELIMINARY REPORT

ABSTRACT

The site of Caltonac is located in the state of Puebla, at the eastern edge of the Mexican Central Altiplano. Preliminary mapping in the course of a geologic survey shows that it is built over a compound andesite flow, and can be divided in three sections, each of which covers an area of approximately 2 km^2. The southern section has a well defined public area, surrounded by what appear to be domestic structures arranged along four major roadways that radiate from the public area. In the northern and northwestern sections the stone-walled habitational (?) structures are arranged in isolated groups surrounding open spaces, or clustered at the rim of the andesite flow. A major rhyolite flow is located ~10 km northwest of the site. The glassy portions of this flow prove to be the source of the D or Zaragoza type obsidian found in Formative to Postclassic Mesoamerican sites, whose provenance was until now uncertain. The chronology of the site is unknown, but an increase during the Classic of the number of sites in which D-type obsidian artifacts are found suggests that by this time local control of the source had been established.

INTRODUCTION

Despite nearly a century of archaeological research, several of the prehistoric population centers of the Central Altiplano of Mexico remain to be studied. Among them is the previously undocumented site of Caltonac or Cantonac, located in the state of Puebla and on the eastern edge of

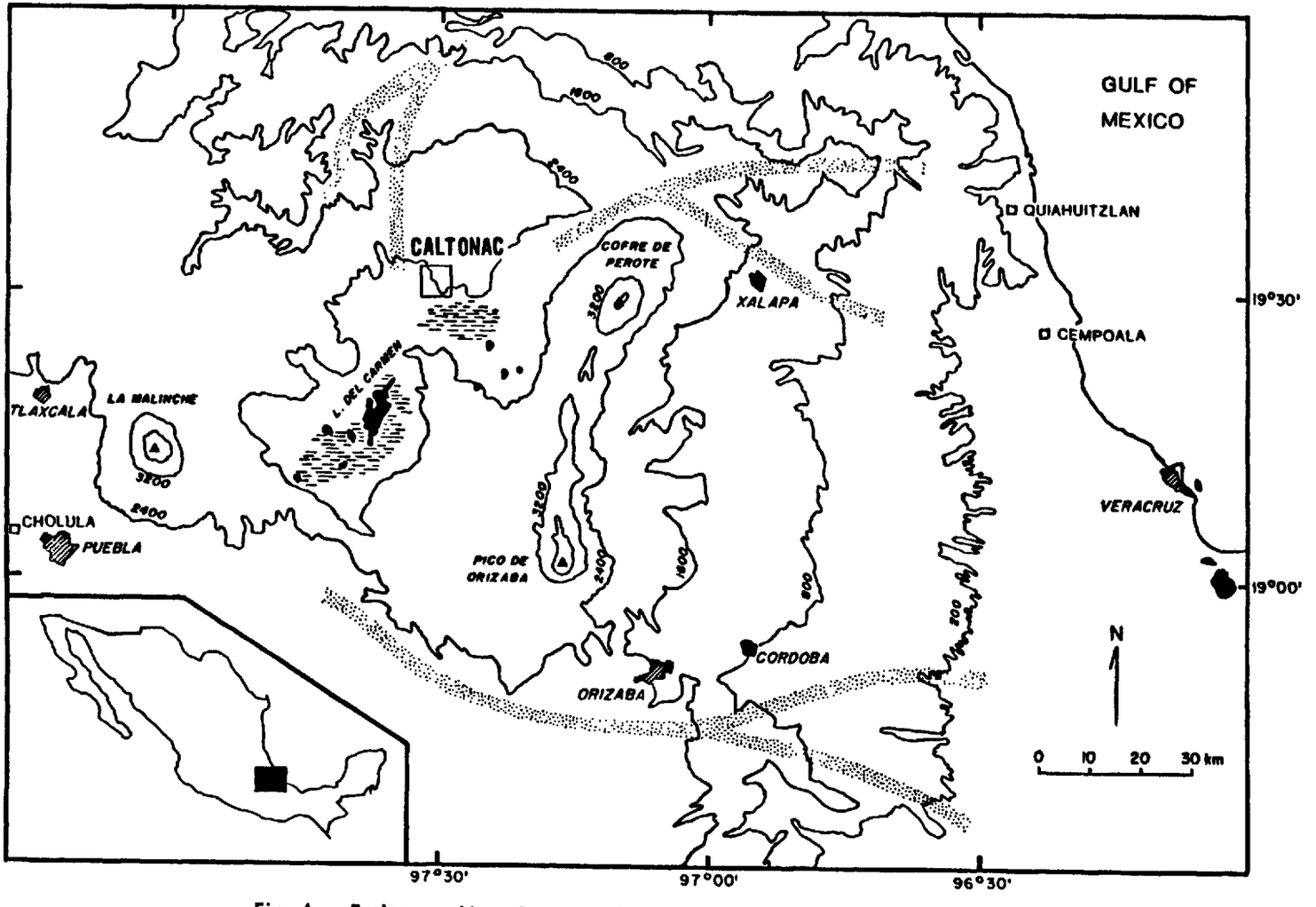

Fig. 1. Eastern portion of central Mexico with cities (diagonal pattern), important archaeological sites (squares), andesitic volcanoes (triangles), lagoons (black), and swamps (dashes) indicated. The contour lines are in meters. The natural routes between the coastal regions and the altiplano are shown by the stippled pattern.

the altiplano (Figure 1). The site was built on the southern slope of the Quaternary Los Humeros volcanic center (Figure 2), where Comision Federal de Electricidad (CFE) -- Mexico's federal power company-- has been conducting geothermal exploration since 1978. As part of its general project of exploration (Ferriz, 1982) and environmental impact assesement, CFE's geologic staff undertook in 1981 the preliminary mapping of the site, the results of which are presented in this paper. This reconaissance work is intended to provide a framework for the planning of the archaeological studies that will have to be performed in case the nearby geothermal field is developed. From the archaeological standpoint, thus, this paper is expected to help formulate questions rather than to provide answers.

Because the ancient builders made use of the volcanic landforms in laying out the site, it is appropriate to point out some significant events in the geologic history of this volcanic center (Ferriz and Mahood, 1984). About 0.46 Ma ago a major pyroclastic eruption took place, leading to the formation of the Xàltipan Ignimbrite. The eruption of this ignimbrite, in which obsidian blocks are ubiquitous, led to the collapse of the Los Humeros caldera (LHC in Figure 2). Several rhyolite domes erupted after collapse along the fractures that bounded the caldera; all but one of these lavas contain crystals. The only rhyolite without crystals is the Caltonac rhyolite flow; its glassy portions most probably constituted the major source of obsidian for the inhabitants of the local area. After the eruption of these

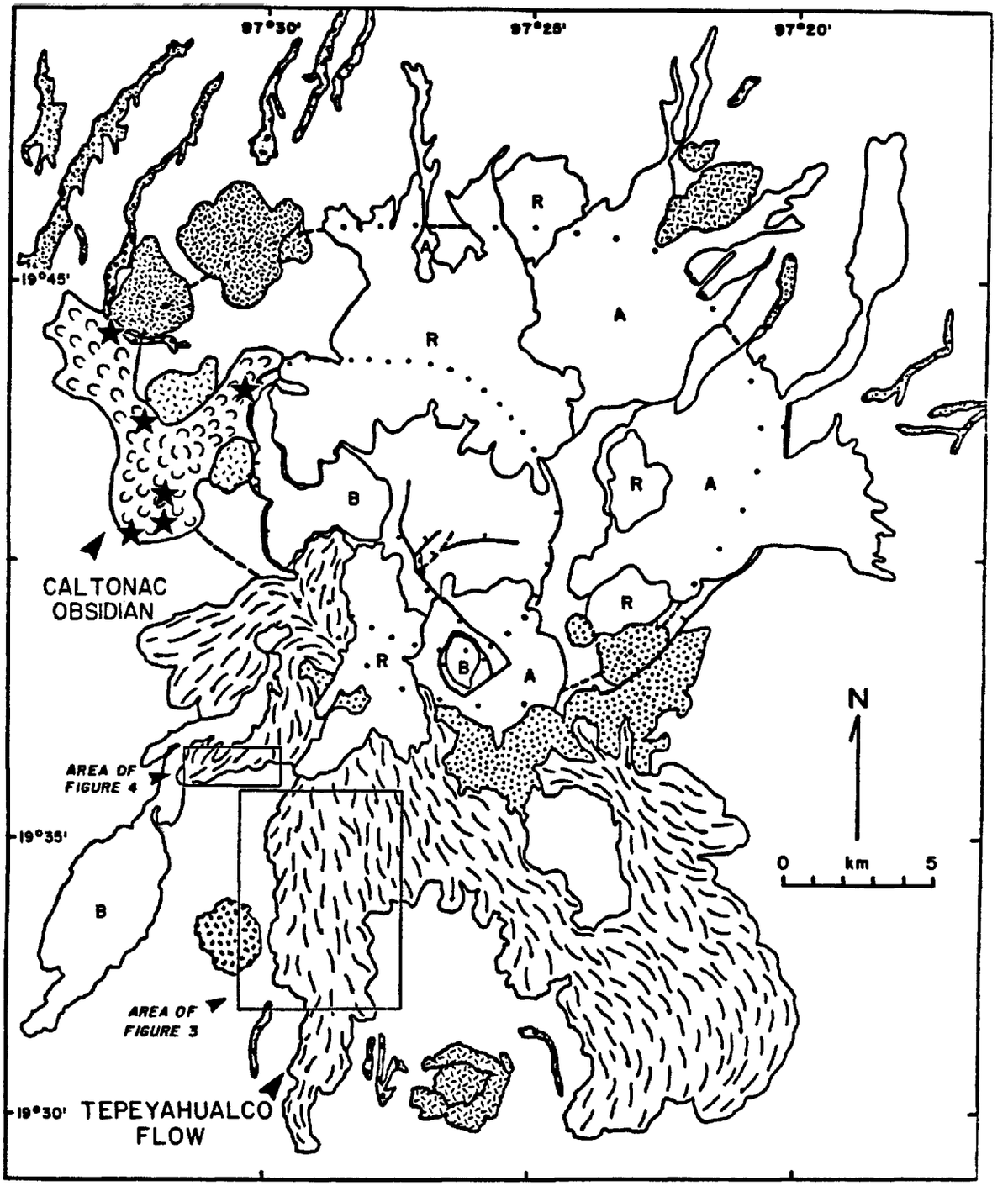

Fig. 2. Simplified geologic map of the Los Humeros volcanic center after Ferriz and Yáñez (1981), showing the Caltonac rhyolite flow (cuspate pattern), rhyolite domes (dashed patterns), pyroclastic deposits (stippled patterns), andesite flows (long dashes and A), rhyodacite flows (R), and olivine basalt flows (B). LHC indicates the inferred rim of the Los Humeros caldera. Outcrops of obsidian within the Caltonac rhyolite flow are shown by black stars. The large rectangle indicates the location of the southern and northern sections of the site of Caltonac (Figure 3), whereas the small rectangle indicates the location of the northwestern section (Figure 4).

lavas, two other major pyroclastic eruptions took place 0.24 Ma ago (Faby Tuff) and 0.1 m.y. ago (Zaragoza Tuff). These younger tuffs cover the Caltonac flow to a large extent so outcrops of obsidian are now mostly restricted to the bottoms of gullies. Between 0.06 and 0.04 Ma ago, a series of andesite flows were erupted along the southern fracture zone of the Los Humeros caldera, spreading to the south over the plains that surrounded the volcanic center. One of these flows, the Tepeyahualco flow (Figure 2), is formed by several flow units (i.e. surges of lava) stacked one upon the other. The site of Caltonac was built on this flow, with the andesite itself providing excellent building material, because of its tendency to break in small blocks. The contrasting elevations provided by the stacking of flow units served to isolate the public area from the living area. Although it will not be further discussed here, volcanic activity continued with the eruption of andesites, rhyodacites, and olivine basalts in other portions of the volcanic center (Figure 2; Ferriz and Mahood, 1984).

DESCRIPTION OF THE SITE

Maps of the three different sections of the Caltonac archaeological site are presented in Figures 3 and 4. Each one of these sections covers an area of about 2 km^2. Mapping was based on 1:20,000 scale aerial photographs of good quality, and was supplemented by field reconaissance. Because the purpose of the work was to help in the planning of further archaeological studies special care was taken not

to disturb the site in any way. Accordingly, no excavation or artifact collection was undertaken. This policy has restricted the archaeological interpretations which follow, but is expected to result in the benefit of future work.

The continuous lines in Figure 3 indicate the boundaries of the andesite flow units mentioned before, and the numbers indicate their relative stratigraphic position from bottom (1) to top (8). Stacking of the flow units resulted in the formation of natural terraces. Flow units are 10 m thick on the average, so where the boundary of flow units 3 and 6 coincides, in the area of densest settlement, there is a total difference of elevation of approximately 20 m between the lower and upper natural terraces.

A group of seven small pyramids stands at the rim of the upper terrace (6 in Figure 3), dominating the living area and the plains that surround the volcanic center to the south. Most of them are quadrangular in map view, their lateral dimensions ranging from 20 to 30 m, and their heights ranging from 8 to 12 m. Ten other pyramids are located behind the rim, as either isolated structures or distributed around plazas. Their outlines are commonly rectangular in plan view, with lateral dimensions ranging from 15 by 20 m to 40 by 60 m, and heights ranging from 6 to 15 m. They commonly have a stone-wall enclosure adjoining one of their sides, and in one case what seems to be a ballcourt. As is the case with all other structures, the pyramids were formed by stacking of rock fragments derived from the underlying lava flow. The fact that there are

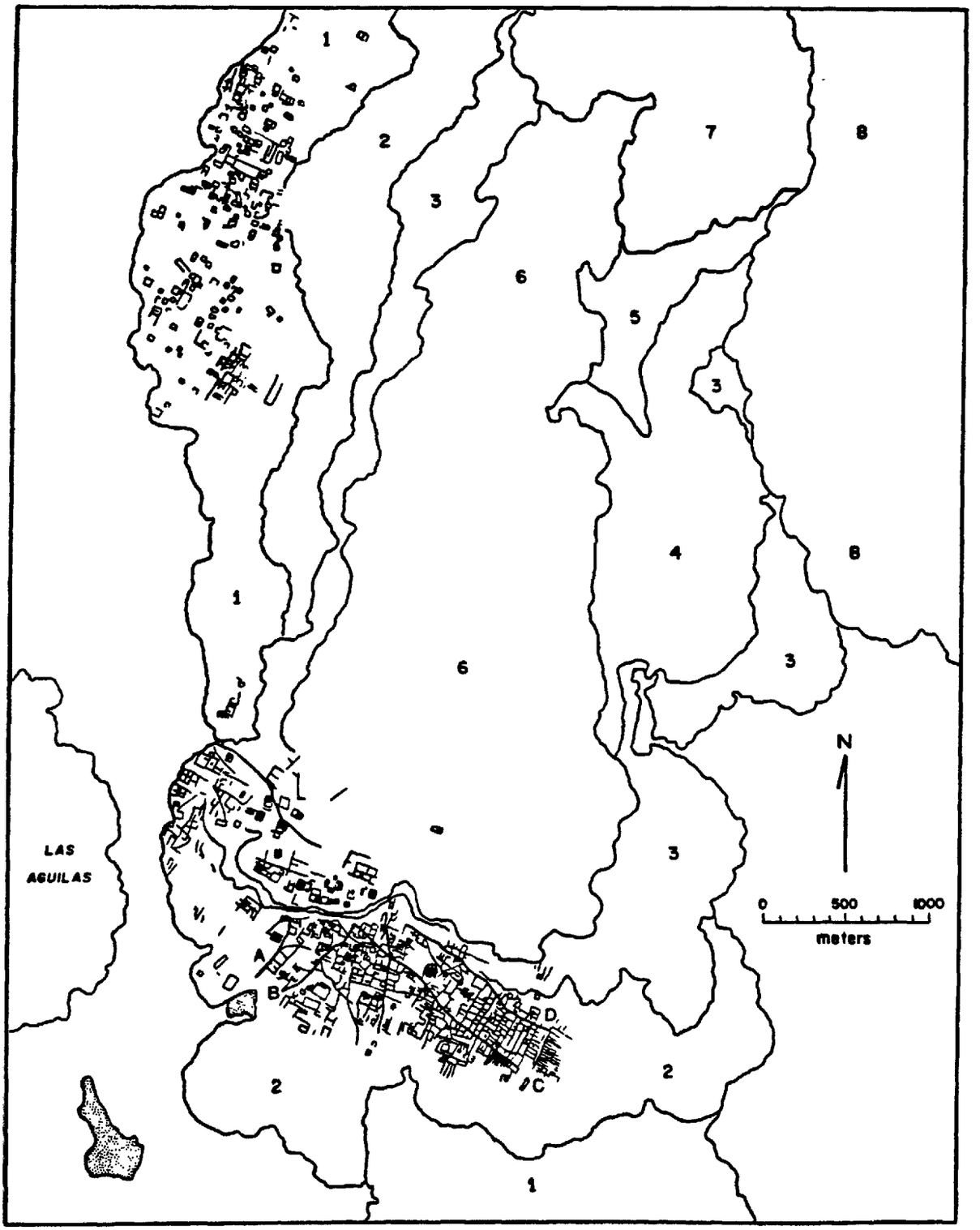

Fig. 3. Map by the author of the southern and northern sections of the site of Caltonac showing main roadways (heavy lines), stone walls (short lines), and pyramids (black squares). The continuous lines indicate the boundaries between andesite flow units (1 being the lowermost and 8 the uppermost), and the stippled pattern indicates limestone outcrops. The surrounding plains are unnumbered and the Las Aguilas rhyolite dome is shown for reference.

relatively few residential structures on the upper terrace suggests that this portion of the site may have been reserved as a public, perhaps ceremonial area.

The lower terrace (2 in Figure 3) shows a high density of probable habitation structures. Field examination reveals that in the southern portion of the site four main roadways (A to D in Figure 3) radiate away from the base of the public center. These roadways are continuous and apparently constituted discrete structural entities; they are connected with each other through a network of alleys. Within the portions limited by the roadways and alleys are rectangular areas bounded by partially destroyed walls, which are up to 1.5 m in height. They were formed by stacking of andesite fragments, apparently without mortar. Some of these walls undoubtedly belong to small rooms within buildings that were up to 100 m long. Most of the walls, however, seem to define the perimeter of single structures which were probably used as living quarters. Only two small pyramids are found on the lower terrace.

The northern section of the site is built on terrace 1 (Figure 3). Although the constructions are of similar proportions to those found in the southern section, their layout is different. Evidence of pyramids and roadways is absent, the density of structures decreases, and some of the structures are located around rectangular open spaces. Structures become more abundant toward the rim of flow unit 1. The layout of the northwest section of the site (Figure 4) is similar to that of the northern section. The main

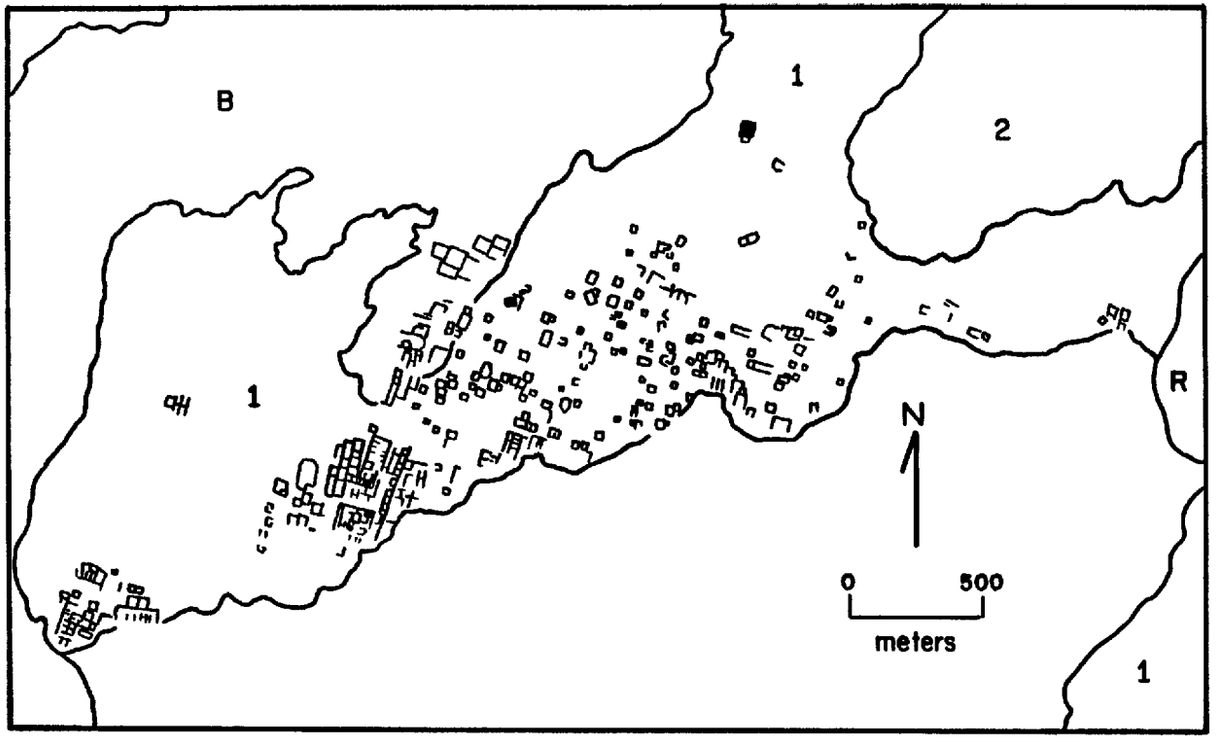

Fig. 4. Map by the author of the northwest section of the site of Caltonac showing stone walls (short lines), and pyramids (black squares). The continuous lines indicate the boundaries between andesite flow units (1 and 2), a rhyodacite flow (R), and a basalt flow (B). The plain to the south is unnumbered.

portion of the former is located on flow unit 1, but some structures are built on the basalt flow (B in Figure 4), whose eruption marked the end of volcanic activity in the area (Ferriz and Mahood, 1984). Two small pyramids and a few vestiges of roadways are preserved. Stone-walled structures are largely arranged in isolated groups around open spaces, or clustered at the rim of flow unit 1.

A minimum of 624 stone-wall enclosures are preserved in the southern section of the site. In the northern and northwestern sections the minimum number of structures is 275 and 351, respectively. These figures do not include the relatively large number of structures that are too poorly preserved to reconstruct their original outlines.

The andesite flow in which the site as a whole is built is arid and unsuitable for raising crops so cultivation must have been restricted to the surrounding plains, which may explain the increased housing density at the rim of the lower terrace observed in the northern (Figure 3) and northwestern (Figure 4) sections of the site. Although characterized by thin profiles the soils developed in the pyroclastic deposits that underlie the plains are fertile. These soils, however, have a low water retention capacity so the population must have depended on seasonal crops which, due to the relatively high altitude of the site (2,500 m), are extremely susceptible to frost, retarded rains, and droughts. As happens today in the area, crop failure may have been alleviated by trade with the fertile coastal regions. Game may have been hunted in the mountain massif

of the volcanic center, and the swamps of the Laguna del Carmen (Figure 1) could have provided fish and wild birds.

Water is now a scarce commodity at the site. Nearby arroyos are seasonal and could not support even a small size population. Springs are unknown in the nearby area although their past existence cannot be ruled out. Because current water wells intersect the phreatic level at depths of approximately 100 m, wells are an unlikely prehistoric source of water. Water may have been brought from the Laguna del Carmen, from one of the small seasonal lagoons that form on the plain south of the site, or may have been collected during the rainy season.

As discussed in the next section, good quality obsidian was one of the major natural resources potentially available to the inhabitants of the site. In addition, wood in the form of pine forests is abundant in the mountain massif of the volcanic center, and in the basalt flow that extends to the west of the site (Figure 2). The pumiceous rhyolite of the Las Aguilas dome (Figure 3) provided an easily carved material for sculptural art. Finally, outcrops of limestone, a basic material in the elaboration of the lime used to prepare staple foods such as maize tortillas, are common in the vicinity of the site (Figure 3; Ferriz and Yáñez, 1981).

OBSIDIAN SOURCES AND DISTRIBUTION

Two possible sources of obsidian are found in the vicinity of the site: obsidian blocks in the Xâltipan Ignimbrite and obsidian from the Caltonac rhyolite flow. The distribution of the Xâltipan Ignimbrite is shown in Figure 5. Obsidian blocks found within this ignimbrite were the source of the samples that Cobean et al. (1971) labeled the Altotonga obsidian. Figure 5 shows that this source of obsidian is not restricted to the vicinity of Altotonga. The obsidian found in blocks within the ignimbrite has no crystals and thus has good flaking characteristics. However, the blocks are sparse, not very large (<15 cm), and commonly show minor vesiculation. It is unlikely that they were quarried on a large scale.

The obsidian from the Caltonac flow is black and lustrous, or light gray and dull due to hydration. Dark gray obsidian with light gray streaks is dominant in some of the outcrops. All types have excellent flaking characteristics, and homogeneous obsidian blocks can reach side dimensions of up to 40 cm. In several outcrops the flow is partially devitrified or pumicitic, and is thus useless for tool manufacturing. Mapped outcrops of good quality obsidian are shown with stars in Figure 2. In the southernmost of these outcrops there is a 30 cm-thick layer of obsidian artifacts and debris. This horizon is covered by a thin veneer of alluvium. Core preforms (20%), blades (10%), and broken projectile points (5%) are found among the debris.

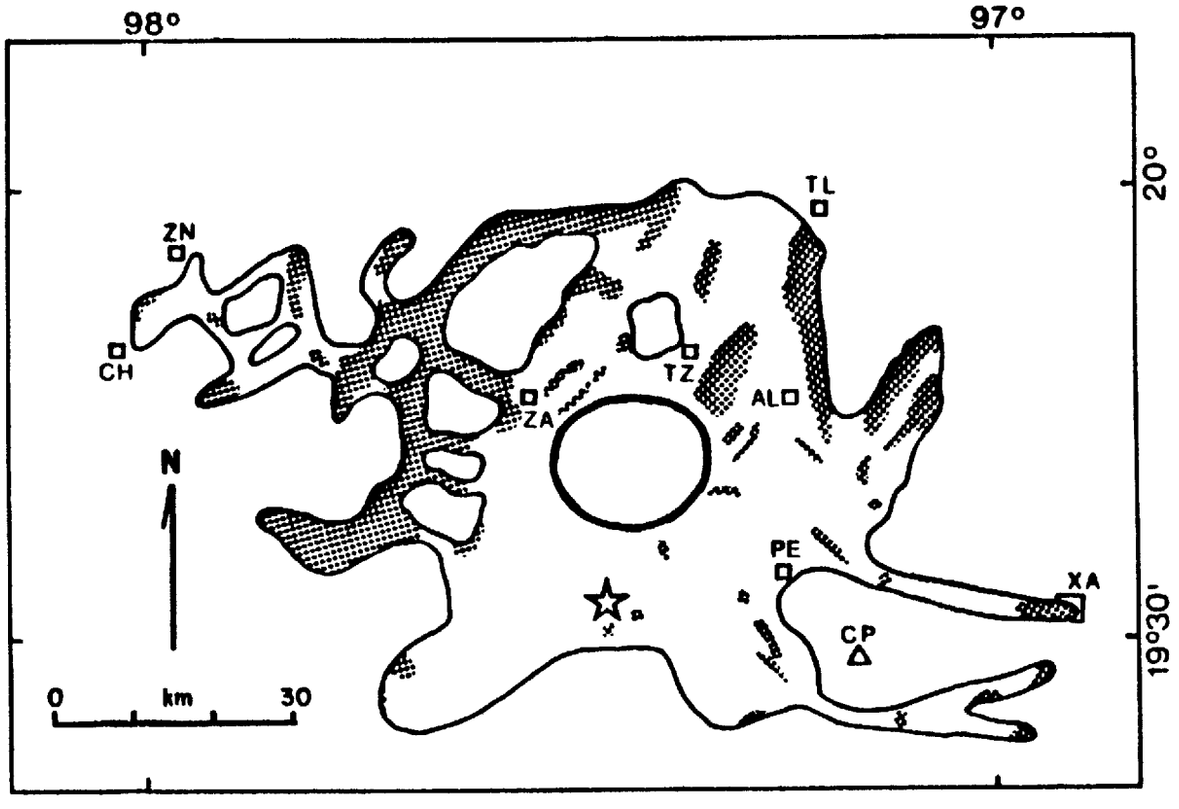

Fig. 5. Inferred distribution of the Xáltipan Ignimbrite with present outcrops indicated by the stippled pattern. The star indicates the location of Caltonac. Squares indicate the towns of Chignahuapan (CH), Zacatlán (ZN), Zaragoza (ZA), Teziutlán (TZ), Tlapacoyan (TL), Altotonga (AL), Perote (PE), and the city of Xalapa (XA). The summit of the Cofre de Perote andesitic volcano (CP) is indicated by the triangle. The solid line indicates the location of the Los Humeros caldera.

Although obsidians from different sources have very similar major element compositions their trace elements compositions are characteristically different, a fact that has allowed archaeologists to correlate obsidian artifacts with specific sources (e.g., Stross et al., 1976). Chemical analyses of geologic samples of Caltonac obsidian (Table 1; Figure 6) have been correlated by the author, based mainly in Rb, Sr, and Zr contents, with analyses of obsidian artifacts found at the sites of Villa Morelos[1], Tula[1], Cholula[2], El Tajin[3], Quiahuitzlan[3], Cempoala[3], Cerro de Las Mesas[4], Tres Zapotes[5], San Lorenzo Tenochtitlan[6], La Venta[7], Laguna Zope[8], Saltillo[8], and Seibal[9] Caltonac obsidian has also been recognized among collections of artifacts from Coxcatlán Viejo, Venta Salada, and San Pedro (F. Asaro, pers. comm., 1983) in the state of Puebla; unfortunately in these last three sites the analyzed artifacts lack stratigraphic control. This type of obsidian has various names in the archaeologic literature, Zaragoza type or D type being the most common. The term Caltonac obsidian is

---

[1] Hester et al. (1973; obsidian D). [2] Hester et al. (1972; obsidian D). [3] Jack et al. (1972; obsidian D). [4] Hester et al. (1971a; obsidian D). [5] Hester et al. (1971b; obsidian D). After analyzing a boulder of obsidian found near the town of Zaragoza, Puebla (Figure 5) the authors correctly inferred that the source of obsidian was located somewhere in the nearby area. [6] Cobean et al., (1971; obsidians C and C'). As pointed out by Stross et al. (1976) the Mn values reported by Cobean et al. are systematically higher than those obtained by other laboratories. (Figure 6). [7] Jack and Heizer (1968; obsidian D) and Hester et al. (1971a; obsidian D). [8] Zeitlin and Heimbuch (1978), Zeitlin (1979), Zeitlin (1982). Caltonac obsidian corresponds to Unknown Source 1, whose chemical composition has been recalculated by Stross et al. (1983). [9] Graham et al. (1972; obsidian D).

Table 1. Chemical Composition of Geologic Samples of Caltonac Obsidian.

	Composition in wt% (1 analysis)		Composition in ppm (5 analyses)	
			Range	Average
SiO_2	74.9	Rb	122-141	132 ± 9
TiO_2	0.13	Sr	31-36	34 ± 2
Al_2O_3	12.8	Zr	142-207	189 ± 26
Fe_2O_3*	1.35	Y	32-34	33 ± 1
MgO	0.13	Nb	18-20	19 ± 1
CaO	0.50			
Na_2O	3.78	Ba	540-700	626 ± 55
K_2O	4.88	La	36-45	42 ± 4
P_2O_5	0.05	Mn	240-270	258 ± 12
		Ni	2.6-3.5	3.1 ± 0.3
H_2O	1.10	Be	4.1-5.5	4.9 ± 0.5
F	0.05	Co	1.7-2.3	2.1 ± 0.2
Cl	0.07	Ga	15-20	19 ± 2
Total	99.74			

Analyses performed by the U.S. Geological Survey Analytical Laboratories. Fe_2O_3* = total iron reported as Fe_2O_3. Major elements, Rb, Sr, Zr, Y and Nb determined by X-ray fluorescence. Other trace elements determined by emission spectrographic analysis. H_2O determined by the Penfield method. F and Cl determined by specific ion electrode techniques.

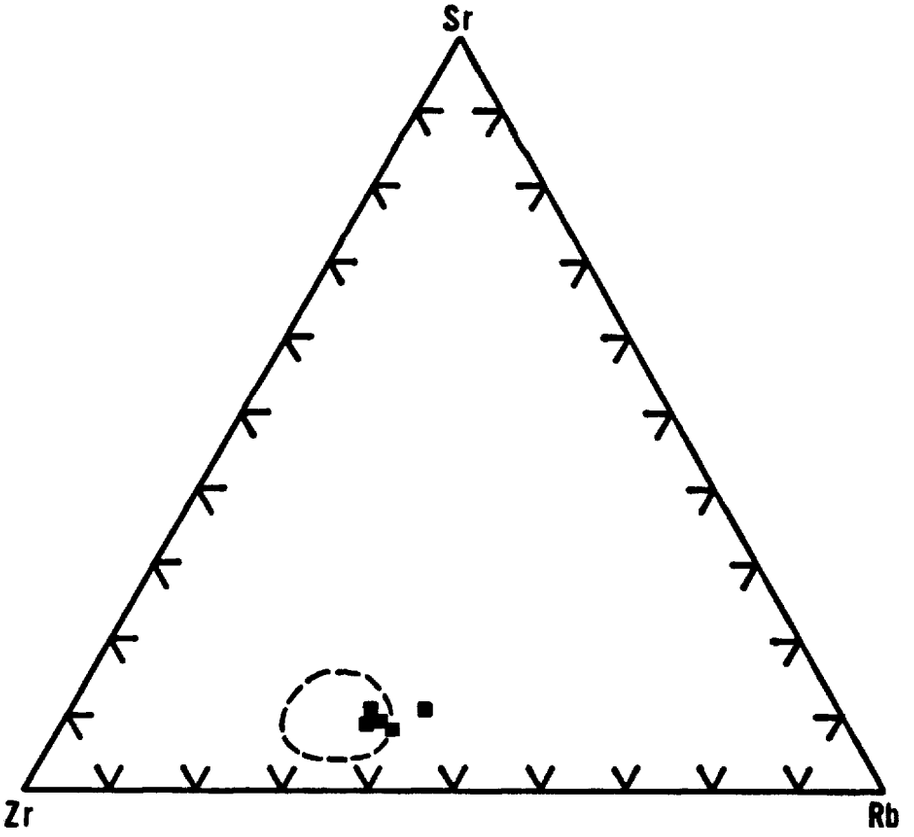

Fig. 6. Relative Rb, Sr, and Zr contents of obsidian artifacts previously called D or Zaragoza type (dashed outline, sources given in notes 1 through 9 in the text) are compared against geologic samples of Caltonac obsidian (black squares). The D obsidian XRF measurements were not corrected for background radiation and for interference of the Sr secondary X-ray peak with the main X-ray peak of Zr and are thus slightly shifted toward Zr values higher than those of the geologic samples.

informally used here to avoid confusions with the geologic literature, in which the name Zaragoza Tuff is used to designate the pyroclastic deposit on which the town of Zaragoza, Puebla is built.

Figure 7 shows the approximate stratigraphic intervals in which Caltonac obsidian has been found at each of the sites mentioned in the previous paragraph, the thickness of the bars indicating its relative abundance with respect to other obsidian types. Unfortunately the stratigraphic control is sound only for the San Lorenzo Tenochtitlan, Laguna Zope, Saltillo, and Seibal occurrences. The overlap of these stratigraphic columns suggests that quarrying of Caltonac obsidian was an important activity during the Classic and Early Postclassic, although Caltonac obsidian was traded from the Middle Formative period (San Lorenzo Tenochtitlan) to Hispanic times (Cempoala).

The relative abundance of core preforms in the quarried area and in the site suggests that obsidian was exported, at least in part, in a semi-processed way, perhaps to minimize damage during transport. This was an apparently common practice in other obsidian quarries (Spence and Parsons, 1972). This suggestion is supported by the abundance of exhausted cores of Caltonac obsidian found in the site of Tres Zapotes (Hester et al., 1971b).

Figure 8 shows the location of the sites where Caltonac obsidian has been reported. Three sites (Villa Morelos, Tula, and Seibal) are closer to other sources of obsidian, which undoubtedly accounts for the small

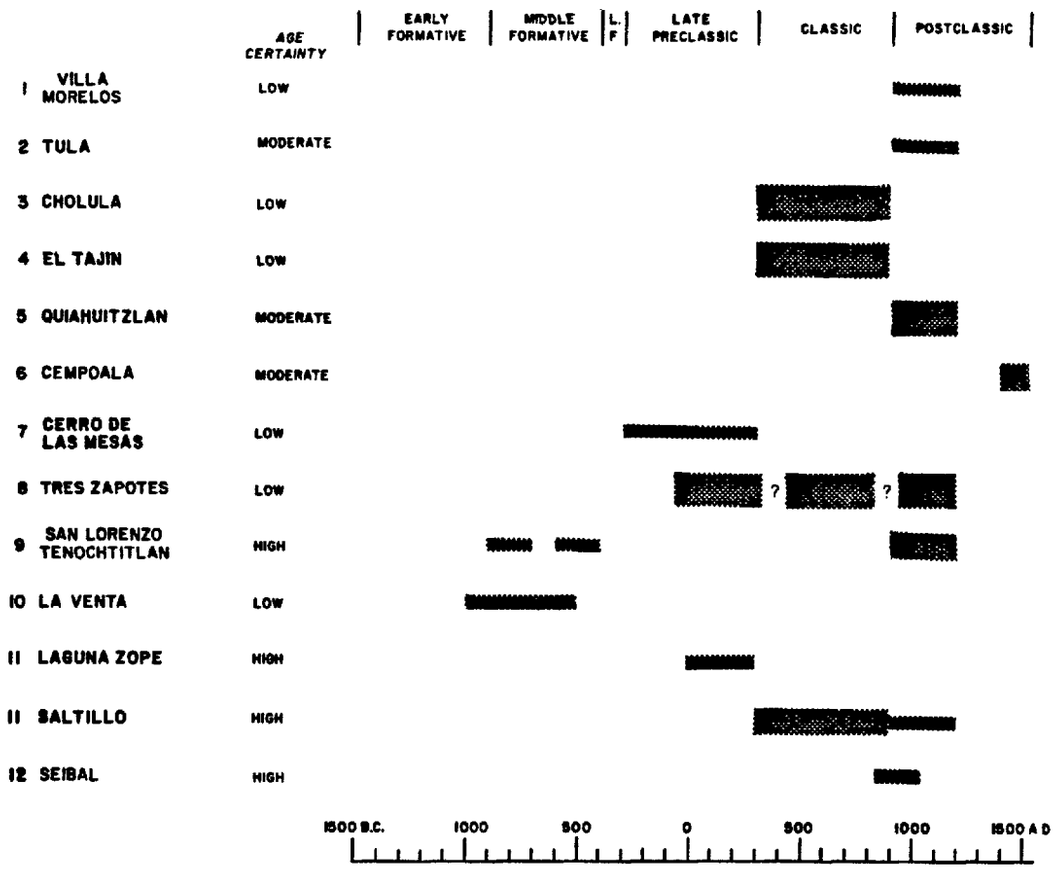

Fig. 7. Some archaeologic sites where Caltonac obsidian has been identified. The bars indicate the stratigraphic interval assigned by the original investigators (sources given in notes 1 through 9 in the text). The thickness of the bar is indicative of the relative abundance of Caltonac obsidian at each site.

proportion of Caltonac obsidian. Since Cholula is located near Caltonac and no major topographic obstacles separate them (Figure 1), Caltonac naturally became an obsidian source to Cholula. All of the other sites, however, are located on the coastal regions, and their access to the obsidian sources of the altiplano is restricted by topographic barriers. The natural access routes between the coastal regions and the altiplano are shown by the stippled pattern in Figure 1. It is evident that for population centers such as El Tajin, Quiahuitzlan, and Cempoala, Caltonac was not only the closest obsidian source but also was on the natural path that would be followed during trade with the altiplano. For centers such as Cerro de Las Mesas, Tres Zapotes, San Lorenzo Tenochtitlan, and La Venta, a more direct route would be the one shown in the lower portion of Figure 1, and closer sources of obsidian would be those located near the Pico de Orizaba andesitic volcano (Cobean et al., 1971). However, this obsidian is crystal-bearing and thus of quality inferior to that of the Caltonac obsidian, a factor that may have overruled the advantages of a shorter trade route.

In addition to the strategic geographic position and superior quality of the Caltonac obsidian, socio-political factors may have influenced the pattern of its distribution. Zeitlin (1982) documented prominent changes with time in the obsidian types utilized at the sites of Laguna Zope and Saltillo (12 in Figure 8), in the southern Isthmus of Tehuantepec. Caltonac obsidian (Unknown Source 1) first

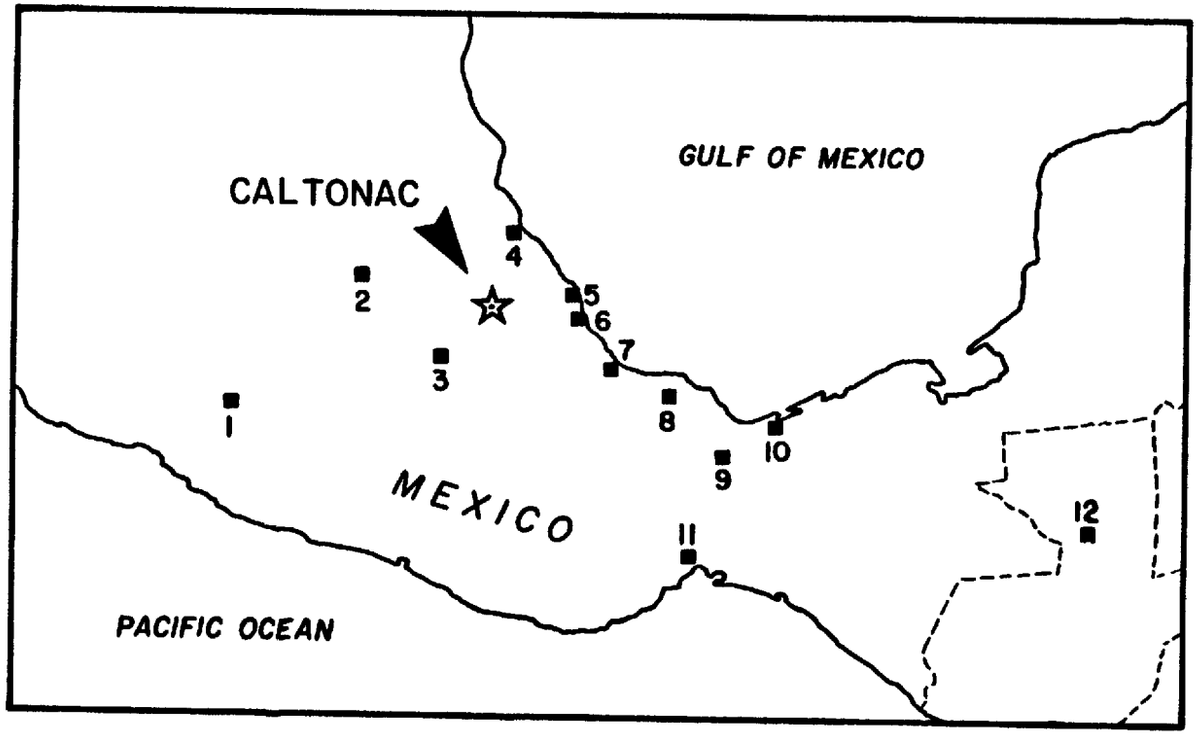

Fig. 8. Location of some of the archaeologic sites where Caltonac obsidian has been identified: 1. Villa Morelos, 2. Tula, 3. Cholula, 4. El Tajin, 5. Quiahuitzlan, 6. Cempoala, 7. Cerro de Las Mesas, 8. Tres Zapotes, 9. San Lorenzo Tenochtitlan, 10. La Venta, 11. Laguna Zope and Saltillo, 12. Seibal.

appeared as replacement of other Mexican and Guatemalan sources during the Late Preclassic, became the dominant source during the Classic, and was completely replaced by other sources by the end of the Early Postclassic. Zeitlin (1982) attributed the waxing and waning of Caltonac obsidian utilization to changes in the socio-political sphere of influence of the population group that at that time controlled the obsidian source or the trade route to the southern Isthmus.

CONCLUSION

Probably among the major factors which led to the founding of Caltonac at this particular locality were: (1) the availability of building material and the peculiar topographic conditions offered by the Tepeyahualco lava flow, (2) the existence of a nearby source of obsidian of excellent quality, and (3) its location at the intersection of two of the natural access routes between the coastal regions and the Central Altiplano. The relative importance of these factors, if any, remains to be assessed. First, it will be necessary to establish the chronology of the site, which as yet remains unknown[10]. If as it is likely the

---

[10] Hernán Cortés (in Lorenzana, 1770) states, in his second letter to King Charles, that after crossing the Cofre de Perote range (Figure 1), he crossed a desolate plain and another mountain pass to arrive at the village of Caltami. Also, in the same book Lorenzana (1770) reproduced the tax records of the Aztec emperor Moctezuma II, who ruled from 1502 to 1520; among the tributary cities in the area of the archaeological site being described there was one whose glyph can be read as Caltepec. The similarities between these names and Caltonac are indeed suggestive of occupation of the site just prior to the arrival of the spaniards.

population center controlled the quarrying of obsidian, the data in Figure 7 suggests the site was occupied for a long period of time. Admittedly, the obsidian might have been quarried long before a major population center was established, but its wide distribution during the Classic is strong evidence that by this time quarrying was an organized activity, most probably under local control.

ACKNOWLEDGEMENTS

This study was supported by Mexico's Comisiòn Federal de Electricidad and Consejo Nacional de Ciencia y Tecnología. The U.S. Geological Survey kindly provided the chemical analyses. Thanks are due to J. Limòn, P. Mari, J. Rick, J. Fox, G. Mahood, T. Hester, R. Zeitlin, J. Parsons, K. Pope, J. Wiseman, and two anonimous reviewers for their help at different stages.

REFERENCES

Cobean,R.H., Coe,M.D., Perry,E.A., Turekian,K.K., Kharkar,D.P, 1971, Obsidian trade at San Lorenzo Tenochtitlan, Mexico: Science, v.174, p.666-671.

Ferriz,H., 1982, Geologic and preliminary reservoir data on the Los Humeros geothermal system, Puebla, Mexico: Proceedings Eight Workshop Geothermal Reservoir Engineering (SGP-TR-60), Stanford University, Stanford, California, December 1982, p.19-24.

Ferriz,H., Mahood,G.A., 1984, Eruption rates and compositional trends at Los Humeros volcanic center, Puebla, Mexico: J. Geophys. Res., v.89, p.8511-8524.

Ferriz,H., Yáñez,C., 1981, Mapa geológico del centro volcánico de Los Humeros, Edición preliminar: Comisión Federal de Electricidad, México, Juán de la Barrera#37, Cd. Satélite, Edo. de Mexico, 53100, MEXICO.

Graham,J.A., Hester,T.R., Jack,R.N., 1972, Sources for the obsidian at the ruins of Seibal, Peten, Guatemala: Contributions from the University of California Archaeological Research Facility, v.16,p.111-116.

Hester,T.R., Heizer,R.F., Jack,R.N., 1971a, Technology and geologic sources of obsidian artifacts from Cerro de Las Mesas, Veracruz, Mexico, with observations on Olmec trade: Contributions form the University of California Archaeological Research Facility, v.13, p.133-141.

Hester,T.R., Jack,R.N., Heizer,R.F, 1971b, The obsidian of Tres Zapotes, Veracruz, Mexico: Contributions from the University of California Archaeological Research Facility, v.13, p.65-131.

Hester,T.R., Jack,R.N., Heizer,R.F., 1972, Trace element analysis of obsidian from the site of Cholula, Mexico: Contributions of the University of California Archaeological Research Facility, v.16, 1972, p.105-110.

Hester,T.R., Jack,R.N., Bonfer,A., 1973, Trace element analyses of obsidian from Michoacan, Mexico: Preliminary results: Contributions of the University of California Archaeological Research Facility, v.18, p.167-176.

Jack,R.N., Heizer,R.F., 1968, 'Finger-printing' of some Mesoamerican obsidian artifacts: Contributions of the University of California Archaeological Research Facility, v.5,p.81-100

Jack,R.N., Hester,T.R., Heizer,R.F., 1972, Geologic Sources of Archaeological Obsidian from Sites in Northern and Central Veracruz, Mexico: Contributions of the University of California Archaeological Research Facility, v.16, p.117-122.

Lorenzana,F.A., 1770, Historia de Nueva-España escrita por su esclarecido conquistador Hernàn Cortès, aumentada con otros documentos, y notas por el Ilustrissimo Señor Don Francisco Antonio Lorenzana, Arzobispo de Mèxico: Imprenta del Superior Gobierno, Mexico City, p.I-IX and Plate 2.

Spence,M.W., Parsons,J.R., 1972, Prehispanic Obsidian Exploitation in Central Mexico, a Preliminary Synthesis: in Miscellaneous Studies in Mexican Prehistory. Museum of Anthropology, Anthropological Papers 45 (University of Michigan: Ann Arbor), p.1-43.

Stross,F.H., Hester,T.R., Heizer,R.F., Jack,R.N., 1976, Chemical and Archaeological Studies of Mesoamerican Obsidians: in R.E. Taylor (editor) Advances in Obsidian Glass Studies (Noyes Press: New Jersey), p.240-258.

Stross,F.H., Asaro,F., H.V. Michel,H.V., 1983, Precise Characterization of Guatemalan Obsidian Sources, and Source Determination of Artifacts from Quirigua: American Antiquity, v.48,p.338-340.

Zeitlin,R.N., 1982, Toward a more comprehensive model of interregional commodity distribution: Political variables and prehistoric obsidian procurement in Mesoamerica: American Antiquity, v.47, p.260-275.

Zeitlin, R.N., 1979, Prehistoric long-distance exchange on the southern Isthmus of Tehuantepec, Mexico: Ph.D. dissertation, Yale University (University Microfilms, Ann Arbor), p.74-79 and 90-98.

Zeitlin,R.N., Heimbuch,R.C., 1978, Trace Element Analysis and the Archaeologic Study of Obsidian Procurement in Precolumbian Mesoamerica: in D.D. Davis (editor) Lithics and Subsistence. Vanderbilt University Publications in Anthropology 20 (Vanderbilt University: Nashville, Tenn.), p.117-159.

APPENDIX

SAMPLE LOCATIONS AND DESCRIPTIONS

Sample	Location	Field description
LH1	19°46'51" N 97°29'43" W	Teziutlán lavas. Light gray, vesicular, porphyritic olivine basalt. 10% phenocrysts: plag, ol.
LH2	19°44'57" N 97°20'51" W	Teziutlán lavas. Green porphyritic andesite. 30% phenocrysts: plag, opx, cpx, ol, ox.
LH3	19°42'36" N 97°33'18" W	Teziutlán lavas. Dark gray, sparsely porphyritic basalt. 5% phenocrysts: plag, cpx, ol.
LH4	19°42'36" N 97°33'18" W	Teziutlán lavas. Medium gray, porphyritic basalt. 25% phenocrysts: pl, cpx, ol.
LH5	19°35'22" N 97°23'42" W	Pre-Xáltipan rhyolite. Light-gray, pumiceous, flow-banded hypersthene rhyolite. 4% phenocrysts: san, plag, opx, ox. Covered by Xáltipan Ignimbrite.
LH6	19°41'48" N 97°17'53" W	Pre-Xáltipan rhyolite. White, pumiceous biotite rhyolite. Restricted spherulitic zones. <1% phenocrysts: bio. Covered by Xáltipan Ignimbrite.
LH7	19°28'40" N 97°42'50" W	Xáltipan Ignimbrite. Sand pit in the road between Libres and Ixtacamaxtitlán. Aphyric rhyolitic pumice.
LH8	19°41'36" N 97°15'15" W	Xáltipan Ignimbrite. Sand pit in the roadway between Perote and Altotonga. Unoxidized core of aphyric rhyolitic pumice.
LH9	19°30'36" N 97°16'22" W	Xáltipan Ignimbrite. Arroyo near Tenextepec. Green aphyric rhyolitic pumice with tubular vesicles.
LH10	19°42'04" N 97°17'00" W	Xáltipan Ignimbrite. White, aphyric rhyolitic pumice with tubular vesicles.
LH11	19°41'36" N 97°15'15" W	Xáltipan Ignimbrite. Same outcrop as LH8. Unoxidized core of rhyodacitic pumice. 5% phenocrysts: plag, bio, cpx, opx, ox.

Sample	Location	Field description
LH13	19°41'36" N 97°15'15" W	Xâltipan Ignimbrite. Same outcrop as LH8. Unoxidized core of rhyodacitic pumice. 5% phenocrysts: plag, bio, cpx, ox.
LH14	19°45'59" N 97°33'41" W	Xâltipan Ignimbrite. Rhyodacitic pumice. 10% phenocrysts: plag, san, bio, cpx, qz (?), ox.
LH15	19°39'40" N 97°19'43" W	Xâltipan Ignimbrite. Mildly oxidized core of rhyodacitic pumice. 5% phenocrysts: plag, bio, cpx, hbl (?), ox. The ignimbrite is covered by a co-ignimbrite ash-fall (X-2) and the eight Upper Xâltipan air-fall tuffs (X-3 to X-10).
LH16	19°39'40" N 97°19'43" W	Upper Xâltipan air-falls. Same location as LH15. Light-cream rhyodacitic pumice from air-fall X-4. 5% phenocrysts: plag, opx, cpx, bio, ox.
LH17	19°39'40" N 97°19'43" W	Upper Xâltipan air-falls. Same outcrop as LH15. Green andesitic pumice from air-fall X-4. 5% phenocrysts: plag, cpx, ol, ox.
LH18	19°39'40" N 97°19'43" W	Upper Xâltipan air-falls. Same outcrop as LH15. Rhyodacitic pumice from air-fall X-5. 4% phenocrysts: plag, opx, cpx, ol(?), ox.
LH19	19°39'40" N 97°19'43" W	Upper Xâltipan air-falls. Same outcrop as LH15. Rhyodacitic, mildly oxidized pumice from air-fall X-7. 8% phenocrysts: plag, opx, cpx, bio, hbl, ol, ox.
LH20	19°39'40" N 97°19'43" W	Upper Xâltipan air-falls. Same outcrop as LH15. Dacitic pumice from air-fall X-7. 4% phenocrysts: plag, opx, cpx, bio, hbl, ol, ox.
LH21	19°39'40" N 97°19'43" W	Upper Xâltipan air-falls. Same outcrop as LH15. Green andesitic scoria from air-fall X-9. 2% phenocrysts: plag, opx, cpx, hbl (?), ox.

Sample	Location	Field description
LH22	19°39'40" N 97°19'43" W	Upper Xàltipan air-falls. Same outcrop as LH15. Rhyodacitic pumice from air-fall X-10. 10% phenocrysts: plag, bio, hbl, opx, cpx, ox. Air-fall X-10 is covered discordantly by the eight air-fall layers of the Faby Tuff.
LH23	19°43'05" N 97°31'49" W	Oyameles biotite rhyolite dome A. Rhyolitic vitrophyre. 3-5% phenocrysts: plag, san, bio, ox.
LH24	19°41'34" N 97°30'20" W	Oyameles biotite rhyolite dome B. Pumiceous rhyolite. 10% phenocrysts: san, plag, qz, bio, ox.
LH25	19°45'47" N 97°29'28" W	Manzanos biotite rhyolite dome. Pink pumiceous rhyolite. 6% phenocrysts: san, plag, bio, opx, ox.
LH26	19°46'58" N 97°20'41" W	Xiutetelco biotite rhyolite dome. Hydrated, friable, and partially devitrified rhyolite. 5% phenocrysts: plag, san, qz(?), bio, ox.
LH27	19°44'20" N 97°32'55" W	Caltonac aphyric rhyolite flow. Rhyolitic obsidian.
LH28	19°45'47" N 97°29'44" W	Ocotepec opx rhyolite dome A. Pumiceous rhyolite fragment from flow breccia. 5% phenocrysts: san, plag, opx, ox.
LH29	19°44'00" N 97°32'02" W	Ocotepec opx rhyolite dome B. Rhyolitic vitrophyre. 5% phenocrysts: san, plag, opx, cpx, ox.
LH30	19°43'28" N 97°34'10" W	Las Trancas opx rhyolite dome. Rhyolitic vitrophyre. 5% phenocrysts: plag, san, opx, ox.
LH31	19°39'40" N 97°19'43" W	Faby Tuff. Same location as LH15. Rhyodacitic pumice from layer F-1. 3% phenocrysts: plag, opx, ox.
LH32	19°39'40" N 97°19'43" W	Faby Tuff. Same location as LH15. Rhyodacitic pumice from layer F-2. 4% phenocrysts: plag, opx, ox.

Sample	Location	Field description
LH33	19°39'40" N 97°19'43" W	Faby Tuff. Same location as LH15. Rhyodacitic pumice from layer F-4. 5% phenocrysts: plag, hbl, opx, bio, ox.
LH34	19°39'40" N 97°19'43" W	Faby Tuff. Same location as LH15. Rhyodacitic pumice from layer F-5. 15% phenocrysts: plag, opx, cpx, ox.
LH35	19°39'40" N 97°19'43" W	Faby Tuff. Same location as LH15. Rhyodacitic pumice from layer F-6. 1% phenocrysts: plag, cpx, opx, ol, tmt.
LH36	19°39'40" N 97°19'43" W	Faby Tuff. Same location as LH15. Rhyodacitic pumice from layer F-7. 15% phenocrysts: plag, opx, cpx, hbl(?), ox.
LH40	19°39'28" N 97°24'43" W	Escarpe rhyodacite flow. Black rhyodacitic vitrophyre. 10% phenocrysts: plag, opx, cpx, ox. Covered by the Lower Zaragoza air-fall tuff.
LH41	19°40'01" N 97°24'30" W	Lower Zaragoza air-fall tuff. Rhyodacitic pumice with glomerophyric texture. 6% phenocrysts: plag, opx, cpx, ox. Covered concordantly by the Zaragoza Ignimbrite.
LH42	19°40'01" N 97°24'30" W	Zaragoza Ignimbrite. Same location as LH41. Silver-gray rhyodacitic pumice with glomerophyric texture. 10% phenocrysts: plag, opx, cpx, ox, ol.
LH43	19°31'29" N 97°24'41" W	Zaragoza Ignimbrite. Dark-gray rhyodacitic pumice with glomerophyric texture from the basal portion of the ignimbrite. 7% phenocrysts: plag, opx, cpx, ox. Sub-milimetric vapor-phase mica.
LH44	19°31'29" N 97°24'41" W	Zaragoza Ignimbrite. Same location as LH43. Greenish-gray rhyodacitic pumice with glomerophyric texture from the middle portion of the ignimbrite. 15% phenocrysts: plag, opx, cpx, ox.

Sample	Location	Field description
LH45	19°31'29" N 97°24'41" W	Zaragoza Ignimbrite. Same location as LH43. Black andesitic scoria from the middle portion of the ignimbrite. 30% phenocrysts: plag, cpx, opx, ox.
LH46	19°31'29" N 97°24'41" W	Zaragoza Ignimbrite. Yellowish-brown dacitic pumice. 40% phenocrysts: plag,opx, ox.
LH47	19°44'44" N 97°33'08" W	Zaragoza Ignimbrite. Black andesitic scoria. 2% phenocrysts: plag, copx, opx, ol, ox.
LH48	19°42'13" N 97°30'29" W	Upper Zaragoza lithic air-fall tuff. Rhyodacitic pumice with glomerophyric texture. 12% phenocrysts: plag, opx, cpx, ox.
LH49	19°46'13" N 97°25'26" W	Las Lineas rhyodacite dome. Hydrated and partially devitrified rhyodacite: 10% phenocrysts: plag, opx, cpx, ox.
LH50	19°40'20" N 97°27'17" W	Cueva Ahumada lavas. Dark gray, porphyritic andesite. 10% phenocrysts: plag, opx, cpx, ol, ox. Cognate (?) inclusions with ol, cpx, plag, and glass.
LH51	19°40'50" N 97°27'20" W	Cueva Ahumada lavas. Dark gray, sparsely porphyritic, vesicular, basaltic andesite. 3% phenocrysts: plag, cpx, ol, ox.
LH52	19°40'07" N 97°27'07" W	Cueva Ahumada lavas. Rhyodacitic vitrophyre. 10% phenocrysts: plag, bio, opx, ox. Covered by the Xoxoctic Tuff.
LH53	19°41'11" N 97°24'24" W	Xoxoctic Tuff. Green dacitic pumice. 2% phenocrysts: cpx, ol, plag, ox.
LH54	19°35'36" N 97°23'31" W	Llano andesitic Ignimbrite. Black andesitic bomb. 7% phenocrysts: plag, opx, cpx, ol, ox.
LH55	19°33'53" N 97°27'37" W	Tepeyahualco compound flow. Dark-gray, sparsely porphyritic, vesicular andesite. 3% phenocrysts: plag, cpx, opx (?), ol. Lowermost in a series of flow units.

Sample	Location	Field description
LH56	19°35'47" N 97°28'55" W	Tepeyahualco compound flow. Black sparsely porphyritic andesite. 3% phenocrysts: plag, cpx, ol. Flow unit above the one of LH55.
LH57	19°35'34" N 97°28'45" W	Tepeyahualco compound flow. Black sparsely porphyritic andesite. 3% phenocrysts: plag, cpx, ol, pigeonite (?), tmt. Flow unit above the one of LH56.
LH58	19°35'23" N 97°28'39" W	Tepeyahualco compound flow. Black sparsely porphyritic andesite. 5% phenocrysts: plag, cpx, ol, ox. Flow unit above the one of LH57.
LH59	19°35'11" N 97°28'11" W	Tepeyahualco compound flow. Black porphyritic andesite. 15% phenocrysts: plag, cpx, ol. Flow unit above the one of LH58.
LH60	19°36'50" N 97°27'53" W	Tepeyahualco compound flow. Black sparsely porphyritic vesicular andesite. 3% phenocrysts: plag, cpx, pigeonite, ox. Flow unit above the one of LH59.
LH61	19°33'56" N 97°27'31" W	Tepeyahualco compound flow. Black porphyritic andesite. Physical mixture of two magmas (?). 15% phenocrysts: plag, cpx, opx, pigeonite, ol, ox. Flow unit above the one of LH60.
LH62	19°29'57" N 97°21'18" W	Limón compound flow. Dark-gray, porphyritic basaltic andesite. 5% phenocrysts: plag, ol. Lowermost of a series of flow units
LH63	19°33'14" N 97°21'01" W	Limón compound flow. Black, porphyritic, vesicular basaltic andesite. 5% phenocrysts: plag, ol, cpx, opx. Physical mixture of two magmas. Flow unit above that of LH62.
LH64	19°34'35" N 97°22'09" W	Limón compound flow. Black, porphyritic,vesicular andesite. 15% phenocrysts: plag, ol, cpx, ox. Flow unit above that of LH63.

Sample	Location	Field description
LH65	19°34'41" N 97°22'28" W	Limón compound flow. Black, porphyritic,vesicular andesite. 20% phenocrysts: plag, ol, cpx. Flow unit above that of LH64.
LH66	19°29'37" N 97°24'01" W	Sarabia compound flow. Black, vesicular sparsely microphyric basaltic andesite. 2% phenocrysts: plag, cpx, ol (?), ox. Lowermost of a series of flow units.
LH67	19°33'14" N 97°21'01" W	Sarabia compound flow. Black, porphyritic basaltic andesite. 5% phenocrysts: plag, cpx, ox. Flow unit above that of LH66.
LH68	19°34'35" N 97°22'09" W	Sarabia compound flow. Black, porphyritic andesite. 20% phenocrysts: plag, cpx, pigeonite, ox. Flow unit above that of LH67.
LH69	19°45'39" N 97°22'49" W	Chiapa shield. Dark gray, slightly vesicular sparsely porphyritic andesite. 3-5% phenocrysts: plag, pigeonite, ol (?), ox. Lowermost of a series of flows.
LH70	19°45'15" N 97°22'53" W	Chiapa shield.Dark gray, vesicular, porphyritic andesite. 8% phenocrysts: plag, cpx, ol. Flow above that of LH69.
LH71	19°44'55" N 97°23'08" W	Chiapa shield. Black, vesicular, sparsely porphyritic andesite. 3-5% phenocrysts: plag, cpx, opx, ox. Flow above that of LH70.
LH72	19°44'03" N 97°23'41" W	Chiapa shield. Black, microvesicular, sparsely microphyric andesite. 3% phenocrysts: plag, cpx, ox. Flow above that of LH71.
LH73	19°39'21" N 97°26'37" W	Xalapazco andesite. Dark gray, porphyritic andesite. 10% phenocrysts: plag, cpx, opx, ox. ~1% of basaltic inclusions.
LH74	19°37'23" N 97°26'26" W	Matzaloya andesite. Black, sparsely microphyric andesite. 3% phenocrysts: plag, opx, cpx, ox. <1% inclusions of vesiculated silicic glass. Physical mixture of two magmas (?). Flow above that of

Sample	Location	Field description
LH75	19°37'12" N 97°25'59" W	Matzaloya andesite. Black vitrophyric andesite. 3% microphenocrysts: plag, opx, cpx, ox. Flow above that of LH74.
LH76	19°39'15" N 97°25'42" W	Cuicuiltic Tuff. Sequence of alternating rhyodacitic and andesitic air-fall tuffs. Rhyodacitic pumice from the lowermost layer. Phenocrysts: plag, opx, cpx, ol (?), ox.
LH77	19°39'15" N 97°25'42" W	Cuicuiltic Tuff. Same outcrop as LH76. Rhyodacitic pumice. Phenocrysts: plag, opx, cpx, ox. Layer above that of LH76.
LH78	19°39'15" N 97°25'42" W	Cuicuiltic Tuff. Same outcrop as LH76. Andesitic scoria. Phenocrysts: plag, cpx, ol. Layer above that of LH77.
LH79	19°39'15" N 97°25'42" W	Cuicuiltic Tuff. Same outcrop as LH76. Rhyodacitic pumice. Phenocrysts: plag, opx, cpx, ol, ox. Layer above that of LH78.
LH80	19°39'15" N 97°25'42" W	Cuicuiltic Tuff. Same outcrop as LH76. Andesitic scoria. Phenocrysts: plag, ol, cpx, opx. Agglomerate above the layer of LH79.
LH81	19°46'02" N 97°26'05" W	San Antonio shield. Northern flank. Black, sparsely porphyritic rhyodacite. 5% phenocrysts: plag, opx, cpx, hbl, ox. Flow below that of LH82.
LH82	19°45'52" N 97°25'46" W	San Antonio shield. Northern flank. Black, rhyodacitic vitrophyre. Glomerophyric texture. 10% phenocrysts: plag, opx, cpx, ox. Flow above that of LH81.
LH83	19°41'13" N 97°24'47" W	San Antonio shield. Southeastern flank. Black rhyodacitic vitrophyre. 15% phenocrysts: plag, opx, ox. Covered by Cuicuiltic Tuff, which is in turn covered by the flow of LH84.

Sample	Location	Field description
LH84	19°42'11" N 97°24'52" W	San Antonio shield. Southeastern flank. Black, sparsely porphyritic andesite. 3% phenocrysts: plag, opx, cpx, ox. Inclusions of vesiculated silicic glass and diorite (cognate?). Flow above that of LH83.
LH85	19°42'17" N 97°25'36" W	San Antonio shield. Southeastern flank. Black, sparsely porphyritic andesite. 3% phenocrysts: plag, cpx, opx, ol, ox. Inclusions of silicic vesiculated glass. Flow above that of LH84.
LH86	19°43'15" N 97°29'34" W	San Antonio shield. Western flank. Black rhyodacitic vitrophyre. 10% phenocrysts: plag, opx, cpx, ox. Mafic inclusions.
LH87	19°43'04" N 97°29'46" W	San Antonio shield. Western flank. Black rhyodacitic vitrophyre. 10% phenocrysts: plag, cpx, opx, ox. Mafic inclusions. Flow above that of LH86.
LH88	19°42'41" N 97°28'49" W	San Antonio shield. Western flank. Black rhyodacite 5% phenocrysts: plag, opx, ox. Flow above that of LH87.
LH89	19°45'28" N 97°26'54" W	San Antonio shield. Northwestern flank. Papata andesite flow. Black, microvesicular, microphyric andesite. 5% phenocrysts: plag, pigeonite, ol, ox. Flow above those of LH81 and LH82.
LH90	19°40'08" N 97°28'10" W	Arenas volcano. Northwestern flank. Black rhyodacitic vitrophyre. 15% phenocrysts: plag, cpx, opx, hbl, ox. Physical mixture of two magmas.
LH91	19°38'31" N 97°28'14" W	Arenas volcano. Summit. Black, sparsely porphyritic rhyodacite. 3% phenocrysts: plag, opx, cpx, hbl, ox. Mafic inclusions. Flow above that of LH92.
LH92	19°37'10" N 97°28'53" W	Arenas volcano. Southwestern flank. Black, sparsely porphyritic rhyodacite. 5% phenocrysts: plag, opx, cpx, ox.

Sample	Location	Field description
LH93	19°39'35" N 97°23'30" W	Cuamilacas rhyodacite flow. Black, sparsely porphyritic rhyodacite. 5% phenocrysts: plag, opx, cpx, hbl, ox. Mafic inclusions.
LH94	19°37'14" N 97°30'20" W	Tenextepec olivine basalt. Light gray, vesicular, porphyritic, intergranular olivine basalt. 5% phenocrysts: ol, plag, ox.
LH95	19°43'09" N 97°29'35" W	Los Humeros olivine basalt. Light gray, vesicular, porphyritic, intergranular olivine basalt. 5% phenocrysts: ol, plag, ox.
LH96	19°38'23" N 97°26'29" W	Xalapazco olivine basalt. Light gray, vesicular, glomerophyric, intergranular olivine basalt. 5% phenocrysts: ol, plag, ox.
LH97	19°33'26" N 97°25'37" W	Sarabia cinder cone. Reddish gray, crystal-poor, basaltic andesite scoria.
LH98	19°32'53" N 97°18'16" W	Guadalupe Victoria cinder cone. Black, crystal-poor, basaltic andesite scoria.
LH99	19°30'06" N 97°26'30" W	Pizarro rhyolite dome. Rhyolitic vitrophyre. 10% phenocrysts: san, qz, bio, ox.
LH100	19°33'09" N 97°30'20" W	Las Aguilas rhyolite dome. Slightly hydrated rhyolitic vitrophyre. 5-10% phenocrysts: san, qz, bio, ox.